Protein Dynamics in Mammalian Genome Maintenance

Angelika Zotter

Cover picture:

"Structure and Function of the Eiffel Tower" by Angelika Zotter

Protein Dynamics in Mammalian Genome Maintenance

Dynamiek van eiwitten betrokken in het genoomonderhoud van zoogdieren

Proefschrift

ter verkrijging van de graad van doctor
aan de Erasmus Universiteit Rotterdam
op gezag van de Rector Magnificus
Prof.dr. S.W.J. Lamberts
en volgens besluit van het College voor Promoties

De openbare verdediging zal plaatsvinden op
woensdag 14 mei 2008 om 9:45 uur

door

Angelika Monika Zotter
geboren te Mödling, Oostenrijk

ERASMUS UNIVERSITEIT ROTTERDAM

Promotiecommissie

Promotor:

Prof.dr. J. H. J. Hoeijmakers

Overige leden:

Prof.dr. J. Trapman

Prof.dr. R. van Driel

Dr. A. B. Houtsmuller

Copromotor:

Dr. W. Vermeulen

Contents

Chapter

1

General Introduction

and

Aim of the Thesis

General Introduction and Aim of the Thesis

The integrity of the genome, carrier of the blueprint for each organism, is under constant attack from environmental as well as endogenous DNA damaging agents. An agent with substantial impact on our DNA is the UV-fraction of sunlight. It inflicts bulky DNA lesions, which can interfere with vital cellular functions, such as DNA replication and transcription of genes, by simply blocking these processes. This can lead to cell death or to mutations, which in higher organisms can in turn lead to inborn diseases and cancer. To counteract these deleterious effects, the specialized multi-component nucleotide excision repair (NER) machinery has evolved which removes and replaces the damaged oligonucleotide in a multi-step process. Defects in this repair pathway are the underlying cause for the inherited UV-sensitive diseases xeroderma pigmentosum, Cockayne syndrome, and trichothiodystrophy. In association with these disorders it has been demonstrated that repair deficiencies do not only lead to mutations and cancer, but also to developmental difficulties, (neuronal) degeneration and premature ageing. In rapidly dividing cells, not all DNA lesions can be repaired by the time a new DNA replication round has begun, even if the corresponding repair pathway is fully functional. Therefore, cells have also evolved specialized lesion-bypass polymerases. Translesion polymerases are capable of resolving DNA polymerase complexes stalled at DNA damage sites by inserting a nucleotide opposite an altered base, enabling the cell to continue to replicate. Importantly, polymerase eta can insert the correct nucleotide opposite UV-induced pyrimidine-pyrimidine adducts such as cyclobutane pyrimidine dimers (CPD), enabling mutation-free replication of DNA past these UV lesions. Without a functioning polymerase eta, unrepaired UV injuries blocking the replication process can only be resolved by mutational translesion synthesis performed by other lesion bypass polymerases. This leads to a highly elevated risk of skin cancer in patients exhibiting a special form of xeroderma pigmentosum due to lack of polymerase eta.

NER and translesion synthesis (TLS) have been extensively studied *in vitro*, resulting in a basic understanding of these processes. The aim of this study is to provide more insight into the dynamic actions and interplay of these vital processes in the living mammalian cell. Using GFP-fusion proteins combined with confocal microscopic techniques, we intended to get a more accurate picture of how mammalian cells deal with UV-induced DNA damage.

As an introduction to the topic, **Chapter 2** provides a review on the dynamic organization of genome surveillance processes. In addition, this chapter gives an overview over future directions in this field. In the experimental **Chapter 3**, a novel approach is presented to study minuscule differences in the nuclear dynamics of biologically functional proteins. This method is then applied to discern the differences in nuclear mobility between diverse subunits of the NER machinery. **Chapter 4** provides a comprehensive study on the active role of the NER endonuclease XPG *in vivo.* **Chapter 5** is an *in vivo* study of the interactions of the Cockayne syndrome B (CSB) protein, implicated in transcription-coupled repair of UV lesions, with the transcription machinery. **Chapter 6** focuses on the nuclear dynamics of the translesion polymerase eta throughout the cell cycle and in response to UV-induced replication stalling.

Chapter 2

Dynamic Organization of Genome Surveillance Processes

To be submitted to

DNA Repair

Dynamic Organization of Genome Surveillance Processes

Angelika Zotter[1], Deborah Hoogstraten[1] and Wim Vermeulen[1,*]

[1]Department of Cell Biology and Genetics, Erasmus MC Rotterdam, P.O. box 2040, 3000 CA Rotterdam, The Netherlands.

*Corresponding author. Phone: (+31) 10 7043194, Fax: (+31) 10 7044743
email: w.vermeulen@erasmusmc.nl

Introduction

Survival of all species depends on the accurate translation of genetic information into functional proteins and a faithful transmission of the genetic code to progeny. This requires precise replication of the genome and distribution of chromosomes over daughter cells. However, DNA is continuously exposed to agents that alter its physico-chemical constitution; these include cellular metabolites, environmental chemicals and electro-magnetic radiation. Superficially innocuous agents such as water, oxygen, sunlight, and food, fundamental to terrestrial live, modify the DNA structure as a result of normal cellular metabolism [1]. DNA lesions directly interfere with efficient gene transcription and genomic replication fidelity, eventually causing premature ageing and cancer [2]. To counteract the severe biological consequences of DNA injuries, different genome defence mechanisms are activated in the cell. The overall cellular DNA damage response (DDR) consists of three distinct though partially overlapping strategies: (i) Direct removal of DNA lesions by distinct specialized DNA repair systems; (ii) damage avoidance processes, and (iii) damage signalling systems that trigger and coordinate the cellular response. Which DDR system is activated depends on the type of lesion encountered, the location of the lesion in the genome and the phase of the cell cycle [3], and probably also the type of cell. The aim of this review is to summarize recent findings on the spatial and temporal organization of the DDR system.

DNA damage repair

The heart of the cellular defence against DNA injuries is formed by a variety of DNA repair mechanisms [4], each having their own damage specificity. Together, they are able to remove the vast majority of injuries from the genome. The simplest

solution that emerged in evolution is the direct reversal of lesions by specialized activities, such as of photolyases that selectively reverse UV-induced DNA damages [5] and the suicide enzyme O^6-methylguanine transferase (MGMT) [6]. Photolyases are not conserved into the mammalian branch and mammals have to rely on more complex mechanisms to remove UV injuries. Nucleotide excision repair (NER) removes a broad spectrum of lesions that interfere with proper base pairing, such as the major UV light-induced damages 6-4 photoproducts ((6-4)PPs) and cyclobutane pyrimidine dimers (CPDs), and bulky chemical adducts. NER is initiated via two pathways, global genome repair (GG-NER) scanning the whole genome for DNA damages, and transcription-coupled NER (TC-NER), promoting the efficient repair of a transcribed strand; it is directly triggered by a DNA polymerase stalled at a lesion site [7-9] (Fig.1). Bases with small chemical alterations, such as oxidative and alkylated damages, are substrate to base excision repair (BER) [10, 11]. Single-strand break repair is closely connected to BER [12]. Lesions for both NER and BER processes only affect one of the DNA strands and are removed in a 'cut-and-patch'-mechanism. The resulting single-stranded gap is filled using the intact complementary strand as template. When both DNA strands are affected, as in the case of double-stranded breaks (DSBs), the cell encounters a more serious problem. In such a case simple removal of a damage-containing stretch of nucleotides and copying information from the un-touched opposite strand like in BER and NER is not possible. Two distinct pathways, homologous recombination (HR) and non-homologous end-joining (NHEJ) deal with DSBs [13, 14]. In somatic mammalian cells, DSB repair is mainly performed by NHEJ based on direct ligation of the broken DNA ends [15, 16]. NHEJ can, however, be considered an error-prone emergency strategy, since it requires processing of DSBs prior to ligation which in a significant number of cases causes loss or changes of a few nucleotides. HR is in principle error-free but requires the presence of a homologous DNA copy (i.e. a sister chromatide); an intact DNA strand has to be used as a template for DNA repair synthesis for no genetic information to be lost [17].
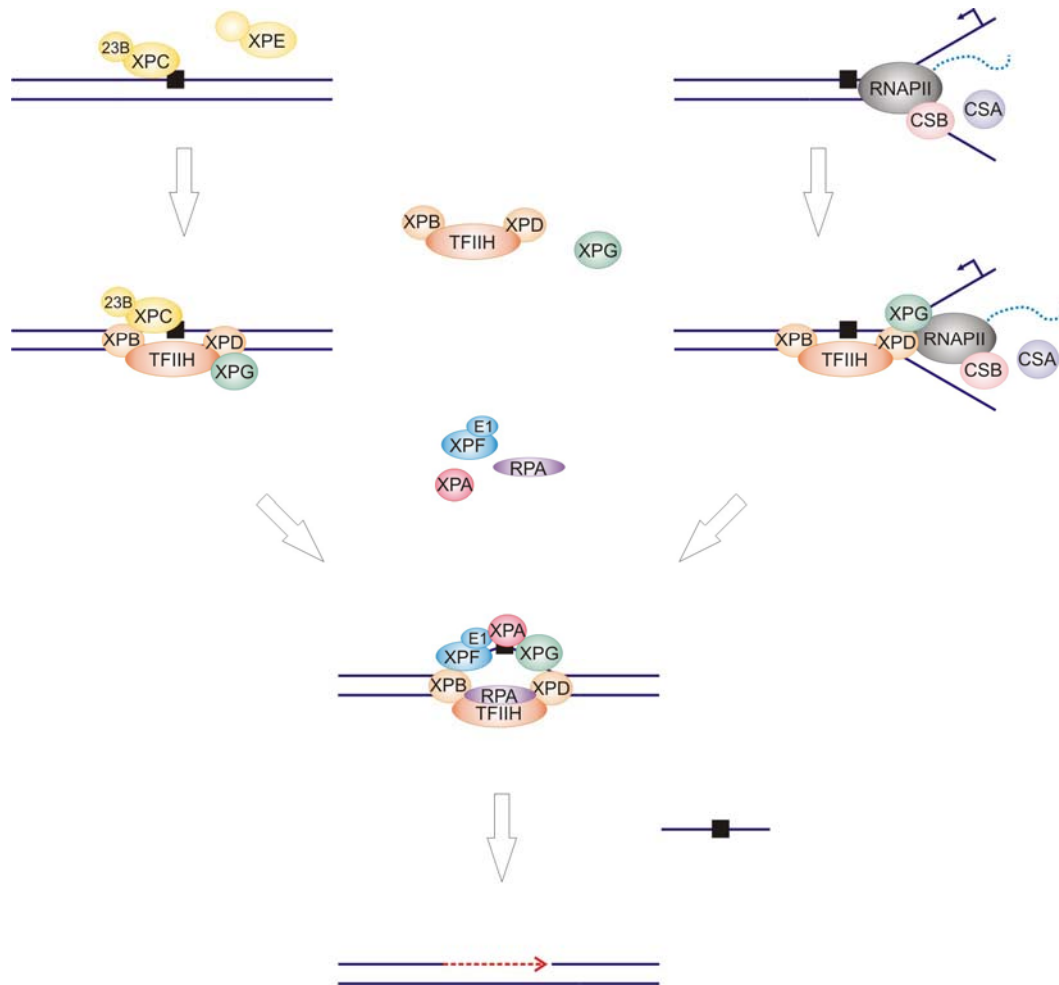
Fig.1. Global genome and transcription-coupled nucleotide excision repair. (A) In GG-NER, bulky DNA lesions (e.g. (6-4)PP) are recognized by the protein dimer XPC-hHR23B. XPC can be aided in DNA damage sensing by XPE, a dimer consisting of the DNA damage binding protein 1 (DDB1) and p48 (this accounts especially for certain less prominent DNA damages like CPDs). Subsequently, the basal transcription factor TFIIH, which includes two helicases of opposite polarities (XPB and XPD), and the 3' endonuclease XPG are recruited. After unwinding of the DNA around the lesion, RPA is required to bind the single-stranded DNA and stabilize the open complex. The XPC-hHR23B duplex is replaced by XPA, which is believed to contribute by verifying the presence of a lesion. Finally, a third protein dimer, ERCC1-XPF, is recruited. Dual incisions are made and to cut out a stretch of DNA containing the lesion. After release of the damaged oligonucleotide, the resulting gap is filled by the replication machinery. (B) Alternatively, a lesion may be recognized when it stalls an elongating RNA polymerase II complex. Such blocks trigger the recruitment of TFIIH, XPG and two additional proteins, CSA and CSB. The resulting complex is probably responsible for removing the stalled polymerase from the transcribed strand so that subsequent repair of the lesion can occur. Black square, bulky DNA damage; XPA-G, Xeroderma pigmentosum complementation group A-G; 23B, hHR23B (human homologue to the yeast Rad23 protein); E1, ERCC1 (human excision repair cross complementation group 1); CSA and CSB, Cockayne syndrome proteins A and B; parental DNA is depicted as dark blue lines, newly synthesized DNA as dotted red line; dotted blue line, newly synthesized RNA.

DNA damage avoidance or tolerance

To guarantee faithful transmission of genetic information to the progeny after cell division, cells rely for a large part on the high fidelity replication of DNA performed in mammals by the DNA polymerases δ/ε and α. The extremely low error-rate of these DNA polymerases is additionally reduced by a factor 2 to 3 as a result of the correcting activities of the mismatch repair (MMR) pathway (reviewed in [18, 19]). MMR distinguishes between the newly synthesized and the original template strand and by this corrects erroneously inserted or modified nucleotides. Also extrahelical loops created by polymerase strand slippages, especially on short repetitive DNA sequences (microsatellites), are reversed by MMR, thereby preventing frameshift mutations.

DNA lesions that are not removed by one of the above mentioned repair mechanisms would interfere with DNA replication. Lesion-stalled replication forks can lead to highly cytotoxic DSB and require a swift response. At least two DNA damage tolerance mechanisms have evolved: translesion synthesis (TLS) and recombination-dependent daughter-strand gap repair (DSGR) [4, 20, 21]. Both processes do not actually remove lesions, but serve as a temporal solution for a stalled replicative DNA polymerase. During translesion synthesis, the regular DNA polymerase (polδ/ε or α) is temporarily exchanged with a damage-specific translesion polymerase (pol ζ-κ) [22-26] (Fig.2 A and B). Though TLS can circumvent lesion-induced replication stalling, the reduced fidelity of the alternative polymerases causes generally enhanced mutagenesis. However, for some defined blocking injuries (e.g. CPDs or specific N_2-adducts on Guanine) a relatively error-free TLS (by polymerase η or κ, respectively) is possible [27-29]. For certain poorly repaired damages it might be especially important to have an accurate bypass mechanism to avoid mutagenesis. Recombination-dependent daughter-strand gap repair, also generally termed "damage avoidance", is mainly described in unicellular eukaryotes such as yeast. This damage avoidance process is essentially error-free and based on the re-initiation of replication downstream of a blocking injury (Fig. 2 C). The regular DNA polymerase uses the newly synthesized DNA of an allelic copy of a gene via recombinatorial strand exchange as a template to fill in the gaps [20, 30].
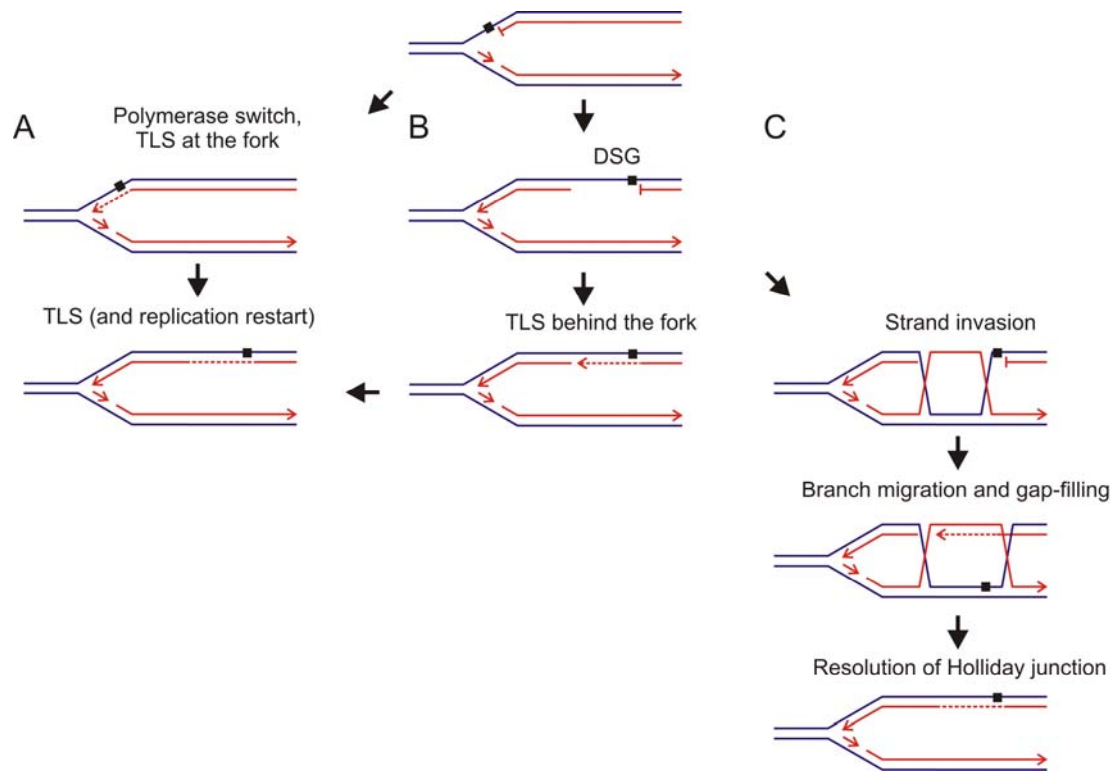
Fig.2. Translesion synthesis (TLS) and recombination-dependent daughter-strand gap repair (DSGR). Both bypass mechanisms are triggered by a replication fork-stalling DNA lesion (indicated by a black square). (A) "Classical" model of translesion synthesis. The regular DNA polymerase is temporarily exchanged for a translesion polymerase, and TLS takes place at the site of the stalled fork, followed by replication restart. (B) Alternatively, replication could restart beyond the blocked fork leaving a gap (DSG) behind, which is subsequently filled in by TLS after the fork has proceeded downstream. (C) Instead of TLS, DSG can trigger recombination-dependent DSGR. The DSG is filled in using the undamaged, newly synthesized strand via recombinatorial strand exchange involving the HR protein Rad51 (or alternatively by fork regression and annealing of the new strand, not shown). Parental strands are shown in blue; daughter strands are shown in red. Dotted lines depict the stretch of lesion bypass synthesis.

Unrepaired DNA lesions also interfere with transcription. While it is known that RNA polymerase II (RNAPII) stalled at bulky DNA damages promotes the efficient recruitment of the transcription-coupled repair (TCR) machinery [31, 32], for non-bulky oxidative lesions this is still a topic of controversy. These DNA modifications could instead be circumvented by transcriptional lesion bypass, resulting in transcriptional mutagenesis [33]. After thorough characterization of this pathway in E. coli [34], a recent publication has confirmed its relevance also in human cells [35]. RNAPII bypass activities were found to reside in transcription elongation factors such as TFIIF, Elongin, CSB, and TFIIS, providing distinct bypass specificities depending on the type of lesion.

Damage signaling

In order to efficiently cope with challenges to the genome, damage sensing is linked to signal transduction that triggers changes in expression and/or posttranslational modifications of DDR proteins. This in turn may result in cell cycle arrest to create an extended time window to allow completion of lesion removal prior to replication or cell division. Depending on the nature of the DNA injury and the phase of the cell cycle in which the lesion is encountered, the cell cycle can be arrested at the G1/S transition, within the S-phase, or at the G2/M transition (reviewed in [36]). Alternatively, apoptosis is triggered when too many injuries are encountered in order to protect the organism from potentially harmful cells [37].

Different DNA lesions trigger distinct kinase cascades that result in cell cycle checkpoint control and DNA repair. For example, DSBs mainly induce the ATM (Ataxia telangiectasia mutated) kinase and its downstream checkpoint kinase Chk2 [38], whereas bulky lesions and replication stress activate ATR (ATM- and Rad3-related) and its key effector kinase Chk1 [39, 40]. A third kinase, DNA-PK (DNA-dependent protein kinase, composed of its catalytic subunit DNA-PKcs and a regulatory Ku70/80 heterodimer), is activated by IR-induced DSBs and UV damage-induced replication stress. It is essential for NHEJ in higher eukaryotes [16] and additionally functions in telomere maintenance and induction of apoptosis [41]. Below we will discuss the spatio-temporal organization of genome surveillance systems including damage signaling.

Intertwined DNA-transacting processes

The distinct DNA surveillance mechanisms are usually represented as separate entities; however, most of them are part of an intricate network. In fact, most repair pathways are in part overlapping and/or connected to other DNA-transacting pathways, often sharing specific essential components (Table 1). Different strategies might be used to employ the multifunctionality of these factors: (*i*) different spatial organization, (*ii*) incorporation into diverse functional complexes, and/or (*iii*) dynamic sharing of these components. Regulation of pleiotropic functionality of proteins into discrete cellular processes by subcellular redistribution, activation and adaptive responses is commonly achieved by distinct posttranslational modifications (PTMs) of proteins. Within DDR different PTMs were identified ranging from phosphorylation, acetylation, methylation, neddylation, mono- and polyubiquitylation, and sumoylation to poly-ADP-ribosylation. These modifications do not only alter the electrostatic charge of the target proteins, but also mask or create

interaction sites for other factors. One of the most common and best-explored PTMs implicated in DDR is by differential phosphorylation/dephosphorylation, mainly driven by the ATM, ATR and DNA-PKcs kinases [36, 42, 43]. Recent research indicates that also differential ubiquitylation (and PTMs by ubiquitin variants) plays an important role in the regulation of DDR [43-52].

Overlapping repair processes

A plethora of repair factors were found to be engaged in multiple DNA maintenance systems. Here we will summarize only a few (typical) examples (see also Table1). (*i*) The hetero-dimeric ERCC1/XPF complex was originally identified as a structure-specific endonuclease that incises 5' of the DNA lesions within NER [53-56]. Further analysis revealed additional functions for this complex in HR [57-61], interstrand cross-link repair [62-64] and telomere maintenance [65]; engagement in mismatch repair has been shown in yeast [66, 67].

Another component of the NER pathway, the GG-NER damage recognition factor XPC/HR23B [68], was found to play an additional role in BER: HR23B and HR23A, the two human Rad23 homologs, stimulate the activity of the BER enzyme 3-methyladenine-DNA glycosylase [69]. In addition, XPC interacts with and stimulates thymine DNA glycosylase (TDG), which initiates BER at G/T mismatches generated by spontaneous deamination of 5-methylcytosine [70]. Very recently, it was shown that the XPC/HR23 complex acts as a cofactor to the BER enzyme OGG1 (8-oxoguanine DNA-glycosylase 1), a glycosylase involved in removing the oxidative base damage 8-hydroxyguanine [71].

As mentioned above, DSBs in mammalian cells are repaired via HR or NHEJ. Even though these processes are mechanistically and structurally distinct, they use some common factors; both are stimulated by ATM and employ the breast cancer susceptibility gene 1 (BRCA1), which promotes HR and facilitates high fidelity NHEJ, possibly by protecting DNA ends from excess trimming [72, 73]. BRCA1 recruits the meiotic recombination 11 (Mre11), Rad50, and Nijmegen breakage syndrome 1 (Nbs1) containing complex (MRN) to DSBs. Also this complex is implicated in both DSB repair pathways as well as mitotic and meiotic recombination, telomere length maintenance, and cell cycle regulation [74].

Transcription and DNA repair

Besides overlap between distinct repair processes, DDR is also linked to other essential DNA transacting mechanisms, such as transcription and replication. A prime example of such a link is the tight connection between NER and

transcription, clearly illustrated by the existence of a specialized transcription-coupled NER pathway (TC-NER) [31, 75, 76]. Several key factors exhibit a dual functionality in NER and transcription, such as the basal RNAPII transcription factor TFIIH [77-81] and the chromatin remodelling factor Cockayne Syndrome B (CSB) [82-84]. Also the NER 3' endonuclease XPG has been proposed to promote transcription elongation by direct interaction with RNAPII [81] and is involved in TC-NER.

The versatile BRCA1, an important DSB repair factor [85-87], links DSB repair to transcription, as shown by its physical interaction with the RNAPII holoenzyme and various transcription factors. Since BRCA1 has a function in RNAPII transcription, in maintenance of heterochromatin, and various DNA repair pathways such as HR and NHEJ, and possibly TCR, it has been hypothesized that it might be involved in the replacement of the elongating RNAPII from the damage and subsequently recruiting repair factors, such as the MRN complex in NHEJ [88].

Table 1. Multiple functions of repair factors.

Protein (complex)	Functions	References
XPC-HRad23A/B	NER	[221]
	Ubiquitin-proteasome complex	[222-225]
	BER	[69, 71]
TFIIH	RNAPII transcription	[77, 78]
	NER	[77, 226]
	RNAPI transcription	[227]
CSB	TC-NER	[228]
	RNAPII transcription	[82, 229]
	RNAPI transcription	[230]
	RNAPIII transcription	[229]
ERCC1-XPF	NER	[54-56]
	HR	[58, 59]
	ICL repair	[63]
XPG	NER	[231]
	BER	[232, 233]
	TC-NER	[81, 127, 234]
RPA	DNA replication	[235]
	HR	[91, 236]
	NER	[92, 237]
	BER	[93]
	MMR	[238, 239]
		reviewed in [94, 96, 97]

HAT p300	Transcription	[122]
	NER	[125, 126, 240]
PCNA	DNA replication	[102, 235, 241, 242]
	Replicative damage bypass	[26, 102, 104]
	Damage avoidance	[102]
	Cell cycle regulation	[243-246]
	Chromatin assembly	[101, 247-251]
	NER	[244, 252, 253]
	BER	[101, 254]
	MMR	[255-257]
		reviewed in [98-100]
RFC	Replication	[258]
	NER	[259]
	BER	[254, 259]
	MMR	[238, 239, 255]
		reviewed in [260]
Rad50-Nbs1-Mre11	HR	
	NHEJ	
	Meiotic and mitotic recombination	
	Cell cycle regulation	
	Telomere length maintenance	reviewed in [74, 261]
		[262, 263]
BRCA1	HR	[73, 264, 265]
	NHEJ	[21, 266]
	Damage avoidance	[88, 267]
	RNAPII transcription	[268]
	Cell cycle control	
	chromatin remodelling and	[269, 270]
	maintenance of heterochromatin	reviewed in [85, 87, 271]
ATM	HR	
	NHEJ	
		[38, 42, 110, 272, 273]

Replication and DNA repair

Multiple links between DNA replication and genome surveillance processes are known, including MMR, lesion bypass synthesis, homologous recombination, and gap-filling synthesis in NER. MMR mends mistakes made by the replication machinery and is directly coupled to and in most cases strictly dependent on replication [19, 89]. Translesion synthesis and recombination-dependent daughter-strand gap repair assist the replication machinery at stalled replication forks.

A range of proteins and protein complexes are shared between replication and genome maintenance pathways. Most relevant within the context of DNA repair

are replication protein A (RPA) and proliferating cell nuclear antigen (PCNA). RPA, a stable complex of three subunits RPA70, RPA32 and RPA14, is essential for DNA replication [90] and several repair pathways, like HR [91], NER [92], and possibly BER [93]. The involvement of RPA within these repair processes is coordinated by a series of RPA-ssDNA and RPA-protein interactions [94]. A specific domain of RPA32 interacts with the HR-associated factor Rad52, the NER-related component XPA, and the major uracil-DNA glycosylase UNG2 involved in BER [95]. The mutually exclusive binding of these components to RPA suggests distinct pathway-specific sub-complex formation. RPA32 becomes hyperphosphorylated upon DNA damage induction or replicative stress, thereby inducing a conformational change which negatively affects the activity of RPA in replication [96, 97], suggesting that part of the pathway selection occurs via differential PTMs.

PCNA is perhaps the most multi-functional protein in DDR, as it is, besides normal DNA replication, involved in cell cycle arrest, chromatin assembly coupled to DNA synthesis, and various repair pathways including NER, BER, MMR, recombination-dependent daughter-strand gap repair and translesion synthesis [98-100]. PCNA assembles into a trimeric ring that encircles the DNA, after which the PCNA clamp can slide freely along the duplex (of naked DNA; what exactly happens in chromatin is not yet known). Its hydrophobic pocket is responsible for the competitive binding of various proteins, like DNA polymerase δ, the cell-cycle inhibitor p21, DNA ligase I and the endonucleases XPG and FEN1 (flap structure-specific endonuclease 1) associated with NER and BER (and replication), respectively [101]. Both RPA and PCNA seem to function by binding to specific affinity sites and serve as a loading platform for various DNA-transacting complexes. Pathway selection via PCNA also involves PTMs, mainly by differential ubiquitylation and SUMOylation (small-ubiquitin-related modifier (SUMO)). SUMO conjugation inhibits the role of PCNA in the recombination-dependent daughter-strand gap repair and suggests a function for the SUMO conjugation in normal DNA replication [102, 103]. Monoubiquitinated PCNA is active in TLS [104], while polyubiquitinated PCNA is functional in the recombination-dependent DSGR pathway [102].

Multiple engagement on chromatin: the signaling network

Dynamic structure of chromatin in genome surveillance

In eukaryotic cells, DNA is packaged into nucleosomes [105], resulting in a considerable barrier for all DNA-transacting proteins. Modification of this compact structure is therefore an important regulatory mechanism for processes such as replication, transcription and DDR. Chromatin remodeling occurs by two processes:

by active ATP-consuming remodeling complexes involving molecular machines of the SWI/SNF-superfamily of DNA-dependent ATPases and by PTMs of the core histones, such as acetylation, methylation, phosphorylation, and ubiquitylation [106]. Additionally, diverse histone variants exist, capable of providing selected chromatin regions with particular properties.

(i) γ-H2AX

The clearest example of a direct relationship between DNA damage response and histone modifications is the rapid phosphorylation of the histone isomer H2AX after DNA damage (by UV-light or ionizing radiation) or replicative stress by the checkpoint kinases ATM, ATR and DNA-PKcs [107-112]; reviewed in [113]). Phosphorylated H2AX (γ-H2AX) is observed shortly after DNA damage induction in ionizing irradiation-induced foci (IRIF) and may serve as a docking site for recruiting DSB repair and signalling factors to DNA breaks (reviewed in [114-116]). UV damage-induced γ-H2AX, on the other hand, is homogenously distributed throughout the nucleus, except when cells are in S-phase. Local UV-irradiation showed that γ-H2AX is restricted to UV-damage sites. H2AX phosphorylation upon UV in non-S-phase cells depends on the NER damage recognition factor XPC and the damage verifier XPA, and shows strikingly similar kinetics to NER of 6-4 photoproducts [109, 117]. Therefore, γ-H2AX might play a role in maintaining an active checkpoint during the period of UV lesion repair.

(ii) Other chromatin modifications

Phosphorylation of H1 regulates the activation of specific genes [118]. In response to DSBs, specific phosphorylation by DNA-PKcs reduces H1 affinity to DNA in the vicinity of lesions and hence enables NHEJ [119]. Phosphorylated H1 is released into the cytosol following ionizing irradiation, where the H1.2 isoform is even engaged in damage-induced apoptosis [120, 121].

Transcriptional activators, but also repair factors, recruit histone acetyl-transferases (HATs) like p300 to promoters [122-127]. Histone acetylation is an important step for subsequent chromatin remodeling and results in the transfer of histone H2A-H2B dimers from nucleosomes to histone chaperones like nucleosome assembly protein 1 (NAP1) [128] as well as H3-H4 tetramers to Anti-silencing function 1 protein (Asf1) [129]. The same histone chaperones are also responsible for deposition of histones onto newly replicated DNA [130]. Importantly, Asf1 is also essential for genetic stability during replication [131, 132]. Further, Asf1 cooperates

with chromatin assembly factor 1 (CAF-1) in nucleosome assembly coupled to NER [133], where CAF-1 also mediates the *de-novo* deposition of H3.1 [134]. These data exclude a mechanism in which chromatin restoration depends on simple recycling of preexisting nucleosomes, raising the question as of whether and how epigenetic information on DNA damage sites is preserved, or whether DNA damage could even be "remembered" by new epigenetic modifications at the repaired damage site.

Also histone methylation, involved in gene expression, may play a role in DNA damage responses, since the p53-binding protein 1 (53BP1), a checkpoint mediator in DNA damage signaling [135-138], specifically recognizes and binds histone H3 methylated at lysine 79. Although this modification is not induced upon DNA damage, it might be more accessible due to chromatin distortions induced by DNA lesions [139]. A similar mechanism seems to be employed in *S. pombe* [140], suggesting a generic relevance of this process.

Recently, also histone ubiquitylation in response to DNA damage was reported (reviewed in [141]). Both H3 and H4 ubiquitylation were observed in response to UV [142], as well as H2B in yeast [143] and H2A in mammals [144]. An early DDB2-dependent (DNA damage sensor in GG-NER) ubiquitylation of H3 and H4 appears to stimulate NER factor assembly [142]. A further NER-dependent H2A mono-ubiquitylation, which only occurs after dual incision, depends on the damage signaling kinase ATR and suggests a role in post repair signaling or epigenetic mark on previously damaged DNA [144].

Recent studies show that IR-induced ubiquitylation of H2A and H2AX by the RING-finger ubiquitylase RNF8 is necessary for the efficient assembly of repair factors to DSBs, as well as the subsequent establishment of G2/M checkpoint arrest [47, 48].

For recent reviews on histone modifications upon DNA damage induction, see [141, 145]

Nuclear Organization of DDR

An important question is how all the above-described multifunctional machines and common factors of DDR are assembled and organized within the complex environment of the mammalian cell nucleus. DNA damage leads to impediment of replication or transcription, and changes in chromatin. How does all this lead to an effective recruitment of factors for lesion repair, damage tolerance, cell cycle arrest, or apoptosis?

(1) Nuclear organization of DSB response

The seminal work of the Lukas laboratories, using a defined laser-assisted subnuclear DSB generating system, has provided insight into the spatio-temporal organization of DDR after DSB induction. This resulted in the dissection of DDR factors into subclasses with respect to the subcellular structures in which they reside after DNA damage [146].

(i) The major checkpoint mediators, such as Mdc1 (mediator of DNA damage checkpoint protein 1), 53BP, ATM and the MRN complex, co-localize with modified DSB-flanking, i.e. γ-H2AX-decorated, chromatin. These findings are in line with previous studies, showing that Mdc1 binds to γ-H2AX [147-149] and is required for Nbs1 recruitment to broken DNA. Nbs1 in turn, as part of the MRN complex involved in HR as well as NHEJ of DSB, further recruits ATM to broken DNA [110, 150]. Also 53BP1 has been shown previously to directly interact with posttranslationally modified histones [139]. γ-H2AX also mediates BRCA1 localization into DSB repair foci, possibly by the RNF8-mediated H2A and H2AX ubiquitylation that further recruits Rap80 which via ABRA1 recruits BRCA1 [43, 46-50]. Concordantly, all these proteins were shown to assemble directly at the DSB-flanking chromatin throughout the cell cycle.

(ii) Another group of DSB-activated proteins assembles in much smaller ssDNA microcompartments surrounded by γ-H2AX-modified chromatin, which are most likely formed by 5' resections at DSB, an important HR intermediate. These "microfoci" are only formed in S and G2-phase cells, and typically accumulate factors directly involved in HR repair, like Rad51, Rad52, BRCA1, and FANCD2 (Fanconi anemia complementation group D2). They also contain the ssDNA-activated checkpoint kinase ATR and proteins required for its recruitment to DSB, like ATR interacting protein (ATRIP) and RPA ([151-153]). ATR is known to be activated by different processes that produce ssDNA intermediates, e.g. NER of UV lesions, HR and replication stress. In living cells, ssDNA is immediately covered by RPA, which triggers ATR binding, promoted by its regulatory partner ATRIP [152, 154], and its subsequent activation ([155-157]). Full activation of ATR/ATRIP also requires the RPA-mediated binding of the DNA damage-specific PCNA-like Rad17/9-1-1 sliding clamp [155, 158]. (Rad 17 is an RFC-like component that is thought to load the 9-1-1 trimeric complex.) Concordantly, also Rad17/9-1-1 was found to accumulate in ssDNA microcompartments.

Of the in this study observed damage signalling components, only the MRN complex and BRCA1 have been shown to interact with both DSB-flanking chromatin

and ssDNA microcompartments. Noteworthy, interaction of Nbs1 or BRCA1 with the latter compartments is not dependent on γ-H2AX or Mdc1, while their recruitment to DSB-flanking chromatin is.

(iii) Several DSB repair factors, particularly those involved in NHEJ (DNA-PKcs, Ku70/80) could not be found to re-localize into microscopically discernible foci. It has therefore been hypothesized that these factors bind (transiently) to unprocessed and/or only partially processed DNA breaks forming microcompartments beyond the resolution of light microscopy. Very recently, however, using microirradiation procedures in live cells which create a high local density of DSBs, microscopically discernible accumulations could be induced [159, 160]. These accumulations likely reflect high local concentrations of repair factors on dense breaks rather than a strict structural organization as the HR and DSB signaling mediators.

(iv) Other factors implicated in DSB processing do not exhibit discernible relocalization, since these proteins are omnipresent on chromatin and simply get post-translationally modified at or near breaks, similarly to the phosphorylation of H2AX. One of them is Smc1 (Structural Maintenance of Chromosomes 1), a structural component of the cohesin complex required for sister chromatid cohesion during S-phase, which is also implicated in DSB repair. Smc1 is phosphorylated by ATM and ATR after exposure to a broad array of stimuli including IR, HU, and UV-light [161]. DSB induce phosphorylation on serine 957 (a key ATM target site) near DNA damage sites.

(v) Upon activation of the key sensor kinases, various targets are phosphorylated and a number of proteins recruited to damaged DNA. Many of the activated proteins remain at the site of damage, while others, like the effector kinases Chk1 and Chk2, are released to activate soluble targets [146, 148], such as p53 and Cdc25A [162]. Also these effectors, crucial for efficient DNA damage-induced gene expression (p53) and cell cycle arrest (Cdc25A, p53), do not accumulate at DNA damage sites.

In summary, these recent spatio-structural studies show that for efficient HR-dependent DSB repair, large assemblies of activities and significant chromatin structural rearrangements are required. Large depositions and chromatin modifications (histone phosphorylation and ubiquitylation) remain relatively long after genomic insult, suggesting that these epigenetic marks play a role in extended signalling, perhaps beyond repair time, to guarantee accurate and versatile DDR.

(2) Nuclear Organization of NER and signalling

Unlike DSB repair, NER factors do not exhibit relocalisation into microscopically discernible subnuclear structures upon DNA damage induction, making it difficult to unravel the structural organization of NER-dependent damage response. Therefore, in spite of detailed biochemical knowledge on the complex formation and proteins involved in the repair process itself, conflicting data on the role of NER in UV-induced damage signalling exist in the literature. A study on primary fibroblasts from NER-defective patients, however, clarified that checkpoint signalling in these cells, similarly to yeast [163], depends on NER in G_0/G_1 and G_2/M phases of the cell cycle. Very recently, it was shown that single strand gaps, which are more pronounced as NER intermediates in primary cells due to lower levels of replication factors in quiescent cells, trigger ATR-signalling and subsequent γ-H2AX [164]. Both recognition and processing of the DNA damage by the GG-NER machinery, but not TC-NER, are necessary to phosphorylate key ATR targets in response to UV [165]. In S-phase cells probably other structures, such as stalled replication forks or strand breaks, contribute to trigger the checkpoint cascade ([165]; see also references therein).

Real-time dynamics in the nucleus

Disclosure of genetic networks, detailed insight into the biochemical properties of crucial DDR factors and establishment of *in vitro* DDR-mimicking reactions have proven fundamental to the current understanding of these complex molecular transactions. The above described and discussed cellular studies further advanced comprehension. Utilization of cellular biological approaches additionally have the advantage that especially the crosstalk between different mechanisms can be studied within the most relevant context, i.e. the cell. Classically, these experiments, however, only were able to monitor subnuclear structures under static conditions and obviously miss possible dynamic transient interactions. The developments in imaging technology and genetically tagging factors with fluorescent proteins (such as the green fluorescent protein, GFP) have made it possible to not only visualize these proteins in living cells and to explore the organization of different cellular processes, but we can also study the interaction-kinetics of factors within these cellular events [166]. The usage of GFP-fused proteins in combination with time-lapse studies as well as quantitative fluorescence methods have revolutionized the field of molecular biology and have provided spectacular new insights into the regulation and organization of cellular processes. Of particular importance in the study of real-time protein dynamics are photobleaching techniques such as

fluorescence recovery after photobleaching (FRAP) and fluorescence loss in photobleaching (FLIP) (reviewed in [167-171].

(1) chromatin

Employing these techniques, various groups have shown that histones in the living cell are not statically bound to chromatin, but show diverse dynamic exchange rates depending on the type of histone and functional state of the chromatin ([172], see also references therein). Histone-DNA interactions are also altered in time in response to various stimuli like replication (reviewed in [173]), regulation of gene expression and cell cycle [174], and DNA damage response. GFP-tagged linker histones H1 have been found to be immobilized in the order of minutes on euchromatin as well as heterochromatin [175], suggesting that H1 is continuously exchanging between chromatin regions, independently of their global activation state. However, transcription-dependent hyperacetylation, as well as phosphorylation, reduce the residence time of the linker histone further, indicating that chromatin modification increases the exchange rate of H1 on chromatin [175-177]. The core histones H2A and H2B exhibit much longer residence times on chromatin, in the order of hours [172, 178]. A small fraction of H2B exchanges rapidly, i.e. in the order of minutes, in a transcription-dependent fashion, likely representing H2B in transcriptionally active chromatin [178]. Unlike H1 and H2B, the core histones H3 and H4 are assembled into chromatin after DNA replication where most of them remain bound until the next round of DNA duplication. On anaphase and telophase chromosomes, however, a significant fraction also of these core histones becomes mobile [174]. The above FRAP experiments on GFP-tagged histones show that although H2A, H2B, H3, and H4 are part of the same nucleosomal structure, their individual stability in chromatin is very different.

(2) transcription

Various groups have demonstrated that most of the components required for rRNA synthesis, as well as proteins involved in processing and ribosome assembly, are rapidly exchanged between the nucleoplasm and the nucleolus harbouring the RNAPI transcription factories [80, 179, 180]. These studies further indicate that most RNAPI factors, including subunits of the RNAPI complex, assemble separately onto an RNAPI promoter and dissociate when their requirement has ended. In contrast, ribosomal subunit proteins, such as S5 and L9, exchange at a much lower rate [179].

Nascent RNAPII transcripts can be seen distributed in a focal pattern throughout the nucleoplasm. These transcription foci seem to be very dynamic and

employ a similar 'on the spot assembly' of all required factors as described for RNAPI transcription. Distinct retention times for different factors indicate a step-wise assembly of the transcription complex [80, 181, 182]. Furthermore, RNAPII itself is engaged in the order of minutes in transcription initiation and elongation, while transcription initiation factors, as well as a series of transcriptional activators and coactivators [181, 183-186], employ a 'hit and run' mechanism and are only employed in transcription for seconds. A recent review summarizing the complex results of combined structure and dynamics studies on the transcription machinery can be found in [187].

(3) DNA repair

In situ studies revealed that HR proteins exhibit re-localization into distinct intranuclear foci upon IR, where they co-localize with components of the replication machinery. In contrast, no such redistribution of NER proteins is visible upon introduction of NER-specific DNA damage. In fact, NER factors that are shared in different nuclear processes, such as TFIIH, seem to redistribute from subnuclear accumulation sites (i.e. RNAPI transcription in nucleoli) into a diffuse nuclear distribution pattern typical for all NER proteins when they are recruited for DNA repair [80]. Based on this difference in subcellular distribution, a distinct strategy on dealing with different lesions can be envisaged.

Recent live-cell as well as *in vitro* studies have led to a better understanding of how DNA repair is organized and have thus shown that both HR and NER are far from being static processes. NER has been shown to be a sequential process, where all separate factors move distinctly throughout the nucleus and assemble individually and sequentially onto damaged DNA when required ([188-190]. GFP-based studies showed that the NER-specific 5'-endonuclease ERCC1/XPF [191], the damaged DNA binding protein DDB2 [192], the damage verification factor XPA [193], the 3' endonuclease XPG [192], and the multifunctional TFIIH complex [80] are not incorporated into large repair 'holo'-complexes, but rather diffuse autonomously (Zotter et al., in preparation) until they encounter an NER site where they are transiently immobilized. A recent study shows corresponding behaviour in this process also for the multi-task component PCNA [194]. Immobilization times of pre-incision NER factors were found to correlate with their participation in one single repair event at the time and subsequent release of the proteins [191]. This suggests that NER components form one stable assembly on the damaged DNA in a relatively short time and are released again after the repair process has been completed. Differences in assembly dynamics of NER factors have been reported [190, 192],

reflecting the sequence of association of distinct components with the repair complex as well as their individual release.

Though DSB repair via HR occurs in DNA repair foci, these too appear to be highly dynamic. Functional repair complexes were also assembled from the diffusing constituents after inducing DNA damage by IR [195]. Photobleaching experiments revealed that repair foci are dynamic structures of which only Rad51 is a relatively stably associated core component. In contrast, Rad52 and Rad54 only transiently interact with these structures, and each protein exhibits individual immobilization dynamics. GFP-Rad51 exists under unchallenged conditions in three distinct nucleoplasmic pools, a mobile part and two relatively immobile fractions resulting from either self-oligomerization or binding to BRCA2 [196]. Upon replication arrest a shift in equilibrium was seen from BRCA2-bound towards transiently mobile GFP-Rad51, indicating that BRCA2 might regulate Rad51 mobilization in response to DNA damage [197].

Similarly, the NHEJ factor Ku70/80, part of the DNA-PK (DNA-dependent protein kinase) complex [160], and DNA-PKcs itself [159] move freely throughout the nucleus of unchallenged cells. After DSB induction they become rapidly immobilized at DNA ends and continuously exchange with the soluble protein pool.

In conclusion, both DSB repair as well as NER exhibits "on-the-spot" assembly of smaller complexes instead of bulky pre-assembled holo-complexes that might have less efficient access to DNA damage sites. So, if the onset is similar, why is there such a difference in the organization of NER versus HR? One explanation could be that fewer DNA lesions are present with equal cytotoxic doses of agents that induce HR (e.g. IR) [198] as compared to NER-inducing lesions (e.g. UV) which are however more difficult to resolve. It has been suggested that the large protein accumulations near DSBs are simply to aid local increase in concentration of relevant enzymes to stimulate the complex and relatively slow repair of these lesions. The strikingly large and long-lasting assemblies are probably required to allow the problematic resolution of DSB repair by HR involving the search for homology, strand invasion, resolution of holiday junctions and subsequent separation of sister chromatids. Apparently in HR, accuracy is preferred over efficiency.

(4) replication

Replication factors accumulate in S-phase nuclei into "replication factories". Dynamics studies have shown that, within these structures, core replication factors are immobilized significantly longer than auxiliary proteins. For example, the main

coordinator of replication, PCNA, remains bound to S-phase foci in the order of several minutes [194, 199-201], while RPA34 [199, 201], DNA methyltransferase 1 (Dnmt1), DNA ligase1 and FEN1 are all individually released after only a few seconds [199, 202, 203]. Diverse specialized associated factors, such as the translesion polymerase eta, also show a very rapid turnover at replication sites ([202]; own unpublished data). Upon stalling of the replication machinery, e.g. due to the encounter of DNA lesions, immobilization times of a variety of replication factors change. PCNA as well as RPA34 are retained significantly longer in replication structures after treatment with diverse fork-stalling agents, but still exhibit a very different turnover from each other [194, 201]. Interestingly, the still relatively rapid exchange of RPA34 at DNA damage sites is at least partially promoted by DNA-PK-dependent phosphorylation, whereas PCNA needs to be mono-ubiquitylated to be at all able to stably associate with repair foci [194, 201]. Polymerase eta, which very similarly accumulates into S-phase foci in undamaged and damaged cells [104], shows prolonged retention in these structures upon the encounter of UV damage, but not after treatment of the cells with MMS ([202]; own unpublished data). FEN1, on the other hand, shows significantly enhanced binding after MMS treatment [202]. Together, the diverse immobilization times of the above mentioned factors at replication sites, distinctly changing with different challenges to the replication machinery, closely mirror the respective tasks of the single components. Moreover, the use of confocal bleaching techniques also revealed the impact of single PTMs on the dynamic functionality of specific factors.

Conclusions

All the above-described chromatin-associated processes are tightly regulated by posttranslational modifications, post-transcriptional control and gene expression. Rather than employing ready-to-go pre-assembled 'holo'-complexes, the cell utilizes smaller components, many of which are capable of performing diverse functions in different processes. Quick and efficient formation of specific complexes on activity sites (lesions, promoters, or origins) occurs by temporal assemblies of all required factors from a freely diffusing pool. Sequential assembly of factors provides a process with elbowroom to regulate in different steps and allows for intermediate abortion of a reaction or the possibility that an inactive factor is replaced by an active factor. It also provides the possibility to use multifunctional protein (complex)es [204, 205], such as PCNA, RPA, and TFIIH, which may allow the coordination of different processes. This gives the cell the flexibility to react adequately to stress conditions, like induction of DNA damage. In addition, these small components can gain more

efficient access to condensed chromatin than bulky 'holo'-complexes, permitting them to be omnipresent and to be always in the vicinity of affinity sites.

Distinct dynamics of engagement into diverse DNA-transacting processes for multi-task entities, such as TFIIH and CSB in transcription and NER [80, 84], and PCNA in replication, translesion synthesis and DNA repair [194], have been observed. The reaction-kinetics of factors involved in DNA-transacting processes suggests that they are engaged in these nuclear events on the basis of simple chemical principles. That is, they diffuse freely through the nucleus and upon collision with sites of activity (or factors with affinity) they are transiently assembled into a reaction complex. Thus, the movement of these factors in the nucleus critically depends on the availability and strength of affinity sites.

Future directions

To obtain a kinetic framework of DNA repair in living mammalian cells, the dynamic properties of NER factors under different conditions were used as input parameters in a simplified sequential mathematical NER reaction model resulting in an interesting insight into reaction kinetics [206]. Monte Carlo simulation appeared an efficient tool to comprehend complex protein dynamic profiles [80, 185]. Further improvements in the combination of *in vivo* and *in silico* experimentation will facilitate the understanding of the sometimes complex behaviour of proteins in living cells. Innovations within the imaging field have already provided highly sensitive microscopes with which previously unexpected resolutions can be obtained in living cells. More developments are expected which will only further broaden the experimental possibilities. In addition, advances in molecular biology, *in vitro* methodology, instrumental improvements, and the ever more emerging new classes of fluorescent probes and their multiple applications (comprehensively reviewed in [207]) are providing the scientific world with new, exciting possibilities to study processes in living cells and multicellular organisms. Since all of these methods have their advantages and drawbacks, the key to fully unravel the function of complex cellular machineries is to combine their beneficial properties. Future directions towards the understanding of genome surveillance processes will hence include the use of diverse means for the exploration of signalling via PTMs, as was found for PCNA and others. Chromatin immunoprecipitation and mass spectrometry will give us further insight into chromatin components and their modifications in response to genomic insults. Detailed spatial information of key components in the context of sub-nuclear structures could be added by the correlation of fluorescent light microscopy with electron microscopy, using a property of fluorophores called

"photoconversion" [208, 209]. Fluorescence resonance energy transfer (FRET), a potent method to study dynamic interactions between proteins or of protein with DNA [210-213], but also to visualize conformational changes within proteins (reviewed in [214-217]), has undergone considerable improvements. In addition, a variety of FRET-based sensors have been developed that can detect ions, cyclic nucleotides, metabolites, neurotransmitters, but also the balance between diverse enzyme activities in specific subcellular compartments [215-218]. FRET might therefore prove an invaluable tool in exploring a multitude of functions in genome surveillance. Other refined microscopic methods, such as fluorescence correlation spectroscopy (FCS), could be used to complement protein mobility data obtained by photobleaching methods, thereby facilitating the resolution of distinct mobility pools in the nucleus (Zotter et al., in preparation). Recently, a two-colour FCS system was developed to detect protein interactions *in vivo* (reviewed in [219, 220]). Together, a multidisciplinary approach of biochemical, cell biological and bioinformatical nature will bring us closer to fully grasp the complex organization of the DNA transacting network.

Obviously, the above summarized newly emerged cell biological approaches and advanced microscopic and spectroscopic techniques have contributed to a fascinating new or adapted insight into cellular processes. However, we have to be careful in directly extrapolating these results obtained in live cells to the real "actual" *in vivo* situation. Without exceptions, dynamic studies on GFP-tagged proteins have been performed on cultured cells and in most cases using immortalized rapidly dividing cells. Cultured cells are however under constant stress (e.g. atmospheric oxygen) and usually in highly replicative status. Moreover, physiological processes critically depend on the cellular context (neighbouring cells, extracellular matrix, etc.). The apparent next challenge is to study live cell protein dynamics on cells embedded within their natural context, i.e. the tissue of living organisms.

References

1.   Lindahl, T., *Instability and decay of the primary structure of DNA.* Nature, 1993. 362: p. 709-715.

2.   Mitchell, J.R., J.H. Hoeijmakers, and L.J. Niedernhofer, *Divide and conquer: nucleotide excision repair battles cancer and ageing.* Curr Opin Cell Biol, 2003. 15(2): p. 232-40.

3.   Essers, J., W. Vermeulen, and A.B. Houtsmuller, *DNA damage repair: anytime, anywhere?* Curr Opin Cell Biol, 2006. 18(3): p. 240-6.

4.   Hoeijmakers, J.H., *Genome maintenance mechanisms for preventing cancer.* Nature, 2001. 411(6835): p. 366-74.

5.   Weber, S., *Light-driven enzymatic catalysis of DNA repair: a review of recent biophysical studies on photolyase.* Biochim Biophys Acta, 2005. 1707(1): p. 1-23.

6.   Friedberg, E.C., G.C. Walker, and W. Siede, *DNA Repair and Mutagenesis.* 2006, Washington: ASM Press. 1118.

7.   de Laat, W.L., N.G. Jaspers, and J.H. Hoeijmakers, *Molecular mechanism of nucleotide excision repair.* Genes Dev., 1999. 13(7): p. 768-785.

8.   Batty, D.P. and R.D. Wood, *Damage recognition in nucleotide excision repair of DNA.* Gene, 2000. 241(2): p. 193-204.

9.   Gillet, L.C.J. and O.D. Scharer, *Molecular Mechanisms of Mammalian Global Genome Nucleotide Excision Repair.* Chem. Rev., 2006. 106(2): p. 253-276.

10.   Lu, A.L., et al., *Repair of oxidative DNA damage: mechanisms and functions.* Cell Biochem Biophys, 2001. 35(2): p. 141-70.

11.   Dizdaroglu, M., *Base-excision repair of oxidative DNA damage by DNA glycosylases.* Mutat Res, 2005. 591(1-2): p. 45-59.

12.   Caldecott, K.W., *Mammalian single-strand break repair: mechanisms and links with chromatin.* DNA Repair (Amst), 2007. 6(4): p. 443-53.

13.   van Gent, D.C., J.H. Hoeijmakers, and R. Kanaar, *Chromosomal stability and the DNA double-stranded break connection.* Nat Rev Genet, 2001. 2(3): p. 196-206.

14.   Cahill, D., B. Connor, and J.P. Carney, *Mechanisms of eukaryotic DNA double strand break repair.* Front Biosci, 2006. 11: p. 1958-76.

15.   Weterings, E. and D.C. van Gent, *The mechanism of non-homologous end-joining: a synopsis of synapsis.* DNA Repair (Amst), 2004. 3(11): p. 1425-35.

16.   Burma, S., B.P. Chen, and D.J. Chen, *Role of non-homologous end joining (NHEJ) in maintaining genomic integrity.* DNA Repair (Amst), 2006. 5(9-10): p. 1042-8.

17.   Wyman, C., D. Ristic, and R. Kanaar, *Homologous recombination-mediated double-strand break repair.* DNA Repair (Amst), 2004. 3(8-9): p. 827-33.

18.   Aquilina, G. and M. Bignami, *Mismatch repair in correction of replication errors and processing of DNA damage.* J Cell Physiol, 2001. 187(2): p. 145-54.

19.   Kunkel, T.A. and D.A. Erie, *DNA mismatch repair.* Annu Rev Biochem, 2005. 74: p. 681-710.

20.   Li, Z., et al., *Identification of a protein essential for a major pathway used by human cells to avoid UV- induced DNA damage.* Proc Natl Acad Sci U S A, 2002. 99(7): p. 4459-64.

21.   Scully, R., N. Puget, and K. Vlasakova, *DNA polymerase stalling, sister chromatid recombination and the BRCA genes.* Oncogene, 2000. 19(53): p. 6176-83.

22.   Lehmann, A.R., *Replication of damaged DNA by translesion synthesis in human cells.* FEBS Lett, 2005. 579(4): p. 873-6.

23.   Friedberg, E.C., W.J. Feaver, and V.L. Gerlach, *The many faces of DNA polymerases: strategies for mutagenesis and for mutational avoidance.* Proc Natl Acad Sci U S A, 2000. 97(11): p. 5681-3.

24.   Friedberg, E.C., A.R. Lehmann, and R.P. Fuchs, *Trading places: how do DNA polymerases switch during translesion DNA synthesis?* Mol Cell, 2005. 18(5): p. 499-505.

25.   Lehmann, A.R., *Translesion synthesis in mammalian cells.* Exp Cell Res, 2006. 312(14): p. 2673-6.

26. Lehmann, A.R., et al., *Translesion synthesis: Y-family polymerases and the polymerase switch.* DNA Repair (Amst), 2007. 6(7): p. 891-9.

27. Masutani, C., et al., *Xeroderma pigmentosum variant (XP-V) correcting protein from HeLa cells has a thymine dimer bypass DNA polymerase activity.* Embo J, 1999. 18(12): p. 3491-501.

28. Masutani, C., et al., *Mechanisms of accurate translesion synthesis by human DNA polymerase eta.* Embo J, 2000. 19(12): p. 3100-9.

29. Jarosz, D.F., V.G. Godoy, and G.C. Walker, *Proficient and accurate bypass of persistent DNA lesions by DinB DNA polymerases.* Cell Cycle, 2007. 6(7): p. 817-22.

30. Lopes, M., M. Foiani, and J.M. Sogo, *Multiple mechanisms control chromosome integrity after replication fork uncoupling and restart at irreparable UV lesions.* Mol Cell, 2006. 21(1): p. 15-27.

31. Mellon, I., et al., *Preferential DNA repair of an active gene in human cells.* Proc Natl Acad Sci U S A, 1986. 83(23): p. 8878-8882.

32. Svejstrup, J.Q., *Transcription repair coupling factor: a very pushy enzyme.* Mol Cell, 2002. 9(6): p. 1151-2.

33. Doetsch, P.W., *Translesion synthesis by RNA polymerases: occurrence and biological implications for transcriptional mutagenesis.* Mutat Res, 2002. 510(1-2): p. 131-40.

34. Bregeon, D., et al., *Transcriptional mutagenesis induced by uracil and 8-oxoguanine in Escherichia coli.* Mol Cell, 2003. 12(4): p. 959-70.

35. Charlet-Berguerand, N., et al., *RNA polymerase II bypass of oxidative DNA damage is regulated by transcription elongation factors.* Embo J, 2006. 25(23): p. 5481-91.

36. Zhou, B.B. and S.J. Elledge, *The DNA damage response: putting checkpoints in perspective.* Nature, 2000. 408(6811): p. 433-9.

37. Bernstein, C., et al., *DNA repair/pro-apoptotic dual-role proteins in five major DNA repair pathways: fail-safe protection against carcinogenesis.* Mutat Res, 2002. 511(2): p. 145-78.

38. Falck, J., et al., *The DNA damage-dependent intra-S phase checkpoint is regulated by parallel pathways.* Nat Genet, 2002. 30(3): p. 290-4.

39. Tibbetts, R.S., et al., *Functional interactions between BRCA1 and the checkpoint kinase ATR during genotoxic stress.* Genes Dev, 2000. 14(23): p. 2989-3002.

40. Chen, Y. and Y. Sanchez, *Chk1 in the DNA damage response: conserved roles from yeasts to mammals.* DNA Repair (Amst), 2004. 3(8-9): p. 1025-32.

41. Burma, S. and D.J. Chen, *Role of DNA-PK in the cellular response to DNA double-strand breaks.* DNA Repair (Amst), 2004. 3(8-9): p. 909-18.

42. Yang, J., et al., *ATM, ATR and DNA-PK: initiators of the cellular genotoxic stress responses.* Carcinogenesis, 2003. 24(10): p. 1571-80.

43. Wang, B., et al., *Abraxas and RAP80 Form a BRCA1 Protein Complex Required for the DNA Damage Response.* Science %R 10.1126/science.1139476, 2007. 316(5828): p. 1194-1198.

44. Bergink, S., N.G. Jaspers, and W. Vermeulen, *Regulation of UV-induced DNA damage response by ubiquitylation.* DNA Repair (Amst), 2007. 6(9): p. 1231-42.

45. Huang, T.T. and A.D. D'Andrea, *Regulation of DNA repair by ubiquitylation.* Nat Rev Mol Cell Biol, 2006. 7(5): p. 323-34.

46. Kolas, N.K., et al., *Orchestration of the DNA-Damage Response by the RNF8 Ubiquitin Ligase.* Science, 2007.

47. Mailand, N., et al., *RNF8 Ubiquitylates Histones at DNA Double-Strand Breaks and Promotes Assembly of Repair Proteins.* Cell, 2007. 131(5): p. 887-900.

48. Huen, M.S., et al., *RNF8 Transduces the DNA-Damage Signal via Histone Ubiquitylation and Checkpoint Protein Assembly.* Cell, 2007. 131(5): p. 901-14.

49. Sobhian, B., et al., *RAP80 Targets BRCA1 to Specific Ubiquitin Structures at DNA Damage Sites.* Science %R 10.1126/science.1139516, 2007. 316(5828): p. 1198-1202.

50. Kim, H., J. Chen, and X. Yu, *Ubiquitin-Binding Protein RAP80 Mediates BRCA1-Dependent DNA Damage Response.* Science %R 10.1126/science.1139621, 2007. 316(5828): p. 1202-1205.

51.   Anindya, R., O. Aygun, and J.Q. Svejstrup, *Damage-induced ubiquitylation of human RNA polymerase II by the ubiquitin ligase Nedd4, but not cockayne syndrome proteins or BRCA1.* Mol Cell, 2007. 28(3): p. 386-97.

52.   Boulton, S.J., *BRCA1-mediated ubiquitylation.* Cell Cycle, 2006. 5(14): p. 1481-6.

53.   Westerveld, A., et al., *Molecular cloning of a human DNA repair gene.* Nature, 1984. 310(5976): p. 425-9.

54.   Mu, D., et al., *Reconstitution of human DNA repair excision nuclease in a highly defined system.* J. Biol. Chem., 1995. 270(6): p. 2415-8.

55.   Sijbers, A.M., et al., *Xeroderma pigmentosum group F caused by a defect in a structure-specific DNA repair endonuclease.* Cell, 1996. 86(5): p. 811-822.

56.   Bessho, T., et al., *Reconstitution of human excision nuclease with recombinant XPF-ERCC1 complex.* J Biol Chem, 1997. 272(6): p. 3833-7.

57.   Adair, G.M., et al., *Role of ERCC1 in removal of long non-homologous tails during targeted homologous recombination.* Embo J, 2000. 19(20): p. 5552-61.

58.   Schiestl, R.H. and S. Prakash, *RAD1, an excision repair gene of Saccharomyces cerevisiae, is also involved in recombination.* Mol. Cell. Biol., 1988. 8(9): p. 3619-3626.

59.   Schiestl, R.H. and S. Prakash, *RAD10, an excision repair gene of Saccharomyces cerevisiae, is involved in the RAD1 pathway of mitotic recombination.* Mol. Cell. Biol., 1990. 10(6): p. 2485-2491.

60.   Niedernhofer, L.J., et al., *The structure-specific endonuclease Ercc1-Xpf is required for targeted gene replacement in embryonic stem cells.* Embo J, 2001. 20(22): p. 6540-9.

61.   Sargent, R.G., et al., *Role of the nucleotide excision repair gene ERCC1 in formation of recombination-dependent rearrangements in mammalian cells.* Nucleic Acids Res, 2000. 28(19): p. 3771-8.

62.   De Silva, I.U., et al., *Defining the roles of nucleotide excision repair and recombination in the repair of DNA interstrand cross-links in mammalian cells.* Mol Cell Biol, 2000. 20(21): p. 7980-90.

63.   Niedernhofer, L.J., et al., *The structure-specific endonuclease Ercc1-Xpf is required to resolve DNA interstrand cross-link-induced double-strand breaks.* Mol Cell Biol, 2004. 24(13): p. 5776-87.

64.   Dronkert, M.L. and R. Kanaar, *Repair of DNA interstrand cross-links.* Mutat Res, 2001. 486(4): p. 217-47.

65.   Zhu, X.D., et al., *ERCC1/XPF removes the 3' overhang from uncapped telomeres and represses formation of telomeric DNA-containing double minute chromosomes.* Mol Cell, 2003. 12(6): p. 1489-98.

66.   Saparbaev, M., L. Prakash, and S. Prakash, *Requirement of mismatch repair genes MSH2 and MSH3 in the RAD1-RAD10 pathway of mitotic recombination in Saccharomyces cerevisiae.* Genetics, 1996. 142(3): p. 727-36.

67.   Prado, F., et al., *Mitotic recombination in Saccharomyces cerevisiae.* Curr Genet, 2003. 42(4): p. 185-98.

68.   Sugasawa, K., *UV-induced ubiquitylation of XPC complex, the UV-DDB-ubiquitin ligase complex, and DNA repair.* J Mol Histol, 2006. 37(5-7): p. 189-202.

69.   Miao, F., et al., *3-Methyladenine-DNA glycosylase (MPG protein) interacts with human RAD23 proteins.* J Biol Chem, 2000. 275(37): p. 28433-8.

70.   Shimizu, Y., et al., *Xeroderma pigmentosum group C protein interacts physically and functionally with thymine DNA glycosylase.* Embo J, 2003. 22(1): p. 164-73.

71.   D'Errico, M., et al., *New functions of XPC in the protection of human skin cells from oxidative damage.* Embo J, 2006. 25(18): p. 4305-15.

72.   Paull, T.T., et al., *Direct DNA binding by Brca1.* Proc Natl Acad Sci U S A, 2001. 98(11): p. 6086-91.

73.   Bau, D.T., et al., *Breast cancer risk and the DNA double-strand break end-joining capacity of nonhomologous end-joining genes are affected by BRCA1.* Cancer Res, 2004. 64(14): p. 5013-9.

74.   Connelly, J.C. and D.R. Leach, *Tethering on the brink: the evolutionarily conserved Mre11-Rad50 complex.* Trends Biochem Sci, 2002. 27(8): p. 410-8.

75.   Bohr, V.A., et al., *DNA repair in an active gene: removal of pyrimidine dimers from the DHFR gene of CHO cells is much more efficient than in the genome overall.* Cell, 1985. 40(2): p. 359-369.

76.   Mellon, I., G. Spivak, and P.C. Hanawalt, *Selective removal of transcription-blocking DNA damage from the transcribed strand of the mammalian DHFR gene.* Cell, 1987. 51(2): p. 241-249.

77.   Schaeffer, L., et al., *DNA repair helicase: a component of BTF2 (TFIIH) basic transcription factor.* Science, 1993. 260: p. 58-63.

78.   Drapkin, R., et al., *Dual role of TFIIH in DNA excision repair and in transcription by RNA polymerase II.* Nature, 1994. 368: p. 769-772.

79.   Egly, J.M., *The 14th Datta Lecture. TFIIH: from transcription to clinic.* FEBS Lett, 2001. 498(2-3): p. 124-8.

80.   Hoogstraten, D., et al., *Rapid Switching of TFIIH between RNA Polymerase I and II Transcription and DNA Repair In Vivo.* Mol Cell, 2002. 10(5): p. 1163-74.

81.   Sarker, A.H., et al., *Recognition of RNA polymerase II and transcription bubbles by XPG, CSB, and TFIIH: insights for transcription-coupled repair and Cockayne Syndrome.* Mol Cell, 2005. 20(2): p. 187-98.

82.   van Gool, A.J., et al., *The Cockayne syndrome B protein, involved in transcription-coupled DNA repair, resides in a RNA polymerase II containing complex.* EMBO J., 1997. 16(19): p. 5955-5965.

83.   Citterio, E., et al., *ATP-Dependent Chromatin Remodeling by the Cockayne Syndrome B DNA Repair-Transcription-Coupling Factor.* Mol Cell Biol, 2000. 20(20): p. 7643-7653.

84.   van den Boom, V., et al., *DNA damage stabilizes interaction of CSB with the transcription elongation machinery.* J Cell Biol, 2004. 166(1): p. 27-36.

85.   Deng, C.X., *BRCA1: cell cycle checkpoint, genetic instability, DNA damage response and cancer evolution.* Nucleic Acids Res, 2006. 34(5): p. 1416-26.

86.   Zhang, J. and S.N. Powell, *The role of the BRCA1 tumor suppressor in DNA double-strand break repair.* Mol Cancer Res, 2005. 3(10): p. 531-9.

87.   Gudmundsdottir, K. and A. Ashworth, *The roles of BRCA1 and BRCA2 and associated proteins in the maintenance of genomic stability.* Oncogene, 2006. 25(43): p. 5864-74.

88.   Mullan, P.B., J.E. Quinn, and D.P. Harkin, *The role of BRCA1 in transcriptional regulation and cell cycle control.* Oncogene, 2006. 25(43): p. 5854-63.

89.   Aquilina, G. and M. Bignami, *Mismatch repair in correction of replication errors and processing of DNA damage.* J Cell Physiol, 2001. 187(2): p. 145-54.

90.   MacNeill, S.A., *DNA replication: partners in the Okazaki two-step.* Curr Biol, 2001. 11(20): p. R842-4.

91.   Park, M.S., et al., *Physical interaction between human RAD52 and RPA is required for homologous recombination in mammalian cells.* J Biol Chem, 1996. 271(31): p. 18996-9000.

92.   Coverley, D., et al., *Requirement for the replication protein SSB in human DNA excision repair.* Nature, 1991. 349(6309): p. 538-541.

93.   DeMott, M.S., S. Zigman, and R.A. Bambara, *Replication protein A stimulates long patch DNA base excision repair.* J Biol Chem, 1998. 273(42): p. 27492-8.

94.   Fanning, E., V. Klimovich, and A.R. Nager, *A dynamic model for replication protein A (RPA) function in DNA processing pathways.* Nucleic Acids Res, 2006. 34(15): p. 4126-37.

95.   Mer, G., et al., *Structural basis for the recognition of DNA repair proteins UNG2, XPA, and RAD52 by replication factor RPA.* Cell, 2000. 103(3): p. 449-56.

96.   Binz, S.K., A.M. Sheehan, and M.S. Wold, *Replication protein A phosphorylation and the cellular response to DNA damage.* DNA Repair (Amst), 2004. 3(8-9): p. 1015-24.

97.   Zou, Y., et al., *Functions of human replication protein A (RPA): from DNA replication to DNA damage and stress responses.* J Cell Physiol, 2006. 208(2): p. 267-73.

98.   Tsurimoto, T., *PCNA binding proteins.* Front Biosci, 1999. 4: p. D849-58.

99.   Warbrick, E., *The puzzle of PCNA's many partners.* Bioessays, 2000. 22(11): p. 997-1006.

100.   Moldovan, G.L., B. Pfander, and S. Jentsch, *PCNA, the maestro of the replication fork.* Cell, 2007. 129(4): p. 665-79.
101.   Warbrick, E., *PCNA binding through a conserved motif.* Bioessays, 1998. 20(3): p. 195-9.
102.   Hoege, C., et al., *RAD6-dependent DNA repair is linked to modification of PCNA by ubiquitin and SUMO.* Nature, 2002. 419(6903): p. 135-41.
103.   Watts, F.Z., *Sumoylation of PCNA: Wrestling with recombination at stalled replication forks.* DNA Repair (Amst), 2006. 5(3): p. 399-403.
104.   Kannouche, P.L., J. Wing, and A.R. Lehmann, *Interaction of human DNA polymerase eta with monoubiquitinated PCNA: a possible mechanism for the polymerase switch in response to DNA damage.* Mol Cell, 2004. 14(4): p. 491-500.
105.   Luger, K., et al., *Crystal structure of the nucleosome core particle at 2.8 A resolution.* Nature, 1997. 389(6648): p. 251-60.
106.   He, H. and N. Lehming, *Global effects of histone modifications.* Brief Funct Genomic Proteomic, 2003. 2(3): p. 234-43.
107.   Burma, S., et al., *ATM phosphorylates histone H2AX in response to DNA double-strand breaks.* J Biol Chem, 2001. 276(45): p. 42462-7.
108.   Ward, I.M. and J. Chen, *Histone H2AX is phosphorylated in an ATR-dependent manner in response to replicational stress.* J Biol Chem, 2001. 276(51): p. 47759-62.
109.   O'Driscoll, M., et al., *A splicing mutation affecting expression of ataxia-telangiectasia and Rad3-related protein (ATR) results in Seckel syndrome.* Nat Genet, 2003. 33(4): p. 497-501.
110.   Falck, J., J. Coates, and S.P. Jackson, *Conserved modes of recruitment of ATM, ATR and DNA-PKcs to sites of DNA damage.* Nature, 2005. 434(7033): p. 605-11.
111.   Friesner, J.D., et al., *Ionizing radiation-dependent gamma-H2AX focus formation requires ataxia telangiectasia mutated and ataxia telangiectasia mutated and Rad3-related.* Mol Biol Cell, 2005. 16(5): p. 2566-76.
112.   Rogakou, E.P., et al., *DNA double-stranded breaks induce histone H2AX phosphorylation on serine 139.* J Biol Chem, 1998. 273(10): p. 5858-68.
113.   Thiriet, C. and J.J. Hayes, *Chromatin in need of a fix: phosphorylation of H2AX connects chromatin to DNA repair.* Mol Cell, 2005. 18(6): p. 617-22.
114.   Franco, S., et al., *H2AX prevents DNA breaks from progressing to chromosome breaks and translocations.* Mol Cell, 2006. 21(2): p. 201-14.
115.   Bassing, C.H. and F.W. Alt, *H2AX may function as an anchor to hold broken chromosomal DNA ends in close proximity.* Cell Cycle, 2004. 3(2): p. 149-53.
116.   Peterson, C.L. and J. Cote, *Cellular machineries for chromosomal DNA repair.* Genes Dev, 2004. 18(6): p. 602-16.
117.   Marti, T.M., et al., *H2AX phosphorylation within the G1 phase after UV irradiation depends on nucleotide excision repair and not DNA double-strand breaks.* PNAS, 2006. 103(26): p. 9891-9896.
118.   Dou, Y., et al., *Phosphorylation of linker histone H1 regulates gene expression in vivo by mimicking H1 removal.* Mol Cell, 1999. 4(4): p. 641-7.
119.   Kysela, B., M. Chovanec, and P.A. Jeggo, *Phosphorylation of linker histones by DNA-dependent protein kinase is required for DNA ligase IV-dependent ligation in the presence of histone H1.* Proc Natl Acad Sci U S A, 2005. 102(6): p. 1877-82.
120.   Konishi, A., et al., *Involvement of histone H1.2 in apoptosis induced by DNA double-strand breaks.* Cell, 2003. 114(6): p. 673-88.
121.   Bree, R.T., et al., *The switch from survival responses to apoptosis after chromosomal breaks.* DNA Repair (Amst), 2004. 3(8-9): p. 989-95.
122.   Shikama, N., J. Lyon, and N.B. La Thangue, *The p300/CBP family: integrating signals with transcription factors and chromatin.* Trends in Cell Biology, 1997. 7(6): p. 230-236.
123.   Roth, S.Y., J.M. Denu, and C.D. Allis, *Histone acetyltransferases.* Annu Rev Biochem, 2001. 70: p. 81-120.
124.   Black, J.C., et al., *A Mechanism for Coordinating Chromatin Modification and Preinitiation Complex Assembly.* Molecular Cell, 2006. 23(6): p. 809-818.

125.   Rapic-Otrin, V., et al., *Sequential binding of UV DNA damage binding factor and degradation of the p48 subunit as early events after UV irradiation.* Nucleic Acids Res, 2002. 30(11): p. 2588-98.

126.   Hasan, S., et al., *Transcription coactivator p300 binds PCNA and may have a role in DNA repair synthesis.* Nature, 2001. 410(6826): p. 387-91.

127.   Fousteri, M., et al., *Cockayne syndrome A and B proteins differentially regulate recruitment of chromatin remodeling and repair factors to stalled RNA polymerase II in vivo.* Mol Cell, 2006. 23(4): p. 471-82.

128.   Ito, T., et al., *p300-mediated acetylation facilitates the transfer of histone H2A-H2B dimers from nucleosomes to a histone chaperone.* Genes Dev, 2000. 14(15): p. 1899-907.

129.   Lorch, Y., B. Maier-Davis, and R.D. Kornberg, *Chromatin remodeling by nucleosome disassembly in vitro.* PNAS, 2006. 103(9): p. 3090-3093.

130.   Tyler, J.K., et al., *The RCAF complex mediates chromatin assembly during DNA replication and repair.* Nature, 1999. 402(6761): p. 555-560.

131.   Prado, F., F. Cortes-Ledesma, and A. Aguilera, *The absence of the yeast chromatin assembly factor Asf1 increases genomic instability and sister chromatid exchange.* EMBO Rep, 2004. 5(5): p. 497-502.

132.   Groth, A., et al., *Human Asf1 regulates the flow of S phase histones during replicational stress.* Mol Cell, 2005. 17(2): p. 301-11.

133.   Mello, J.A., et al., *Human Asf1 and CAF-1 interact and synergize in a repair-coupled nucleosome assembly pathway.* EMBO Rep, 2002. 3(4): p. 329-34.

134.   Polo, S.E., D. Roche, and G. Almouzni, *New histone incorporation marks sites of UV repair in human cells.* Cell, 2006. 127(3): p. 481-93.

135.   Wang, H. and S.J. Elledge, *Genetic and physical interactions between DPB11 and DDC1 in the yeast DNA damage response pathway.* Genetics, 2002. 160(4): p. 1295-304.

136.   DiTullio, R.A., Jr., et al., *53BP1 functions in an ATM-dependent checkpoint pathway that is constitutively activated in human cancer.* Nat Cell Biol, 2002. 4(12): p. 998-1002.

137.   Fernandez-Capetillo, O., et al., *DNA damage-induced G2-M checkpoint activation by histone H2AX and 53BP1.* Nat Cell Biol, 2002. 4(12): p. 993-7.

138.   Ward, I.M., et al., *p53 Binding protein 53BP1 is required for DNA damage responses and tumor suppression in mice.* Mol Cell Biol, 2003. 23(7): p. 2556-63.

139.   Huyen, Y., et al., *Methylated lysine 79 of histone H3 targets 53BP1 to DNA double-strand breaks.* Nature, 2004. 432(7015): p. 406-11.

140.   Sanders, S.L., et al., *Methylation of histone H4 lysine 20 controls recruitment of Crb2 to sites of DNA damage.* Cell, 2004. 119(5): p. 603-14.

141.   Dai, Q. and H. Wang, *"Cullin 4 makes its mark on chromatin".* Cell Div, 2006. 1: p. 14.

142.   Wang, H., et al., *Histone H3 and H4 ubiquitylation by the CUL4-DDB-ROC1 ubiquitin ligase facilitates cellular response to DNA damage.* Mol Cell, 2006. 22(3): p. 383-94.

143.   Giannattasio, M., et al., *The DNA damage checkpoint response requires histone H2B ubiquitination by Rad6-Bre1 and H3 methylation by Dot1.* J Biol Chem, 2005. 280(11): p. 9879-86.

144.   Bergink, S., et al., *DNA damage triggers nucleotide excision repair-dependent monoubiquitylation of histone H2A.* Genes Dev, 2006. 20(10): p. 1343-52.

145.   Groth, A., et al., *Chromatin challenges during DNA replication and repair.* Cell, 2007. 128(4): p. 721-33.

146.   Bekker-Jensen, S., et al., *Spatial organization of the mammalian genome surveillance machinery in response to DNA strand breaks.* J Cell Biol, 2006. 173(2): p. 195-206.

147.   Stewart, G.S., et al., *MDC1 is a mediator of the mammalian DNA damage checkpoint.* Nature, 2003. 421(6926): p. 961-6.

148.   Lukas, C., et al., *Distinct spatiotemporal dynamics of mammalian checkpoint regulators induced by DNA damage.* Nat Cell Biol, 2003. 5(3): p. 255-60.

149.   Stucki, M., et al., *MDC1 directly binds phosphorylated histone H2AX to regulate cellular responses to DNA double-strand breaks.* Cell, 2005. 123(7): p. 1213-26.

150. You, Z., et al., *ATM activation and its recruitment to damaged DNA require binding to the C terminus of Nbs1.* Mol Cell Biol, 2005. 25(13): p. 5363-79.

151. Cortez, D., et al., *ATR and ATRIP: partners in checkpoint signaling.* Science, 2001. 294(5547): p. 1713-6.

152. Ball, H.L., J.S. Myers, and D. Cortez, *ATRIP binding to replication protein A-single-stranded DNA promotes ATR-ATRIP localization but is dispensable for Chk1 phosphorylation.* Mol Biol Cell, 2005. 16(5): p. 2372-81.

153. Kumagai, A., S.M. Kim, and W.G. Dunphy, *Claspin and the activated form of ATR-ATRIP collaborate in the activation of Chk1.* J Biol Chem, 2004. 279(48): p. 49599-608.

154. Ball, H.L. and D. Cortez, *ATRIP oligomerization is required for ATR-dependent checkpoint signaling.* J Biol Chem, 2005. 280(36): p. 31390-6.

155. Zou, L., D. Liu, and S.J. Elledge, *Replication protein A-mediated recruitment and activation of Rad17 complexes.* Proc Natl Acad Sci U S A, 2003. 100(24): p. 13827-32.

156. Cortez, D., *Unwind and slow down: checkpoint activation by helicase and polymerase uncoupling.* Genes Dev, 2005. 19(9): p. 1007-12.

157. Kim, S.M., et al., *Phosphorylation of Chk1 by ATM- and Rad3-related (ATR) in Xenopus egg extracts requires binding of ATRIP to ATR but not the stable DNA-binding or coiled-coil domains of ATRIP.* J Biol Chem, 2005. 280(46): p. 38355-64.

158. Zou, L., D. Cortez, and S.J. Elledge, *Regulation of ATR substrate selection by Rad17-dependent loading of Rad9 complexes onto chromatin.* Genes Dev, 2002. 16(2): p. 198-208.

159. Uematsu, N., et al., *Autophosphorylation of DNA-PKCS regulates its dynamics at DNA double-strand breaks.* J Cell Biol, 2007. 177(2): p. 219-29.

160. Mari, P.O., et al., *Dynamic assembly of end-joining complexes requires interaction between Ku70/80 and XRCC4.* Proc Natl Acad Sci U S A, 2006. 103(49): p. 18597-602.

161. Kim, J.S., et al., *Specific recruitment of human cohesin to laser-induced DNA damage.* J Biol Chem, 2002. 277(47): p. 45149-53.

162. Kastan, M.B. and J. Bartek, *Cell-cycle checkpoints and cancer.* Nature, 2004. 432(7015): p. 316-23.

163. Giannattasio, M., et al., *Physical and functional interactions between nucleotide excision repair and DNA damage checkpoint.* Embo J, 2004. 23(2): p. 429-38.

164. Matsumoto, M., et al., *Perturbed gap-filling synthesis in nucleotide excision repair causes histone H2AX phosphorylation in human quiescent cells.* J Cell Sci, 2007. 120(Pt 6): p. 1104-12.

165. Marini, F., et al., *DNA nucleotide excision repair-dependent signaling to checkpoint activation.* Proc Natl Acad Sci U S A, 2006. 103(46): p. 17325-30.

166. Tsien, R.Y. and A. Miyawaki, *Seeing the machinery of live cells.* Science, 1998. 280(5371): p. 1954-5.

167. White, J. and E. Stelzer, *Photobleaching GFP reveals protein dynamics inside live cells.* Trends Cell Biol., 1999. 9(2): p. 61-65.

168. Houtsmuller, A.B. and W. Vermeulen, *Macromolecular dynamics in living cell nuclei revealed by fluorescence redistribution after photobleaching.* Histochem Cell Biol, 2001. 115(1): p. 13-21.

169. Phair, R.D. and T. Misteli, *Kinetic modelling approaches to in vivo imaging.* Nat Rev Mol Cell Biol, 2001. 2(12): p. 898-907.

170. Lippincott-Schwartz, J., E. Snapp, and A. Kenworthy, *Studying protein dynamics in living cells.* Nat Rev Mol Cell Biol, 2001. 2(6): p. 444-56.

171. Lippincott-Schwartz, J., N. Altan-Bonnet, and G.H. Patterson, *Photobleaching and photoactivation: following protein dynamics in living cells.* Nat Cell Biol, 2003. Suppl: p. S7-14.

172. Kimura, H., *Histone dynamics in living cells revealed by photobleaching.* DNA Repair (Amst), 2005. 4(8): p. 939-50.

173. Falbo, K.B. and X. Shen, *Chromatin remodeling in DNA replication.* J Cell Biochem, 2006. 97(4): p. 684-9.

174. Chen, D., et al., *Condensed mitotic chromatin is accessible to transcription factors and chromatin structural proteins.* J Cell Biol, 2005. 168(1): p. 41-54.

175. Misteli, T., et al., *Dynamic binding of histone H1 to chromatin in living cells.* Nature, 2000. 408(6814): p. 877-81.
176. Dou, Y., et al., *Phosphorylation and an ATP-dependent process increase the dynamic exchange of H1 in chromatin.* J Cell Biol, 2002. 158(7): p. 1161-70.
177. Contreras, A., et al., *The dynamic mobility of histone H1 is regulated by cyclin/CDK phosphorylation.* Mol Cell Biol, 2003. 23(23): p. 8626-36.
178. Kimura, H. and P.R. Cook, *Kinetics of core histones in living human cells: little exchange of H3 and H4 and some rapid exchange of H2B.* J Cell Biol, 2001. 153(7): p. 1341-53.
179. Chen, D. and S. Huang, *Nucleolar components involved in ribosome biogenesis cycle between the nucleolus and nucleoplasm in interphase cells.* J Cell Biol, 2001. 153(1): p. 169-76.
180. Dundr, M., et al., *A kinetic framework for a mammalian RNA polymerase in vivo.* Science, 2002. 298(5598): p. 1623-6.
181. Chen, D., et al., *TBP dynamics in living human cells: constitutive association of TBP with mitotic chromosomes.* Mol Biol Cell, 2002. 13(1): p. 276-84.
182. Kimura, H., K. Sugaya, and P.R. Cook, *The transcription cycle of RNA polymerase II in living cells.* J Cell Biol, 2002. 159(5): p. 777-82.
183. McNally, J.G., et al., *The glucocorticoid receptor: rapid exchange with regulatory sites in living cells.* Science, 2000. 287(5456): p. 1262-5.
184. Becker, M., et al., *Dynamic behavior of transcription factors on a natural promoter in living cells.* EMBO Rep, 2002. 3(12): p. 1188-94.
185. Farla, P., et al., *The androgen receptor ligand-binding domain stabilizes DNA binding in living cells.* J Struct Biol, 2004. 147(1): p. 50-61.
186. Rayasam, G.V., et al., *Ligand-specific dynamics of the progesterone receptor in living cells and during chromatin remodeling in vitro.* Mol Cell Biol, 2005. 25(6): p. 2406-18.
187. Jackson, D.A., *The amazing complexity of transcription factories.* Brief Funct Genomic Proteomic, 2005. 4(2): p. 143-57.
188. Volker, M., et al., *Sequential Assembly of the Nucleotide Excision Repair Factors In Vivo.* Molecular Cell, 2001. 8(1): p. 213-224.
189. Riedl, T., F. Hanaoka, and J.M. Egly, *The comings and goings of nucleotide excision repair factors on damaged DNA.* Embo J, 2003. 22(19): p. 5293-5303.
190. Mone, M.J., et al., *In vivo dynamics of chromatin-associated complex formation in mammalian nucleotide excision repair.* Proc Natl Acad Sci U S A, 2004. 101(45): p. 15933-7.
191. Houtsmuller, A.B., et al., *Action of DNA repair endonuclease ERCC1/XPF in living cells.* Science, 1999. 284(5416): p. 958-961.
192. Zotter, A., et al., *Recruitment of the nucleotide excision repair endonuclease XPG to sites of UV-induced dna damage depends on functional TFIIH.* Mol Cell Biol, 2006. 26(23): p. 8868-79.
193. Rademakers, S., et al., *Xeroderma pigmentosum group A protein loads as a separate factor onto DNA lesions.* Mol Cell Biol, 2003. 23(16): p. 5755-67.
194. Essers, J., et al., *Nuclear dynamics of PCNA in DNA replication and repair.* Mol Cell Biol, 2005. 25(21): p. 9350-9.
195. Essers, J., et al., *Nuclear dynamics of RAD52 group homologous recombination proteins in response to DNA damage.* Embo J, 2002. 21(8): p. 2030-7.
196. Yu, D.S., et al., *Dynamic control of Rad51 recombinase by self-association and interaction with BRCA2.* Mol Cell, 2003. 12(4): p. 1029-41.
197. Abaji, C., I. Cousineau, and A. Belmaaza, *BRCA2 regulates homologous recombination in response to DNA damage: implications for genome stability and carcinogenesis.* Cancer Res, 2005. 65(10): p. 4117-25.
198. Aten, J.A., et al., *Dynamics of DNA double-strand breaks revealed by clustering of damaged chromosome domains.* Science, 2004. 303(5654): p. 92-5.
199. Sporbert, A., et al., *DNA polymerase clamp shows little turnover at established replication sites but sequential de novo assembly at adjacent origin clusters.* Mol Cell, 2002. 10(6): p. 1355-65.

200. Sporbert, A., et al., *PCNA acts as a stationary loading platform for transiently interacting Okazaki fragment maturation proteins.* Nucleic Acids Res, 2005. 33(11): p. 3521-8.
201. Solomon, D.A., M.C. Cardoso, and E.S. Knudsen, *Dynamic targeting of the replication machinery to sites of DNA damage.* J Cell Biol, 2004. 166(4): p. 455-63.
202. Solovjeva, L., et al., *High mobility of flap endonuclease 1 and DNA polymerase eta associated with replication foci in mammalian S-phase nucleus.* Mol Biol Cell, 2005. 16(5): p. 2518-28.
203. Schermelleh, L., et al., *Dynamics of Dnmt1 interaction with the replication machinery and its role in postreplicative maintenance of DNA methylation.* Nucleic Acids Res, 2007. 35(13): p. 4301-12.
204. Kowalczykowski, S.C., *Some assembly required.* Nat Struct Biol, 2000. 7(12): p. 1087-9.
205. Vermeulen, W. and A.B. Houtsmuller, *The transcription cycle in vivo. A blind watchmaker at work.* Mol Cell, 2002. 10(6): p. 1264-6.
206. Politi, A., et al., *Mathematical modeling of nucleotide excision repair reveals efficiency of sequential assembly strategies.* Mol Cell, 2005. 19(5): p. 679-90.
207. Giepmans, B.N., et al., *The fluorescent toolbox for assessing protein location and function.* Science, 2006. 312(5771): p. 217-24.
208. Maranto, A.R., *Neuronal mapping: a photooxidation reaction makes Lucifer yellow useful for electron microscopy.* Science, 1982. 217(4563): p. 953-5.
209. Deerinck, T.J., et al., *Fluorescence photooxidation with eosin: a method for high resolution immunolocalization and in situ hybridization detection for light and electron microscopy.* J Cell Biol, 1994. 126(4): p. 901-10.
210. Galperin, E., V.V. Verkhusha, and A. Sorkin, *Three-chromophore FRET microscopy to analyze multiprotein interactions in living cells.* Nat Methods, 2004. 1(3): p. 209-17.
211. He, L., et al., *Determination of tumor necrosis factor receptor-associated factor trimerization in living cells by CFP->YFP->mRFP FRET detected by flow cytometry.* Nucleic Acids Res, 2005. 33(6): p. e61.
212. Cremazy, F.G., et al., *Imaging in situ protein-DNA interactions in the cell nucleus using FRET-FLIM.* Exp Cell Res, 2005. 309(2): p. 390-6.
213. van Royen, M.E., et al., *Compartmentalization of androgen receptor protein-protein interactions in living cells.* J. Cell Biol., 2007. 177(1): p. 63-72.
214. Truong, K. and M. Ikura, *The use of FRET imaging microscopy to detect protein-protein interactions and protein conformational changes in vivo.* Curr Opin Struct Biol, 2001. 11(5): p. 573-8.
215. Zhang, J., et al., *Creating new fluorescent probes for cell biology.* Nat Rev Mol Cell Biol, 2002. 3(12): p. 906-18.
216. Jares-Erijman, E.A. and T.M. Jovin, *FRET imaging.* Nat Biotechnol, 2003. 21(11): p. 1387-95.
217. Wallrabe, H. and A. Periasamy, *Imaging protein molecules using FRET and FLIM microscopy.* Curr Opin Biotechnol, 2005. 16(1): p. 19-27.
218. Wu, X., et al., *Measurement of two caspase activities simultaneously in living cells by a novel dual FRET fluorescent indicator probe.* Cytometry A, 2006. 69(6): p. 477-86.
219. Haustein, E. and P. Schwille, *Single-molecule spectroscopic methods.* Curr Opin Struct Biol, 2004. 14(5): p. 531-40.
220. Kohl, T. and P. Schwille, *Fluorescence correlation spectroscopy with autofluorescent proteins.* Adv Biochem Eng Biotechnol, 2005. 95: p. 107-42.
221. Masutani, C., et al., *Purification and cloning of a nucleotide excision repair complex involving the xeroderma pigmentosum group C protein and a human homolog of yeast RAD23.* EMBO J., 1994. 13(8): p. 1831-1843.
222. Schauber, C., et al., *Rad23 links DNA repair to the ubiquitin/proteasome pathway.* Nature, 1998. 391(6668): p. 715-8.
223. Hiyama, H., et al., *Interaction of hHR23 with S5a. The ubiquitin-like domain of hHR23 mediates interaction with S5a subunit of 26 S proteasome.* J Biol Chem, 1999. 274(39): p. 28019-25.

224. Kim, I., K. Mi, and H. Rao, *Multiple interactions of rad23 suggest a mechanism for ubiquitylated substrate delivery important in proteolysis.* Mol Biol Cell, 2004. 15(7): p. 3357-65.

225. Richly, H., et al., *A series of ubiquitin binding factors connects CDC48/p97 to substrate multiubiquitylation and proteasomal targeting.* Cell, 2005. 120(1): p. 73-84.

226. Drapkin, R., et al., *Dual role of TFIIH in DNA excision repair and in transcription by RNA polymerase II.* Nature, 1994. 368(6473): p. 769-72.

227. Iben, S., et al., *TFIIH Plays an Essential Role in RNA Polymerase I Transcription.* Cell, 2002. 109(3): p. 297-306.

228. Troelstra, C., et al., *ERCC6, a member of a subfamily of putative helicases, is involved in Cockaynes syndrome and preferential repair of active genes.* Cell, 1992. 71(6): p. 939-953.

229. Yu, A., et al., *Activation of p53 or Loss of the Cockayne Syndrome Group B Repair Protein Causes Metaphase Fragility of Human U1, U2, and 5S Genes.* Molecular Cell, 2000. 5: p. 801-810.

230. Bradsher, J., et al., *CSB Is a Component of RNA Pol I Transcription.* Mol Cell, 2002. 10(4): p. 819-29.

231. O'Donovan, A., et al., *XPG endonuclease makes the 3' incision in human DNA nucleotide excision repair.* Nature, 1994. 371: p. 432-435.

232. Bessho, T., *Nucleotide excision repair 3' endonuclease XPG stimulates the activity of base excision repairenzyme thymine glycol DNA glycosylase.* Nucleic. Acids Res., 1999. 27(4): p. 979-983.

233. Klungland, A., et al., *Base excision repair of oxidative DNA damage activated by XPG protein.* Mol. Cell, 1999. 3(1): p. 33-42.

234. Svejstrup, J.Q., et al., *Different forms of TFIIH for transcription and DNA repair: holo-TFIIH and a nucleotide excision repairosome.* Cell, 1995. 80(1): p. 21-8.

235. Fairman, M.P., et al., *Replication of SV40 in vitro using proteins derived from a human cell extract.* J Cell Sci Suppl, 1989. 12: p. 161-9.

236. Heyer, W.D., et al., *An essential Saccharomyces cerevisiae single-stranded DNA binding protein is homologous to the large subunit of human RP-A.* EMBO J., 1990. 9(7): p. 2321-2329.

237. Coverley, D., et al., *A role for the human single-stranded DNA binding protein HSSB/RPA in an early stage of nucleotide excision repair.* Nucl. Acids Res., 1992. 20(15): p. 3873-3880.

238. Constantin, N., et al., *Human mismatch repair: reconstitution of a nick-directed bidirectional reaction.* J Biol Chem, 2005. 280(48): p. 39752-61.

239. Dzantiev, L., et al., *A defined human system that supports bidirectional mismatch-provoked excision.* Mol Cell, 2004. 15(1): p. 31-41.

240. Frit, P., et al., *Transcriptional activators stimulate DNA repair.* Mol Cell, 2002. 10(6): p. 1391-401.

241. Prelich, G., et al., *The cell-cycle regulated proliferating cell nuclear antigen is required for SV40 DNA replication in vitro.* Nature, 1987. 326(6112): p. 471-5.

242. Prelich, G. and B. Stillman, *Coordinated leading and lagging strand synthesis during SV40 DNA replication in vitro requires PCNA.* Cell, 1988. 53(1): p. 117-26.

243. Chuang, L.S., et al., *Human DNA-(cytosine-5) methyltransferase-PCNA complex as a target for p21WAF1.* Science, 1997. 277(5334): p. 1996-2000.

244. Gary, R., et al., *The DNA repair endonuclease XPG binds to proliferating cell nuclear antigen (PCNA) and shares sequence elements with the PCNA-binding regions of FEN-1 and cyclin-dependent kinase inhibitor p21.* J Biol Chem, 1997. 272(39): p. 24522-9.

245. Matsuoka, S., M. Yamaguchi, and A. Matsukage, *D-type cyclin-binding regions of proliferating cell nuclear antigen.* J Biol Chem, 1994. 269(15): p. 11030-6.

246. Pagano, M., et al., *Cyclin D1-mediated inhibition of repair and replicative DNA synthesis in human fibroblasts.* Genes Dev, 1994. 8(14): p. 1627-39.

247. Henderson, D.S., et al., *Mutagen sensitivity and suppression of position-effect variegation result from mutations in mus209, the Drosophila gene encoding PCNA.* Embo J, 1994. 13(6): p. 1450-9.

248. Zhang, Z., K. Shibahara, and B. Stillman, *PCNA connects DNA replication to epigenetic inheritance in yeast.* Nature, 2000. 408(6809): p. 221-5.

249.   Shibahara, K. and B. Stillman, *Replication-dependent marking of DNA by PCNA facilitates CAF-1-coupled inheritance of chromatin.* Cell, 1999. 96(4): p. 575-85.

250.   Moggs, J.G., et al., *A CAF-1-PCNA-mediated chromatin assembly pathway triggered by sensing DNA damage.* Mol Cell Biol, 2000. 20(4): p. 1206-18.

251.   Krawitz, D.C., T. Kama, and P.D. Kaufman, *Chromatin assembly factor I mutants defective for PCNA binding require Asf1/Hir proteins for silencing.* Mol Cell Biol, 2002. 22(2): p. 614-25.

252.   Shivji, M.K.K., M.K. Kenny, and R.D. Wood, *Proliferating cell nuclear antigen is required for DNA excision repair.* Cell, 1992. 69(2): p. 367-74.

253.   Nichols, A.F. and A. Sancar, *Purification of PCNA as a nucleotide excision repair protein.* Nucleic Acids Res., 1992. 20: p. 2441-2446.

254.   Matsumoto, Y., *Molecular mechanism of PCNA-dependent base excision repair.* Prog Nucleic Acid Res Mol Biol, 2001. 68: p. 129-38.

255.   Kadyrov, F.A., et al., *Endonucleolytic function of MutLalpha in human mismatch repair.* Cell, 2006. 126(2): p. 297-308.

256.   Lee, S.D. and E. Alani, *Analysis of interactions between mismatch repair initiation factors and the replication processivity factor PCNA.* J Mol Biol, 2006. 355(2): p. 175-84.

257.   Umar, A., et al., *Requirement for PCNA in DNA mismatch repair at a step preceding DNA resynthesis.* Cell, 1996. 87(1): p. 65-73.

258.   Tsurimoto, T. and B. Stillman, *Purification of a cellular replication factor, RF-C, that is required for coordinated synthesis of leading and lagging strands during simian virus 40 DNA replication in vitro.* Mol Cell Biol, 1989. 9(2): p. 609-19.

259.   McAlear, M.A., K.M. Tuffo, and C. Holm, *The Large Subunit of Replication Factor C (Rfc1p/Cdc44p) Is Required for DNA Replication and DNA Repair in Saccharomyces cerevisiae.* Genetics, 1996. 142(1): p. 65-78.

260.   Majka, J. and P.M. Burgers, *The PCNA-RFC families of DNA clamps and clamp loaders.* Prog Nucleic Acid Res Mol Biol, 2004. 78: p. 227-60.

261.   Assenmacher, N. and K.P. Hopfner, *MRE11/RAD50/NBS1: complex activities.* Chromosoma, 2004. 113(4): p. 157-66.

262.   Cortez, D., et al., *Requirement of ATM-dependent phosphorylation of brca1 in the DNA damage response to double-strand breaks.* Science, 1999. 286(5442): p. 1162-6.

263.   Moynahan, M.E., et al., *Brca1 controls homology-directed DNA repair.* Mol Cell, 1999. 4(4): p. 511-8.

264.   Zhong, Q., et al., *Deficient nonhomologous end-joining activity in cell-free extracts from Brca1-null fibroblasts.* Cancer Res, 2002. 62(14): p. 3966-70.

265.   Zhong, Q., et al., *BRCA1 facilitates microhomology-mediated end joining of DNA double strand breaks.* J Biol Chem, 2002. 277(32): p. 28641-7.

266.   Nagaraju, G. and R. Scully, *Minding the gap: the underground functions of BRCA1 and BRCA2 at stalled replication forks.* DNA Repair (Amst), 2007. 6(7): p. 1018-31.

267.   Krum, S.A., et al., *BRCA1 associates with processive RNA polymerase II.* J Biol Chem, 2003. 278(52): p. 52012-20.

268.   Ye, Q., et al., *BRCA1-induced large-scale chromatin unfolding and allele-specific effects of cancer-predisposing mutations.* J Cell Biol, 2001. 155(6): p. 911-21.

269.   Ganesan, S., et al., *BRCA1 supports XIST RNA concentration on the inactive X chromosome.* Cell, 2002. 111(3): p. 393-405.

270.   Silver, D.P., et al., *Further evidence for BRCA1 communication with the inactive X chromosome.* Cell, 2007. 128(5): p. 991-1002.

271.   Starita, L.M. and J.D. Parvin, *The multiple nuclear functions of BRCA1: transcription, ubiquitination and DNA repair.* Curr Opin Cell Biol, 2003. 15(3): p. 345-50.

272.   Bakkenist, C.J. and M.B. Kastan, *DNA damage activates ATM through intermolecular autophosphorylation and dimer dissociation.* Nature, 2003. 421(6922): p. 499-506.

273.   Lobrich, M. and P.A. Jeggo, *Harmonising the response to DSBs: a new string in the ATM bow.* DNA Repair (Amst), 2005. 4(7): p. 749-59.

Chapter

3

Molecular Size-dependent Nuclear Mobility of Nucleotide Excision Repair Factors in the Absence of UV-induced DNA Damage

To be submitted

Molecular Size-dependent Nuclear Mobility of Nucleotide Excision Repair Factors in the Absence of UV-induced DNA Damage

Angelika Zotter[1], [#], Shehu M. Ibrahim[2], [#], Karin A. Mattern[2], W.A. van Cappellen[3], Bart Geverts[2], Jan H. J. Hoeijmakers[1], Wim Vermeulen[1] and Adriaan B. Houtsmuller[2], [*]

[#]Authors contributed equally to this work

[1]Department of Cell Biology and Genetics, Erasmus MC Rotterdam, P.O. box 2040, 3000 CA Rotterdam, The Netherlands.

[2] Department of Pathology, Josephine Nefkens Institute, Erasmus MC Rotterdam, P.O. box 2040, 3000 CA Rotterdam, The Netherlands.

[3] Department of Reproduction and Development, Erasmus MC Rotterdam, P.O. box 2040, 3000 CA Rotterdam, The Netherlands.

*Corresponding author. Phone: (+31) 10 7044456, Fax: (+31) 10 7044762
email: a.houtsmuller@erasmusmc.nl

Abstract

Many crucial cellular reactions take place within the cell nucleus. To facilitate these reactions, the cell often employs complex assemblies of proteins to interact with DNA, which in most cases is packed into chromatin. The sites of protein action are often randomly dispersed throughout the nucleus, specifically in the case of DNA damage. Considering the crowded nuclear environment, it is still not completely understood how chromatin-transacting proteins move through the nucleus, assemble into functional complexes and onto DNA, and act synchronically at their respective sites of need. To study the movement of functional nuclear proteins in the living cell, we combined two microscopic methods, fluorescence correlation spectroscopy (FCS) and fluorescence recovery after photobleaching (FRAP). In order to assess the general influence of the nuclear environment on the mobility of proteins with different molecular size and shape, this combined method was first tested and calibrated on an array of biologically inert GFP-fusion constructs with increasing size. Subsequently, we employed the well-characterized multi-subunit nucleotide excision repair (NER) machinery to study the

mobility of proteins that have a biological function in the cell nucleus. Systematic comparison of mobility parameters of diverse functional, physiologically expressed GFP-tagged NER subunits in the absence of induced DNA damage revealed that the mobility of the core factors XPA, XPG and ERCC1 is mainly determined by their molecular size. The 10-subunit TFIIH complex, which has an additional function in transcription initiation, and the primary NER damage sensor XPC, showed significant retention indicative of biological action also in the absence of NER-inducing DNA damage.

Introduction

Understanding complex cellular processes requiring the assembly of multiple proteins is of fundamental importance in biological research. How these multiple components reach their respective targets in an ordered and timely fashion is a matter of debate and has led to controversies in models describing these processes [1]. Particularly, nuclear DNA transacting processes are thought to be influenced by molecular crowding in the nucleoplasm.

It has been hypothesized that nuclear factors reside in pre-assembled holo-complexes or modules to facilitate their timely assembly when required at sites of action. Some nuclear proteins and RNAs have also been shown to accumulate consistently in distinct nuclear compartments believed to be specialized centres for DNA replication [2], transcription [3-5], RNA processing [6, 7], or ribosome biogenesis [8] (reviewed in [9]). The purpose of such distinct nuclear assemblies could be to enable resident enzymes to carry out their vital functions (e.g. replication) in a concerted manner. However, the association of nuclear factors with these structures has been shown to be far from static, in fact they generally seem to be highly dynamic [10-13]. Whether these "nuclear factories" themselves are kept in place via attachment to a nuclear matrix is still a matter of controversy [14-17] (reviewed in [16, 18-20]).

Similarly, the manner of subnuclear translocation in order to assemble at such structures, or other sites of action, is still under debate. Studies on numerous nuclear bodies such as ribonucleoprotein (RNP) particles, and chromosome fibres have shown that the movement of some nuclear solutes is largely diffusion-based but in some cases rely on energy-dependent processes [21] (reviewed in [22]). Many nuclear proteins observed, though showing random movement independent of ATP-based energy, still exhibit substantially slower mobility than inert solutes like GFP [23]. Therefore, it has been suggested that nuclear protein mobility is mainly determined by stop-and-go binding events [23]. Likewise, the impact of chromatin structure on protein mobility, especially a "sieving effect" for larger nuclear solutes, is still under debate ([24, 25]; reviewed in [26]).

To investigate the nature of nuclear protein mobility, we combined two complementary methods of fluorescence microscopy, FCS and FRAP. FCS with its microscopic detection volume is capable of accurate determination of an effective diffusion coefficient and concentration of a protein [27]. The method is fast and diffusing species of sufficient disparity are distinguishable. However, the limitation of the sensitive volume to a minute spot makes the technique less suitable for the characterization of long range dynamic parameters such as binding rates involving long residence times (> 3 s). Immobile fluorescent molecules in the detection volume of an FCS system are susceptible to bleaching resulting in a high apparent number of molecules and faster than normal diffusion coefficients [28]. FRAP involves the measurement of the recovery of fluorescence in a bleached, relatively large, observation area due to the influx of (unbleached) fluorescent molecules from the unbleached region. The recovery kinetics reflects the mobility of many molecules over a longer range and time, and is influenced by the interactions they undergo within the nucleus. The long range and the multitude of parameters involved make the analysis of FRAP recovery kinetics very challenging. Simplified mathematical algorithms used to model FRAP recovery kinetics are only able to extract the apparent effective diffusion coefficients (D_{eff}) that may be weighted averages of two or more diffusing species or diffusion coupled with transient binding events [29-31]. However, if properly modelled, the diffusion coefficients, mobile and immobile fractions, as well as average residence times at binding sites of the labelled molecules can be extracted from a recovery profile [30-34]. In more rigorous evaluation of FRAP data, computer simulation of the FRAP process is applied to generate curves with varying diffusion coefficients and kinetic parameters [30, 35, 36]. The input parameters of the simulated curve that best fits the experimental curve are then ascribed to experimental data. The choice of parameters to associate with the experimental curve is influenced by a prior knowledge of some properties of the dynamics of the protein under investigation.

To investigate the effect of the nuclear environment and molecular size on the mobility of proteins, we used various sizes of biologically inert tandem constructs with GFP measured in solutions and when expressed in live cell nuclei. We compared the dynamic properties of the tandem constructs of the EGFP obtained with FCS to those obtained using FRAP.

To investigate the nuclear mobility of biologically active proteins, we chose the nucleotide excision repair (NER) complex as a model system. NER is a highly conserved multi-step and multi-subunit DNA repair pathway, specialized in the removal of UV-induced DNA damage. The NER pathway has been extensively studied in vitro, resulting in a detailed model for its core reaction (reviewed in [37-40]. To clarify the in vivo

functioning and organization of the NER machinery, several subunits of the NER complex have been tagged with GFP in our lab, and have been introduced into corresponding NER-defective mutant cell lines. Their functionality was tested by their capability to restore UV resistance to the respective complemented cell lines, and cells were selected for expression at physiological levels. Within this background, DNA repair factors have been shown to move throughout the nucleus as distinct proteins or smaller multimeric subunits of a complex, and to assemble step by step at their active sites as individual factors that transiently interact only at DNA damage sites [12, 29, 41-44].

In order to find out what factors determine their individual mobility within the nucleus, we compared the mobility of different NER proteins in cells that were not subjected to UV irradiation. In these cells, DNA damage was minimal, and therefore also the repair activity of the NER enzymes. Using FCS and FRAP in cells stably expressing GFP-tagged NER proteins at physiologically relevant concentrations, combined with mathematical analysis and direct comparison with biologically inert GFP tandem constructs, we characterized the nuclear dynamics of biologically functional nuclear proteins.

Materials and Methods

Generation of EGFP-NFP$_n$ and EGFP-NFP$_n$-NLS fusion constructs

A non-fluorescent variant of EGFP, in which glycine 67 is replaced by a valine [45], was generated using the Quikchange Site-Directed Mutagenesis Kit (Stratagene, Cedar Creek, TX), and primers 5'-GTGACCACCCTGACCTACG<u>TA</u>GTGCAGTGCT TCAGCCGC-3' and 5'-GCGGCTGAAGCACTGCAC<u>TA</u>CGTAGGTCAGGGTGGTCAC-3' and by removing the authentic start codon of the EGFP. The resulting <u>n</u>on-<u>f</u>luorescent <u>p</u>rotein was designated NFP. The EGFP-NFP$_n$ and EGFP-NFP$_n$-NLS constructs were generated by the insertion of multiple *Pin*AI-*Xma*CI fragments containing NFP into the *Xma*CI-site of EGFP-C1 vector (Clontech, Mountain View, CA). An extra sequence encoding for a polyhistidine (His$_6$) and hemagglutinin (HA)-tag at the N-terminus of EGFP (between the *Nhe*I and *Nco*I sites) was added. The EGFP-NFP$_n$-NLS constructs also contain three tandem copies of the SV40 Large T-antigen nuclear localization signal (NLS) inserted by cloning the *Bgl*II/*Bam*HI-fragment from pEYFP-Nuc (Clontech, Mountain View, CA) in the *Bam*HI site of EGFP-C1. The constructs additionally contain a FLAG-tag at the C-terminus.

Cell lines expressing the protein constructs were generated by the transfection of EGFP-NFP$_n$ plasmid DNA into Hep3B and EGFP-NFP$_n$-NLS plasmid DNA into Chinese hamster ovary (CHO) cells using FugENE 6 transfection reagent (Roche, Indianapolis,

IN). Stable clones were picked after selection with G418 Sulphate (Sigma, St. Louis, MO, 0.6 mg/ml active concentration). The molecular weights of the protein constructs expressed by the G418 resistant clones were checked by Western blotting using an anti-EGFP antibody (Ab290, Abcam, Cambridge, UK) and horseradish peroxidase-conjugated secondary antibody. The signal was visualized with Super Signal West Pico Luminol solution (Pierce, Rockford, IL).

Construction of GFP-tagged NER proteins and generation of stably expressing cell lines

Full-length human XPC was tagged on the C-terminus with EGFP by in-frame ligation into the His_6HA-EGFP-N1 vector, a derivative of the pEGFP-N1 vector (Clontech, Mountain View, CA). In this vector, a His_6-HA-tag was added at the C-terminus of EGFP. Simian virus 40 (SV40)-transformed XP20MA (XP-C) cells were transfected with the corresponding plasmids, following selection with 0.3mg/ml of gentamycin (G418; Clontech, Mountain View, CA), and subsequently for UV resistance (three times irradiation with $4J/m^2$ UV with 1-day interval). An equal procedure was applied for the other NER constructs used here [12, 29, 43, 44]. All the fusion proteins were tested for functionality and physiological expression levels [12, 29, 43, 44].

Cell lines

Cell strains used in this study include Hep3B-cells stably expressing free EGFP or EGFP fused to the EGFP(G67V) variant designated NFP, and CHO cells expressing EGFP fused to increasing numbers of NFP containing a triple NLS. Further, SV40-immortalized human fibroblasts XP20S (XP-A), stably expressing EGFP-XPA (clone 40; [44]), XPCS2BA (XP-B; [46]) stably expressing XPB-EGFP [12], XP20MA (XP-C) stably expressing XPC-EGFP, the CHO cell lines 43-3B (ERCC-1) expressing ERCC1-GFP [29], and UV135 (XP-G) stably expressing XPG-EGFP [43], were used. All cell lines were cultured in a 1:1 mixture of DMEM/Ham's F10 medium containing Ultra-Glutamine (Cambrex Corporation, New Jersey, USA), 100 i.u. penicillin and 100 U streptomycin per ml, and 10% fetal calf serum at 37°C in an atmosphere of 5% CO_2.

Assayed solutions

Stock solutions of rhodamine Rh6G and Alexa Fluor 488 (Molecular Probes, Inc., Willow Creek Road, Eugene, OR) were prepared by dissolving the dyes in DMSO at concentrations of 5 and 10 mM, respectively. The recombinant EGFP (rEGFP) used in this work was from Clonetech (Clonetech laboratories, Inc., Terra Bella Avenue,

Mountain View, CA). Protein extracts from our cell lines were produced as previously described [47]. Dilutions of the assayed fluorophores were made in phosphate buffered saline solution (PBS).

Microscopy

Fluorescence autocorrelation measurements were performed on a Carl Zeiss LSM510 microscope upgraded to ConfoCor2/LSM510 combi. A combined setup enabled easy positioning of the cells at the laser focus of the FCS head and images taken before and after FCS measurements aided in data interpretation [48, 49]. For excitation, the 488 nm line of an Ar laser was used at a tube current of 6.1 A. An additional shutter situated at the exit of the laser ensured complete blockage of the 458, 477 and 514 lines when the 488-line was being used. FCS measurements were performed at a laser power of about 1.75 µW/µm^2 using the C-Apochromat 40x water immersion objective (1.2 n.a.) with a band pass filter BP 505-550 nm (BP530-560 for Rh6G) and behind a 488 nm dichroic mirror at a detector pinhole setting of 70 µm.

Photobleaching experiments were performed on a Zeiss LSM-META confocal Microscope using a Plan-Neofluar 40x/1.3 n.a. oil immersion objective. Excitation was by the 488-nm line of an Ar ion laser and EGFP fluorescence was detected by photomultiplier tubes (PMTs) after passing through a 505-550 nm band pass filter.

Both of the microscopes were equipped with a Zeiss 37-2 digital incubation system to keep cells under physiological conditions.

FCS measurement of liquid specimens

Dilute solutions of the assayed compounds (Rh6G, Alexa488, EGFP-chains) were prepared in PBS. 100-150 µl of the solution to be measured was then dropped onto a 24-mm silica glass coverslip mounted on a sample dish placed on the microscope stage. Five to ten repeated twenty-seconds-long FCS measurements were then carried out 200 µm above the glass. The autocorrelation functions were corrected for background obtained from measurements on clear PBS and then fitted to Eqn.1 for EGFP containing solutions and Eqn.3 for non-EGFP solutions to obtain the diffusion times and apparent number of molecules in the sample volume.

FCS measurement in cells

Cells for measurement were grown on 24-mm silica glass coverslips and then transferred to a sample dish with the growth medium replaced by phenol-red free medium. The dish was placed in a sample holder and mounted on the microscope stage in a heated chamber connected to a CO_2 supply. The chamber and the objective lens

were kept at 37°C. With the aid of LSM imaging the cell to be studied was identified and the desired point for measuring positioned at the FCS beam. The location of the FCS centre with respect to the LSM centre was identified by focusing with high laser intensity in FCS mode at a thin layer of precipitated Rh6G and then examining the bleached spot in LSM mode.

Evaluation of autocorrelation curves

Autocorrelation curves measured from intracellular GFP tagged proteins in living cells are generally analysed using the Levenberg-Marquardt non-linear least-squares method to fit the data to a single- or multi-component anomalous diffusion model corrected for the triplet state and blinking fluctuations [50-52].

$$G(\tau) = a_0 + \frac{1}{<N>} \cdot G_{tr} \cdot G_{bl} \cdot \sum_{i}^{n} \left[w_i \left(1 + \left(\frac{\tau}{\tau_{d,i}} \right)^{2/d_{w,i}} \right)^{-1} \left(1 + \frac{1}{S^2} \left(\frac{\tau}{\tau_{d,i}} \right)^{2/d_{w,i}} \right)^{-1/2} \right] \qquad \text{(Eqn.1)}$$

whereby the triplet state correction is given by

$$G_{tr}(\tau) = \frac{\left(1 - T + Te^{-\tau/\tau_{tr}} \right)}{1 - T} \qquad \text{(Eqn.1a)}$$

and the blinking correction by

$$G_{bl}(\tau) = \frac{\left(1 - \omega_{bl} + \omega_{bl} \cdot e^{-\tau/\tau_{bl}} \right)}{1 - \omega_{bl}} \qquad \text{(Eqn.1b)}$$

$<N>$ in Eqn.1 is the average number of molecules in the detection volume, the diffusional autocorrelation time, $\tau_{d,i}$ of the *i-th* diffusing species represents the average time it takes the molecule of a weight fraction w_i to traverse the detection volume described by the structure parameter, $S = \omega_z/\omega_{xy}$ (ratio of axial radius ω_z to the lateral radius ω_{xy} of the ellipsoid forming the detection volume). $d_{w,i}$ denotes the anomaly parameters of the diffusing components and a_0 is an offset to compensate for the non-zero baseline of the autocorrelation function arising from drifts in the fluorescence signal.

In the triplet term, G_{tr}, T denotes the equilibrium molar fraction of fluorophores in the triplet state [52-55] and τ_{tr} is the triplet lifetime. The "blinking term", G_{bl} accounts for the conformational fluctuations between fluorescent and dark state formation. ω_{bl} is the fraction of fluorophores in the detection volume in the dark state and τ_{bl} is the corresponding relaxation time.

The diffusion time can be converted to a diffusion coefficient (D) using the equation:

$$D_i = \frac{\omega_{xy}^2}{4\tau_{d,i}}$$
(Eqn.2)

The radii ω_{xy} and ω_z are obtained by calibrating the system with a dilute solution of a dye of known concentration and diffusion coefficient. Rh6G of molecular mass 0.479 kDa is commonly used for its small size and photostability. In such dilute solution (~10 nM), diffusion is simply Brownian and of a single component. Eqn.1 then simplifies to

$$G(\tau) = a_0 + \frac{1}{<N>} \cdot G_{tr} \cdot \left(1 + \left(\frac{\tau}{\tau_d}\right)\right)^{-1} \left(1 + \frac{1}{S^2}\left(\frac{\tau}{\tau_d}\right)\right)^{-1/2}$$
(Eqn.3)

The diffusion time, τ_d obtained from a Levenberg-Marquardt non-linear least-squares method fit to Eqn.3 and the diffusion coefficient of Rh6G (280 μm^2/s) are used in Eqn.2 to obtain ω_{xy}. An estimate of ω_z can then be obtained from the fit result of S or rigorously determined from measurements of a series of dilute concentrations of the dye. For a given concentration of dye, the average number of molecules in the detection volume can be expressed in terms of the dimensions of the ellipsoidal sensitive volume in the optical plane and the molar concentration c:

$$N = N_A c \pi^{3/2} \omega_{xy}^2 \omega_z$$
(Eqn.4)

N_A is Avogadro's number. Thus, $\omega_{xy}^2 \omega_z$ can be derived from the slope of a plot of the apparent number of particles, N, against the dye concentration.

FCS System Calibration

We calibrated the FCS system by evaluating the autocorrelation curves obtained for measurements on different concentrations of Rh6G solutions. Autocorrelation curves

obtained at the excitation laser power of 2.88 µW/µm^2 could be fitted well with the single component model of Eqn.3. Typical calibration measurements on 20, 38, 76, 80 and 100 nM Rh6G solutions in buffer yielded an average diffusion time of 30.6 +/- 1.1 µs and the slope of the plot of apparent number of particles, N, versus dye concentration (N/C M^{-1}) was 0.117 (plot not shown). Using these in Eqn.1 and Eqn.3, we calculated the radial and axial radii to be 0.185 µm and 1.02 µm respectively, resulting in a structural parameter, S, of 5.53. For subsequent fittings using equations Eqn.1 and Eqn.3, S was fixed at this value. We used this to fit the autocorrelation curves we obtained from measurements on a 30 nM solution of Alexa488 in PBS to recover a diffusion coefficient of 220 µm^2/s and a triplet time of 4.2 µs. The diffusion coefficient is close to 230 µm^2/s obtained by Bacia et al. for Alexa488 in water [55].

Accurate analysis of the autocorrelation curves of EGFP-tagged nuclear proteins requires knowledge of the nonfluorescent-triplet and -blinking state parameters (τ_{tr} and ω_{tr}, and τ_b and ω_b, respectively) associated with the GFP. To determine these parameters we analysed a solution of rEGFP in buffer and fitted the autocorrelation curves with Eqn.1 for a single component keeping the structural parameter, S fixed at the value of 5.53. For a 23 nM solution we obtained a triplettime of 9.4 +/- 0.6 µs with a triplet fraction of 0.15 +/- 0.08 and a blinking relaxation time of 296 +/- 15 µs with a fraction of 0.12 +/- 0.4. The diffusion coefficient of 86.35 +/-3.31 µm^2/s recovered for EGFP in buffer along with the blink parameters in the single component fit are comparable with previous results [52, 54, 56, 57].

The blink parameters were appropriately substituted into Eqn.1 to fit the measured autocorrelation curves of a solution of EGFP-XPA diluted in PBS. The diffusion coefficient of 54.6 µm2/s obtained for the protein is in conformity with the expected diffusion coefficient of a 54-kDa protein in PBS.

Fluorescence recovery after photobleaching (FRAP)

Cells for photobleaching experiments were chosen to minimize cell-to-cell nuclear size variation. Using the cropping function of the microscope cells were centred, aligned upright and focused for an equatorial 512 x 512 pixel (38.4 µm x 38.4µm) image of 2µm optical slice thickness recorded at zoom 6 and a pinhole setting of 160 µm. With the same settings the FRAP experiments were carried out with the use of the bleach-control macro provided with the Zeiss LSM software. The program was set to measure the average fluorescence intensity of a 10 pixel (0.7µm) strip spanning the entire nucleus every 21 ms for 4 s at a monitor laser power of 0.8% or 550-650 nW, followed by a bleach-scan of the strip at 100% laser power (140-180 µW) and then monitoring the

post-bleach intensity of the strip every 21 ms for 20 to 60 s at the low laser intensity. Mean fluorescence intensities of the bleached region were corrected for background taken from non-expressing cells. FRAP data for 10 to 60 cells were averaged to obtain a mean recovery curve for each cell line.

Analysis of FRAP-data

FRAP data were analysed with a custom-written LabView program employing the non-linear Levenberg-Marquardt algorithm for the general model accounting for both free and anomalous (hindered) diffusion [58]. In the absence of directed transport and assuming that recovery after bleaching is solely due to a single diffusing species, the fluorescence intensity f_t at any time for a Gaussian laser beam can be approximated [58] by the equation:

$$f_t = \frac{f_0 + f_\infty \left(t/t_{1/2}\right)^\alpha}{1 + \left(t/t_{1/2}\right)^\alpha} \qquad \text{(Eqn.6)}$$

where f_0 is the fluorescence intensity immediately after photobleaching, f_∞ is the maximum recovered intensity attainable after a long time, $t_{1/2}$ is the time to half of the maximum recovery (i.e. $(f_\infty + f_0)/2$), and α is the anomaly parameter [58], which has a value of 1 for free diffusion, and smaller than 1 for hindered ("anomalous") diffusion.

The mobile fraction (percentage recovery of fluorescence) is determined by

$$R = \frac{f_\infty - f_0}{f^0 - f_0} \qquad \text{(Eqn.7a)}$$

while the immobile fraction is given by

$$Im = \frac{f^0 - f_\infty}{f^0 - f_0} \qquad \text{(Eqn.7b)}$$

The 3-dimensional diffusion coefficient of the mobile molecules is obtained from the half-time of recovery, $t_{1/2}$ by

$$D = \frac{\gamma \omega^2}{6 t_{1/2}} \qquad \text{(Eqn.8)}$$

where ω is the bleached width and γ, the bleach parameter, is obtained as described by Wolf et al. [59].

However, if a fraction q, of the molecules undergoes reversible binding events with a fast binding rate compared to the diffusion (high turn over), then the calculated effective diffusion coefficient would be reduced by a factor of $(1+q)$ [31], so that the measurable effective diffusion coefficient becomes

$$D_{eff} = D/(1+q)$$ (Eqn.10)

On the other hand, if the binding and dissociation rates are slow compared to diffusion, the resulting FRAP curve is said to exhibit biphasic behaviour (a fast diffusion phase and a slow turnover phase) [31, 60] and the fluorescence intensity at time t on the recovery curve can be written as

$$f_t = \frac{k}{1+k} f_{imm} + \frac{1}{1+k} f_{free}$$ (Eqn.11)

whereby the bound fraction $v = k/(1+k)$ and $k = k_b/k_d$ is the ratio of the binding and dissociation rates. If the dissociation is exponential with a rate constant k_b then the concentration of released molecules diffusing in and out of the observation volume is

$$c_b = \left[v(1-e^{-k_d t}) \frac{(t/t_{1/2})^\alpha}{1+(t/t_{1/2})^\alpha} \right]$$ (Eqn.12a)

While the concentration of freely diffusing molecules is given by

$$c_d = (1-v) \frac{(t/t_{1/2})^\alpha}{1+(t/t_{1/2})^\alpha}$$ (Eqn.12b)

Thus if the fluorescence intensity increases from f_0 to f_∞ after equilibrium, then the fluorescence intensity at any time during the experiment can be written as

$$f_t = f_0 + (f_\infty - f_0) \left[(1-v) \frac{(t/t_{1/2})^\alpha}{1+(t/t_{1/2})^\alpha} + v(1-e^{-k_d t}) \frac{(t/t_{1/2})^\alpha}{1+(t/t_{1/2})^\alpha} \right]$$

or

$$f_t = f_0 + (f_\infty - f_0)(1 - ve^{-k_d t}) \frac{(t/t_{1/2})^\alpha}{1 + (t/t_{1/2})^\alpha}$$

(Eqn.13)

Eqn.13 enables the estimation of important biological information such as average residence time of the bound molecules ($t_r = 1/k_d$) and the steady state proportions of bound, $\dfrac{k}{1+k}$ and free, $\dfrac{1}{1+k}$ molecules contributing to the recovery dynamics.

Results

Characterization of functionally inert EGFP-chains expressed in Hep3B and CHO-cells

We used FCS and FRAP to study the mobility of EGFP and fusions of EGFP with increasing numbers of a <u>n</u>on-<u>f</u>luorescent EGF<u>P</u> mutant NFP, which we termed EGFP-chains (Table 1). Since the constructs have no function in the host nuclei, they are a useful set of proteins to study the properties of the cell nucleus with respect to macromolecular mobility. Moreover, they facilitate a comparison between FCS and FRAP analyses in live cells.

Table 1.

Protein	Molecular weights of constituents [kDa]				
	linker	GFP	HisH$_A$ + Flag	NLS	Total
EGFP	0 x 2	1 x 27	1 x 3	0 x 3	30
EGFP-NFP	1 x 2	2 x 27	1 x 3	0 x 3	59
EGFP-NLS	1 x 2	1 x 27	1 x 3	1 x 3	35
EGFP-NFP-NLS	2 x 2	2 x 27	1 x 3	1 x 3	64
EGFP-NFP$_2$-NLS	3 x 2	3 x 27	1 x 3	1 x 3	93
EGFP-NFP$_3$-NLS	4 x 2	4 x 27	1 x 3	1 x 3	122
EGFP-NFP$_4$-NLS	5 x 2	5 x 27	1 x 3	1 x 3	151

Composition and calculated molecular weights of tandem GFP constructs. Each construct is made up of a fluorescent EGFP (MW = 27 kDa) tagged to a number of non-fluorescent mutants of the protein (NFP = EGFP(G67V), MW = 27 kDa). They all contain a His$_6$-H$_A$ and a FLAG tag (MW = 3 kDa), and fusions to NFPs and NFP to NLS (MW =3kDa) are achieved by linkers (MW = 2kDa).

We first characterized the integrity, expression levels and subcellular distribution of the fusion proteins by Western blotting and confocal microscopy (Fig. 1). We were able to fuse a maximum of four NFPs to EGFP and stably express the intact fusion product in Hep3B and CHO-cells. As expected, EGFP (MW=30 kDa, Table 1) and the

twice as large EGFP-NFP (MW=59 kDa) were able to pass the nuclear envelope both with and without a nuclear localization signal (Fig. 1A and B), although the larger construct without NLS migrated to the nucleus to a lesser extent. EGFP-NFP$_2$, EGFP-NFP$_3$, and EGFP-NFP$_4$ were not able to sufficiently pass the nuclear envelope. To facilitate the uptake of these into the host nuclei, three tandem copies of the SV40 Large T-antigen nuclear localization signal (NLS) were fused to the ends of these constructs, after which efficient nuclear transport was observed (Fig. 1C to G). To investigate the effect of the presence of the triple-NLS, EGFP and EGFP-NFP were also fused to the triple-NLS. All EGFP-chains carrying an NLS were stably expressed in CHO cells. The NLS-free EGFP and EGFP-NFP were studied after transient transfection into Hep3B-cells.
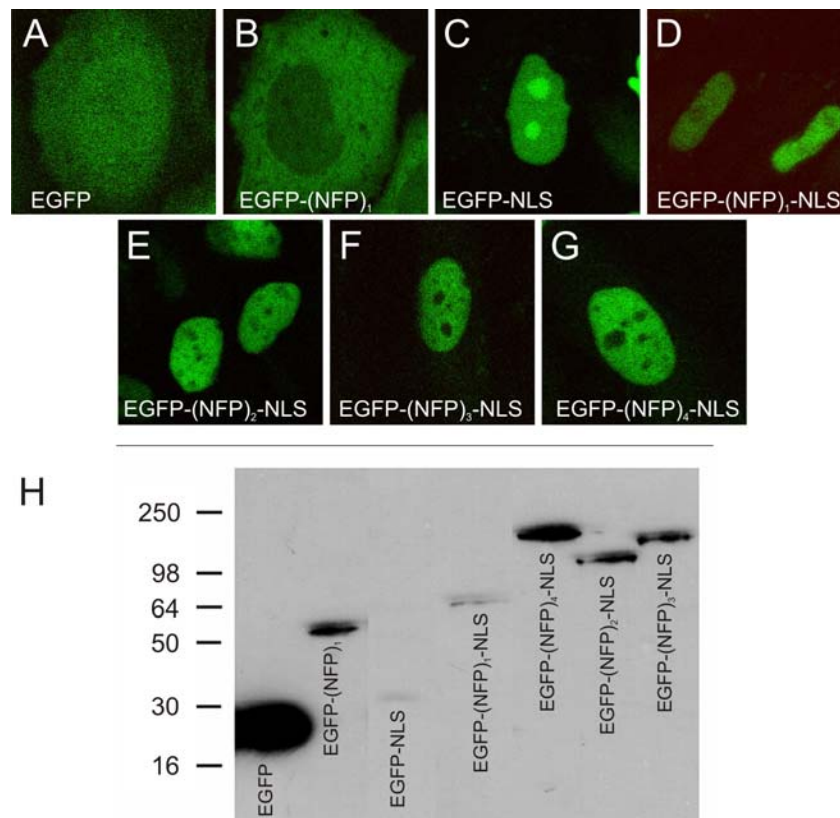
Fig.1. Hep3B and CHO cells expressing tandem constructs of EGFP. (A) and (B) Confocal optical sections of Hep3B cells expressing EGFP and EGFP-NFP, respectively. (C-G) CHO cells expressing EGFP-NLS, EGFP-NFP-NLS, EGFP-NFP$_2$-NLS, EGFP-NFP$_3$-NLS, and EGFP-NFP$_4$-NLS. (H) Western blot of whole-cell extracts of Hep3B cells expressing EGFP (lane 1) or EGFP-NFP$_1$ (lane 2), and of CHO cells expressing EGFP-NLS (lane 3), EGFP-NFP$_1$-NLS (lane 4), EGFP-NFP$_4$-NLS (lane 5), EGFP-NFP$_2$-NLS (lane 6), EGFP-NFP$_3$-NLS (lane 7).

FCS analysis of the nuclear mobility of EGFP-chains in living CHO-cells

We then investigated the mobility of EGFP-chains in the nuclei of living cells by FCS. In FCS, only a volume less than 1 femto-liter inside the nucleus is monitored. Therefore, data obtained with this method reflect the diffusion of nuclear proteins in the nucleoplasm, largely excluding the influence of globally distributed binding sites and large obstacles. We avoided the nucleoli during these measurements and took care that the microscope objective was also adjusted properly in the z-direction to ensure that the focal volume of the laser was within the nucleus. Fluorescence autocorrelation curves collected for the various EGFP-chains are shown in Fig. 2A. Triplet and blinking parameters established earlier for the fluorescent EGFP (see materials and methods) were used in fitting the autocorrelation curves (Fig. 2B). Interestingly, curves of the NLS-free EGFP and EGFP-NFP fitted best to a one component diffusion model (Eqn.1) with good residuals (Fig. 2C), whereas the autocorrelation curves for the NLS-appended constructs required fitting to a two component model to obtain good residuals. The single EGFP protein showed the highest diffusion coefficient of 29.8 ±1.3 μm^2/s (Table 2). Two-

Table 2.

Protein	MW [kDa]	ω_1 [%]	D_1 [μm^2/s]	D_2 [μm^2/s]	dw_1	dw_2
EGFP	30	-	**29.8** *±1.3*	-	**2.2** *± 0.1*	-
EGFP-NFP	35	71 ± 17	**27.4** ± 2.5	**2.5** ± 1.4	**2.4** *± 0.4*	**1.9** *± 0.2*
EGFP-NLS	59	-	**18.6** *± 1.8*	-	**2.8** *± 0.3*	-
EGFP-NFP-NLS	64	82 ± 5	**17.6** *± 1.7*	**1.3** ± 0.5	**2.6** *± 0.2*	**1.9** *± 0.3*
EGFP-NFP$_2$-NLS	93	68 ± 14	**13.0** ± 0.5	**0.8** ± 0.5	**2.6** *± 0.4*	**2.2** *± 0.2*
EGFP-NFP$_3$-NLS	122	76 ± 4	**11.5** *± 1.8*	**1.4** ± 0.6	**3.1** *± 0.7*	**2.9** *± 1.0*
EGFP-NFP$_4$-NLS	151	71 ±8	**8.7** ± 2.3	**0.8** ± 0.4	**2.6** ± 0.4	**2.4** *± 0.3*

FCS analysis of intranuclear mobility of EGFP-chains. FCS diffusion parameters are presented as mean ± SEM. Data were obtained by fitting the autocorrelation curves derived from FCS measurements on EGFP and EGFP-NFP expressed in Hep3B cells and constructs with NLS appendage in CHO cells to a one- or two- component diffusion model of Eqn.1. Indexes 1 and 2 refer to the fast and slow components. D_1 and D_2 are the diffusion constants, ω_1 is the fraction of constructs associated with the fast component, and dw is the anomaly parameter which in FCS formalism is 2 for Brownian diffusion.

component analysis of the autocorrelation curves of EGFP-NLS suggested that a fast component of 71 ± 17% had a diffusion coefficient of 27.4 ± 2.5 μm^2/s, similar to the NLS-free EGFP, whereas the slow component had a diffusion coefficient of 2.5 ± 1.4 μm^2/s. EGFP- NFP, EGFP-NFP$_2$, EGFP-NFP$_3$, and EGFP-NFP$_4$ had increasingly slower diffusion coefficients, but somewhat higher anomaly parameters (Table 2). This clearly shows that the size of a protein can in principle be determined from its diffusion coefficient. In addition, the slow components obtained from NLS-appended EGFP-chains

were not dependent on their size, suggesting that their mobility is reduced to more or less the same extent by the NLS. This is most likely due to transient interactions of the triple-NLS used here with immobile structures in the nucleus.
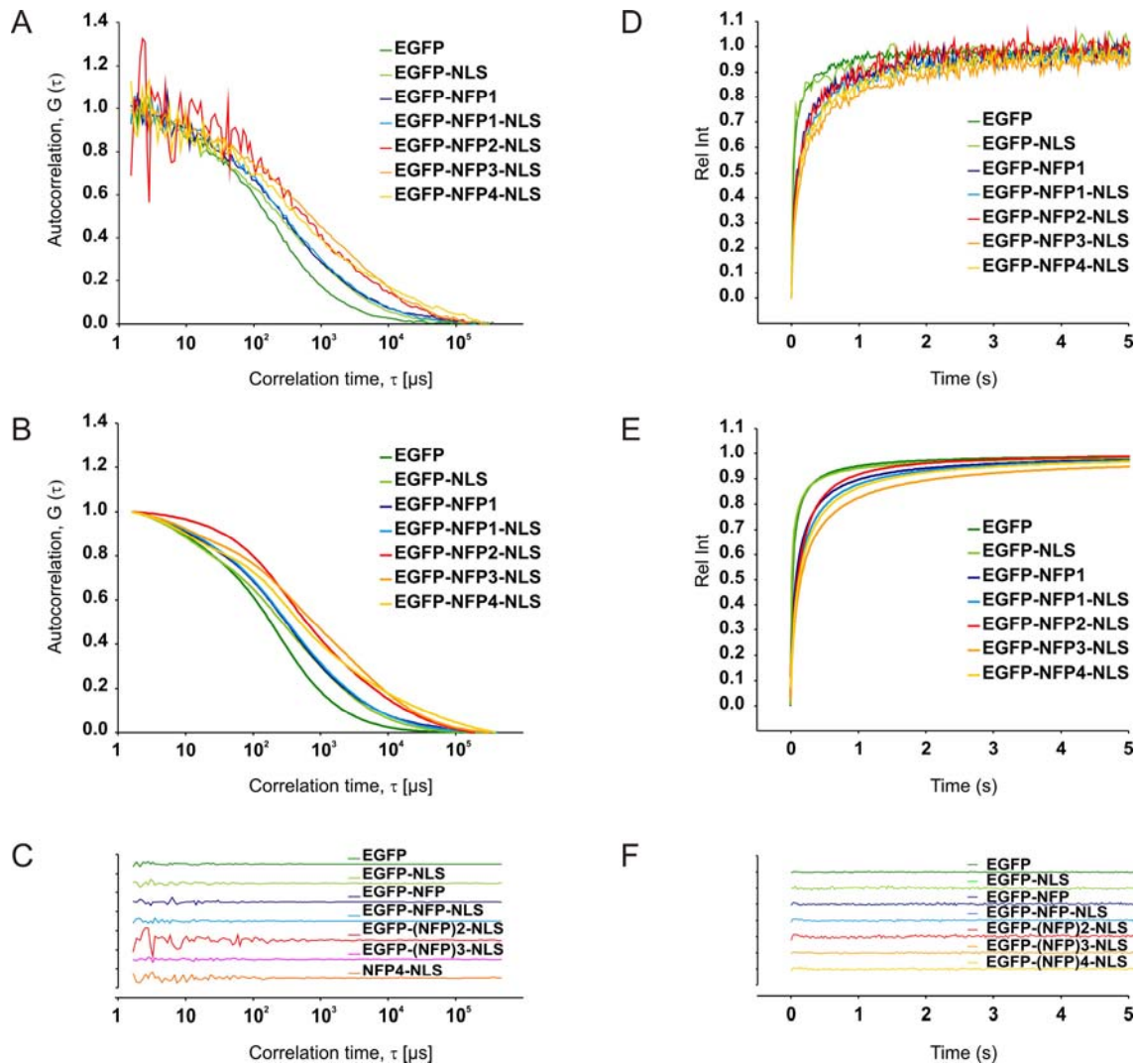

Fig.2. FCS and FRAP analysis of cells expressing tandem constructs of GFP of increasing sizes. (A) Normalized autocorrelation functions of fluorescence measured in defined positions of the nuclei from Hep3B cells expressing EGFP (dark green), EGFP-NFP (dark blue), and in CHO cells expressing EGFP-NLS (light green), EGFP-NFP-NLS (light blue), EGFP-NFP$_2$-NLS (red), EGFP-NFP$_3$-NLS (orange), EGFP-NFP$_4$-NLS (dark yellow). (B) Best fitting curves to the correlation functions in (A). The correlation functions could be described by the anomalous diffusion model of Eqn.1 with corrections for EGFP blinking and triplet state. (C) Panels showing the corresponding fit residuals. (D)-(F) FRAP analysis of same cell lines as used in (A)-(C). (D) For a clear visualization, fluorescent curves are expressed relative to the first measurement after bleaching and total recovery of fluorescence after photobleaching. (E) Corresponding best fitting curves, shown in the same normalization as the experimental data. Experimental data were fitted to the anomalous diffusion model of Eqn.6. (F) Panel showing the residuals of the fits. Rel Int, relative fluorescence intensity.

FCS analysis of the mobility of EGFP-chains in aqueous solution

To assess the effect of the nuclear environment on the mobility of the constructs, nuclear extracts were obtained of the cells expressing the various EGFP-chains, diluted 5 times in PBS and the mobility of the chains was determined by FCS. EGFP had a roughly three times higher diffusion coefficient than in the living cell nucleus (81.2 μm2/s), similar to that of the purified recombinant EGFP in aqueous solution (see materials and methods). The diffusion coefficients obtained for increasingly long EGFP chains showed an inverse cube root dependence on their molecular weight (Fig. 3). The ratio between measured intranuclear diffusion coefficient and the in vitro diffusion coefficient also showed an inverse dependence on molecular weight indicating that the effect of the nuclear environment increases with size.
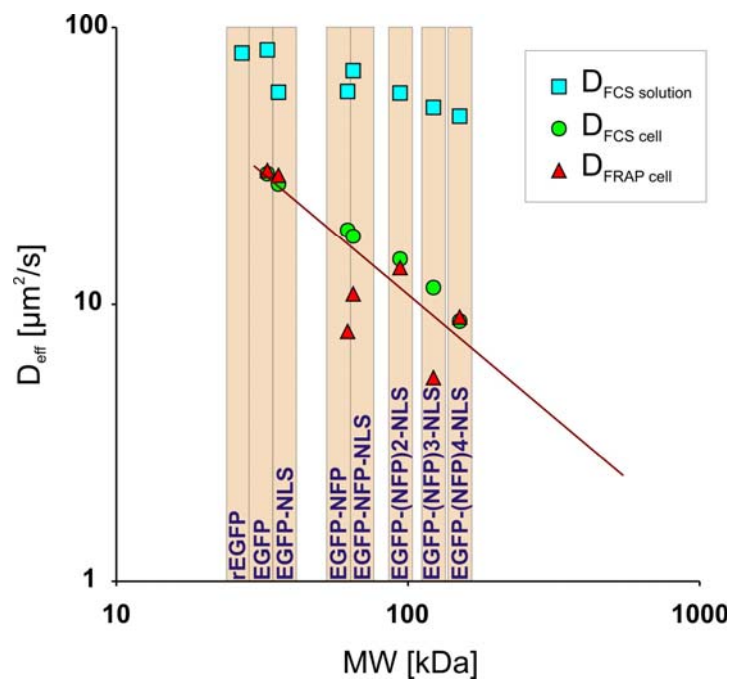
Fig.3. Relationship between protein molecular weight and mobility of GFP constructs. Light blue squares: Diffusion coefficients plotted against molecular weight of GFP constructs in cell extracts in dilute solution of PBS, and a purchased recombinant EGFP in aqueous solution (rEGFP), measured by FCS; green circles: the fast components of intranuclear diffusion coefficients of the constructs in Hep3B and CHO cells measured by FCS; red triangles: the measured intranuclear effective diffusion coefficients of the proteins measured by FRAP; D_{eff}, effective diffusion coefficient; MW, molecular weight.

FRAP analysis of the nuclear mobility of EGFP-chains in living CHO-cells

We performed FRAP experiments on the same transfected cells that were used for the FCS measurements. Fluorescence recovery curves obtained for the respective constructs are shown in Fig. 2D. Modelling the recovery curve obtained for EGFP and EGFP-NLS with simple Brownian recovery (Eqn.6) produced a poor fit at the beginning of recovery (first 100 ms) but the fit was improved using the anomalous diffusion model, i.e. setting the anomaly parameter α in Equn.6 to <1. However, the larger constructs required modifying the diffusion equation to account for transient immobilization (Eqn.10) before good fits to the recovery kinetics could be obtained (Fig. 2E and F, Table 3). The recovery curves did not show large variations in the anomaly parameter, with EGFP-NFP_1 deviating the most from simple Brownian diffusion, and EGFP-NLS and EGFP-NFP_2-NLS showing the least anomaly (α closest to 1). Since dense nuclear structures can constrain random motion and hence affect otherwise free mobility (resulting in anomalous diffusion, "corralled diffusion"), we express the determined mobilities of all nuclear factors measured by FRAP as an effective diffusion rate (D_{eff}). The D_{eff} measured for EGFP, EGFP-NLS, EGFP-NFP_2-NLS and EGFP-NFP_4-NLS (29.2 ±1.6, 29.6 ±5.1, 13.5 ±1.7 and 9.0 ±2.3 μm^2/s respectively) agree with values obtained from FCS (Fig 3) but the apparent diffusion coefficients extracted for EGFP-NFP_1, EGFP-NFP_1-NLS and EGFP-NFP_3-NLS (10.2 ±0.8, 10.9 ±0.7, and 7.0 ±0.4 μm^2/s respectively) are slower than the fast components measured by FCS for these proteins. Using Eqn.10

Table 3.

Protein	MW [kDa]	α	D_{eff} [μm^2/s]	Bound [%]	Residence time [s]	Brief obstruction
EGFP	30	0.97 ±0.04	29.2 ±1.6	-	-	-
EGFP-NFP	35	0.98 ±0.15	29.6 ± 5.1	-	-	-
EGFP-NLS	59	0.90 ±0.03	10.2 ± 0.8	10 ± 2	1.1 ± 0.1	41%
EGFP-NFP-NLS	64	0.97 ±0.04	10.9 ± 0.7	19 ± 1	1.2 ± 01	31%
EGFP-NFP_2-NLS	93	0.98 ±0.09	13.5 ± 1.7	25 ± 3	0.8 ± 0.1	-
EGFP-NFP_3-NLS	122	0.96 ±0.19	7.0 ± 0.4	14 ± 8	2.1 ± 0.5	47%
EGFP-NFP_4-NLS	151	0.97 ±0.04	9.0 ± 2.3	19 ± 2	1.3 ± 0.1	35%

FRAP analysis of intranuclear mobility of EGFP-chains. The FRAP diffusion parameters are presented as mean ± SEM. Data was obtained by fitting the recovery curves obtained from FRAP measurements on EGFP and EGFP-NFP expressed in Hep3B cells and constructs with NLS appendage in CHO cells to the anomalous diffusion model of Eqn.6, corrected for transient binding events (Eqn.10) in the case of the larger GFP chains. D_{eff} is the apparent diffusion coefficient extracted from the recovery curve, α is the anomaly parameter which is 1 for Brownian diffusion.

to calculate immobilized fractions and assuming that diffusion coefficients obtained from FCS represent the intranuclear diffusion rates of the proteins, we deduced that in addition to the one-second-duration restriction to mobility experienced by a subpopulation (10, 19, 14 and 19 % for EGFP-NFP$_1$, EGFP-NFP$_1$-NLS, EGFP-NFP$_3$-NLS and EGFP-NFP$_4$-NLS respectively) of these proteins, a further 41, 31, 47 and 35 % of the proteins, respectively, experience brief obstructions to their movements (Table 3). For EGFP-NFP2-NLS, we did not find an additional transient obstruction by comparing FRAP with FCS-derived data, but could instead calculate that a fraction of 25 % shows a retention of less than a second. Together, these data point towards an increase of the influence of molecular shape on nuclear diffusion with range.

Distribution of functional GFP-tagged NER factors within the cell

After the establishment of the above-described combined microscopic analysis method, we used it to characterize the nuclear mobility of diverse core factors of the nucleotide excision repair (NER) machinery. All these GFP-tagged NER factors were stably expressed in mammalian cells carrying inactivating mutations in their respective NER gene. Cell populations with physiological expression levels of the fusion protein were selected. In addition, fusion proteins had been tested for their biological activity before being used in nuclear protein dynamics studies.

In living cells, the GFP-tagged NER factors XPA, XPG and ERCC1 (Fig.4A to C) exhibited a homogeneous nuclear distribution, as described before [29, 43, 44]. XPG and ERCC1 additionally showed lower concentrations within nucleoli. This pattern is also similar to the above-described GFP-NFP chains containing NLS (Fig. 1). XPB-GFP (Fig.4D), as an integral part of TFIIH, showed in transcriptionally active cells homogeneous nuclear distribution with additional inhomogeneous accumulation in nucleoli [12]. XPC-GFP (Fig.4E) exhibited an inhomogeneous nuclear distribution that largely mimicked the non-uniform distribution of genomic DNA or chromatin in interphase mammalian nuclei [61].
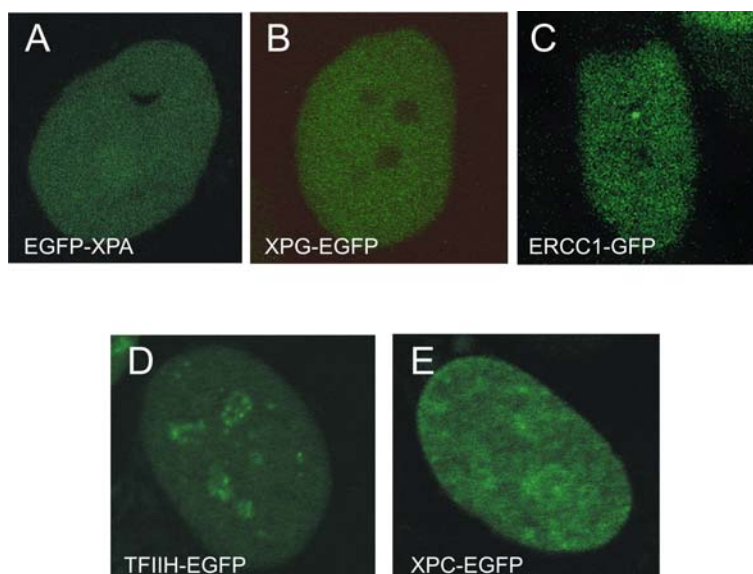
Fig.4. Nuclear distribution of various GFP-tagged NER proteins expressed in corresponding deficient cell lines. (A) and (B) Confocal optical sections of human cells expressing EGFP-XPA and XPG-EGFP, respectively. (C) CHO cell expressing ERCC1-GFP. (D) and (E) Confocal sections of human cells expressing TFIIH-EGFP and XPC-EGFP, respectively. Note the nucleolar accumulations of TFIIH actively engaged in RNA polymerase I transcription, and the uneven distribution pattern of XPC throughout the nucleus.

FCS and FRAP on GFP-tagged NER factors

In previous experiments [12, 29, 43, 44, 61], we have determined the mobilities of a number of different GFP-tagged NER factors by using various FRAP techniques. The corresponding measurements were performed over a period spanning several years, in which experimental conditions, such as microscopic settings and laser intensities, as well as the type of microscope used, varied. This hampered proper comparison of the mobility parameters of the diverse GFP-tagged NER factors. To systematically determine mobilities of the distinct nuclear proteins that are part of this DNA-transacting process and comprehensively analyze the factors that influence their differential mobility, we used the above-described combined FCS and FRAP approach.

To assess the mobility of GFP-tagged NER proteins in the absence of UV-induced DNA damage, we examined untreated mammalian cells at physiological temperature (37°C). Under these conditions, the activity of the highly specialized NER system was assumed to be minimal. Using exactly the same microscope and laser settings for all, for the first time the mobilities of the following GFP-tagged NER proteins were compared directly with each other using FRAP (Fig. 5A-C) and FCS (Fig. 6A-C): the relatively small lesion verification factor XPA (61 kDa); the 3'-endonuclease XPG (163 kDa); the 5'-endonuclease ERCC1 (as part of a stable dimer with XPF, 165 kDa);

the damage sensor XPC (about 200 kDa as a heterotrimeric complex of XPC, hHR23B and centrin 2 (CEN2) [62]; and the helicase XPB (400-510 kDa as integral part of the ten-subunit TFIIH complex [63].
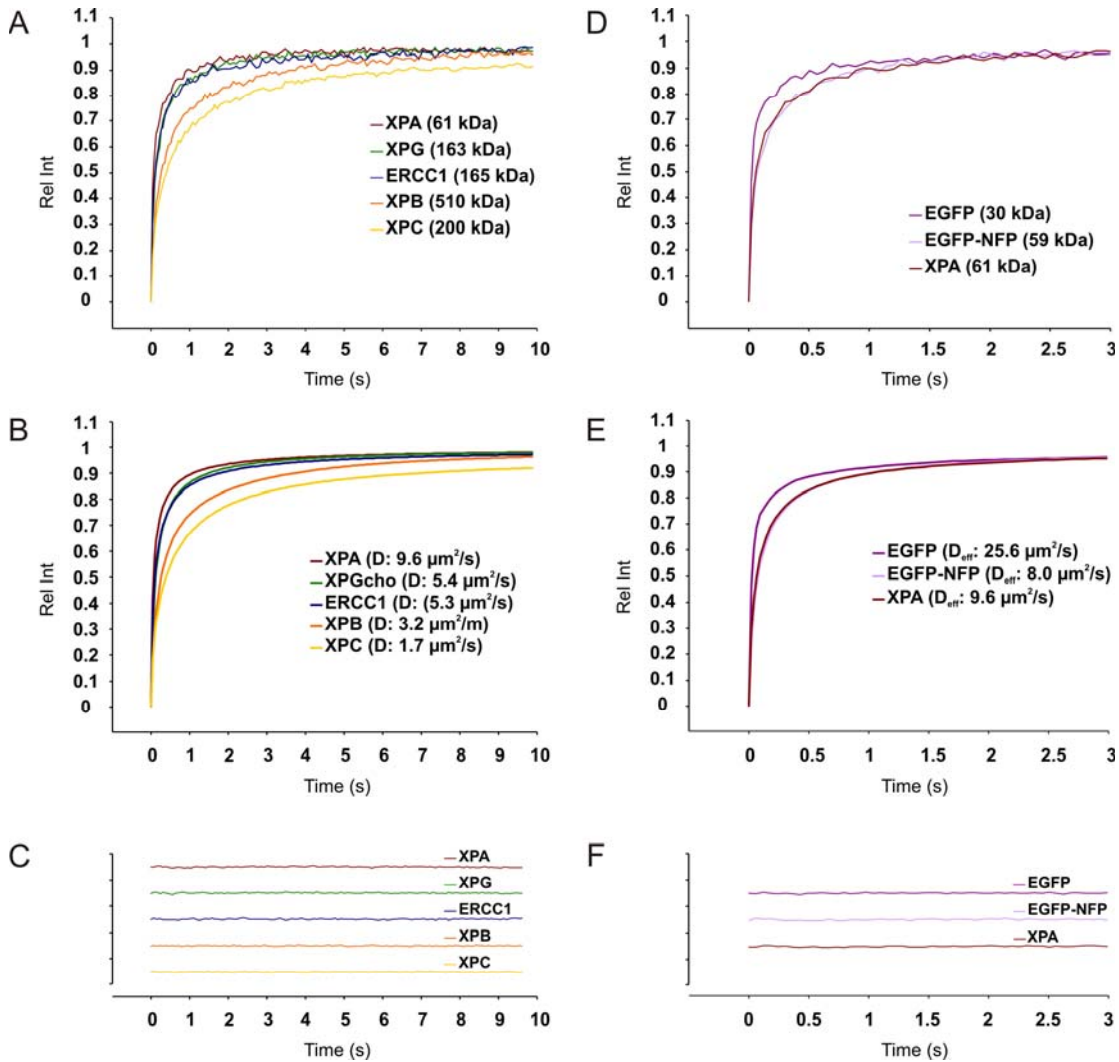

Fig.5. FRAP analysis of cells expressing GFP-tagged NER proteins. As a control and direct comparison, also EGFP and EGFP-NFP were included into this set of measurements. (A and D) FRAP curves are expressed relative to the first measurement after bleaching and total recovery of fluorescence after photobleaching. (B and E) Corresponding best fitting curves shown in the same normalization as the experimental data. Experimental data were fitted to the anomalous diffusion model of Eqn.3.6. (C and F) Residuals of the fits. Red lines, EGFP-XPA, green lines, XPG-EGFP, dark blue lines, ERCC1-GFP, orange lines, XPB-EGFP, dark yellow lines, XPC-EGFP, violet lines, EGFP, lavender lines, EGFP-NFP, Rel Int, relative fluorescence intensity.

To better visualize the nature of NER protein mobility, we included two of the previously characterized biologically inert EGFP chains, EGFP and EGFP-NFP, directly in the same set of measurements as the NER factors (Fig. 5D-F).

Analysis of the nuclear mobility of NER factors

To comprehensively investigate NER factor mobility, we first analysed the respective FRAP curves (Fig. 5A and D). Already from the experimental data curves it was visible that the lightest NER protein, EGFP-XPA (61 kDa), exhibited the highest mobility. Strikingly, the recovery pattern of the equally-sized molecule EGFP-NFP was very similar to EGFP-XPA, revealing that these proteins, in spite of their entirely different properties and biological functions, show equal nuclear mobilities (Fig. 5D); the single EGFP exhibited a clearly faster recovery. The equally-sized XPG-EGFP (163 kDa) and ERCC1/XPF-GFP (165 kDa) showed a very similar recovery pattern. GFP-tagged XPB, as an integral subunit of a large multi-protein complex, exhibited a clearly slower mobility than the previously mentioned NER proteins. Together, these results point towards protein mobility being determined mostly by size and shape of the examined nuclear factors. XPC-EGFP, on the other hand, showed a significantly different behaviour. Surprisingly, it appeared to be even slower than XPB, though it is part of a complex much smaller than TFIIH, with an estimated molecular mass of only 200 kDa. Clearly, this protein moved much slower than expected on the basis of its molecular size.

Fitting the FRAP curves to Eqn.6 for anomalous diffusion, XPA, XPG and ERCC1 produced D_{eff} corresponding to their respective molecular weight (see Table 4 and Fig. 7). Importantly hereby, the equally-sized proteins XPG and ERCC1/XPF produced very similar D_{eff} (5.4 and 5.3 $\mu m^2/s$, respectively), which were significantly different from the smaller factor XPA (9.6 $\mu m^2/s$) and the large TFIIH complex (3.2 $\mu m^2/s$). Furthermore, analysis of the NER protein EGFP-XPA (61 kDa) mobility curve resulted in a D_{eff} very similar to the one obtained for EGFP-NFP (9.6 $\mu m^2/s$ as compared to 8.0 $\mu m^2/s$; see Table 4). The recovery curve of XPC, however, despite its good fit to equations for anomalous Brownian diffusion, produced a strikingly low D_{eff} (1.7 $\mu m^2/s$).

Analysis of both XPB and XPC recovery curves also revealed transiently bound fractions. About 9 % of XPB-EGFP was immobilized for around 3 s (Table 4), which was consistent with its previously determined dynamic engagement in transcription [61]. An equal percentage of XPC-EGFP molecules were immobilized for only little more than 1 s (Table 4).

Table 4.

Protein	MW [a] [kDa]	Nuclear function	D_{FCS} [µm²/s]	$D_{eff(FRAP)}$ [µm²/s]	bound fraction	brief obstruction
EGFP	30	none	29.2 ±1.6	25.6 ± 2.6	-	-
EGFP-NFP	59	none	29.6 ± 5.1	15.0 ± 3.6 [*] 8.0 ± 3.6	22.7% (0.72 s) -	- 43%
EGFP-XPA	61	NER lesion verification	10.2 ± 0.8	9.6 ± 0.4	-	-
ERCC1-GFP	165[1]	5' endonuclease	10.9 ± 0.7	5.3 ±1.0	-	24%
XPG-EGFP	163	3' endonuclease	13.5 ± 1.7	5.4 ±1.1	-	-
XPB-EGFP	400-510[2]	helicase	7.0 ± 0.4	3.2 ± 0.9 [*]	8.8% (2.90 s)	-
XPC-EGFP	200[3]	NER lesion recognition	9.0 ± 2.3	1.7 ± 0.4 [*]	9.1% (1.23 s)	64%

[a] all molecular weights are estimates including tags and linkers

[1] in complex with XPF; [2] as part of TFIIH complex +/-CAK; [3] in complex with hHR23B + centrosome component CEN2

[*] anomalous FRAP fit corrected for binding

Analysis of intranuclear mobility of functionally inert and biologically active nuclear factors in living cells based on FRAP and FCS measurements. Diffusion coefficients obtained by FCS and FRAP measurements are presented as mean ± SEM. FCS data were obtained by fitting the autocorrelation curves derived from FCS measurements to a one- or two- component diffusion model of Eqn.3.1. FRAP data was obtained by fitting the recovery curves obtained from FRAP measurements to the anomalous diffusion model of Eqn.3.6; where indicated, best fits were achieved by adjusting the equation for transient binding. Subsequently, additional obstructions were calculated from the differences between FCS and FRAP mobility parameters. Brief obstructions of less than 15 % of the protein are not shown (statistically not relevant).

Complementation of the mobility parameters obtained by FRAP with diffusion coefficients derived from FCS (Fig. 6, Table 4) revealed that none of the NER factors exhibited significant additional retention which would become apparent over a longer range, with the exception of XPC (see also Fig. 7). Nearly 2/3 of the XPC molecules appeared to undergo short retention additionally to the calculated immobilized fraction, providing an explanation for the apparent slow diffusion in FRAP. These transient obstructions are in the order of only a fraction of a second and largely correspond to anomalous (corralled) diffusion that could be due to sterical hindrance by dense nuclear structures and be influenced by the molecular shape of the protein. Additionally, they could account for a fraction of the protein being transiently immobilized in a biologically relevant action, i.e. in the case of XPC, probing DNA or chromatin for DNA damage.
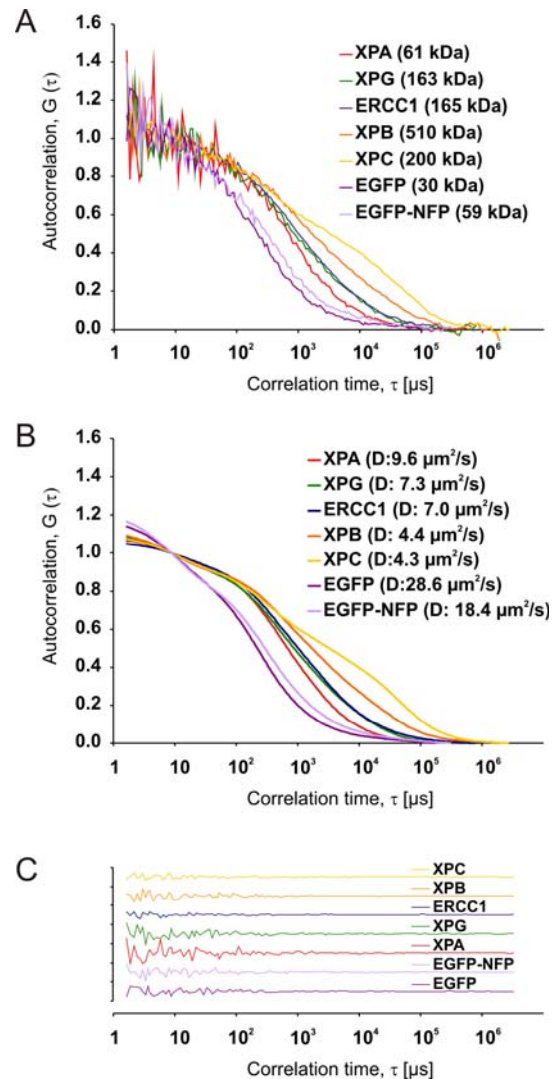
Fig.6. FCS analysis of cells expressing GFP-tagged NER proteins. (A) Normalized autocorrelation functions of fluorescence measured in defined positions within cell nuclei, (B) corresponding best fitting curves and (C) residuals of the fits. EGFP and EGFP-NFP measurements were included as a control and direct comparison. Red lines, EGFP-XPA, green lines, XPG-EGFP, dark blue lines, ERCC1-GFP, orange lines, XPB-EGFP, dark yellow lines, XPC-EGFP, violet lines, EGFP, lavender lines, EGFP-NFP.

3.5. Discussion

How nuclear processes function in their required precision and efficiency in an environment that is believed to be relatively crowded is a question of fundamental importance. The nature of nuclear protein motion in order to arrive at dispersed sites of enzymatic action is of special interest in the case of cellular emergency functions such as DNA repair.

To analyse the nuclear mobility of DNA-interacting proteins background we chose the NER machinery as a model system. This system provided several crucial advantages: the multi-protein NER machinery has already been extensively studied in

vitro, resulting in a profound knowledge of its core reaction [37, 64]; the GFP-tagged NER core factors used in this study were expressed in physiologically relevant amounts in corresponding mutant cell lines and have been shown to be functional in NER [12, 29, 43, 44, 61]; the NER machinery can be switched on (by inducing global or local NER-specific DNA damage) or, importantly, be studied in a situation where DNA repair is at a minimum i.e. in the absence of UV-induced DNA damage. Therefore, NER proteins are an excellent model system to study the behaviour of nuclear proteins when they are not exerting their primary function.

By tagging various NER proteins with GFP and expressing them at physiologically relevant levels in corresponding mutant cell lines that lack the protein under investigation, we could study the molecular mobility of each of the subunits separately. Using the same microscope and the same settings for all of the factors measured facilitated a direct comparison of the only slightly divergent protein mobilities. Moreover, by combining two different novel microscopic approaches and mathematical analysis, we could establish individual mobility parameters for each of the factors examined.
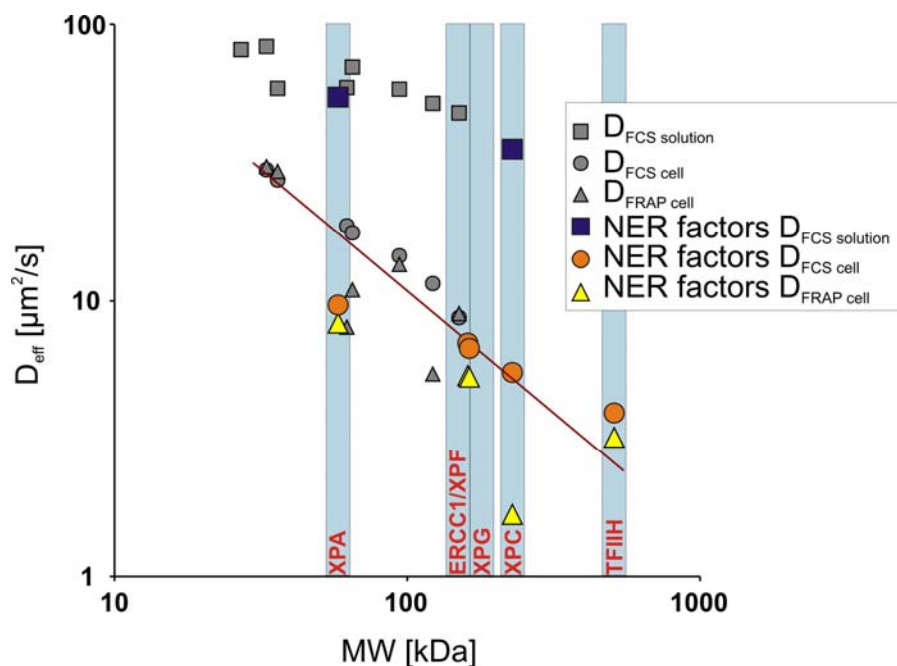
Fig.7. Molecular mass dependence of in vitro- and intranuclear mobility of GFP-tagged NER proteins. Diffusion coefficients of the cell extracts of EGFP-XPA and XPC-EGFP in dilute solution of PBS measured by FCS (dark blue squares), the fast components of intranuclear diffusion coefficients of the constructs in human and CHO cells measured by FCS (orange circles), and the measured intranuclear effective diffusion coefficients of the proteins measured by FRAP (yellow triangles) are plotted as function of the calculated molecular weights. For additional comparison, the calibrating measurements of the GFP tandem constructs (Fig.3) are given in grey. D_{eff}, effective diffusion coefficient; MW, molecular weight.

Our results show that individual NER subunits, in the absence of DNA damage, exhibit passive diffusion at a rate mainly determined by their molecular size or that of the protein complex they are a stable part of (Fig. 7). Only the helicase XPB and the lesion recognition factor XPC showed partial immobilization in time frames consistent with biological function.

XPB is an integral part of the ten-subunit TFIIH complex [63], that besides NER also functions in RNA polymerase I and II transcription initiation [65-67]. Concomitantly, the mobility parameters of XPB are consistent with the diffusion of a protein complex the size of TFIIH. We found that only a small percentage (9%) of the TFIIH pool is immobilized for a short time also in cells not subjected to DNA damage. These data are in concordance with earlier studies that already suggested transient binding of TFIIH to transcription sites [12]. The fact that redistribution of XPB is further slowed down at lower temperatures ([12] and unpublished data) indicates that the observed transient immobilization of TFIIH is due to its involvement in a temperature dependent process in which it gets immobilised, most likely by DNA binding.

Despite the very slow redistribution of the damage recognition factor XPC, we found that its calculated immobilized fraction (9%, equal to XPB) is relatively small, and the time of immobilization very short (a little more than 1s). However, an additional large fraction (about 2/3) of the XPC pool is transiently retained for even less than 1s. This short stalling could either be interpreted as constrained, "corralled", diffusion, or as very short binding events at immobile nuclear structures. XPC has been shown to be additionally slowed down at lower temperatures, indicating temperature-dependent binding or dissociation of this protein [61]. We hypothesize therefore that most of the nuclear XPC pool might be engaged in continuous probing of DNA for NER damage, also in unchallenged cells. It might attach to distorted or perhaps partly remodelled patches of chromatin and dissociate quickly from these structures if no damage is detected. Another indication of this is the fact that XPC, unlike the other NER factors, is not homogeneously distributed throughout the nucleus but rather co-localizes with DNA-dense regions [61]. The retention time of XPC could be too short to be resolved by our combined methods, which would explain the outcome of our calculations. The percentage of stalled XPC could also be underrated since very densely distributed binding sites for XPC might have influenced FCS measurements. The FCS data therefore may not only represent free diffusion of the XPC complex, but also be influenced by transiently bound molecules. Consequently, the obtained data might not contribute as much to resolving immobilized fractions of XPC undetected by FRAP measurements. Further, there might be two or more pools of transiently immobilized

protein (indicated also by the biphasic FCS autocorrelation curve in Fig. 6), which we could not resolve with our combined methods.

In summary, our study presents the first direct mobility comparison of functional NER proteins within the nucleus of mammalian cells in an unchallenged condition. Our data show that chromatin-transacting proteins that are not engaged in their respective function are freely mobile throughout the nucleus. Our results therefore provide further support for a general model of chromatin-transacting processes in which free diffusion and random collision allows the efficient formation of functional and adaptable protein complexes directly at the site of need. Individual factors can hereby be easily exchanged or used for multiple actions within one or more processes, rendering a cell capable of adapting quickly and efficiently to environmental or internal challenges.

References

1.   Misteli, T., *Concepts in nuclear architecture.* BioEssays, 2005. **27**(5): p. 477-487.
2.   Hozak, P., D.A. Jackson, and P.R. Cook, *Replication factories and nuclear bodies: the ultrastructural characterization of replication sites during the cell cycle.* J Cell Sci, 1994. **107 (Pt 8)**: p. 2191-202.
3.   Kimura, H., et al., *Quantitation of RNA polymerase II and its transcription factors in an HeLa cell: little soluble holoenzyme but significant amounts of polymerases attached to the nuclear substructure.* Mol Cell Biol, 1999. **19**(8): p. 5383-92.
4.   Francastel, C., W. Magis, and M. Groudine, *Nuclear relocation of a transactivator subunit precedes target gene activation.* Proc Natl Acad Sci U S A, 2001. **98**(21): p. 12120-5.
5.   Pombo, A., et al., *Regional specialization in human nuclei: visualization of discrete sites of transcription by RNA polymerase III.* Embo J, 1999. **18**(8): p. 2241-53.
6.   Smith, K.P., et al., *Processing of endogenous pre-mRNAs in association with SC-35 domains is gene specific.* J Cell Biol, 1999. **144**(4): p. 617-29.
7.   Sacco-Bubulya, P. and D.L. Spector, *Disassembly of interchromatin granule clusters alters the coordination of transcription and pre-mRNA splicing.* J Cell Biol, 2002. **156**(3): p. 425-36.
8.   Dundr, M., et al., *A kinetic framework for a mammalian RNA polymerase in vivo.* Science, 2002. **298**(5598): p. 1623-6.
9.   Jackson, D.A., *The principles of nuclear structure.* Chromosome Res, 2003. **11**(5): p. 387-401.
10.   Lamond, A.I. and D.L. Spector, *Nuclear speckles: a model for nuclear organelles.* Nat Rev Mol Cell Biol, 2003. **4**(8): p. 605-12.
11.   Phair, R.D. and T. Misteli, *High mobility of proteins in the mammalian cell nucleus.* Nature, 2000. **404**(6778): p. 604-9.
12.   Hoogstraten, D., et al., *Rapid switching of TFIIH between RNA polymerase I and II transcription and DNA repair in vivo.* Mol Cell, 2002. **10**(5): p. 1163-74.
13.   Kimura, H., K. Sugaya, and P.R. Cook, *The transcription cycle of RNA polymerase II in living cells.* J Cell Biol, 2002. **159**(5): p. 777-82.
14.   Philimonenko, V.V., J.E. Flechon, and P. Hozak, *The nucleoskeleton: a permanent structure of cell nuclei regardless of their transcriptional activity.* Exp Cell Res, 2001. **264**(2): p. 201-10.
15.   Nickerson, J., *Experimental observations of a nuclear matrix.* J Cell Sci, 2001. **114**(Pt 3): p. 463-74.
16.   Pederson, T., *Half a century of "the nuclear matrix".* Mol Biol Cell, 2000. **11**(3): p. 799-805.
17.   Philimonenko, A.A., et al., *Dynamics of DNA replication: an ultrastructural study.* J Struct Biol, 2004. **148**(3): p. 279-89.

18. Cook, P.R., *The organization of replication and transcription.* Science, 1999. **284**(5421): p. 1790-5.

19. Bode, J., et al., *From DNA structure to gene expression: mediators of nuclear compartmentalization and dynamics.* Chromosome Res, 2003. **11**(5): p. 435-45.

20. Barboro, P., et al., *An intranuclear frame for chromatin compartmentalization and higher-order folding.* J Cell Biochem, 2003. **88**(1): p. 113-20.

21. Calapez, A., et al., *The intranuclear mobility of messenger RNA binding proteins is ATP dependent and temperature sensitive.* J Cell Biol, 2002. **159**(5): p. 795-805.

22. Carmo-Fonseca, M., M. Platani, and J.R. Swedlow, *Macromolecular mobility inside the cell nucleus.* Trends Cell Biol, 2002. **12**(11): p. 491-5.

23. Phair, R.D., et al., *Global nature of dynamic protein-chromatin interactions in vivo: three-dimensional genome scanning and dynamic interaction networks of chromatin proteins.* Mol Cell Biol, 2004. **24**(14): p. 6393-402.

24. Misteli, T., *Protein dynamics: implications for nuclear architecture and gene expression.* Science, 2001. **291**(5505): p. 843-7.

25. Shav-Tal, Y., et al., *Dynamics of single mRNPs in nuclei of living cells.* Science, 2004. **304**(5678): p. 1797-800.

26. Verkman, A.S., *Solute and macromolecule diffusion in cellular aqueous compartments.* Trends Biochem Sci, 2002. **27**(1): p. 27-33.

27. Webb, W., *Fluorescence Correlation Spectroscopy: Inception, Biophysical Experimentations, and Prospectus.* Appl. Opt., 2001. **40**: p. 3969-3983.

28. Lippincott-Schwartz, J., E. Snapp, and A. Kenworthy, *Studying protein dynamics in living cells.* Nat Rev Mol Cell Biol, 2001. **2**(6): p. 444-56.

29. Houtsmuller, A.B., et al., *Action of DNA repair endonuclease ERCC1/XPF in living cells.* Science, 1999. **284**(5416): p. 958-61.

30. Sprague, B.L., et al., *Analysis of Binding Reactions by Fluorescence Recovery after Photobleaching.* Biophys. J., 2004. **86**(6): p. 3473-3495.

31. Carrero, G., et al., *Characterizing fluorescence recovery curves for nuclear proteins undergoing binding events.* Bull Math Biol, 2004. **66**(6): p. 1515-45.

32. Houtsmuller, A.B. and W. Vermeulen, *Macromolecular dynamics in living cell nuclei revealed by fluorescence redistribution after photobleaching.* Histochem Cell Biol, 2001. **115**(1): p. 13-21.

33. White, J. and E. Stelzer, *Photobleaching GFP reveals protein dynamics inside live cells.* Trends in Cell Biology, 1999. **9**(2): p. 61-65.

34. Klonis, N., et al., *Fluorescence photobleaching analysis for the study of cellular dynamics.* Eur Biophys J, 2002. **31**(1): p. 36-51.

35. Houtsmuller, A.B., *Fluorescence Recovery after Photobleaching: Application to Nuclear Proteins*. Advances in Biochemical Engineering/Biotechnology : Microscopy Techniques. Vol. 95/2005. 2005, Berlin / Heidelberg: Springer. 177-199.

36. Mueller, F., P. Wach, and J.G. McNally, *Evidence for a common mode of transcription factor interaction with chromatin as revealed by improved quantitative FRAP.* Biophys J, 2008.

37. de Laat, W.L., N.G.J. Jaspers, and J.H.J. Hoeijmakers, *Molecular mechanism of nucleotide excision repair.* Genes Dev., 1999. **13**(7): p. 768-785.

38. Araujo, S.J., et al., *Nucleotide excision repair of DNA with recombinant human proteins: definition of the minimal set of factors, active forms of TFIIH, and modulation by CAK.* Genes Dev., 2000. **14**(3): p. 349-359.

39. de Boer, J. and J.H. Hoeijmakers, *Nucleotide excision repair and human syndromes.* Carcinogenesis, 2000. **21**(3): p. 453-60.

40. Schärer, O.D., *Chemistry and Biology of DNA Repair.* Angewandte Chemie International Edition, 2003. **42**(26): p. 2946-2974.

41. Volker, M., et al., *Sequential Assembly of the Nucleotide Excision Repair Factors In Vivo.* Molecular Cell, 2001. **8**(1): p. 213-224.

42. Mone, *In vivo dynamics of chromatin-associated complex formation in mammalian nucleotide excision repair.* Proc Natl Acad Sci U S A, 2004.

43. Zotter, A., et al., *Recruitment of the Nucleotide Excision Repair Endonuclease XPG to Sites of UV-induced DNA Damage Depends on Functional TFIIH.* Mol. Cell. Biol., 2006: p. MCB.00695-06.

44. Rademakers, S., et al., *Xeroderma pigmentosum group A protein loads as a separate factor onto DNA lesions.* Mol Cell Biol, 2003. **23**(16): p. 5755-67.

45. Cubitt, A.B., et al., *Understanding, improving and using green fluorescent proteins.* Trends in Biochemical Sciences, 1995. **20**(11): p. 448-455.

46. Vermeulen W, S.R., Rodgers S, Muller HJ, Cole J, Arlett CF, Kleijer WJ, Bootsma D, Hoeijmakers JH, Weeda G, *Clinical heterogeneity within xeroderma pigmentosum associated with mutations in the DNA repair and transcription gene ERCC3.* Am J Hum Genet., 1994. **, 54**(2): p. 191-200.

47. Segers-Nolten, G.M.J., et al., *Scanning confocal fluorescence microscopy for single molecule analysis of nucleotide excision repair complexes 10.1093/nar/gkf599.* Nucl. Acids Res., 2002. **30**(21): p. 4720-4727.

48. Brock, R. and T.M. Jovin, *Fluorescence correlation microscopy (FCM)-fluorescence correlation spectroscopy (FCS) taken into the cell.* Cell Mol Biol (Noisy-le-grand), 1998. **44**(5): p. 847-56.

49. Brock, R., et al., *Rapid characterization of green fluorescent protein fusion proteins on the molecular and cellular level by fluorescence correlation microscopy 10.1073/pnas.96.18.10123.* PNAS, 1999. **96**(18): p. 10123-10128.

50. Schwille, P., J. Korlach, and W.W. Webb, *Fluorescence correlation spectroscopy with single-molecule sensitivity on cell and model membranes.* Cytometry, 1999. **36**(3): p. 176-82.

51. Gennerich, A. and D. Schild, *Fluorescence correlation spectroscopy in small cytosolic compartments depends critically on the diffusion model used.* Biophys J, 2000. **79**(6): p. 3294-306.

52. Wachsmuth, M., W. Waldeck, and J. Langowski, *Anomalous diffusion of fluorescent probes inside living cell nuclei investigated by spatially-resolved fluorescence correlation spectroscopy.* J Mol Biol, 2000. **298**(4): p. 677-89.

53. Widengren, J., Ü. Mets, and R. Rigler, *Fluorescence correlation spectroscopy of triplet states in solution: A theoretical and experimental study.* J. Phys. Chem., 1995. **99**: p. 13368-13379.

54. Schwille, P., et al., *Molecular dynamics in living cells observed by fluorescence correlation spectroscopy with one- and two-photon excitation.* Biophys J, 1999. **77**(4): p. 2251-65.

55. Bacia, K. and P. Schwille, *A dynamic view of cellular processes by in vivo fluorescence auto- and cross-correlation spectroscopy.* Methods, 2003. **29**(1): p. 74-85.

56. Rusu, L., et al., *Fluorescence Correlation Spectroscopy Studies of Peptide and Protein Binding to Phospholipid Vesicles 10.1529/biophysj.104.039958.* Biophys. J., 2004. **87**(2): p. 1044-1053.

57. Hess, S.T. and W.W. Webb, *Focal Volume Optics and Experimental Artifacts in Confocal Fluorescence Correlation Spectroscopy.* Biophys. J., 2002. **83**(4): p. 2300-2317.

58. Feder, T.J., et al., *Constrained diffusion or immobile fraction on cell surfaces: a new interpretation.* Biophys J, 1996. **70**(6): p. 2767-73.

59. Wolf, D.E. and M. Edidin, *Methods of measuring diffusion and mobility of molecules in surface membranes*, in *Techniques in Cellular Physiology*, P. Baker, Editor. 1981, Elsevier/North Holland Biomedical Press: Amsterdam. p. 1-14.

60. Carrero, G., et al., *Using FRAP and mathematical modeling to determine the in vivo kinetics of nuclear proteins.* Methods, 2003. **29**(1): p. 14-28.

61. Hoogstraten, D., et al., *Versatile DNA damage probing by the global genome nucleotide excision repair protein XPC.* in preparation.

62. Araki, M., et al., *Centrosome protein centrin 2/caltractin 1 is part of the xeroderma pigmentosum group C complex that initiates global genome nucleotide excision repair.* J Biol Chem, 2001. **276**(22): p. 18665-72.

63. Giglia-Mari, G., et al., *A new, tenth subunit of TFIIH is responsible for the DNA repair syndrome trichothiodystrophy group A.* Nat Genet, 2004. **36**(7): p. 714-9.

64. Riedl, T., F. Hanaoka, and J.-M. Egly, *The comings and goings of nucleotide excision repair factors on damaged DNA.* EMBO J., 2003. **22**(19): p. 5293-5303.

65. Wang, Z., et al., *Transcription factor b (TFIIH) is required during nucleotide-excision repair in yeast.* Nature, 1994. **368**(6466): p. 74-6.

66. Van Vuuren, A.J., et al., *Correction of xeroderma pigmentosum repair defect by basal transcription factor BTF2 (TFIIH).* EMBO J., 1994. **13**(7): p. 1645-1653.

67. Iben, S., et al., *TFIIH Plays an Essential Role in RNA Polymerase I Transcription.* Cell, 2002. **109**(3): p. 297-306.

Chapter

4

Recruitment of the Nucleotide Excision Repair Endonuclease XPG to Sites of UV-induced DNA Damage Depends on Functional TFIIH

Recruitment of the Nucleotide Excision Repair Endonuclease XPG to Sites of UV-induced DNA Damage Depends on Functional TFIIH

Angelika Zotter [1] [#], Martijn S. Luijsterburg [2] [#], Daniël O. Warmerdam [2], Shehu Ibrahim [1,3], Alex Nigg [3], Wiggert A. van Cappellen[4], Jan H. J. Hoeijmakers[1], Roel van Driel [2], Wim Vermeulen [1] [*] and Adriaan B. Houtsmuller [3]

[#] Authors contributed equally to this work

[1] Department of Cell Biology and Genetics, Erasmus MC Rotterdam, P.O. box 2040, 3000 CA Rotterdam, The Netherlands.

[2] Swammerdam institute for life sciences, BioCentrum Amsterdam, University of Amsterdam, Kruislaan 318, 1098 SM Amsterdam, The Netherlands.

[3] Department of Pathology, Josephine Nefkens Institute, Erasmus MC Rotterdam, P.O. box 2040, 3000 CA Rotterdam, The Netherlands.

[4] Department of Endocrinology and Reproduction, Erasmus MC Rotterdam, P.O. box 2040, 3000 CA Rotterdam, The Netherlands.

*Corresponding author: Phone: (+31) 10 4087194, Fax: (+31) 10 4089468
email: w.vermeulen@erasmusmc.nl

Abstract

The structure-specific endonuclease XPG is an indispensable core protein of the nucleotide excision repair (NER) machinery. XPG cleaves the DNA strand at the 3' side of the DNA damage. XPG binding stabilizes the NER pre-incision complex and is essential for the 5' incision by the ERCC1/XPF endonuclease. We have studied the dynamic role of XPG in its different cellular functions in living cells. We have created mammalian cell lines that lack functional endogenous XPG and stably express eGFP-tagged XPG. Life cell imaging shows that in undamaged cells XPG-eGFP is uniformly distributed throughout the cell nucleus, diffuses freely and is not stably associated with other nuclear proteins. XPG is recruited to UV-damaged DNA with a $t_{0.5}$ of 200 s and is

bound for 4 min in NER complexes. Recruitment requires functional TFIIH, although some TFIIH mutants allow slow XPG recruitment. Remarkably, binding of XPG to damaged DNA does not require the DDB2 protein, which is thought to enhance damage recognition by NER factor XPC. Together, our data present a comprehensive view of the *in vivo* behaviour of a protein that is involved in a complex chromatin associated process.

Introduction

Nucleotide excision repair (NER) is a versatile DNA repair mechanism that removes different types of helix-distorting damage from the genome, including UV light-induced DNA damage, such as cyclobutane pyrimidine dimers (CPD) and 6-4 photoproducts (6-4 PP) (10, 22). The severe clinical features of three photo-hypersensitive hereditary NER disorders underscore its biological importance: the cancer-prone syndrome xeroderma pigmentosum (XP), the neuro-developmental conditions Cockayne syndrome (CS) and trichothiodystrophy (TTD) (28). The multi-step NER process requires the coordinated actions of at least 25 polypeptides (11). The general *modus operandi* for NER comprises the following steps: 1) recognition of DNA damage, 2) unwinding around the lesion, 3) dual incision on both sides of the damage, 4) removal of the excised oligonucleotide, and 5) filling the generated gap by DNA polymerase and ligase (5). Two different modes of NER exist, i.e. transcription-coupled NER (TC-NER) and global genome NER (GG-NER) (21). TC-NER removes lesions exclusively from the transcribed strand of active genes, whereas GG-NER repairs damage at any other position in the genome. GG-NER protects against damage-induced mutagenesis and can thus be considered a cancer-preventing process, whereas TC-NER primarily promotes cellular survival and therefore may counteract aging (30). The damage sensor for 6-4 PP in GG-NER is the heterotrimeric XPC/HR23B/centrin2 complex (48, 60). In addition, the UV-damaged DNA binding protein (UV-DDB) assists XPC in the recognition of CPD (9, 61) and facilitates 6-4 PP repair (33). In TC-NER lesions are detected by stalled elongating RNA polymerase II (54). After lesion-detection the two NER sub-pathways funnel into a common mechanism. Damage sensing is followed by the recruitment of the ten-subunit TFIIH complex (13), which utilizes its helicase components XPB and XPD to locally unwind the DNA around the lesion. The structure-specific endonuclease XPG subsequently binds and promotes formation of an open DNA complex around the lesion (8). The next proteins that bind to the repair

complex are the single-stranded DNA (ssDNA) binding Replication Protein A (RPA) and the damage verification factor XPA, which play an important role in the correct positioning of the 3' endonuclease XPG and the 5' endonuclease ERCC1/XPF (4). After dual incision a stretch of ~30 nucleotides ssDNA containing the damage is released, after which the replication factors RPA, PCNA and DNA polymerase δ/ε fill in the resulting gap (45). In the last step the newly synthesized DNA is sealed by DNA ligase I and the original chromatin structure is restored by chromatin assembly factor I (CAF I) (15).

In vitro studies have resulted in a number of models for the assembly of the NER complex onto damaged DNA, proposing a completely pre-assembled holo-complex (50), a partly pre-assembled NER complexes (16-19)(Mu, 1997, and the sequential assembly of individual NER factors, assuming conflicting assembly sequences (41, 48, 62, 63). Assembly studies in intact cultured cells using locally damaged nuclei support the sequential assembly scenario (60). We have previously studied the *in vivo* kinetics of the NER components ERCC1/XPF (24, 31), TFIIH (23, 31), XPA (40), XPC (38), and CSB (54). Together, these studies culminate to a model in which NER factors move freely throughout the nucleus and are incorporated one-by-one into repair complexes after the induction of DNA damage. However, the above-mentioned studies could not unambiguously identify the precise role of XPG, including at what stage the protein is incorporated in the NER complex. Therefore, we have carried out a comprehensive *in vivo* analysis of the behaviour of XPG in DNA repair.

Results

Generation of cell lines stably expressing functional XPG-eGFP

To study the nuclear distribution and dynamics of the XPG protein in living cells we tagged the protein with enhanced green fluorescent protein (eGFP). eGFP was fused to the carboxy-terminus of human XPG (Fig. 1A), resulting in an XPG-eGFP fusion protein, which was stably expressed in XPG-deficient human fibroblasts (XPCS1RO-Sv) and in Chinese Hamster Ovary cells (UV135). Fluorescently tagged XPG is predominantly located in the nucleus of both cell types in which it is uniformly distributed, with nucleoli being less populated (Fig. 1B). These observations are in accordance with earlier findings for fixed cells (6, 53, 60). Immuno-blot analysis of whole cell extracts of both cell types, using anti-XPG antibodies, showed that XPG-eGFP migrates in SDS-

PAGE with a mobility corresponding to the expected size of the full-length fusion protein (~180 kDa, Fig. 1C (36)). Labelling with anti-eGFP antibodies did not reveal the presence of any other GFP-containing polypeptides in the crude extracts (data not shown). This implies that all microscopy-based studies in this paper truly reflect the behaviour of XPG-eGFP. The Western blot in Fig. 1C indicates that XPG-eGFP is expressed at about the same level as endogenous XPG in wild type (HeLa) cells. Importantly, XPG-eGFP was able to restore normal UV-sensitivity of XP-G cells (Fig. 1D), showing that the fusion protein is functional in NER when expressed at physiologically levels.
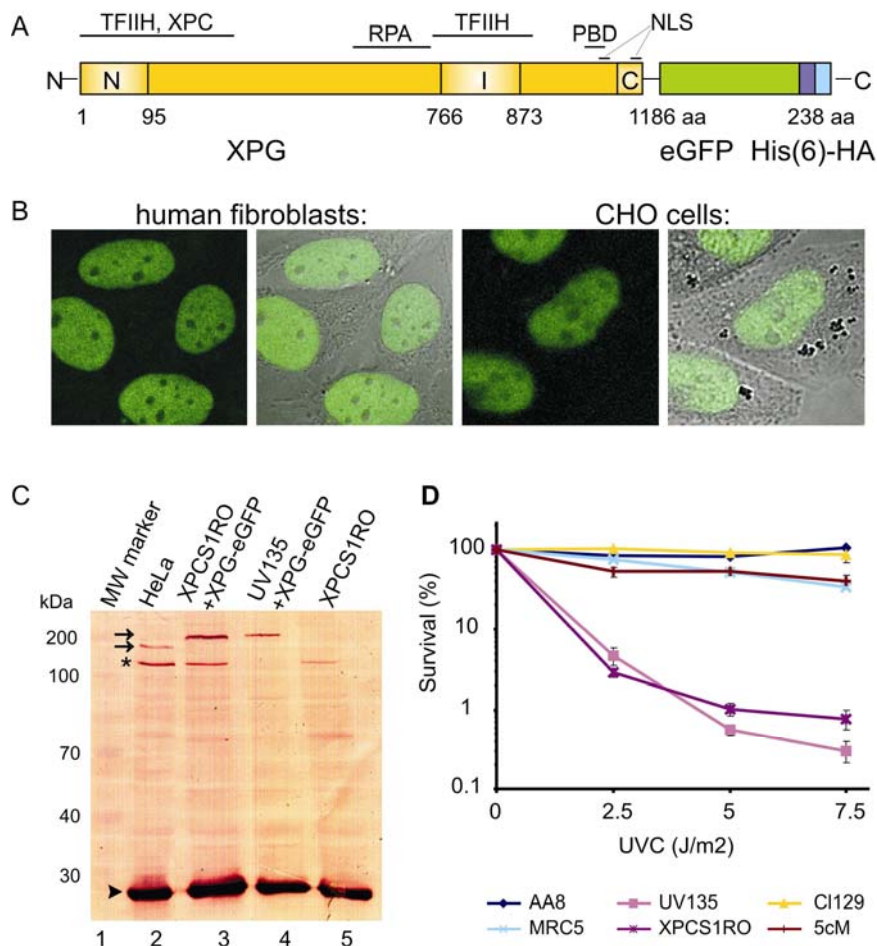
Fig. 1. Expression and functionality of XPG-eGFP. (A) Schematic representation of the XPG-eGFP-His(9)-HA fusion gene with the N-terminal and C-terminal nuclease domains (N and C, respectively) and different interaction domains indicated. I, Internal domain; PBD, PCNA binding domain; NLS, probable

nuclear localization signal; aa, amino acids. (B) Localization of the XPG fusion protein in human fibroblasts (left two images, showing the fluorescence signal and an overlay of fluorescence and phase contrast) and CHO cells (right two images). XPG-eGFP is present mainly in the nucleus, except in the nucleoli. (C) Immuno-blot, probed with monoclonal anti-XPG, of 40 µg of whole-cell extract from HeLa (lane 2), human XPCS1RO-Sv (XP-G) expressing XPG-eGFP (lane 3), CHO (UV135) cells expressing XPG-eGFP (lane 4) and untransfected XPCS1RO-Sv (lane 5). The molecular mass of protein markers is indicated in kilodaltons (kDa). eGFP-tagged XPG migrates slower than endogenous XPG (upper and lower arrow, respectively). No XPG protein was detected in the human fibroblasts in which the severely truncated XPG-mRNA is probably highly unstable or not recognized. Chinese hamster XPG cannot be detected with our anti-XPG serum. Loading control: PCNA (arrowhead), asterisk indicates cross-reacting non-specific band only present in human cell extracts. (D) UV-survival of repair-proficient human MRC5 cells (wild type; light blue line), XPCS1RO cells (violet line), XPCS1RO cells stably expressing XPG-eGFP (clone 5cM; brown line), wild type CHO cells (AA8; dark blue line), XPG-deficient CHO cells (UV135; purple line), and UV135 cells expressing XPG-eGFP (clone 129; yellow line). The transfected cell lines show a correction of UV sensitivity to the wild type level.
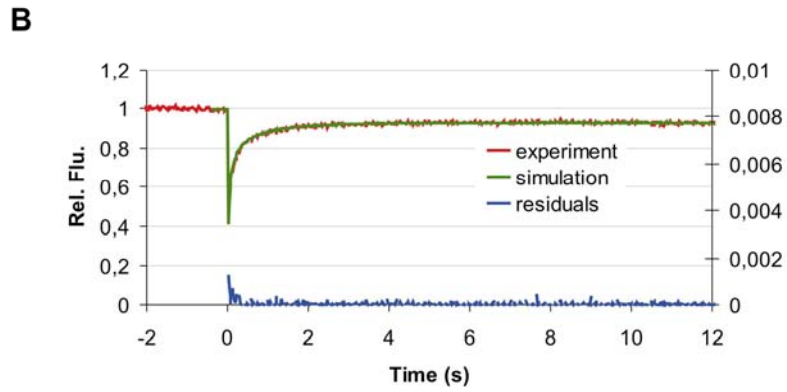
Mobility of XPG-eGFP in the nucleus

XPG has been reported to interact with other DNA repair proteins and with transcription factors and might therefore be part of a larger protein complex (42). To investigate whether XPG either moves freely through the nucleoplasm, is part of a larger complex, or is bound to immobile nuclear structures, we used FRAP (Fluorescence Recovery after Photo-bleaching; Fig. 2A). XPG-eGFP molecules in a specific nuclear region are bleached by a short light pulse, followed by monitoring the kinetics and extent of recovery of fluorescence due to the diffusion of non-bleached XPG-eGFP molecules into the bleached area. In non-UV irradiated living cells, monitored at 37°C, essentially all XPG-eGFP was mobile. The same redistribution kinetics were found for XPG-eGFP in CHO cells (Fig. 2B) and in human fibroblasts (Fig. 2C), indicating that XPG-eGFP mobility is independent of cell type and organism. Curve fitting shows that the effective diffusion coefficients (D_{eff}) of XPG-eGFP in CHO cells and human fibroblasts are very similar, i.e. 6.1 ± 1.5 µm^2/s and 4.0 ± 0.8 µm^2/s, respectively (Fig. 2B and 2C). These diffusion coefficients were significantly different than other NER-GFP fusions (XPA, TFIIH) tested in parallel (A. Zotter unpublished data and (23, 40)). Using combined FLIP and FRAP (23) we showed that the mobility of XPG is the same at 27° and 37°C (Fig 2D). Similar results have been obtained for other NER factors (24, 40), except for TFIIH (23) in which temperature-sensitive mobility was thought to be due to binding to transcription complexes. Together, this indicates that XPG in undamaged cells is not

part of a larger complex, e.g. with TFIIH as has been suggested elsewhere (1, 19), and does not interact with immobile nuclear components, such as chromatin.

A pre-bleach | 1s post bleach | 2s post bleach | 6s post bleach

FRAP XPG CHO
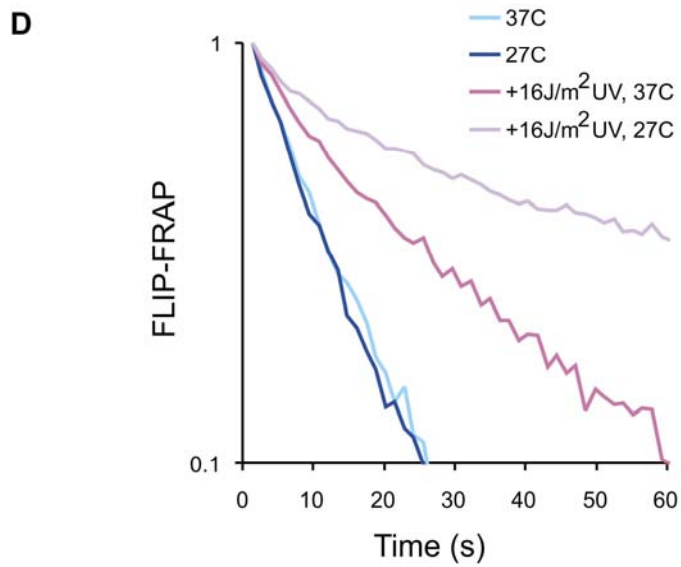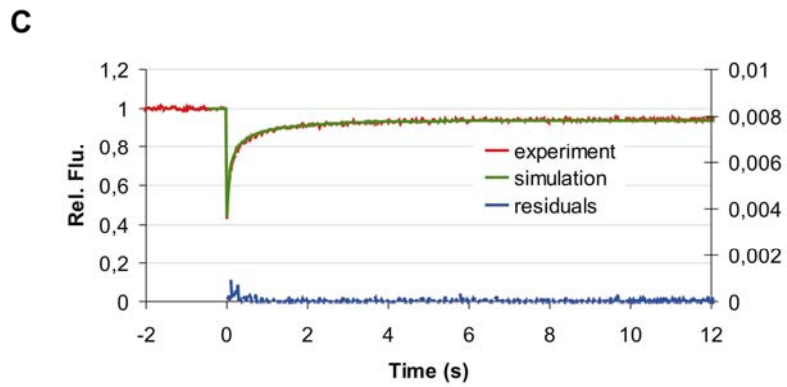
B

FRAP XPG human

C

D
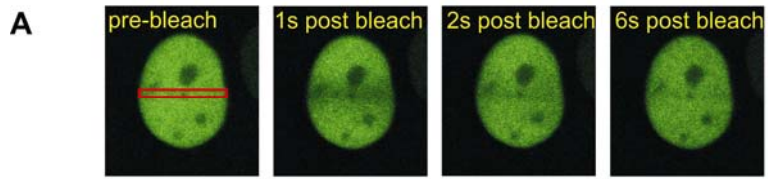
Fig. 2. FRAP analysis of XPG mobility. (A) Example of FRAP analysis to determine effective diffusion coefficients in non UV-irradiated cells. A strip (red rectangle) spanning the nucleus containing eGFP-tagged protein is bleached at high laser intensity. Subsequently, fluorescence recovery after photobleaching is monitored in the strip. (B-C) Graphical representation of FRAP analysis of eGFP-XPG in non-UV irradiated CHO cells (B) and human fibroblasts (C), the mean relative fluorescence (flu. after bleaching/flu. before bleaching) is plotted against the indicated time in seconds. Red lines: experimental data; green lines: simulated curves; blue lines at the bottom of each graph represent residuals which are a measure for the quality of the fits. (D) Simultaneous FLIP/FRAP analysis of XPG mobility in the nucleus of CHO cells. A small area at one pole of the nucleus is bleached for 1 s, subsequently fluorescence is monitored in time in the bleached (FRAP) and unbleached area (FLIP). The difference in eGFP intensity between the two areas after the bleach pulse is plotted on a log scale as a function of time. Light blue line, XPG redistribution at 37°C; dark blue line, XPG redistribution at 27°C; purple line, XPG redistribution in UV irradiated cells at 37°C; violet line, XPG redistribution in UV irradiated cells at 27°C. Experiments on UV-irradiated cells were performed between 10 min and 30 min after global UV-C irradiation.

In vivo assembly of XPG-eGFP into the NER complex

Analysis of the *in vivo* kinetics of NER complex assembly has shown that incorporation of TFIIH and ERCC1/XPF into the pre-incision complex is not diffusion-limited (31). Association of the ERCC1/XPF incision factor depended on the presence of functional TFIIH (31). To determine how XPG-eGFP is incorporated into the repair complex *in vivo*, we analysed its recruitment kinetics in nuclei that had been locally UV-irradiated (Fig 3A, (31)). XPG-eGFP accumulation in the damaged area reached a plateau after about 10 min (Fig 3B). This plateau reflects a pseudo steady state in which DNA repair takes place at a constant rate and the number of XPG molecules that are incorporated into repair complexes per unit time equals the number of molecules that are released after a repair event. The rate of incorporation of XPG-eGFP was the same in CHO cells and in human fibroblasts, with a $t_{0.5}$ of ~200s for both cell types (Fig 3B). This shows that the absence of the DDB2 subunit of the UV-DDB protein in CHO cells has no effect on the kinetics of incorporation of XPG in NER complexes that assemble on UV-damaged DNA. To investigate the role of DDB2 more directly, we transfected CHO cells that stably express XPG-eGFP transiently with DDB2 fused to the red fluorescent protein mCherry (44). Subsequently, binding of XPG-eGFP was measured in cells that also expressed DDB2-mCherry. The rate of incorporation of XPG-eGFP was the same in transfected and non-transfected cells, i.e. with and without expression of DDB2 (Fig 3B). Our experiments show that DDB2 does not changes the incorporation kinetics of XPG into the NER pre-incision complex.
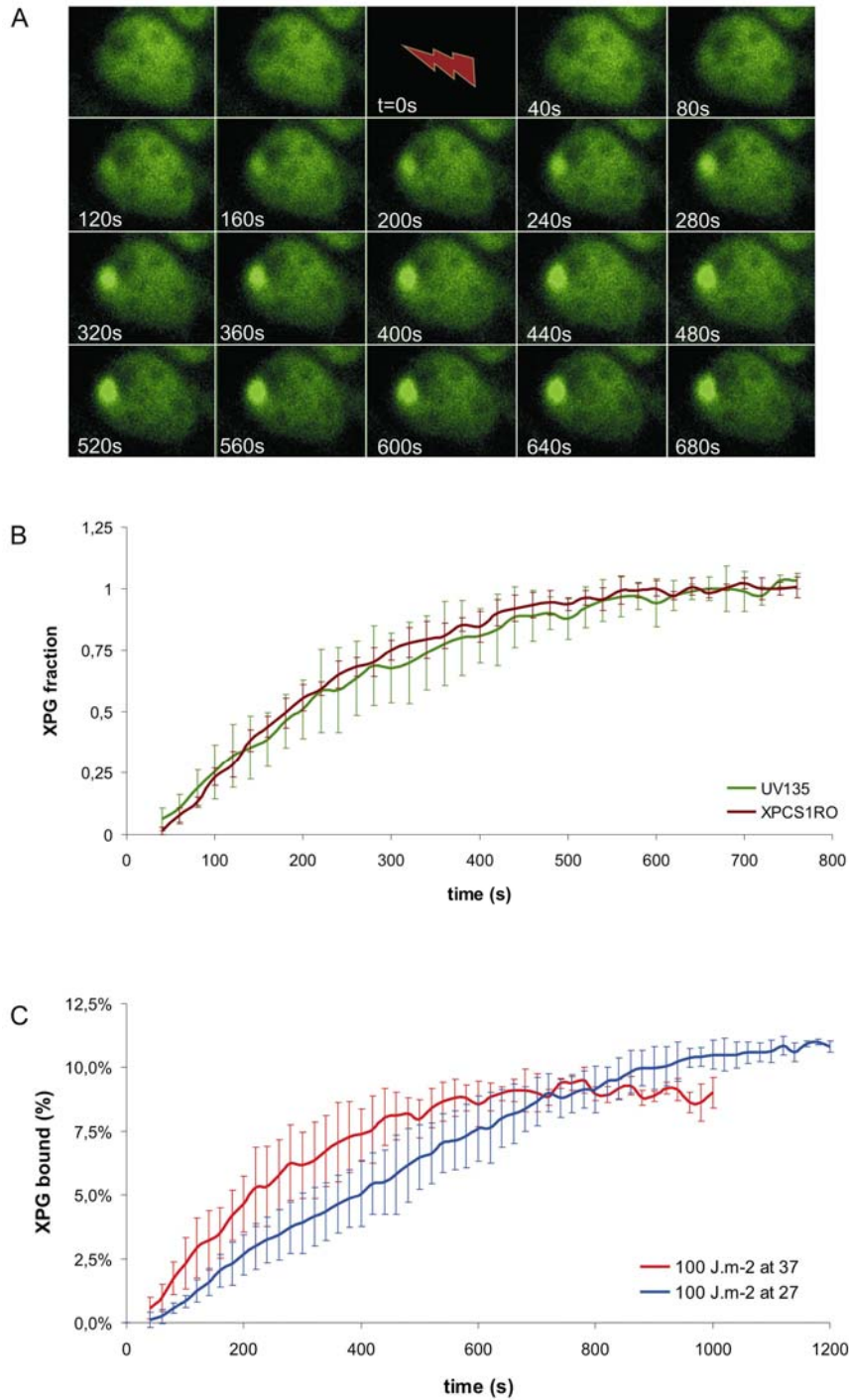
Fig. 3. Accumulation of XPG-eGFP after local UV-DNA damage. (A) Time-lapse series of XPG-eGFP expressed in CHO UV135 cells prior and immediately after UV-C irradiation (100 J/m^2). After taking pre-irradiation images cells were irradiated for 39s (lightning arrow), subsequently images were taken with 20s interval. (B) Incorporation kinetics of XPG-eGFP in CHO cells (UV135 – green line, n=5), CHO cells transfected with DDB2-mCherry (UV135 + DDB2 – red line, n=5) and human fibroblasts (XPCS1RO – blue

line, n=5) at UV-damaged areas after 100 J/m^2 UV-C. The local relative accumulation of XPG-eGFP was measured versus time. (C) Incorporation kinetics of XPG-eGFP in UV135 cells at 37°C (red line, n=5) and 27°C (blue line, n=5). The local accumulation of XPG-eGFP was measured and plotted as a percentage of the total eGFP fluorescence of the cell nucleus (37°C n=11, 27°C n=20) versus time after start of UV irradiation. Error bars represent SD between different experiments.

Binding of XPG depends on the presence of functional TFIIH

The rate of binding of XPG-eGFP to the nascent NER complex is temperature-dependent. The initial rate of XPG-eGFP incorporation at 37°C is about 1.5%/min and at 27°C about 0.5%/min (Fig 3C). Analogous to previous studies of the *in vivo* kinetics of incorporation of ERCC1/XPF it is likely that the temperature-dependent step in NER complex formation is the DNA unwinding process, catalysed by the helicase activity of TFIIH (43). Previous studies, using fixed cells and *in vitro* NER assembly, were not conclusive about the question whether XPG incorporation required functional TFIIH (6, 41, 53). To determine whether XPG binding depends on functional TFIIH, we measured the UV-induced accumulation of XPG (using a specific antibody) at different time points after local UV-irradiation in various cell lines mutated in the TFIIH helicases XPB or XPD (Table 1) and in wild-type cells. Accumulation of XPG, measured 10 min after local UV-induced DNA damage, was strongly reduced in all TFIIH mutants tested, in comparison to wild type cells. In contrast, XPC, which binds to DNA damage before TFIIH, accumulated normally in all mutants (Fig. 4). However, some XPG accumulation was observed in all mutant TFIIH cell lines 30 min after local UV damage, except in TTD cells (Fig. 4). These results show that functional TFIIH is required for normal XPG binding. However, several TFIIH mutants still support what seems a slow or limited XPG incorporation in the NER complex.

Table 1. Human cell-lines used for local damage induction.

Cell strain	TFIIH mutation	Affected function	Syndrome	Reference
C5RO	none		wild type	
XPCS1BA	F99S in XPB	unknown	mild XP/CS	(57)
XP131MA	frame-shift 742 in XPB	helicase activity	XP/CS	(8)
XP6BE	R638W in XPD	p44 interaction	XP	(39)
XPCS2	G602D in XPD	helicase activity	XP	(58)
TTD1BEL	R722W in XPD	p44 interaction	TTD	(52)
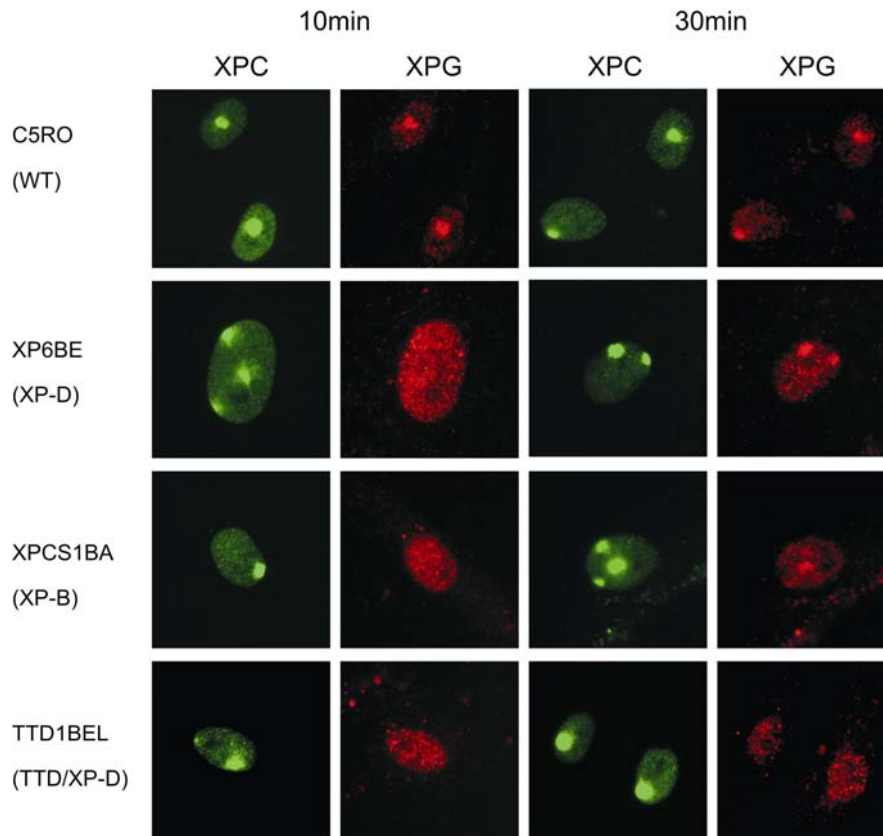
Fig. 4. **Accumulation of XPC and XPG after local UV-damage in human wild-type cells (C5RO) and various TFIIH mutants:** 10 min (columns 1 and 2) and 30 min after UV-irradiation (columns 3 and 4). Columns 1 and 3, immunofluorescence labelling with anti-XPC antibody (green); columns 2 and 4, labelling with anti-XPG antibody (red).

XPG-eGFP is transiently immobilized by UV-damaged DNA

In addition to the binding (i.e. pre-steady state) kinetics of XPG-eGFP into the nascent NER complex, we have analysed the steady state kinetics and the nuclear redistribution after UV damage. Different UV-C doses have been employed, i.e. 2, 4, 8, and 16 J/m^2. Whole cell exposure to UV-light induces a uniform distribution of DNA lesions in the nucleus. This did not result in a detectable redistribution of XPG-eGFP, in contrast to the study by Park *et al.* that reported the formation of XPG foci upon UV irradiation in fixed cells (37). However, these XPG foci could be the result of the fixation procedure. FRAP analyses performed between 10 and 45 min after UV-treatment (when incorporation of XPG is in steady state), showed incomplete fluorescence recovery in human fibroblasts

and in CHO cells within the time frame of 8 seconds after photobleaching (Fig. 5A and 5B, compare to untreated cells). This indicates that maximally 20-30% of the XPG-eGFP molecules are immobile. The mobility of unbound XPG-eGFP did not change upon UV irradiation, as shown by the recovery plots of Fig. 5C and 5D. This demonstrates that the XPG molecules that do not participate in NER have the same mobility and therefore the same molecular size before and after UV irradiation. Similar to other NER factors (23, 24, 40) we conclude that the observed immobilization of XPG-eGFP reflects its incorporation in the NER complex.

Despite exhibiting similar total cellular fluorescence intensities (representing the expression levels of XPG-eGFP), human fibroblasts showed less XPG-eGFP immobilization at a NER-saturating UV dose than CHO cells, i.e. 20% and 30%, respectively (Fig. 5E and 5F). Furthermore, a quantitatively different response to UV-dose was observed for both cell types. While in human cells a larger fraction of the XPG-eGFP molecules was immobilized at low UV-doses (saturating at 8J/m^2) CHO cells show a significant increase in immobilized XPG-eGFP up to 16J/m^2 (Fig. 5E and 5F). This shows that the fraction of immobilized XPG-eGFP of the total cellular amount of XPG is different in both cell types. This is probably due to the fact that the concentration of other NER factors is different. If cells were cultured at 27°C instead of at 37°C, a significantly larger fraction of XPG-eGFP was immobilized at the same UV dose in both cell lines (Fig. 5E and 5F), indicating that at any given time point more XPG-eGFP molecules participate in NER events. Combined FRAP and FLIP at 27°C instead of 37°C, confirmed a decrease in mobility of XPG-eGFP after UV-irradiation (Fig 2D). This implies that the dissociation of XPG-eGFP from the NER complex (presumably after dual incision) is temperature-dependent, resulting in a longer residence time at lower temperature and thus increased immobilization.

In addition to a role in NER, XPG has been shown to be involved in base excision repair of oxidative DNA lesions *in vitro* (26). To investigate a possible role of XPG in BER *in vivo* we treated cells with ionising radiation or paraquat. Both procedures induce oxidative lesions that are removed by BER. After treatment with these agents, we did not observe increased immobilization of XPG-eGFP (data not shown), suggesting that XPG does not play a major role in BER. However, we cannot rule out that the number of lesions introduced by these procedures is too low to detect changes in XPG-eGFP immobilization or that the kinetics of XPG in BER are different and do not result in

detectable immobilization of XPG. Besides a role in BER, it has been suggested that XPG associates with transcription bubbles containing stalled RNAPII molecules together
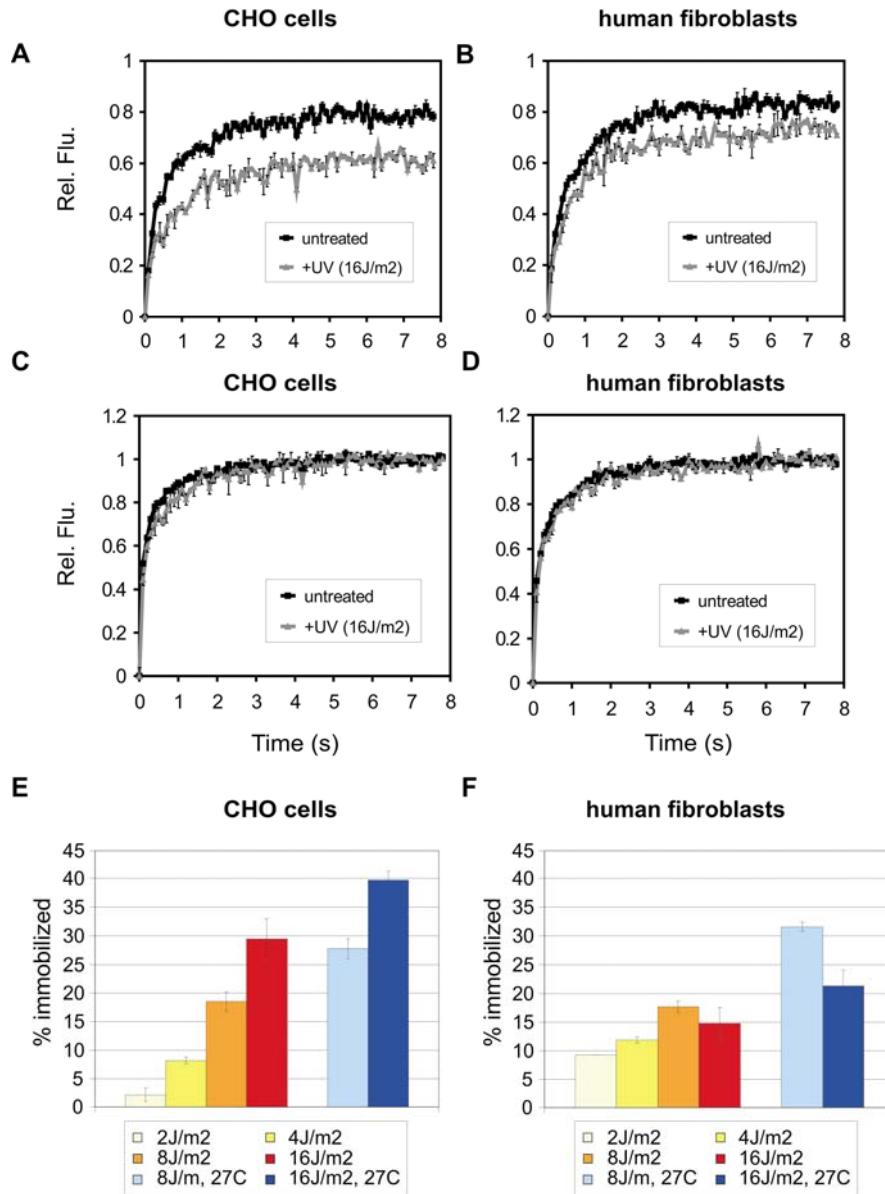

Fig. 5. FRAP analysis of UV-treated and untreated cells to visualize DNA damage-dependent immobilization of XPG-eGFP. (A, B) FRAP recovery curves (normalized to pre-bleach intensity set to one) in CHO cells and human fibroblasts, respectively. Black curves: XPG-eGFP recovery in untreated cells (as a reference); grey curves: recovery in UV irradiated cells. (C, D) FRAP recovery curves (normalized to maximum recovery post-bleach set to one) of XPG-eGFP in CHO cells and human fibroblasts, respectively. Black curves: XPG recovery in untreated cells (as a reference); grey curves: recovery in UV irradiated cells.

(E, F) Immobilized XPG-eGFP fractions in CHO cells and human fibroblasts, respectively, in response to different UV doses. Light blue and dark blue bars depict measurements in cells cultured at 27ºC, after 8 and 16J/m2 UV, respectively. Error bars show the standard error of the mean.

with TFIIH and CSB (42). In addition, the *S. cerevisiae* XPG homologue Rad 2 has been shown to be required for RNAPII activity (27). We showed that the mobility of TFIIH, which is involved in RNAPI and RNAPII activity, is affected by treatment with transcription inhibitors (e.g. 5,6-dichloro-1-D-ribofuranosyl benzimid azole or DRB (23, 25)). We did not observe any effect on XPG-eGFP mobility after treatment with DRB (data not shown) and were thus not able to confirm a role of XPG in transcription bubbles *in vivo* (42). It cannot be excluded that the interaction of XPG with transcription bubbles is too transient or involves only a very small fraction of molecules escaping detection.

The residence time of XPG-eGFP in the NER complex is in the order of minutes

To determine the residence time of XPG in a NER complex we applied a FRAP variant on locally damaged cells. Briefly, an elongated area distant from the local damage is bleached. Subsequently, the fluorescence redistribution is monitored (Fig. 6A). The time required to re-establish the pre-irradiation distribution of XPG-eGFP is a measure for the mean residence time of molecules in the NER complex. A new equilibrium between bleached and non-bleached molecules was reached with a $t_{0.9}$ of approximately 3 to 4 minutes. (Fig. 6B), reflecting the residence time of XPG in the NER complex. This value is similar to the measured residence time of other components of the NER complex (23, 24, 40).
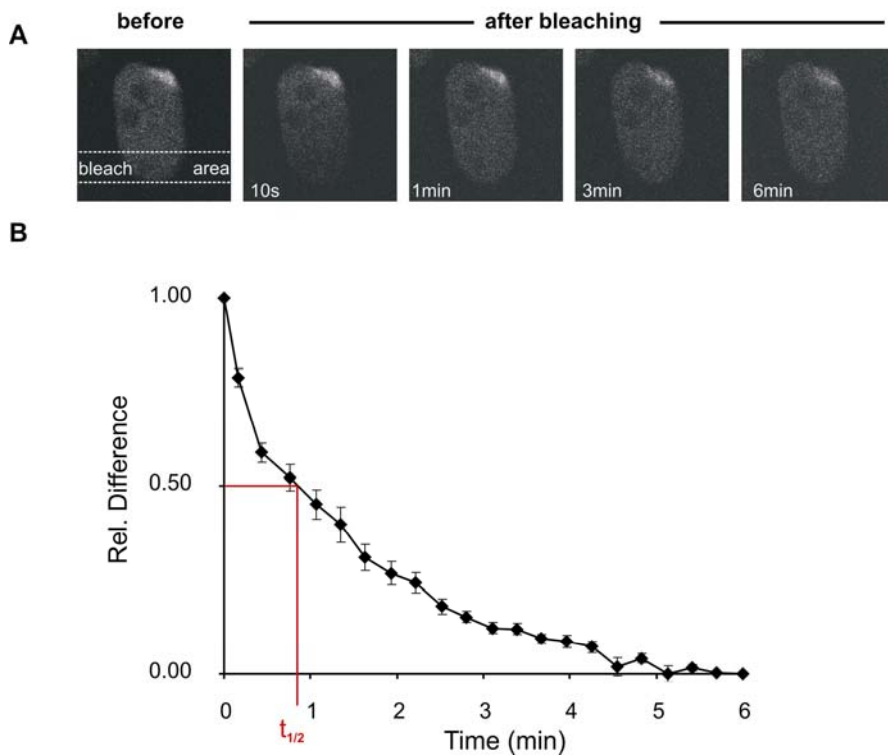
Fig. 6. FLIP analysis of locally UV-damaged areas in the nucleus. (A) A strip opposite a locally damaged area in the nucleus is bleached and the redistribution of bleached and unbleached XPG-eGFP is monitored in time. (B) FLIP curve of the locally damaged nucleus. The relative difference between redistribution in the damaged versus the non-damaged area is plotted in time. Error bars depict the standard error of the mean.

Discussion

The endonuclease XPG is a multi-functional nuclear protein. It plays a central role in nucleotide excision repair (NER) of helix-distorting DNA damage and is thought to be involved in transcription, transcription-coupled repair of non-helix distorting DNA lesions and in base excision repair (BER) (26, 27, 42). In the NER complex XPG carries out the incision at the 3' side of the damage and stabilises the protein complex on the locally unwound DNA (5). In this study we present a comprehensive analysis of the dynamic behaviour of XPG inside the nucleus of living CHO cells and human fibroblasts that do not contain functional endogenous XPG and that stably express human XPG-eGFP at levels similar to endogenous XPG in wild type cells (Fig. 1). Since these cells show normal UV-resistance, the XPG-eGFP is fully functional.

XPG only interacts with NER components on damaged DNA

Evidence has been presented that XPG associates with TFIIH (1, 19, 34). Our FRAP measurements on cells expressing functional XPG-eGFP show that *in vivo* in undamaged cells the majority of the protein is not associated with TFIIH, because of the observed difference in mobility rate and differential dependence of the mobility on temperature. Importantly, also after UV damage the XPG molecules that are not engaged in DNA repair show the same *in vivo* mobility, indicating that XPG only interacts with other nuclear components if it binds to the NER complex that assembles on damaged DNA (Fig. 5). This is supported by the finding that other NER proteins show apparent diffusion rates that are different from what is observed here for XPG-eGFP (14, 23, 24, 40). Moreover, the mobility of TFIIH differs at 27 and 37°C, whereas that of XPG-eGFP is temperature independent (Fig. 2). Also the kinetics of incorporation of these two proteins into the NER complex is different ($t_{0.5}$ of 200 s for XPG and 110 s for TFIIH (Fig. 3 and (31))). The observation that endonuclease XPG does not associate with nuclear components except in the DNA damage-induced NER complex, supports the notion that this protein is only involved in DNA repair.

The dynamics of XPG engagement in NER

After UV-induced DNA damage XPG-eGFP is incorporated into the NER complex with a $t_{0.5}$ of incorporation of about 200 s at 37°C (Fig 3). CHO cells and human fibroblasts show the same assembly rate. This rate of incorporation is somewhat lower than that of XPC and TFIIH ($t_{0.5}$ is 100 and 110 s, respectively (31, 38)) and significantly lower than the 5' endonuclease ERCC1/XPF ($t_{0.5}$ is 65 s (31)). A quantitative model has been proposed that is able to at least partly explain these differences in rates of incorporation (38). After about 5 min, XPG incorporation into NER complexes reaches a steady state. FRAP experiments show that the protein remains incorporated for about 3.5 min (Fig. 6). This is similar to what has been found for XPA (4 to 6 min), TFIIH (4 min) and ERCC1/XPF (4 min) (23, 24, 40) and probably reflects the time required by the NER complex to repair a DNA lesion. XPC has a significantly lower residence time (1-2 min), probably because it leaves the NER complex before repair is complete (Hoogstraten and Vermeulen, unpublished results, (38)) in line with *in vitro* studies (41).

Under steady state condition, at the highest UV doses used here (16 J.m^{-2}), maximally about 30% of the XPG-eGFP molecules are associated with a NER complex

and therefore engaged in NER (Fig. 5). Similar values have been obtained for ERCC1/XPF, XPA and TFIIH (23, 24, 40). These results support a model in which the NER complex assembles from its individuals components on a time scale of minutes, remains intact for 3 to 4 min (maybe except for XPC) during which the actual repair takes place and subsequently dissociates allowing its components to reassemble on another lesion.

Although the dynamic behaviour of XPG is largely the same in CHO cells and in human fibroblasts, a difference is observed in the degree of XPG immobilization under steady state conditions at high UV dose (16 J.m^{-2}). In CHO cells an almost two-fold larger fraction of the XPG-eGFP molecules becomes engaged in NER than observed for human fibroblasts (at 37$^{°}$C 20% and 30%, respectively (Fig 6)). The simplest explanation is that the expression levels of XPG and/or other NER proteins differ in the two cell types. Alternatively, the endogenous truncated, non-functional XPG protein that is present in the human fibroblasts may compete with the functioning of XPG-eGFP, resulting in a lower immobilized fraction. The XPG mutation in CHO UV135 cells is unknown but can be considered a null mutation, since XPG mRNA can hardly be detected in these cells (29).

DDB2 (p48) does not affect the rate of XPG incorporation kinetics

The kinetics of incorporation of XPG into the NER complex and its residence time in the NER complex are the same in CHO cells and in human fibroblasts (Fig. 3, Fig. 6). This is remarkable, since CHO cells lack functional DDB2 (p48), which is a subunit of the UV-DDB complex that is thought to enhance the association of the damage recognition protein XPC with DNA lesions, in particular pyrimidine dimers (33, 49, 51). Since XPC binding precedes incorporation of XPG into the NER complex, it was expected that XPG binding in CHO cells would be slower that in human fibroblasts, which contain endogenous DDB2. Expression of DDB2 in CHO cells did not result in accelerated binding of XPG to UV-induced DNA damage (Fig. 3). These results indicate that UV-DDB does not significantly increase the rate of binding of XPG to UV-damaged DNA.

Recruitment of XPG requires functional TFIIH

Previous experiments showed that the incorporation of core NER factors into the NER complex occurs in a specific sequence (40, 60). However, the precise timing of XPG incorporation could not be established unambiguously. Here we show that incorporation of XPG into the NER complex is temperature-dependent (Fig 3). The same has been found for ERCC1/XPF, whereas binding of TFIIH and XPC are temperature-independent ((31), M.S. Luijsterburg and R. Van Driel, unpublished data). This was interpreted that binding of ERCC1 requires an enzyme activity, i.e. the helicase activity of the TFIIH subunits XPB and XPD (31). Therefore, our data suggests that also XPG binding requires TFIIH helicase activity, indicating that TFIIH binding must precede XPG incorporation. Studies in cell lines that have a mutated *XPB* or *XPD* gene show that impairment of TFIIH function severely affects XPG incorporation into the NER complex (Fig. 4, Table 1).

Comparison of the effect of different TFIIH mutation indicates which parts of the TFIIH molecule are important for XPG binding. XP/TTD cells (47, 55, 56), which carry a C-terminal R722W substitution in XPD (46), exhibit the most severe reduction of XPG recruitment. This suggests that XPD plays an important role in the recruitment of XPG to sites of UV damage in vivo. Recent findings demonstrate that the stability of the TFIIH complex is severely affected in TTD cells (D. Hoogstraten and W. Vermeulen, unpublished data) (2, 13). Therefore, it is conceivable that impaired recruitment of XPG in TTD cells is due to the compromised stability, rather than a direct interaction of XPG with the C-terminus of XPD. A recent study demonstrated that phosphorylation of S751 of XPB controls the 5' incision by ERCC1/XPF, whereas the 3' incision by XPG is unaffected (3). Accordingly, our experiments show that XPG binding is only moderately affected in the XPB mutant, which has a truncated C-terminal domain, lacking the serine 751 residue (Fig. 4). This suggests that another part of the TFIIH complex controls the 3' incision by XPG, possibly the N-terminal PH-fold of p62, which has been shown to interact directly with XPG (12). Nonetheless, our results unambiguously show that stable recruitment of XPG to the pre-incision complex depends on functional TFIIH.

Summarising, our results unfold a consistent and simple picture for the dynamic behaviour of XPG in living CHO cells and human fibroblasts. The protein diffuses freely as a monomer, not showing any prominent interactions other than the nascent NER complex that is formed in UV-damaged cells after binding of XPC and TFIIH. The in vivo

dynamics of the XPG protein are remarkably similar in human cells and Chinese hamster cells, showing that major differences in genetic background hardly affect XPG behaviour.

Materials and Methods

Cell lines.

Cell lines used in this study were simian virus 40 (SV-40)-immortalized human fibroblasts MRC5 (NER-proficient), XPCS1RO (XPG-deficient); HeLa cells (NER-proficient), CHO AA8 (NER-proficient), CHO UV135 (XPG-deficient), 3T3 cells (inducible eGFP expression) and the primary human fibroblasts C5RO (NER-proficient), XPCS1BA (XPB-deficient), XP131MA (XPB-deficient), XP6BE (XPD-deficient), XPCS2 (XPD-deficient) and TTD1BEL (XPD-deficient). All cell lines were cultured in a 1:1 mixture of DMEM/Ham's F10 medium containing Ultra-Glutamine (Cambrex Corporation, New Jersey, USA) supplemented with antibiotics and 10% FCS at 37°C in an atmosphere of 5% CO_2.

Generation of cells expressing XPG-eGFP and construction of DDB2-mCherry.

eGFP-tagged XPG was generated by in-frame ligation of full length human XPG cDNA into a eGFP N1 vector (Clontech Laboratories, California, USA)). This resulted in a fusion gene under control of a cytomegalovirus promoter encoding an XPG-eGFP hybrid polypeptide. The fusion gene was expressed in the XPG-deficient CHO cell line UV135 and the XPG-deficient SV40-transformed human fibroblast cell line, XPCS1RO-Sv (7). After subsequent rounds of selection on the presence of the neomycin resistance gene (by G418-resistance selection) and UV-irradiation (to select for functional XPG expression) stable expressing clones were isolated for each of the cell types. The pDDB2-eYFP (33) plasmid was digested with *AgeI* and *BsrGI* in order to replace the eYFP for mCherry (44) to yield pDDB2-mCherry

Immunoblot analysis and UV survival.

Cell extracts were generated by sonication, separated by sodium dodecyl sulfate polyacrylamide gel (8%) electrophoresis and transferred to nitrocellulose membranes. Expression of the fusion protein was analysed by immunoblotting with a mouse monoclonal anti-XPG antibody (IB5 T.C., 1:100 in PBS/0.05% Tween-20; a gift from Dr.

J.M. Egly), followed by a secondary antibody (goat anti-mouse conjugated with alkaline phosphatase (Biosource International, California, USA) and detection using bromo-4-chloro-3-indolyl phosphate (BCIP) and nitro blue tetrazolium (NBT). As loading control, mouse monoclonal anti-PCNA antibody (Dako, Glostrup, Denmark) at a dilution of 1:1000 was used. For UV-survival experiments, cells were exposed to different UV doses 2 days after seeding. Survival was determined 3 days after UV-irradiation by measuring cell proliferation with the aid of [^{3}H] thymidine pulse-labelling at 37°C, as described previously (20)

Immunofluorescence.

Cells were grown on 24 mm glass coverslips and fixed with 3% paraformaldehyde in PBS with 0.3% Triton X-100 for 20 min at room temperature (RT). Coverslips were washed three times for 10 min with phosphate-buffered saline (PBS) containing 0.1% Triton X-100, and were subsequently incubated for 1 h with PBS containing 1% BSA. Cells were incubated at RT with the primary antibody for 1.5 - 2h in a moist chamber. Subsequently, coverslips were washed three times for 10 min with PBS-Triton X-100 and 5 min with PBS 1% BSA. Incubation with the secondary antibody was for 30 min – 1 h at RT (dark chamber) followed by extensive washing with PBS 1% BSA and finally PBS. Samples were embedded in Vectashield (Vector Laboratories, California, USA) mounting medium containing 0.1 mg of DAPI (4'-6'-diamidino-2-phenylindole) per ml. Primary antibodies used for immunolabeling were: mouse monoclonal antibody against XPG (8H7, Lab Vision Fremont, California, united States, 1:2000), and affinity-purified rabbit monoclonal antibody against XPC (35). Secondary antibody: cy3-conjugated goat anti-mouse antiserum and FITC-conjugated anti-rabbit antiserum (Both from Jackson ImmunoResearch Laboratories, West Grove, Pennsylvania, USA). All antibodies were diluted in PBS containing 0.15% glycine and 0.5% bovine serum albumin. Fluorescence microscopy images were obtained with a Leica DMRBE microscope (Leica Microsystems, Wetzlar, Germany) equipped with epifluorescence optics, a PL-FLUOTAR 100x, 1.3-numerical aperture oil immersion lens and a Hamamatsu (Hamamatsu Photonics, Hamamatsu City, Japan) dual mode cooled CCD camera.

Confocal imaging.

Digital images of eGFP-expressing living cells were obtained using a Zeiss LSM 410 microscope equipped with a 60-mW Ar laser (488 nm) and a 40x, 1.3-numerical aperture oil immersion lens and a Zeiss LSM 510 equipped with a 60-mW Ar laser (488 nm) and a 40x, 1.2-n.a., or 63x Planapochromat, n.a. 1.4, oil immersion lens (Zeiss, Oberkochen, Germany). Both microscopes were equipped with an objective heater. Unless stated otherwise, living cells were examined at 37°C.

UV irradiation.

For induction of global UV DNA damage, cultured cells on coverslips were rinsed with PBS and irradiated with a Phillips TUV lamp (254 nm) at a dose rate of ~0.8 $J/m^2/s$. To induce local UV-damage, cells were UV-irradiated through an polycarbonate filter (Millipore Billerica, Massachusetts, USA) with pores of 5µm diameter, as described previously (32, 60). At indicated time points after filter removal the cells were either microscopically examined, or fixed with 2% paraformaldehyde and further processed for immuno-histochemistry as described above. For kinetic measurements on locally UV-damaged cells that express XPG-eGFP were grown to confluency in glass bottom dishes (MatTek, Ashland, Massachusetts, USA). Local UV-irradiation was performed as described (31). Briefly, a petridish was filled with microscopy medium (137 mM NaCl, 5,4 mM KCl, 1,8 mM $CaCl_2$, 0,8 mM $MgSO_4$, 20 mM D-glucose and 20 mM HEPES) and a small piece of Alcian blue-coated filter (5 µm pores) was sunk onto the cells. A glass ring was carefully placed on top of the filter after which the petridish was sealed with a lid containing a quartz window. The cells were transferred to an Zeiss Axiovert 200 M microscope with a 37° incubator and an objective heater, to ensure the appropriate temperature for this live cell experiment. Subsequently, irradiation was performed using a homemade box, containing four UV lamps (Philips TUV 9W PL-S) above the microscope stage. The UV dose rate was measured to be 3 $W.m^{-2}$ at 254 nm. Cells were irradiated for 39 s, resulting in a UV dose of 100 $J.m^{-2}$

FRAP and fluorescence loss in photobleaching (FLIP).

For all experiments cells were seeded onto 24 mm glass coverslips three days prior to the experiments.

FRAP experiments. Using a Zeiss LSM510 META confocal microscope, equipped with a 60 mW Argon laser and a 40x oil immersion lens (1.2 n.a.), mobility measurements were

performed by FRAP analysis at high time resolution (Strip-FRAP; (23), modified). A strip spanning the nucleus was photo-bleached for 20 ms at 100% laser intensity (120-160µW, argon laser at 488nm). Recovery of fluorescence within the strip was monitored with 20 ms intervals at low laser intensity (450-750nW) to avoid photobleaching by the probe beam. Measurements were performed at 37˚C, using a heated stage with feedback temperature control. Raw data were corrected for background and fluctuations in the monitoring laser power.

Fluorescence Loss in Photobleaching (FLIP). To determine the residence time of XPG at locally UV-irradiated areas local UV irradiation was applied as described above. Using a Zeiss LSM 410 microscope equipped with a 60 mW Argon laser (488 nm) and a 40x, 1.3 n.a. oil immersion lens, a strip was bleached (at 100% 488 nm) for 5 s near the edge of the nucleus opposite to the local damage site. Redistribution of fluorescence was monitored over time (at 488 nm). Evaluation was performed by comparing the loss of fluorescence of bound protein over time (in local damaged area) versus non-bound protein (outside the damaged area) of eGFP-tagged protein. The residence time of XPG in a NER complex was calculated as described elsewhere (24)

Combined FLIP-FRAP analysis. Using a Zeiss LSM510 META confocal microscope, equipped with a 60-mW Argon laser and a 40x oil immersion lens (1.2 n.a.), a 2 µm (30-pixel) strip spanning the cell nucleus at one pole was bleached for 1s at a laser power of 120-160 µW. Redistribution of fluorescence throughout the nucleus was recorded at low laser power (1.6-1.9 µW), keeping monitoring bleaching to a minimum (<5 %). We compared the difference between the fluorescence in the bleached and the unbleached area (at a distance of 150 pixels = 10.2 µm) of the nucleus, and plotted the fluorescence values against time. Unless otherwise specified, measurements were performed at 37˚C, using a heated stage with feedback temperature control. At least 9 independent measurements were averaged to form a single mobility curve. Redistribution of fluorescence was corrected for lateral cell movement. Rotating cells, or cells moving out of focus were excluded from evaluation.

FRAP analysis

For analysis of FRAP data, FRAP curves were normalized to pre-bleach values and the best fitting curve (least squares) was picked from a large set of computer simulated FRAP curves in which three parameters representing mobility properties were

varied: diffusion rate (ranging from 0.04 to 25 μm^2/s), immobile fraction (0, 10, 20, 30, 40, 50 %) and time spent in immobile states, ranging from very short residence times (0.02, 0.04, 0.08, …, 1 s) to relatively long residence times (2, 4, 8, 16, 32, 64, 128, ∞ s). Monte Carlo computer simulations used to generate FRAP curves were based on a model of diffusion in an ellipsoid volume representing the cell nucleus, and simple binding kinetics representing binding to immobile elements in the cell nucleus. Simulations were performed at unit time steps corresponding to the experimental sample rate of 21 ms. Diffusion was simulated by each step deriving novel positions M(x+ dx, y+ dy, z+ dz) for all mobile molecules M(x, y, z), where dx = G(r_1), dy = G(r_2) and dz= G(r_3), r_i is a random number (0 ≤ r_i ≤ 1) chosen from a uniform distribution, and G(r_i) is an inversed cumulative Gaussian distribution with μ = 0 and σ^2 = 6Dt, where D is the diffusion coefficient and t is time measured in unit time steps. Immobilization was based on simple binding kinetics described by: k_{on}/k_{off} = F_{imm} / (1 - F_{imm}), where F_{imm} is the relative number of immobile molecules. The chance for each particle to become immobilized (representing chromatin-binding) was defined as $P_{immobilise}$ = k_{on} = k_{off} · F_{imm} / (1 - F_{imm}), where k_{off} = 1/ t_{imm}, and t_{imm} is the average time spent in immobile complexes measured in unit time steps; the chance to release was $P_{mobilise}$ = k_{off} = 1/ t_{imm}. The FRAP procedure was simulated on the basis of an experimentally derived 3D laser intensity profile providing a chance based on 3D position for each molecule to get bleached during simulation of the bleach pulse.

Assembly at local damaged sites.

For analyzing the dynamics of NER complex assembly cells were kept on an Axiovert 200M microscope stage at the appropriate temperature, using a temperature-controlled microscope chamber. The objective (Zeiss Apochromat 100X) was temperature-controlled with an objective heater. One image was taken to determine the position and the GFP fluorescence intensity of the cells (monochromator at 470 nm, bandwidth 20 nm). A reflection image of the filter was obtained moving up in the z-direction. Images of the cells and the filter were overlaid to determine which nuclei are located under a filter pore. The distance between cells and filter was measured with a Piezo electrical element and had to be less than 7 um to obtain a well-defined damaged area. CHO cells were transiently transfected with DDB2-mCherry with lipofectamine 2000 (Invitrogen, Breda, the Netherlands) according to the manufacturer's instructions.

The cells were irradiated (100 J.m^{-2}) and images were collected at 20 s interval for 30 minutes to allow eGFP accumulation in the locally damaged area to reach a plateau level. DDB2-mCherry accumulation was monitored with 550 ± 20 nm. The accumulation of XPG-eGFP at sites of local damage was quantified with Object-Image software (59). A macro was written to determine the centre of gravity of the fluorescent spot at every time point. Next, the average fluorescence intensity was measured in a region of 20 μm^2 around the centre of gravity for every time point. The average intensity of the entire nucleus, except the damaged area, was also measured, representing the unbound protein pool. The eGFP signal in the undamaged area was subtracted from the damaged area. The resulting value represents the NER-related bound protein fraction. All values were corrected for photo bleaching. Time courses were normalized with respect to the plateau level. Start of the UV irradiation was defined as t=0. Assembly curves were normalized to 1 or to the bound fraction calculated by the equation: Bound (%) = (I_{spot}-$I_{outspot}$)* pixels$_{spot}$ / ($I_{nucleus}$-$I_{background}$)* pixels$_{nucleus}$, where I_{spot} and $I_{outspot}$ are the average pixel intensities inside the damaged spot and outside the spot, respectively. $I_{nucleus}$ is the average pixel intensity of the nucleus, including the spot and $I_{background}$ is the average pixel intensity outside the cell.

Acknowledgement

References

1. **Araujo, S. J., E. A. Nigg, and R. D. Wood.** 2001. Strong functional interactions of TFIIH with XPC and XPG in human DNA nucleotide excision repair, without a preassembled repairosome. Mol Cell Biol **21:**2281-91.

2. **Botta, E., T. Nardo, A. R. Lehmann, J. M. Egly, A. M. Pedrini, and M. Stefanini.** 2002. Reduced level of the repair/transcription factor TFIIH in trichothiodystrophy. Hum Mol Genet **11:**2919-28.

3. **Coin, F., J. Auriol, A. Tapias, P. Clivio, W. Vermeulen, and J. M. Egly.** 2004. Phosphorylation of XPB helicase regulates TFIIH nucleotide excision repair activity. Embo J **23:**4835-46.

4. **de Laat, W. L., E. Appeldoorn, K. Sugasawa, E. Weterings, N. G. Jaspers, and J. H. Hoeijmakers.** 1998. DNA-binding polarity of human replication protein A positions nucleases in nucleotide excision repair. Genes Dev **12:**2598-609.

5. **de Laat, W. L., N. G. Jaspers, and J. H. Hoeijmakers.** 1999. Molecular mechanism of nucleotide excision repair. Genes Dev **13:**768-85.

6. **Dunand-Sauthier, I., M. Hohl, F. Thorel, P. Jaquier-Gubler, S. G. Clarkson, and O. D. Scharer.** 2005. The spacer region of XPG mediates recruitment to nucleotide excision repair complexes and determines substrate specificity. J Biol Chem **280:**7030-7.

7. **Ellison, A. R., T. Nouspikel, N. G. Jaspers, S. G. Clarkson, and D. C. Gruenert.** 1998. Complementation of transformed fibroblasts from patients with combined xeroderma pigmentosum-Cockayne syndrome. Exp Cell Res **243:**22-8.

8. **Evans, E., J. G. Moggs, J. R. Hwang, J. M. Egly, and R. D. Wood.** 1997. Mechanism of open complex and dual incision formation by human nucleotide excision repair factors. Embo J **16:**6559-73.

9. **Fitch, M. E., S. Nakajima, A. Yasui, and J. M. Ford.** 2003. In vivo recruitment of XPC to UV-induced cyclobutane pyrimidine dimers by the DDB2 gene product. J Biol Chem **278:**46906-10.

10. **Friedberg, E. C.** 2001. How nucleotide excision repair protects against cancer. Nat Rev Cancer **1:**22-33.

11. **Friedberg, E. C.** 2005. Suffering in silence: the tolerance of DNA damage. Nat Rev Mol Cell Biol **6:**943-53.

12. **Gervais, V., V. Lamour, A. Jawhari, F. Frindel, E. Wasielewski, S. Dubaele, J. M. Egly, J. C. Thierry, B. Kieffer, and A. Poterszman.** 2004. TFIIH contains a PH domain involved in DNA nucleotide excision repair. Nat Struct Mol Biol **11:**616-22.

13. **Giglia-Mari, G., F. Coin, J. A. Ranish, D. Hoogstraten, A. Theil, N. Wijgers, N. G. Jaspers, A. Raams, M. Argentini, P. J. van der Spek, E. Botta, M. Stefanini, J. M. Egly, R. Aebersold, J. H. Hoeijmakers, and W. Vermeulen.** 2004. A new, tenth subunit of TFIIH is responsible for the DNA repair syndrome trichothiodystrophy group A. Nat Genet **36:**714-9.

14. **Giglia-Mari, G., C. Miquel, A. F. Theil, P. O. Mari, D. Hoogstraten, J. M. Ng, C. Dinant, J. H. Hoeijmakers, and W. Vermeulen.** 2006. Dynamic Interaction of TTDA with TFIIH Is Stabilized by Nucleotide Excision Repair in Living Cells. PLoS Biol **4:**e156.

15. **Green, C. M., and G. Almouzni.** 2003. Local action of the chromatin assembly factor CAF-1 at sites of nucleotide excision repair in vivo. Embo J **22:**5163-74.

16. **Guzder, S. N., P. Sung, L. Prakash, and S. Prakash.** 1996. Nucleotide excision repair in yeast is mediated by sequential assembly of repair factors and not by a pre-assembled repairosome. J Biol Chem **271:**8903-10.

17. **Guzder, S. N., P. Sung, L. Prakash, and S. Prakash.** 1999. Synergistic interaction between yeast nucleotide excision repair factors NEF2 and NEF4 in the binding of ultraviolet-damaged DNA. J Biol Chem **274:**24257-62.

18. **Guzder, S. N., P. Sung, L. Prakash, and S. Prakash.** 1997. Yeast Rad7-Rad16 complex, specific for the nucleotide excision repair of the nontranscribed DNA strand, is an ATP-dependent DNA damage sensor. J Biol Chem **272:**21665-8.

19. **Habraken, Y., P. Sung, S. Prakash, and L. Prakash.** 1996. Transcription factor TFIIH and DNA endonuclease Rad2 constitute yeast nucleotide excision repair factor 3: implications for nucleotide excision repair and Cockayne syndrome. Proc Natl Acad Sci U S A **93:**10718-22.

20. **Hamel, B. C., A. Raams, A. R. Schuitema-Dijkstra, P. Simons, I. van der Burgt, N. G. Jaspers, and W. J. Kleijer.** 1996. Xeroderma pigmentosum--Cockayne syndrome complex: a further case. J Med Genet **33:**607-10.

21. **Hanawalt, P. C.** 2000. DNA repair. The bases for Cockayne syndrome. Nature **405:**415-6.

22. **Hoeijmakers, J. H.** 2001. Genome maintenance mechanisms for preventing cancer. Nature **411:**366-74.

23. **Hoogstraten, D., A. L. Nigg, H. Heath, L. H. Mullenders, R. van Driel, J. H. Hoeijmakers, W. Vermeulen, and A. B. Houtsmuller.** 2002. Rapid switching of TFIIH between RNA polymerase I and II transcription and DNA repair in vivo. Mol Cell **10:**1163-74.

24. **Houtsmuller, A. B., S. Rademakers, A. L. Nigg, D. Hoogstraten, J. H. Hoeijmakers, and W. Vermeulen.** 1999. Action of DNA repair endonuclease ERCC1/XPF in living cells. Science **284:**958-61.

25. **Iben, S., H. Tschochner, M. Bier, D. Hoogstraten, P. Hozak, J. M. Egly, and I. Grummt.** 2002. TFIIH plays an essential role in RNA polymerase I transcription. Cell **109:**297-306.

26. **Klungland, A., M. Hoss, D. Gunz, A. Constantinou, S. G. Clarkson, P. W. Doetsch, P. H. Bolton, R. D. Wood, and T. Lindahl.** 1999. Base excision repair of oxidative DNA damage activated by XPG protein. Mol Cell **3:**33-42.

27. **Lee, S. K., S. L. Yu, L. Prakash, and S. Prakash.** 2002. Requirement of yeast RAD2, a homolog of human XPG gene, for efficient RNA polymerase II transcription. implications for Cockayne syndrome. Cell **109:**823-34.

28. **Lehmann, A. R.** 2003. DNA repair-deficient diseases, xeroderma pigmentosum, Cockayne syndrome and trichothiodystrophy. Biochimie **85:**1101-11.

29. **MacInnes, M. A., J. A. Dickson, R. R. Hernandez, D. Learmonth, G. Y. Lin, J. S. Mudgett, M. S. Park, S. Schauer, R. J. Reynolds, G. F. Strniste, and et al.** 1993. Human ERCC5 cDNA-cosmid complementation for excision repair and bipartite amino acid domains conserved with RAD proteins of Saccharomyces cerevisiae and Schizosaccharomyces pombe. Mol Cell Biol **13:**6393-402.

30. **Mitchell, J. R., J. H. Hoeijmakers, and L. J. Niedernhofer.** 2003. Divide and conquer: nucleotide excision repair battles cancer and ageing. Curr Opin Cell Biol **15:**232-40.

31. **Mone, M. J., T. Bernas, C. Dinant, F. A. Goedvree, E. M. Manders, M. Volker, A. B. Houtsmuller, J. H. Hoeijmakers, W. Vermeulen, and R. van Driel.** 2004. In vivo dynamics of chromatin-associated complex formation in mammalian nucleotide excision repair. Proc Natl Acad Sci U S A **101:**15933-7.

32. **Mone, M. J., M. Volker, O. Nikaido, L. H. Mullenders, A. A. van Zeeland, P. J. Verschure, E. M. Manders, and R. van Driel.** 2001. Local UV-induced DNA damage in cell nuclei results in local transcription inhibition. EMBO Rep **2:**1013-7.

33. **Moser, J., M. Volker, H. Kool, S. Alekseev, H. Vrieling, A. Yasui, A. A. van Zeeland, and L. H. Mullenders.** 2005. The UV-damaged DNA binding protein mediates efficient targeting of the nucleotide excision repair complex to UV-induced photo lesions. DNA Repair (Amst) **4:**571-82.

34. **Mu, D., C. H. Park, T. Matsunaga, D. S. Hsu, J. T. Reardon, and A. Sancar.** 1995. Reconstitution of human DNA repair excision nuclease in a highly defined system. J Biol Chem **270:**2415-8.

35. **Ng, J. M., W. Vermeulen, G. T. van der Horst, S. Bergink, K. Sugasawa, H. Vrieling, and J. H. Hoeijmakers.** 2003. A novel regulation mechanism of DNA repair by damage-induced and RAD23-dependent stabilization of xeroderma pigmentosum group C protein. Genes Dev **17:**1630-45.

36. **O'Donovan, A., A. A. Davies, J. G. Moggs, S. C. West, and R. D. Wood.** 1994. XPG endonuclease makes the 3' incision in human DNA nucleotide excision repair. Nature **371:**432-5.

37. **Park, M. S., J. A. Knauf, S. H. Pendergrass, C. H. Coulon, G. F. Strniste, B. L. Marrone, and M. A. MacInnes.** 1996. Ultraviolet-induced movement of the human DNA repair protein, Xeroderma pigmentosum type G, in the nucleus. Proc Natl Acad Sci U S A **93:**8368-73.

38. **Politi, A., M. J. Mone, A. B. Houtsmuller, D. Hoogstraten, W. Vermeulen, R. Heinrich, and R. van Driel.** 2005. Mathematical Modeling of Nucleotide Excision Repair Reveals Efficiency of Sequential Assembly Strategies. Mol Cell **19:**679-690.

39. **Protic-Sabljic, M., S. Seetharam, M. M. Seidman, and K. H. Kraemer.** 1986. An SV40-transformed xeroderma pigmentosum group D cell line: establishment, ultraviolet sensitivity, transfection efficiency and plasmid mutation induction. Mutat Res **166:**287-94.

40. **Rademakers, S., M. Volker, D. Hoogstraten, A. L. Nigg, M. J. Mone, A. A. Van Zeeland, J. H. Hoeijmakers, A. B. Houtsmuller, and W. Vermeulen.** 2003. Xeroderma pigmentosum group A protein loads as a separate factor onto DNA lesions. Mol Cell Biol **23:**5755-67.

41. **Riedl, T., F. Hanaoka, and J. M. Egly.** 2003. The comings and goings of nucleotide excision repair factors on damaged DNA. Embo J **22:**5293-303.

42. **Sarker, A. H., S. E. Tsutakawa, S. Kostek, C. Ng, D. S. Shin, M. Peris, E. Campeau, J. A. Tainer, E. Nogales, and P. K. Cooper.** 2005. Recognition of RNA polymerase II and transcription bubbles by XPG, CSB, and TFIIH: insights for transcription-coupled repair and Cockayne Syndrome. Mol Cell **20:**187-98.

43. **Schaeffer, L., R. Roy, S. Humbert, V. Moncollin, W. Vermeulen, J. H. Hoeijmakers, P. Chambon, and J. M. Egly.** 1993. DNA repair helicase: a component of BTF2 (TFIIH) basic transcription factor. Science **260:**58-63.

44. **Shaner, N. C., R. E. Campbell, P. A. Steinbach, B. N. Giepmans, A. E. Palmer, and R. Y. Tsien.** 2004. Improved monomeric red, orange and yellow fluorescent proteins derived from Discosoma sp. red fluorescent protein. Nat Biotechnol **22:**1567-72.

45. **Shivji, M. K., V. N. Podust, U. Hubscher, and R. D. Wood.** 1995. Nucleotide excision repair DNA synthesis by DNA polymerase epsilon in the presence of PCNA, RFC, and RPA. Biochemistry **34:**5011-7.

46. **Stefanini, M., P. Lagomarsini, S. Giliani, T. Nardo, E. Botta, A. Peserico, W. J. Kleijer, A. R. Lehmann, and A. Sarasin.** 1993. Genetic heterogeneity of the excision repair defect associated with trichothiodystrophy. Carcinogenesis **14:**1101-5.

47. **Stefanini, M., W. Vermeulen, G. Weeda, S. Giliani, T. Nardo, M. Mezzina, A. Sarasin, J. I. Harper, C. F. Arlett, J. H. Hoeijmakers, and et al.** 1993. A new nucleotide-excision-repair gene associated with the disorder trichothiodystrophy. Am J Hum Genet **53:**817-21.

48. **Sugasawa, K., J. M. Ng, C. Masutani, S. Iwai, P. J. van der Spek, A. P. Eker, F. Hanaoka, D. Bootsma, and J. H. Hoeijmakers.** 1998. Xeroderma pigmentosum group C protein complex is the initiator of global genome nucleotide excision repair. Mol Cell **2:**223-32.

49. **Sugasawa, K., Y. Okuda, M. Saijo, R. Nishi, N. Matsuda, G. Chu, T. Mori, S. Iwai, K. Tanaka, and F. Hanaoka.** 2005. UV-induced ubiquitylation of XPC protein mediated by UV-DDB-ubiquitin ligase complex. Cell **121:**387-400.

50. **Svejstrup, J. Q., Z. Wang, W. J. Feaver, X. Wu, D. A. Bushnell, T. F. Donahue, E. C. Friedberg, and R. D. Kornberg.** 1995. Different forms of TFIIH for transcription and DNA repair: holo-TFIIH and a nucleotide excision repairosome. Cell **80:**21-8.

51. **Tang, J. Y., B. J. Hwang, J. M. Ford, P. C. Hanawalt, and G. Chu.** 2000. Xeroderma pigmentosum p48 gene enhances global genomic repair and suppresses UV-induced mutagenesis. Mol Cell **5:**737-44.

52. **Taylor, E. M., B. C. Broughton, E. Botta, M. Stefanini, A. Sarasin, N. G. Jaspers, H. Fawcett, S. A. Harcourt, C. F. Arlett, and A. R. Lehmann.** 1997. Xeroderma

pigmentosum and trichothiodystrophy are associated with different mutations in the XPD (ERCC2) repair/transcription gene. Proc Natl Acad Sci U S A **94:**8658-63.

53. **Thorel, F., A. Constantinou, I. Dunand-Sauthier, T. Nouspikel, P. Lalle, A. Raams, N. G. Jaspers, W. Vermeulen, M. K. Shivji, R. D. Wood, and S. G. Clarkson.** 2004. Definition of a short region of XPG necessary for TFIIH interaction and stable recruitment to sites of UV damage. Mol Cell Biol **24:**10670-80.

54. **van den Boom, V., E. Citterio, D. Hoogstraten, A. Zotter, J. M. Egly, W. A. van Cappellen, J. H. Hoeijmakers, A. B. Houtsmuller, and W. Vermeulen.** 2004. DNA damage stabilizes interaction of CSB with the transcription elongation machinery. J Cell Biol **166:**27-36.

55. **Vermeulen, W., E. Bergmann, J. Auriol, S. Rademakers, P. Frit, E. Appeldoorn, J. H. Hoeijmakers, and J. M. Egly.** 2000. Sublimiting concentration of TFIIH transcription/DNA repair factor causes TTD-A trichothiodystrophy disorder. Nat Genet **26:**307-13.

56. **Vermeulen, W., S. Rademakers, N. G. Jaspers, E. Appeldoorn, A. Raams, B. Klein, W. J. Kleijer, L. K. Hansen, and J. H. Hoeijmakers.** 2001. A temperature-sensitive disorder in basal transcription and DNA repair in humans. Nat Genet **27:**299-303.

57. **Vermeulen, W., R. J. Scott, S. Rodgers, H. J. Muller, J. Cole, C. F. Arlett, W. J. Kleijer, D. Bootsma, J. H. Hoeijmakers, and G. Weeda.** 1994. Clinical heterogeneity within xeroderma pigmentosum associated with mutations in the DNA repair and transcription gene ERCC3. Am J Hum Genet **54:**191-200.

58. **Vermeulen, W., M. Stefanini, S. Giliani, J. H. Hoeijmakers, and D. Bootsma.** 1991. Xeroderma pigmentosum complementation group H falls into complementation group D. Mutat Res **255:**201-8.

59. **Vischer, N. O., P. G. Huls, R. I. Ghauharali, G. J. Brakenhoff, N. Nanninga, and C. L. Woldringh.** 1999. Image cytometric method for quantifying the relative amount of DNA in bacterial nucleoids using Escherichia coli. J Microsc **196 (Pt 1):**61-8.

60. **Volker, M., M. J. Mone, P. Karmakar, A. van Hoffen, W. Schul, W. Vermeulen, J. H. Hoeijmakers, R. van Driel, A. A. van Zeeland, and L. H. Mullenders.** 2001. Sequential assembly of the nucleotide excision repair factors in vivo. Mol Cell **8:**213-24.

61. **Wakasugi, M., A. Kawashima, H. Morioka, S. Linn, A. Sancar, T. Mori, O. Nikaido, and T. Matsunaga.** 2002. DDB accumulates at DNA damage sites immediately after UV irradiation and directly stimulates nucleotide excision repair. J Biol Chem **277:**1637-40.

62. **Wakasugi, M., and A. Sancar.** 1998. Assembly, subunit composition, and footprint of human DNA repair excision nuclease. Proc Natl Acad Sci U S A **95:**6669-74.

63. **Wakasugi, M., and A. Sancar.** 1999. Order of assembly of human DNA repair excision nuclease. J Biol Chem **274:**18759-68.

Chapter 5

Dynamics of Polymerase Eta in Living Mammalian Cells

Manuscript in preparation

Dynamics of Polymerase Eta in Living Mammalian Cells

Angelika Zotter[1], Audrey Gourdin[1], Shehu Ibrahim[2], Wiggert A. van Capellen[3], Adriaan B. Houtsmuller[2], Patricia Kannouche[4], Alan Lehmann[4*], Wim Vermeulen[1].

[1]Department of Cell Biology and Genetics, Erasmus MC Rotterdam, P.O. box 2040, 3000 CA Rotterdam, The Netherlands.

[2] Department of Pathology, Josephine Nefkens Institute, Erasmus MC Rotterdam, P.O. box 2040, 3000 CA Rotterdam, The Netherlands.

[3] Department of Reproduction and Development, Erasmus MC Rotterdam, P.O. box 2040, 3000 CA Rotterdam, The Netherlands.

[4] Genome Damage and Stability Centre, University of Sussex, Falmer, Brighton BN1 9RQ, United Kingdom.

*Corresponding author. email: a.r.lehmann@sussex.ac.uk

Abstract:

The translesion polymerase eta (Polη) is an important lesion bypass polymerase in eukaryotes, capable of bypassing the main UV-induced DNA lesion, cyclobutane pyrimidine dimer (CPD), in an error-free manner. In order to complement the vast amount of *in vitro* and biochemical studies performed on this important DNA damage tolerance factor with *in vivo* analysis, the full-length human protein was tagged with EGFP and stably expressed in Polη-deficient human cells [1]. We have studied the cell-cycle-dependent dynamic redistribution of the functional fusion protein in response to UV-induced DNA damage in living mammalian cells, using confocal microscopy, time-lapse and photo-bleaching experiments. We have found that Polη, when not associated with S-phase foci, moves rapidly throughout the nucleus, suggesting that most of the protein is freely mobile and not stably integrated into a large complex. In S-phase, a fraction relocates to replication foci, where it becomes immobilized very transiently, in the order of a few seconds. The extent and duration of Polη immobilization within these structures is increased after UV damage induction, but remains highly dynamic. The association of Polη with replication structures is dependent on the amount of DNA

lesions. Time-lapse studies of cells with and without locally induced DNA damage showed that the distribution pattern throughout S-phase highly resembles the one of proliferating cell nuclear antigen (PCNA), supporting previous *in vitro* studies and observations on fixed cells showing that Polη efficiently associates with PCNA in replication foci. Our results underline the highly dynamic, cell cycle-dependent association of Polη with chromatin structures, fine-tuned by the replicative state of the DNA.

Introduction:

Proper maintenance of genomic DNA is of crucial importance for all cells. The integrity of the genome is constantly challenged by different environmental as well as metabolic agents. To counteract the severe consequences of DNA lesions, a variety of specialized repair mechanisms have evolved. At the same time, damage avoidance mechanisms ensure that DNA, from which not all damage has been removed, can still be replicated. In mammalian cells, translesion synthesis (TLS) is believed to be the principal mechanism to resolve replication complexes blocked or stalled at DNA damage sites and thus prevent replication forks from becoming either permanently arrested or being processed into highly cytotoxic double strand breaks (DSB). The rather recently characterized Y-family of DNA polymerases are low-stringency DNA polymerases that are structurally related to each other but quite distinct from classical DNA polymerases [2, 3]. They are capable of replicating past a specific subset of lesions, mostly at the expense of a somewhat elevated mutation frequency (reviewed in [4]). An important translesion polymerase, specialized to bypass the most common UV-induced lesion, the cyclobutane pyrimidine dimers (CPDs), is defective in the variant form of the sun-sensitive, cancer-prone disorder xeroderma pigmentosum (XP).

The xeroderma pigmentosum variant gene (XPV) encodes for polymerase eta (Polη), also referred to as hRad30. Notably, Polη is capable of performing relatively error-free translesion synthesis opposite CPDs [5, 6]. It is also able to perform more error-prone lesion bypass of several other damages and diverse chemical adducts. CPDs are generally poorly repaired by the nucleotide excision repair (NER) machinery and therefore remain longer on the DNA. NER is a multi-step 'cut and patch' repair system for a wide range of lesions that disrupt base-pairing and distort the helical structure of DNA [7, 8]. Among these are numerous chemical adducts as well as UV-induced 6-4 photoproducts and with much slower kinetics CPD lesions. Inherited defects

in the NER genes XPA-XPG cause XP. The lack of Polη causes clinical features similar to an NER deficiency, highlighting the importance of this specialized bypass polymerase. The highly elevated sunlight-induced carcinogenesis in XP-V patients indicates that other bypass polymerases carry out TLS past CPDs in the absence of Polη, but they are error-prone and therefore mutagenic.

Though especially the lesion-bypass properties of several Y-family polymerases have been studied extensively *in vitro* (reviewed in [9]), data on their mode of action within intact cells are scarce. In the present study, we analysed the dynamic involvement of Polη in nuclear processes within the living cell, with special emphasis on responses to blockage/stalling of the DNA replication machinery by UV-induced damages. To this end, the polymerase was provided with an EGFP-tag and stably integrated into Polη-deficient human cell lines, thereby correcting their UV sensitivity (Kannouche et al., 2001). Dynamic changes in Polη localization and mobility inside living cells were investigated employing photobleaching techniques and time-lapse microscopy.

Results and discussion:

To study the dynamics of Polη, we used a previously generated cell line that stably expresses an N-terminally GFP-tagged Polη (Fig. 1A) in XPV mutant cells (XP30RO-SV; [1]). As shown previously, the fusion protein is predominantly localized in the nuclei and biologically functional by its capacity to complement the UV-sensitivity of XP30RO cells in the presence of caffeine [1]. About 10% of the cells stably expressing the fusion protein exhibited focal accumulations (Fig. 1B) that, as reported by Kannouche et al., co-localize with PCNA, a well-known marker for replication foci [1, 10]. 5-9 h upon UV-C irradiation (7 – 8 J/m2), the number of cells exhibiting such foci is greatly increased to about 60%. This prolongation of the S-phase as a response to UV-induced DNA damage is indicative of the accumulation of DNA replication forks stalled at DNA damage sites, to which TLS polymerases such as Polη are recruited. Stalled replication complexes can potentially lead to highly cytotoxic DNA double-strand breaks (DSB) [11-13]. Polη and other lesion bypass polymerases are believed to be recruited to such blocked replication sites in order to resolve the stalled replication complex before DSB can occur and thus enable the cell to proceed throughout the cell cycle.
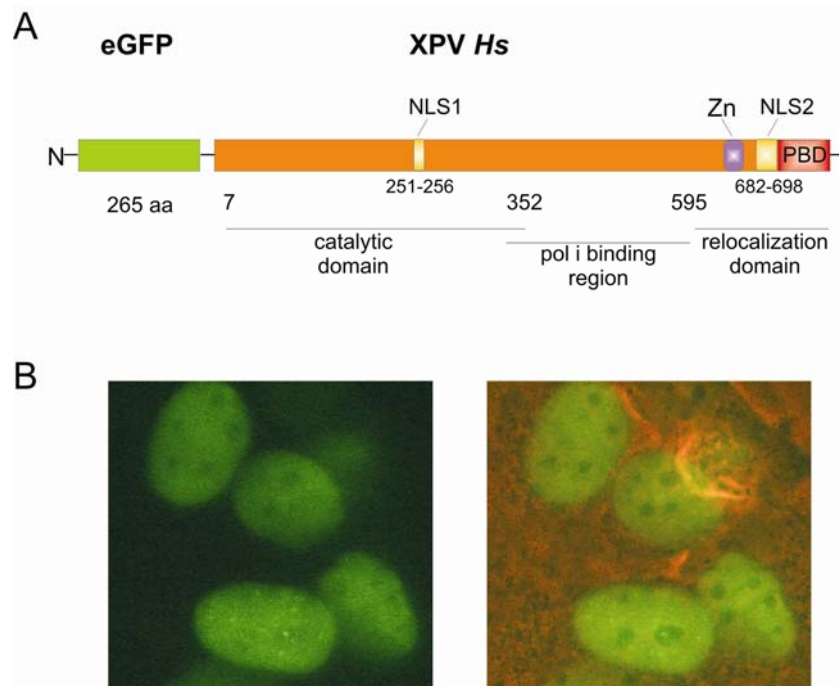
Fig. 1. eGFP-XPV and Polη expression in XP30RO cells. (A) Schematic representation of the eGFP-XPV fusion gene, with the N-terminal catalytic domain of XPV containing a putative nuclear localization signal (NLS1), the polymerase iota (polι) interaction region, and the C-terminal relocalization domain with a Zink-finger (Zn), a nuclear localization signal (NLS2), and the PCNA-binding domain (PBD). aa, amino acids. (B) Localization of EGFP-Polη in the human XP-V cell line XP30ROsv. Left panel, fluorescence signal. Right panel, overlay of fluorescence and phase contrast. The fusion protein shows a diffuse nuclear expression, with about 10% of the cells exhibiting focal accumulations of EGFP-Polη (cell at the bottom of the picture).

To avoid artefacts that can be due to overexpression of the tagged Polη, we selected a subpopulation of XP30RO cells that moderately expressed the GFP-tagged protein for a comprehensive analysis of protein location and mobility within living cells. Protein (re-) location and mobility studies were thus performed using a functional protein expressed under (close to) physiological conditions.

Mobility of EGFP-Polη in the absence of externally introduced DNA damage

Using Fluorescence recovery after photobleaching (FRAP), we first determined the mobility of Polη in cells that had not been subjected to DNA damage, and were not in S-phase (no discernible EGFP-Polη foci). In these stages of the cell cycle (G1 or G2), Polη was not expected to be engaged in translesion synthesis.
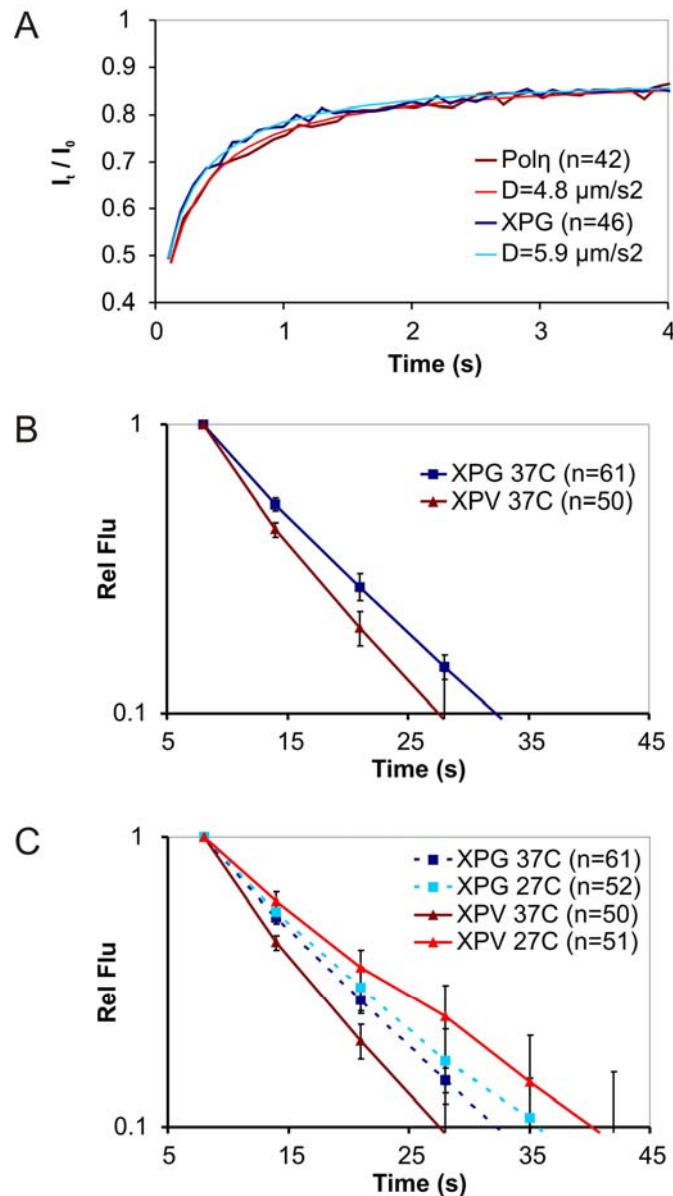
Fig. 2. FRAP analysis of Polη mobility in comparison with the NER endonuclease XPG. (A) FRAP analysis of a narrow strip in the nucleus (Strip-FRAP). A 0.2μm strip spanning the nucleus was bleached at high laser power and the subsequent influx of fluorescence into this strip monitored a low laser power. The mean relative fluorescence values (fluorescence after bleaching/fluorescence before bleaching, I_t/I_0) after the bleach pulse are plotted against the indicated times in seconds. Thick lines, experimental data; n, number of analysed cells; thin lines, mathematical fitting curves; D, apparent diffusion coefficient. (B) Simultaneous FRAP/FLIP analysis of Polη and XPG in the nucleus. A rectangular area spanning the nucleus at one pole was bleached for four seconds. Subsequently, fluorescence was monitored in the bleached area (FRAP) and the unbleached area on the opposite site of the nucleus (FLIP). The normalized difference between these two areas (FLIP-FRAP; see Materials and Methods) following the bleach pulse was plotted on a log scale against time. The x-axis crosses at 90% redistribution of the proteins. Dark red line, Polη;

dark blue line, XPG; n depicts the number of analysed cells. Error bars indicate standard deviations (STD) between experiments. (C) Simultaneous FRAP/FLIP analysis of Polη mobility in the nucleus at different temperatures. Dark red line, Polη at 37°C; red line, Polη at 27°C; dotted dark blue line, XPG at 37°C; dotted light blue line, XPG at 27°C; n, number of cells analysed. Error bars indicate STD between experiments.

We bleached a narrow strip spanning the cell nucleus and monitored the subsequent fluorescence recovery in this previously bleached strip (Strip-FRAP; see Materials and Methods [14-16]. Mathematical fitting of the recovery curves obtained in this manner yields apparent diffusion rates (also "effective Diffusion rates", D_{eff}), which enable us to uncover and compare subtle differences in protein mobility. As a reference for the characterization of Polη mobility, we used a previously well-studied protein with this method, the NER endonuclease XPG. This protein moves through the nucleus, in the absence of UV-induced DNA damage, by passive diffusion mainly determined by its molecular size and shape ([16]; Zotter, Ibrahim et al., in preparation). The observed recovery of EGFP-Polη in cells not subjected to DNA-damaging agents and without microscopically discernible foci suggests a somewhat slower mobility for Polη than anticipated based on its molecular size. Despite its considerably smaller molecular weight than XPG-EGFP, EGFP-Polη exhibited strikingly similar redistribution after photobleaching to the nearly double-sized NER endonuclease (MW XPG-GFP: 190 kDa; MW Polη - GFP: 108kDa; Fig. 2A). Mathematical fitting of the mobility patterns of XPG-EGFP and EGFP-Polη generated effective diffusion constants that differ only slightly from each other, and rather imply a somewhat slower apparent diffusion of Polη than XPG (D_{eff} XPG=5.9, D_{eff} Polη = 4.8; Fig. 2A). This result indicates either a short-lived retention of the lesion bypass polymerase at intranuclear sites, or also a possible di- or oligomerisation with (an)other protein(s). Previous work has indeed shown that Rad18, necessary for the recruitment of Polη to replication foci, constitutively physically interacts with Polη [17]. This interaction could cause a slight delay in diffusion.

To obtain a more global view on live cell mobility of Polη, we subjected the cells to a combined FRAP and FLIP (fluorescence loss in photobleaching) analysis [14, 16]. In this procedure, part of the cell nucleus is bleached at one end, followed by the subsequent monitoring of the whole nucleus until the overall pre-bleach distribution of the fluorescence is re-established. The difference in fluorescence between bleached and unbleached area in time is plotted in log-scale to visualize the protein's velocity and mode of redistribution. The time required for re-establishing 90% of the prebleach-distribution of fluorescence is used as a measure for its mobility over longer distances.

As in the Strip-FRAP method described above, Polη showed a rather similar velocity of redistribution as XPG (a mean of 27 sec versus 32 sec, respectively; Fig 2B). Surprisingly, we found that Polη showed a significant delay in redistribution at lower temperatures (90% redistribution in 40s (27°C), as compared to 27s (37°C); Fig2C). This temperature-dependent retention is indicative of energy-dependent transient binding to more rigid nuclear structures, which could be due to active engagement in enzymatic processes or temperature-dependent reduction of the off-rate when transiently bound. XPG, in comparison, does not show significant retardation at 27°C in the absence of UV-induced DNA damage (Fig 2C), suggesting that the mobility of this protein is merely derived from passive diffusion, as diffusion is hardly affected by this relatively small temperature change. However, the mobility of XPG is strongly affected by temperature reduction when it is engaged in NER [16], which is consistent with the notion that the NER reaction involves several temperature-sensitive enzymatic, energy-requiring steps. Other nuclear factors, such as TFIIH and CSB, have been shown to exhibit similar additional retention at lower temperatures as Polη has, in cells that had not undergone any genotoxic treatment. In these cases temperature-dependent mobilities have been attributed to active engagement in transcription [14, 18].

Also Polη has been shown to have additional roles in the DNA metabolism of higher eukaryotes, like in certain (physiological) homologous recombination (HR) events, but not, for example, in γ-irradiation induced HR (Kawamoto et al., 2005). Since untreated cells without discernible foci were chosen for our analysis, two explanations for the observed retention of Polη are possible: Polη might be transiently immobilized to rigid nuclear structures different from S-phase foci in G1 and/or G2 cells, or the cells contained S-phase foci that were microscopically unrecognisable under our monitoring conditions. Since HR is taking place in G2 cells, interactions with this complex DNA-transacting machinery could potentially explain a temperature-sensitive retention in cells that are not in S-phase.

Cell cycle-dependent mobility of Polη

To exclude the influence of S-phase cells containing poorly visible foci on our dataset, we synchronized part of the cell population by performing mitotic shake-off. Thereby, mitotic cells were detached mechanically from the bottom of a culture dish and transferred into new culture dishes where they were further incubated. No chemical cell cycle inhibitors were used that could potentially produce artefacts by influencing the

dynamics of Polη directly or indirectly. FACS analysis showed that most of the cells were in G1 phase 5-6 h after this procedure. 9-12 h later, most of the cells had entered S-phase (data not shown). Unfortunately, the considerable size difference between G1 and S-phase cells (Fig 3A) rendered them less suitable for optimal comparison using the combined FRAP/FLIP procedure, a method significantly influenced by the size of the nuclei to be analysed. Strip-FRAP experiments, however, did not reveal a significant difference of protein mobility between synchronized G1, S-phase and non-synchronized
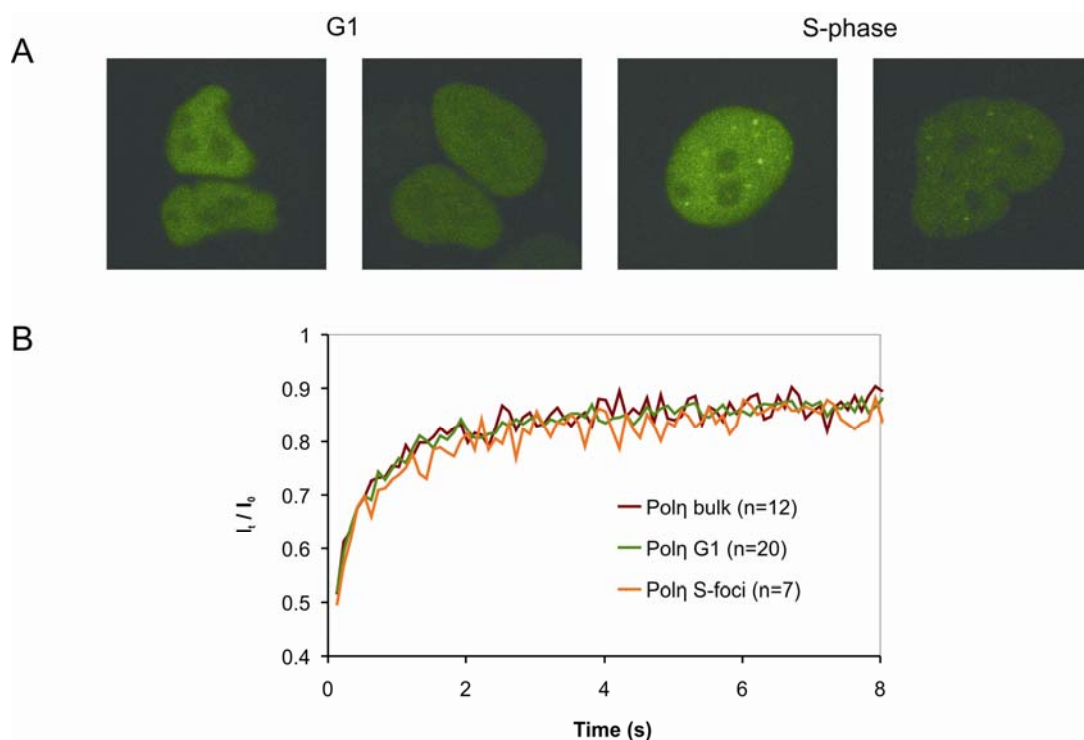

Fig.3. Localization and mobility of Polη in different phases of the cell cycle. (A) The two pictures on the left side depict fluorescent images of Polη–expressing cells in G1 (5-6h after mitotic shake-off). On the right, 2 examples of cells in S-phase are shown (9-12h after mitotic shake-off). Note the size difference and the relatively faint replication foci in moderately expressing cells in the absence of UV-induced DNA damage. For optimal accuracy, G1 cells were selected for their appearance as equally-sized "twins" at the indicated times after mitotic shake-off. (B) Strip-FRAP analysis of cells in G1 and S-phase, in comparison to unsynchronized cells without discernible foci. For simplicity, we show experimental data only, in order to better visualize the minute differences. Dark red line, Polη mobility in unsynchronized cells; green line, G1 cells; orange line, S-phase cells; n, number of cells analysed; I_t/I_0, relative fluorescence (fluorescence after bleaching/fluorescence before bleaching).

cells (Fig 3B). S-phase cells exhibiting clear foci formation showed consistently a slightly though statistically not significant slower mobility indicative for a small fraction of the protein shortly immobilized. The same measurements have also been performed using cells exhibiting foci after irradiation with 7.5 J/m^2 UV or treatment with the replication inhibitors hydroxyurea (HU) and cytosine arabinosid (ara-C). Also here, the observed differences in mobility were minute (data not shown). UV-irradiated cells or cells treated with replication inhibitors but not containing foci did not exhibit any slower redistribution, indicating that the observed retention is mainly due to transient binding to these visible subnuclear structures. In conclusion, the here applied FRAP (strip bleaching) method suggests that Polη interacts very shortly and in a replication dependent manner with S-phase foci; however, it has not proven suitable to readily detect these rather faint and short-term binding events.

UV-induced DNA damage influences nuclear distribution and mobility of Polη in a UV dose-dependent manner

To further investigate the dynamic association of Polη with the replication machinery in the presence of UV lesions, we concentrated on S-phase cells after UV light. UV irradiation of unsynchronised XP30RO cells expressing EGFP-Polη resulted in an accumulation of cells exhibiting S-phase foci after 5-9h. Cells irradiated with different doses of UV-C all showed accumulation of Polη into easily discernible foci without exhibiting a clear increase in the number or size of these structures (Fig 4A). We used combined FRAP/FLIP analysis to compare Polη mobility in these cells with its mobility in untreated cells not exhibiting foci. A clear UV dose-dependent response was observed, resulting in diverse degrees of delay in Polη redistribution due to transient immobilization to subnuclear structures (Fig 4B). Most likely, this retardation is entirely due to the recruitment of Polη into replication foci, in order to perform translesion synthesis past UV damages. Accordingly, higher UV doses resulted in a more pronounced delay in redistribution, reaching a maximum after irradiation with 12-16 J/m^2, with a redistribution time of about 50s, as compared to around 27s in untreated cells not exhibiting foci (Fig 4B). Higher UV doses than the saturating ones resulted again in less delay in redistribution of Polη, despite its clear accumulation in foci (see supplementary figure S1). This not even 2-fold delay in redistribution at the saturating UV-dose indicates a rather short binding time for Polη in these subnuclear structures, probably only for the duration of seconds. Alternatively, only a small fraction of the Polη pool might be

immobilized to replication foci. Similarly short retention times in subnuclear structures, for example, have been shown for TFIIH [14] and CSB [18], for their engagement in the order of seconds in transcription initiation and elongation, respectively.
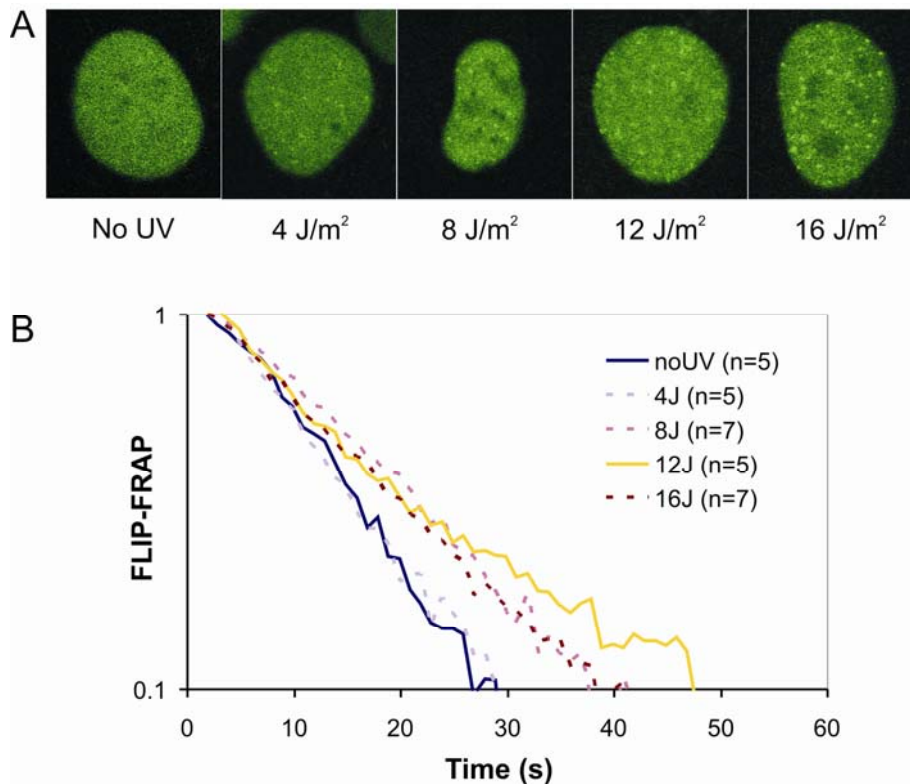

Fig.4. Localization and mobility of Polη in response to UV-C irradiation. (A) Representative images of XP30RO cells expressing EGFP-Polη after the indicated doses of UV. Note the relatively small differences of abundance and size of foci between the different doses of UV. (B) Combined FRAP/FLIP analysis of whole nuclei after exposure to augmenting doses of UV. The procedure, analysis and plotting was performed as described in Fig. 2. B. Polη redistribution after photobleaching is delayed in a UV dose-dependent manner. Maximum delay is reached at around 12 J/m^2, which we therefore determined as the saturating dose for the engagement of Polη in XP30RO cells. Dark blue line, Polη mobility in untreated cells not exhibiting foci; dotted violet line, Polη redistribution after 4 J/m^2; dotted pink line, Polη mobility after 8 J/m^2; yellow line, after 12 J/m^2. n, number of cells analysed.

The binding time of Polη to UV-induced foci is in the order of seconds

The above experiments already indicated a rather short retention of Polη in replication foci after UV-damage induction, and/or the binding of only a very small proportion of the GFP-tagged proteins to immobile nuclear structures. To uncover the

actual binding time of Polη within these replication foci, we performed a specifically adapted FRAP/FLIP procedure on cells exhibiting foci 5-9h after UV-C irradiation with 7.5 J/m^2. We did not choose a higher UV dose to minimize the influence of other stress response mechanisms and rather monitor the engagement of Polη in lesion bypass synthesis. Half of the nucleus of cells containing foci was bleached, and subsequently the re-establishment of the pre-bleach redistribution of fluorescence monitored in time. In the bleached half of the nucleus, fluorescence regain after photobleaching was measured within foci (= largely bound fraction) and separately in the circular surrounding area containing protein not bound to foci (= predominantly free fraction; Fig 5A). Simultaneously, fluorescence loss was measured the same way in the non-bleached half of the nucleus, again separately for the immobilized and free fraction of Polη. From the mathematically fitted difference in redistribution times between free and immobilized fractions of the protein, we could calculate the approximate binding time of Polη to UV-induced foci to be around 16s (Fig 5B; see also Materials and Methods).

This short binding time is in striking contrast to the DNA polymerase clamp PCNA which exhibits a retention time within replication structures in the order of 15-20 minutes [19, 20], highlighting the difference in their function. PCNA physically surrounds the DNA helix as a trimeric protein complex, serves as a central loading platform for an array of replication enzymes [21, 22] including the Y-family translesion polymerases [23, 24] and remains stably associated with the replication machinery [19, 22]. Polη, on the other hand, seems to be recruited continuously from a freely diffusing nucleoplasmic pool and be released again after very transient engagement in TLS of UV-lesions. It has to be considered though that the fact that Polη, as well as many other replication factors, can be seen in focal accumulations at replication factories, points towards a local concentration of many more proteins in these regions than could be directly engaged in actual enzymatic reactions. A number of TLS factors, such as Polη, could therefore adhere to locally altered chromatin that is modified because of ongoing replication, arrested replication forks or perhaps more likely to PCNA that is modified (e.g. ubiquitinated). This can serve as a transient binding platform to increase the local free concentration of TLS factors and thereby speed up the required reaction at the arrested replication fork that involves only a few Polη molecules to facilitate bypass synthesis, which otherwise would take too long, because of the low overall Polη concentration. The same is postulated for e.g. the foci of the homologous recombination repair proteins Rad52 and Rad54 [25]. Therefore the actual binding of the Polη molecules that are

directly engaged in the TLS event may be very different from the retention times of the majority of Polη molecules in a focus, and this may be even very difficult to determine as it is perhaps a very small fraction of the total proteins in a focus.
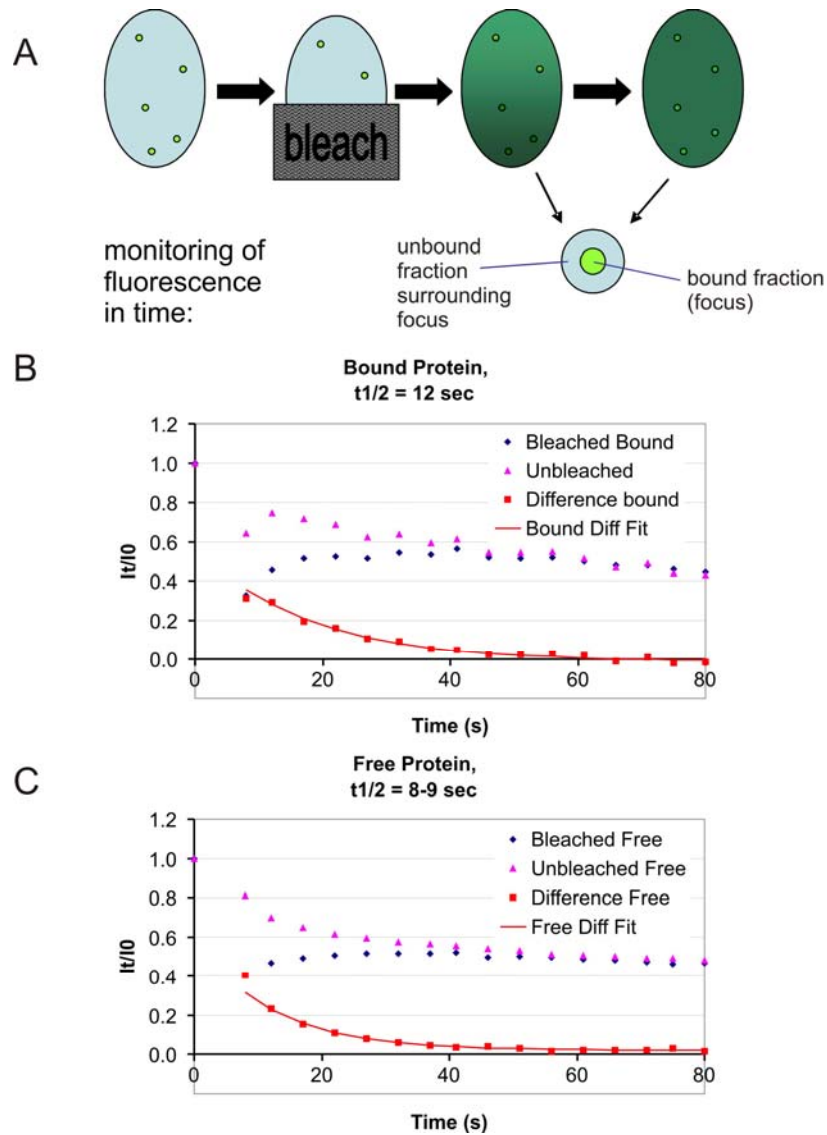

Fig.5. Simultaneous FRAP/FLIP analysis to compare mobility of foci-bound versus freely diffusing fraction of EGFP-Polη. (A) Schematic representation of the procedure. Half of the nucleus containing foci is bleached followed by monitoring of the redistribution of fluorescence over the whole nucleus in time. Simultaneous FRAP (in the bleached area) and FLIP (in the unbleached area) is measured within foci (bound fraction) and the circular surrounding area (free fraction). (B) and (C) Relative fluorescence values (fluorescence after bleaching / fluorescence before bleaching, I_t/I_0) of FRAP and FLIP are plotted as a function of time, separately for the free and the bound fraction of the protein. The differences (FLIP-FRAP) in

time between bleached and unbleached area are fitted mathematically to obtain half times ($t_{1/2}$) of redistribution. The mean binding time within the replication structures is calculated from the difference of the $t_{1/2}$ between bound and free fraction. (B) Redistribution of Polη immobilized to replication structures. (C) Redistribution of the free fraction of Polη. The graphs depict the mean values obtained from 3 independent experiments. Purple triangles, FLIP; dark blue diamonds, FRAP; red squares, FLIP-FRAP; red line, mathematical fit of FLIP-FRAP.

Consistent with this, even shorter residence times (about 2s) have been reported for Polη in S-phase foci of undamaged, as well as methyl-methanesulfonate (MMS)-treated, cells [26]. MMS causes stalling of replication forks [27] and recruitment of Polη to replication sites [1]. These results are indicative of a prolonged association with the replication machinery when Polη is recruited to lesions it is capable of bypassing efficiently, like UV-induced CPDs. In biochemical *in vitro* studies, Washington et al. have found that Polη dissociates from DNA after having incorporated a mismatching nucleotide instead of the correct one, while it can extend efficiently from matched base pairs [28]. This could also account for a shorter *in vivo* binding time of this TLS polymerase when attempting to bypass lesions for which it is not specialized. This notion is supported by the fact that *in vivo* binding of Flap endonuclease 1 (FEN1), in comparison, is significantly prolonged after treatment with MMS, suggesting that this protein plays a major role in MMS-derived lesion bypass in comparison to Polη [26]. Alternatively, the shorter residence times found by Solovjeva et al. might also be derived from the fact that transiently transfected cells were used, which therefore exhibited a higher overexpression of EGFP-Polη, in addition to the endogenous protein. (A masking effect of significantly more free protein concentrated around the binding area might lead to shorter apparent binding times in the subnuclear structures.) In our study, we deliberately chose for moderately fluorescent cells of a stably expressing culture of a cell line corrected for its XPV-deficiency by our construct.

Short binding, in comparison to PCNA, to replication foci has been shown for other replication factors, like the single-stranded DNA binding protein RPA34 [19], which recovers from photobleaching within 1-2min. DNA methyltransferase 1 (Dnmt1), DNA ligase1 and FEN1 show very short association with replication structures, strikingly similar to Polη, in the order of seconds [22, 26, 29]. Together, these data argue for transient interactions of replication-associated factors with the main replication machinery as a common feature. Most of these factors contain a PCNA Binding Domain (PBD) allowing direct interaction with PCNA. In addition, translesion polymerases have

ubiquitin binding sites (designated UBM and UBZ), and their targeting to stalled replication sites involves mono-ubiquitylation of PCNA triggered by replication fork stalling (reviewed in [9]). Hence, association of specific factors might at least partially be mutually exclusive and regulated by post-translational modifications of PCNA. Continuous and dynamic exchange of several distributive replication factors allows a flexible and versatile probing of replication forks by distinct auxiliary factors. Stable assemblies are less flexible, and taking the high number of reported PCNA interacting factors during replication into account these large assemblies would simply not fit onto the relatively small PCNA trimer.

Local UV damage induction reveals cell cycle-dependent relocalization of Polη to DNA damage sites

In order to verify whether Polη relocalises to actual DNA damage sites when cells are in S-phase, we irradiated XP30RO cells expressing Polη–EGFP locally with UV-C [30] and recorded localization over an extended period (time-lapse imaging). Cells were covered with a UV-shielding polycarbonate filter containing pores of 8µm diameter prior to irradiation with a relatively high dose of UV. Only nuclear DNA located directly under a filter pore will be damaged by UV. Focal accumulations of Polη at UV-damaged areas of living cells were observed several hours after UV (Fig 6A). In agreement with previous observations on fixed cells [1, 23], the distribution of the protein within these areas is similar to PCNA on local damage sites in S-phase cells [20]. Unlike NER factors and also PCNA in G1/G2 cells, no diffuse local accumulation was observed with Polη. This indicates that Polη is associated with stalled replication forks at the sites of DNA damages, rather than showing direct binding to lesions.

A time-lapse study of EGFP-Polη redistribution in locally UV-damaged cells revealed a cell-cycle-dependent local accumulation of the translesion polymerase. Relocalisation into foci within locally damaged areas becomes visible in S-phase, in addition to evenly distributed S-phase foci. The UV-damage-induced local accumulations seem to exist longer than the general replication foci but finally disappear in G2 (Fig 6B and M1). After cell division, they do not re-appear in G1. A similar pattern has been shown for PCNA, which in addition shows accumulation in G1 when being engaged in NER, disappears in early S-phase and reappears at unrepaired damage sites, most likely CPDs, in the transition to mid S-phase [20]. Since monoubiquinated PCNA has been shown to recruit Polη to stalled replication forks [23, 31], it is probable that Polη

follows the pattern of PCNA in S-phase. Therefore it is likely that our cells were at the transition of early to mid S-phase when Polη accumulation became visible at the locally damaged area. Unlike PCNA, however, Polη does not show any damage accumulation outside S-phase. Unrepaired sites could remain after TLS even until the next S-phase, where Polη would accumulate again. A pattern like this has also been shown for PCNA, which reappeared at similar sites in the daughter cells, showing a similar distribution as in the parent cells [32].
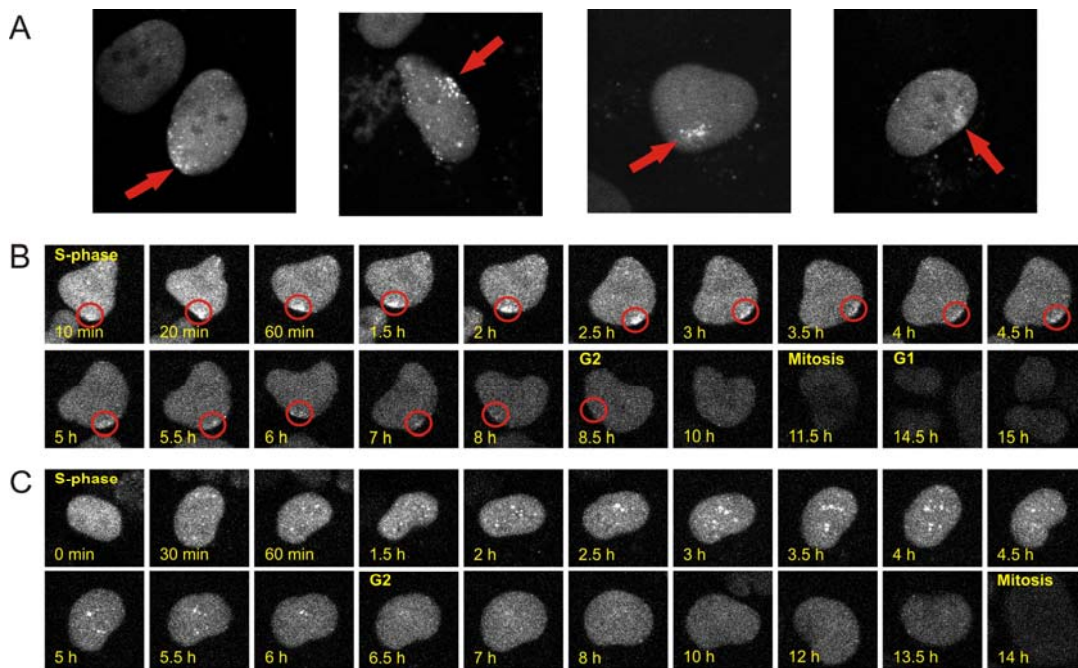

Fig. 6. Relocalisation of EGFP-Polη to confined damaged areas of the nucleus. (A) Four examples of locally damaged nuclei of XP30RO cells. The pictures show the fluorescence signal of EGFP-Polη in living cells obtained between 2 and 14 h after irradiation with 64 J/m^2 UV-C through a polycarbonate membrane bearing 8 μm pores (see Materials and Methods). Note the relatively faint overall S-phase foci in comparison to the locally damaged areas (indicated by red arrows). (B) Image series of a cell bearing local UV-induced DNA lesions. Fluorescence images were obtained every 10 min, using low laser power, for a duration of 15 h starting 10 min after UV filter irradiation. Depicted here is a locally damaged cell which is, in accordance to similar data obtained with PCNA [20], in the first image probably in early/mid S-phase. Subsequently, it shifts into late S-phase, G2, mitosis and G1. The local damage area (red circle), is visible throughout the S-phase and disappears in G2. Indicated at the bottom of the images are the times after local damage induction. (C) Image series of an undamaged S-phase cell in the same time-lapse experiment. An undamaged cell in (probably) early S-phase moves into the picture (1 h into the sequence, indicated time = 0 min), subsequently showing mid- and, even more clearly, late- S-phase patterns strikingly similar to PCNA, before entering mitosis. See M1 for the complete movie.

Undamaged cells in the same experiment show S-phase distribution of Polη in a pattern that mimics the one of PCNA (though less pronounced; [10, 20, 33], exhibiting smaller, evenly distributed foci in early/mid S-phase and fewer, bigger structures in the centre of the nucleus in late S-phase (Fig 6C and M1). Surprisingly, we could not observe a significant delay in cell-cycle progression (and in particular S-phase duration) in cells containing local UV-damage versus non-damaged cells. It should be stated, however, that the cells under investigation are SV40-immortalized and therefore have lost important DNA damage–induced checkpoints by SV40 Large T-inactivation of p53.

M1. Time-lapse experiment of XP30RO cells stably expressing EGFP-Polη, after introducing local UV damage using a polycarbonate filter. The red arrow indicates a locally damaged cell that could be monitored until it underwent mitosis and entered G1. A white arrow indicates an undamaged cell that entered the monitoring field when it was in (probably) early S-phase one hour into the time-lapse recording and remained visible until it underwent mitosis. Both cells show redistribution patterns throughout the cell cycle which strikingly resemble the ones of PCNA [20], with the exception that no accumulation of Polη is visible in G1 cells bearing local DNA damage. Note that EGFP-Polη foci are less distinct than PCNA foci. The probable reason for this is that PCNA is more stably bound to replication structures than Polη, resulting in easier discernible subnuclear structures.

The above results are consistent with the following scenario for Polη engagement in TLS. Upon arrest of the high-fidelity regular replication machinery by persistent DNA damage (e.g. UV-induced CPDs that are poorly repaired by global genome NER) modification (ubiquitination) of a large number of PCNA trimers occurs. These serve as a transient binding platform for the TLS machinery including a series of TLS polymerases and auxiliary factors, explaining the foci that contain in the order of 100 or more GFP-tagged molecules. The transient binding to modified PCNA trimers creates a locally elevated concentration of free TLS factors (such as Polη). This in turn speeds up the complicated polymerase switches that need to find the most appropriate TLS polymerase that allows (relatively error-free) bypass of the lesion.

Together, our data provide insight into the highly dynamic behaviour of Polη within the context of living cells. Clearly, more experiments are required to fully uncover the cell-cycle specific responses of Polη in the nucleus, to UV-induced and other challenges to DNA replication forks. Additional analysis of diverse mutant proteins, especially with mutations that impair interaction with mono-ubiquitinated PCNA, and the interaction and cooperation between diverse TLS polymerases, especially polι, would be highly interesting. Future work will hopefully shed more light on how this fascinating aspect of chromatin-associated processes, translesion synthesis, functions in the living cell.

Materials and Methods:

Cell lines and culture conditions:

For all studies on Polη, SV40-transformed XP30RO cells (XP-V; [34]) were used, stably expressing the peGFP-polη plasmid described in [1]. The plasmid contains the full-length human polη gene, except its first ATG, fused in-frame downstream of the eGFP-cDNA. XPG was studied in XPG-deficient human (XPCS1RO) and CHO (UV135) cells stably expressing the functional fusion gene of full-length human XPG and EGFP [16]. The cells were grown in a 1:1 mixture of Dulbecco's Modified Eagle medium and Ham's F10 medium containing Ultra-Glutamine (Cambrex Corporation) supplemented with antibiotics and 10 % foetal calf serum (FCS), at 37°C in an atmosphere of 5% CO_2.

UV irradiation and drug treatment:

For induction of global UV DNA damage, cultured cells on coverslips were rinsed with PBS and irradiated with a Phillips TUV lamp (254 nm) at a dose rate of ~0.8 J/m^2/s. To induce local UV damage, cells were UV irradiated through a polycarbonate filter (Millipore Billerica) with pores of 8 µm diameter, as described previously [14, 30].

HU and Ara-C (Sigma) were dissolved in water and added to the culture for 30 min at an end concentration of 0.1mM and 2mM, respectively.

Live cell microscopy:

Cells were seeded onto 24 mm glass cover slips, unless indicated otherwise about 3 days before imaging. Digital images of EGFP-expressing living cells were obtained using a Zeiss LSM 410 confocal microscope equipped with a 60-mW Ar laser (488 nm) and a 40x, 1.3 n.a. or a 63x 1.4 n.a. oil immersion lens or a Zeiss LSM 510 META equipped with a 60-mW Ar laser (488 nm) and a 40x, 1.2 n.a. or 63x Planapochromat 1.4 n.a. oil immersion lens (Zeiss, Oberkochen, Germany). Both microscopes were equipped with an objective heater and a heated scan stage. Time-lapse experiments longer than 45 min were conducted with a Zeiss LSM 510 META equipped with a heated chamber providing an atmosphere with 5% CO_2. Unless stated otherwise, cells were examined at 37°C.

FRAP experiments:

Using a Zeiss LSM 410 confocal microscope, mobility measurements were performed by FRAP analysis at a high time resolution (Strip-FRAP; [14, 16, 18]). A 0.2 µm (2-pixel) strip spanning the nucleus was photobleached for 200 ms at 100% laser intensity (120 to 160 µW; argon laser at 488 nm). Recovery of fluorescence within the strip was monitored using 100-ms intervals and low laser intensity (around 800 nW) to avoid photobleaching by the probe beam.

FRAP analysis:

FRAP data were analysed with a custom-written LabView program employing the nonlinear Levenberg-Marquardt algorithm for the general model accounting for both free and anomalous (hindered) diffusion ([35]; Ibrahim et al., in preparation). Assuming that recovery after bleaching is solely due to a single diffusing species, the fluorescence intensity f_t at any time for a Gaussian laser beam was approximated by the equation: $f_t=[f_0+f_\infty(t/t_{1/2})^\alpha]/[(1+t/t_{1/2})^\alpha]$, where f_0 is the fluorescence intensity immediately after photobleaching, f_∞ is the maximum recovered intensity attainable after a long time, $t_{1/2}$ is the time to half of the maximum recovery (i.e $(f_\infty+ f_0)/2)$; α is the anomaly parameter,

which in our FRAP studies was set to 1 assuming free diffusion. A 3-dimensional diffusion coefficient D_{eff} of the mobile molecules is obtained from $t_{1/2}$ by $D=(\gamma\omega^2)/(6t_{1/2})$, where ω is the width of the bleached strip and γ a bleach parameter obtained as described by [36].

Combined FRAP and FLIP:

Using a Zeiss 510 META confocal LSM, a 2 µm (30-pixel) strip spanning the cell nucleus at one pole was bleached for 4 s at a laser power of 120 to 160 µW. Redistribution of fluorescence throughout the nucleus was recorded at low laser power (1.6 to 1.9 µW), keeping monitoring bleaching to a minimum (<5%). We compared the difference between the fluorescence in the bleached and in the unbleached area (at a distance of 150 pixels = 10.2 µm) of the nucleus $\{\Delta I_{rel}(t) = [(I_t/I_0)\text{unbleached} - (I_t/I_0)\text{bleached}]$, whereby I_0 is the fluorescence intensity before bleaching$\}$ and normalized to the first datum point after bleaching. The fluorescence values were plotted on a log scale against time, and the indicated times of 90% redistribution were used as reference values for the mobility of the proteins (beyond this the data become too noisy for a meaningful representation in a log scale). Images were analysed using a custom-written Labview program. Redistribution of fluorescence was corrected for lateral cell movement and rotating cells or cells moving out of focus were excluded from evaluation.

Simultaneous FRAP/FLIP to determine binding time in foci:

Cells containing foci were analysed 4-9h after irradiating them with 8 J/m^2 UV-C. A Zeiss 410 META Confocal microscope was used to photobleach about half the nucleus for 1 s at 140 µW laser intensity [37]. Redistribution of fluorescence after the bleach pulse was monitored with 4-s time intervals at 7.5 µW. For bleaching as well as imaging a 63x Planapochromat 1.4 n.a. oil immersion lens was used. Images were analysed using KS400 software (Zeiss) and subsequently a custom-written Labview program. The differences between relative fluorescence intensities of bleached (FRAP) and unbleached (FLIP) regions were calculated as in the combined FRAP-FLIP procedure described above $\{\Delta I_{rel}(t) = [(I_t/I_0)\text{unbleached} - (I_t/I_0)\text{bleached}]\}$, the resulting curves fitted to a simple exponential decay function of the form $y = y_0 + a*e^{-ct}$ and the half-times of recovery ($t_{1/2}$) derived from the decay constant c using the expression $t_{1/2} = ln(2)/c$. The mean binding time of the protein has been calculated as the difference of the two $t_{1/2}$ (bound and unbound fraction) multiplied with 4.5. *a* depicts the amplitude in the decay function, in this case it relates to the fluorescence intensity at the beginning.
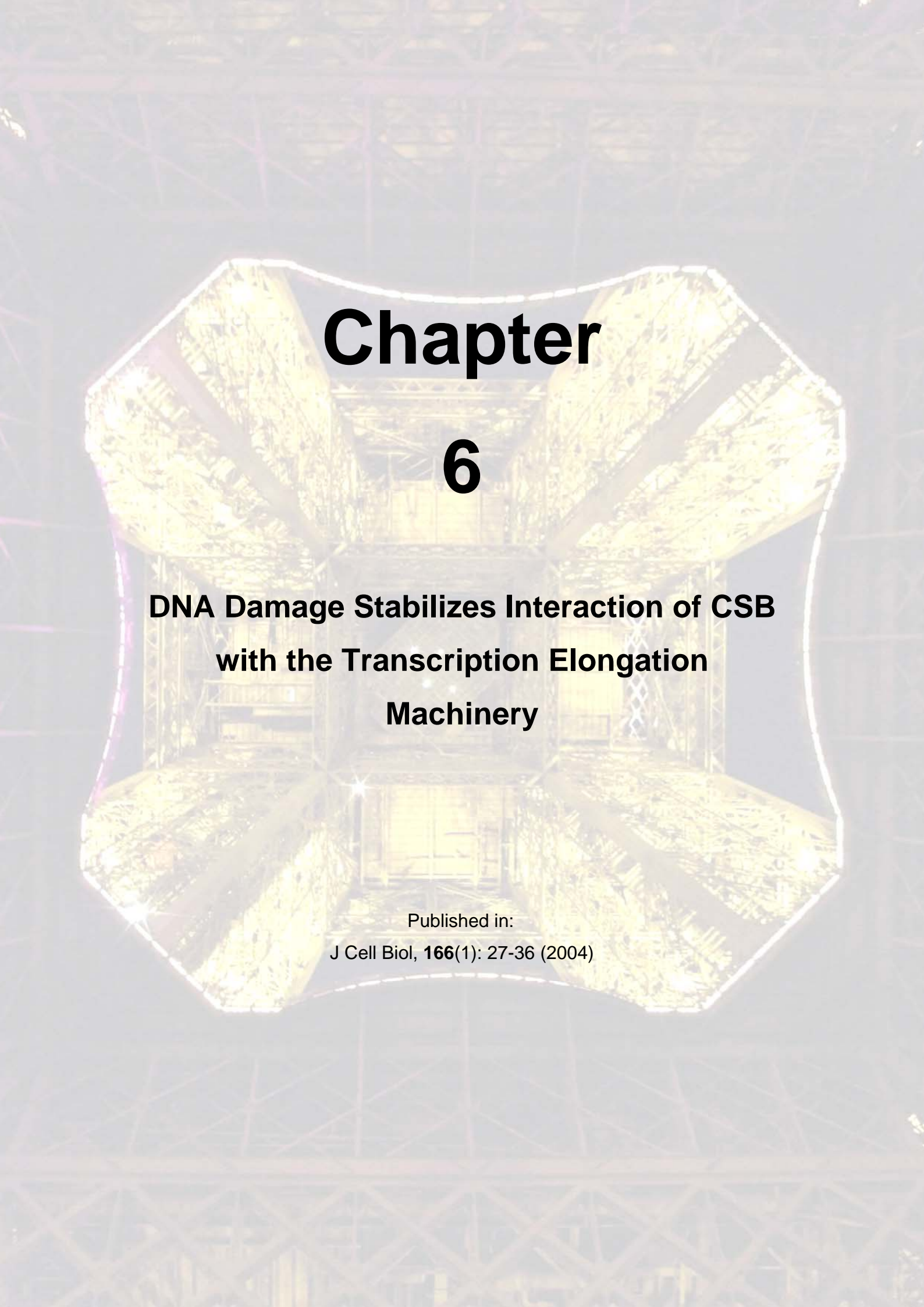
References:

1. Kannouche, P., et al., *Domain structure, localization, and function of DNA polymerase eta, defective in xeroderma pigmentosum variant cells.* Genes Dev, 2001. **15**(2): p. 158-72.

2. Woodgate, R., *A plethora of lesion-replicating DNA polymerases.* Genes Dev, 1999. **13**(17): p. 2191-5.

3. Ohmori, H., et al., *The Y-family of DNA polymerases.* Mol Cell, 2001. **8**(1): p. 7-8.

4. Goodman, M.F., *Error-prone repair DNA polymerases in prokaryotes and eukaryotes.* Annu Rev Biochem, 2002. **71**: p. 17-50.

5. Johnson, R.E., et al., *Fidelity of human DNA polymerase eta.* J Biol Chem, 2000. **275**(11): p. 7447-50.

6. Masutani, C., et al., *Mechanisms of accurate translesion synthesis by human DNA polymerase eta.* Embo J, 2000. **19**(12): p. 3100-9.

7. de Laat, W.L., N.G. Jaspers, and J.H. Hoeijmakers, *Molecular mechanism of nucleotide excision repair.* Genes Dev., 1999. **13**(7): p. 768-785.

8. Gillet, L.C.J. and O.D. Scharer, *Molecular Mechanisms of Mammalian Global Genome Nucleotide Excision Repair.* Chem. Rev., 2006. **106**(2): p. 253-276.

9. Lehmann, A.R., et al., *Translesion synthesis: Y-family polymerases and the polymerase switch.* DNA Repair (Amst), 2007. **6**(7): p. 891-9.

10. Leonhardt, H., et al., *Dynamics of DNA replication factories in living cells.* J Cell Biol, 2000. **149**(2): p. 271-80.

11. Limoli, C.L., et al., *Inaugural article: polymerase eta deficiency in the xeroderma pigmentosum variant uncovers an overlap between the S phase checkpoint and double-strand break repair.* Proc Natl Acad Sci U S A, 2000. **97**(14): p. 7939-46.

12. Cleaver, J.E., et al., *Polymerase eta and p53 jointly regulate cell survival, apoptosis and Mre11 recombination during S phase checkpoint arrest after UV irradiation.* DNA Repair (Amst), 2002. **1**(1): p. 41-57.

13. Limoli, C.L., et al., *UV-induced replication arrest in the xeroderma pigmentosum variant leads to DNA double-strand breaks, gamma -H2AX formation, and Mre11 relocalization.* Proc Natl Acad Sci U S A, 2002. **99**(1): p. 233-8.

14. Hoogstraten, D., et al., *Rapid Switching of TFIIH between RNA Polymerase I and II Transcription and DNA Repair In Vivo.* Mol Cell, 2002. **10**(5): p. 1163-74.

15. Rademakers, S., et al., *Xeroderma pigmentosum group A protein loads as a separate factor onto DNA lesions.* Mol Cell Biol, 2003. **23**(16): p. 5755-67.

16. Zotter, A., et al., *Recruitment of the nucleotide excision repair endonuclease XPG to sites of UV-induced dna damage depends on functional TFIIH.* Mol Cell Biol, 2006. **26**(23): p. 8868-79.

17. Watanabe, K., et al., *Rad18 guides poleta to replication stalling sites through physical interaction and PCNA monoubiquitination.* Embo J, 2004. **23**(19): p. 3886-96.

18. van den Boom, V., et al., *DNA damage stabilizes interaction of CSB with the transcription elongation machinery.* J Cell Biol, 2004. **166**(1): p. 27-36.

19. Sporbert, A., et al., *DNA polymerase clamp shows little turnover at established replication sites but sequential de novo assembly at adjacent origin clusters.* Mol Cell, 2002. **10**(6): p. 1355-65.

20. Essers, J., et al., *Nuclear dynamics of PCNA in DNA replication and repair.* Mol Cell Biol, 2005. **25**(21): p. 9350-9.

21. Maga, G. and U. Hubscher, *Proliferating cell nuclear antigen (PCNA): a dancer with many partners.* J Cell Sci, 2003. **116**(Pt 15): p. 3051-60.

22. Sporbert, A., et al., *PCNA acts as a stationary loading platform for transiently interacting Okazaki fragment maturation proteins.* Nucleic Acids Res, 2005. **33**(11): p. 3521-8.

23. Kannouche, P.L., J. Wing, and A.R. Lehmann, *Interaction of human DNA polymerase eta with monoubiquitinated PCNA: a possible mechanism for the polymerase switch in response to DNA damage.* Mol Cell, 2004. **14**(4): p. 491-500.

24. Lehmann, A.R., *Clubbing together on clamps: The key to translesion synthesis.* DNA Repair (Amst), 2006. **5**(3): p. 404-7.

25. Essers, J., et al., *Nuclear dynamics of RAD52 group homologous recombination proteins in response to DNA damage.* Embo J, 2002. **21**(8): p. 2030-7.

26. Solovjeva, L., et al., *High mobility of flap endonuclease 1 and DNA polymerase eta associated with replication foci in mammalian S-phase nucleus.* Mol Biol Cell, 2005. **16**(5): p. 2518-28.

27. Merrick, C.J., D. Jackson, and J.F. Diffley, *Visualization of altered replication dynamics after DNA damage in human cells.* J Biol Chem, 2004. **279**(19): p. 20067-75.

28. Washington, M.T., et al., *Mismatch extension ability of yeast and human DNA polymerase eta.* J Biol Chem, 2001. **276**(3): p. 2263-6.

29. Schermelleh, L., et al., *Dynamics of Dnmt1 interaction with the replication machinery and its role in postreplicative maintenance of DNA methylation.* Nucleic Acids Res, 2007. **35**(13): p. 4301-12.

30. Volker, M., et al., *Sequential Assembly of the Nucleotide Excision Repair Factors In Vivo.* Molecular Cell, 2001. **8**(1): p. 213-224.

31. Stelter, P. and H.D. Ulrich, *Control of spontaneous and damage-induced mutagenesis by SUMO and ubiquitin conjugation.* Nature, 2003. **425**(6954): p. 188-91.

32. Essers, J., et al., *Dynamics of relative chromosome position during the cell cycle.* Mol Biol Cell, 2005. **16**(2): p. 769-75.

33. Somanathan, S., et al., *Targeting of PCNA to sites of DNA replication in the mammalian cell nucleus.* J Cell Biochem, 2001. **81**(1): p. 56-67.

34. Cleaver, J.E., et al., *Increased ultraviolet sensitivity and chromosomal instability related to P53 function in the xeroderma pigmentosum variant.* Cancer Res, 1999. **59**(5): p. 1102-8.

35. Feder, T.J., et al., *Constrained diffusion or immobile fraction on cell surfaces: a new interpretation.* Biophys J, 1996. **70**(6): p. 2767-73.

36. Wolf, D.E., and M. Edidin. , ed. *Methods of measuring diffusion and mobility of molecules in surface membranes* In Techniques in Cellular Physiology, ed. P. Baker. Vol. 1. 1981, Elsevier/North Holland Biomedica: Amsterdam. 105.

37. Mattern, K.A., et al., *Dynamics of protein binding to telomeres in living cells: implications for telomere structure and function.* Mol Cell Biol, 2004. **24**(12): p. 5587-94.
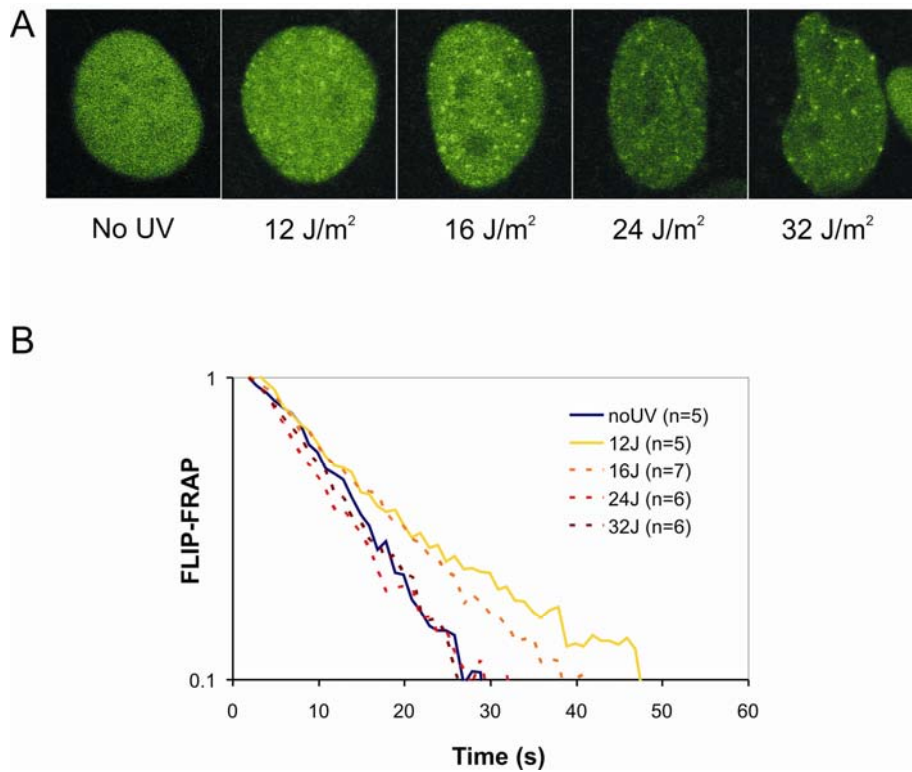
S1. Localization and mobility of Polη in response to higher than saturating UV-C doses. (A) Representative images of XP30RO cells expressing EGFP-Polη after the indicated doses of UV. (B) Simultaneous FRAP/FLIP analysis after UV doses higher than 12 J/m^2. The delay in Polη redistribution after photobleaching is declining in a UV dose-dependent manner, in spite of the cells exhibiting clear foci (S1.A). As a reference, mobility curves in untreated cells and after 12 J/m^2 UV are reproduced from Fig. 4. B. Dark blue line, Polη mobility in untreated cells not exhibiting foci; yellow line, after 12 J/m^2; dotted lines represent redistribution curves after higher UV doses: dotted brown line, after 16 J/m^2; red, after 24 J/m^2; dark red, after 32 J/m^2; n, number of cells analyzed.

Chapter

6

DNA Damage Stabilizes Interaction of CSB with the Transcription Elongation Machinery

DNA Damage Stabilizes Interaction of CSB with the Transcription Elongation Machinery

Vincent van den Boom[1]*, Elisabetta Citterio[2]*, Deborah Hoogstraten[1], Angelika Zotter[1], Wiggert A. van Cappellen[3], Jan H.J. Hoeijmakers[1], Adriaan B. Houtsmuller[4,5] and Wim Vermeulen[1,5]

[1] Department of Cell Biology and Genetics, Medical Genetic Cluster, Erasmus MC Rotterdam, P.O. box 2040, 3000 CA Rotterdam, The Netherlands.

[2] Present address: IFOM-FIRC Institute of Molecular Oncology, via Adamello 16, 20139 Milano, Italy.

[3] Department of Endocrinology and Reproduction, Medical Genetic Cluster, Erasmus MC Rotterdam, P.O. box 2040, 3000 CA Rotterdam, The Netherlands.

[4] Department of Pathology, Josephine Nefkens Institute, Erasmus MC Rotterdam, P.O. box 2040, 3000 CA Rotterdam, The Netherlands;

*these authors contributed equally to this work

[5] To whom correspondence should be addressed.

Abstract

The Cockayne syndrome B (CSB) protein is essential for transcription-coupled DNA repair (TCR), which is dependent on RNA polymerase II elongation. TCR is required to quickly remove the cytotoxic transcription-blocking DNA lesions. Functional GFP-tagged CSB, expressed at physiological levels, was homogeneously dispersed throughout the nucleoplasm in addition to bright nuclear foci and nucleolar accumulation. Photobleaching studies showed that GFP-CSB, as part of a high molecular weight complex, transiently interacts with the transcription machinery. Upon (DNA damage-induced) transcription arrest CSB binding these interactions are prolonged, most likely reflecting actual engagement of CSB in TCR. These findings are consistent with a model in which CSB monitors progression of transcription by regularly probing elongation complexes and becomes more tightly associated to these complexes when TCR is active.

Introduction

Metabolic by-products such as reactive oxygen species (ROS), environmental compounds and short-wave electromagnetic radiation (γ and UV) continuously jeopardize the DNA structure. DNA injuries directly disturb vital DNA-transacting processes such as replication, transcription and cell cycle progression. Evidence in the literature suggests that DNA damage-induced transcriptional interference triggers apoptosis (Ljungman and Zhang, 1996; Yamaizumi and Sugano, 1994). Our previous work on repair-deficient mice provided strong support for our hypothesis that this damage-induced apoptosis leads to segmental ageing (de Boer et al., 2002). Moreover, DNA lesions may result in permanent mutations in the DNA sequence, eventually causing cancer. In order to prevent the severe consequences of genetic erosion a variety of distinct and partially overlapping DNA repair pathways has evolved, each specialized in the removal of specific types of damage (Friedberg et al., 1995; Hoeijmakers, 2001). Priority is given to remove the highly cytotoxic transcription-blocking injuries, allowing quick resumption of transcription. This process, referred to as transcription-coupled repair (TCR) (Mellon et al., 1987), is directly triggered by lesion-induced obstruction of elongating RNA polymerase II (RNAP II). An example of transcription-blocking lesions are DNA helix distorting, UV-induced cyclo-butane pyrimidinedimers (CPDs) and 6-4 photoproducts (6-4PPs. Dependent on the type of lesion stalled RNAP II complexes are first identified by TCR-specific factors and further processed by the core nucleotide and perhaps base excision repair (NER and BER, respectively) factors (Le Page et al., 2000). Removal of lesions in non-transcribed areas of the genome is dependent on global genome repair (GGR).

Inherited defects within genes involved in the TCR-pathway give rise to the rare autosomal recessive disorder Cockayne syndrome (CS; Venema et al., 1990; Van Hoffen et al., 1993). CS patients display mainly progeroid symptoms, growth failure and severe neurological abnormalities and are not cancer-prone (Nance and Berry, 1992). Most of the salient clinical symptoms expressed among CS individuals, except sun-sensitive skin, are difficult to explain by a DNA repair defect only. Within classical Cockayne syndrome two genes are involved, CSA and CSB (Troelstra et al., 1992; Henning et al., 1995). The proteins encoded by these genes are essential for TCR, however their exact function in this process remains elusive. The 44 kD CSA protein contains 5 WD repeats; polypeptides with these repeats are usually involved in formation of macromolecular complexes via the WD-repeat regions (Neer et al., 1994). The 168 kD CSB protein is a member of the SWI2/SNF2 protein family of putative helicases, which includes a variety of proteins involved in transcriptional

regulation, chromatin remodelling and DNA repair (Pazin and Kadonaga, 1997). Biochemical studies showed that recombinant CSB is a DNA-dependent ATPase and is able to remodel chromatin at the expense of ATP (Citterio et al., 1998; Citterio et al., 2000).

Because TCR only occurs in the presence of active transcription, it was suggested that the CS proteins probably interact with elongating RNA polymerase complexes. Moreover, besides a pivotal role in TCR, several lines of evidence suggest an additional function of CS proteins, particularly CSB, in the elongation phase of RNAP II transcription. Gel filtration and immuno-precipitation studies showed that CSB resides in a high molecular weight complex and that a part of these higher order assemblies contain RNAP II (van Gool et al., 1997). Gel mobility shift assays further revealed that CSB interacts with a ternary complex of DNA, RNAP II and nascent RNA (Tantin et al., 1997) and *in vitro* transcription experiments showed that CSB stimulates RNAP II elongation (Selby and Sancar, 1997). In addition, Rad26 (the yeast counterpart of CSB) was found to be required for transcription *in vivo* (Lee et al., 2001). Recently, in a genetic screen for suppressor mutants of Rad26, Spt4 was identified (Jansen et al., 2000). Spt4 is part of a protein complex known to associate with and regulate the processivity of RNAP II, further supporting a function of CSB in transcription elongation (Hartzog et al., 1998; Wada et al., 1998).

A potential problem for the repair machinery is that lesion-stalled polymerases impede the accessibility of repair factors to these lesions by sterical hindrance (Donahue et al., 1994). Several models have been suggested that describe the function of the CS proteins and the fate of stalled RNAP II complexes at lesions: (*i*) backtracking of the RNAP II complex, providing access to lesions (Tornaletti and Hanawalt, 1999); (*ii*) pushing the elongating polymerase past the lesion, translesion transcription; (*iii*) physical removal of the complex; (*iv*) proteolytic degradation of the stalled polymerase; or (*v*) recruiting NER proteins that compete with RNAP II. Efforts to set up an *in vitro* system for TCR have met with little success. A possible explanation is that *in vitro* systems lack the structural elements that are required for proper TCR function (such as nuclear matrix attachment or chromatinated DNA). Particularly, the topological and ATP-dependent chromatin remodelling activity of CSB suggests a role for this protein in remodelling the chromatin structure or the interaction surface of the stalled RNAP II with DNA, to permit admission of the NER machinery to the lesion. However, an adequate model at which stage the TCR factors CSA and CSB are operational is lacking.

To address some of these issues, we investigated the involvement of CSB in TCR and RNAP II transcription elongation in the most relevant context, the living cell. We generated a cell line that stably expresses physiologically relevant levels of a biologically active fusion protein of the green fluorescent protein (GFP) and CSB. Spatial and temporal distribution of GFP-CSB was monitored with live cell confocal microscopy. In addition we determined the *in vivo* reaction parameters of this protein when engaged in repair and transcription by using FRAP (for fluorescence recovery after photobleaching) analysis to measure the mobility of GFP-CSB in untreated transcriptionally active cells and compared these with transcription-inhibited cells and cells challenged with a high dose of UV-light (DNA damage induction).

Results

Expression of GFP-CSB in human fibroblasts

To study the nuclear localization and dynamics of the CSB protein in living cells, we tagged the protein with GFP. Enhanced GFP was fused to the amino-terminus of CSB (Fig. 1A), resulting in a GFP-CSB fusion protein, which was stably expressed in CSB-deficient human fibroblasts (CS1AN-Sv). Immunoblot analysis, using anti-CSB (Fig. 1B) and anti-GFP (data not shown) antibodies, showed that GFP-CSB migrates at the expected height of full-length fusion protein (~195 kD) in two independent clones, and was expressed at physiological levels. In addition, the GFP-CSB cDNA was able to fully correct the UV-sensitivity of CS-B cells (Fig. 1C), stressing that GFP-CSB is functional *in vivo*.

Localization of GFP-CSB in living cells

Confocal microscopy demonstrated that CSB-GFP predominantly resided in the nucleus (Fig. 1D), where it accumulated in small bright foci, in addition to a homogeneous distribution in the nucleoplasm. The foci were present in a large fraction of the investigated cells in varying number and size. In addition, the fusion protein was enriched in nucleoli (Fig. 1D). Immuno-fluorescence studies in MRC5-SV and HeLa cells, using affinity-purified polyclonal anti-CSB antibodies to determine endogenous non-tagged CSB, revealed a more disrupted focal pattern than GFP-imaging in live cells. Immuno-staining of GFP-tagged CSB with anti-HA (GFP is tagged with HA) showed the same disrupted pattern (data not shown) as endogenously stained CSB. From these observations we conclude that the disrupted foci are caused by the applied fixation procedure. Together these data suggest that

the observed distribution is not due to GFP-tagging or to over-expression of the protein and likely reflects the physiologically relevant nuclear organization of CSB.
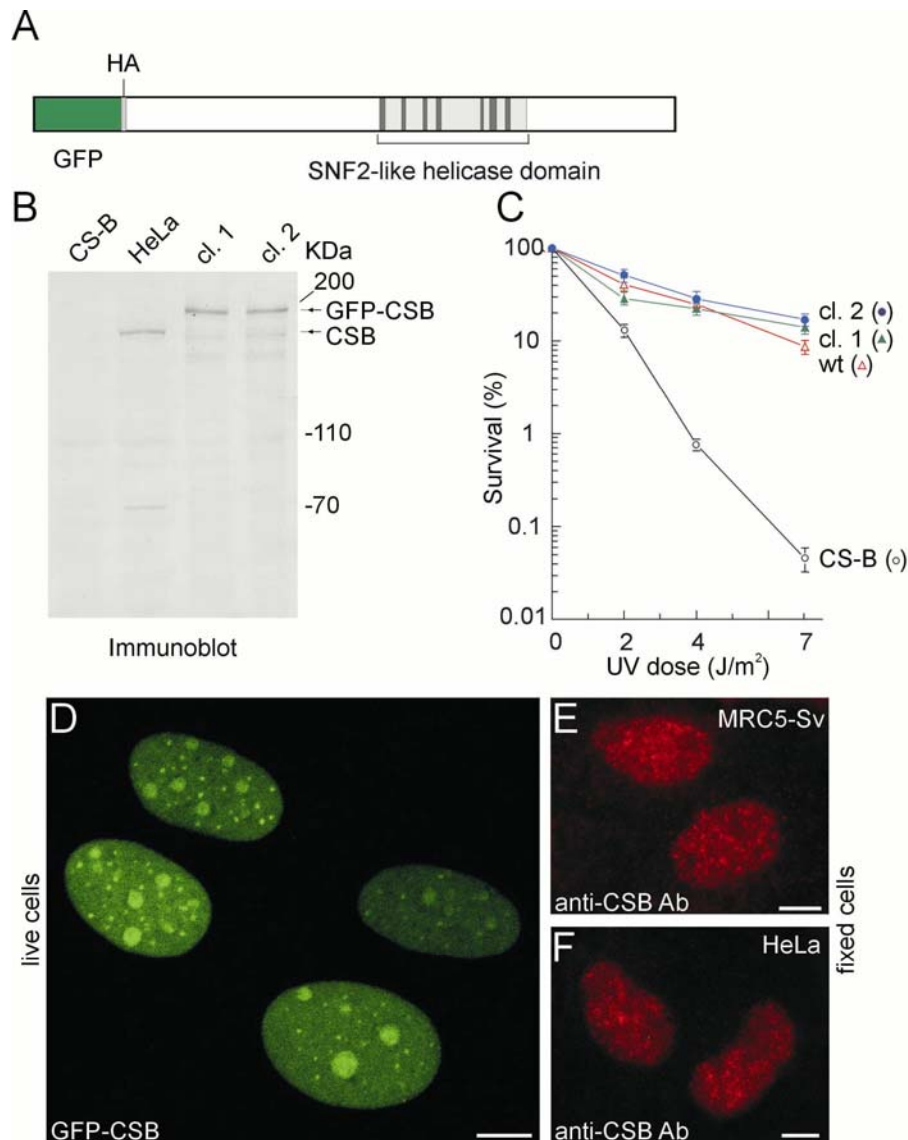

Fig. 1. Characterization of stably expressed GFP-CSB in CS1AN-Sv human fibroblasts. (A) Schematic representation of GFP-CSB fusion protein. The SNF2-like helicase domain is indicated. In between the GFP cDNA and the CSB open reading frame an HA tag is present. (B) Immunoblot analysis of GFP-CSB expression. Equal amounts of whole cell extracts (WCE) from CS1AN-Sv, HeLa and GFP-CSB transfected CS1AN-Sv fibroblasts (two independent clones, 1 and 2 respectively) were probed with affinity-purified polyclonal anti-CSB antibodies. (C) UV-survival of GFP-CSB expressing fibroblasts. The percentage of surviving cells is plotted against the applied UV dose. Survival of clones 1 and 2 and control cell lines after UV-treatment was determined by pulse labelling with ^{3}H-thymidine: CS1AN-Sv, CS-B (black open circles); VH10-Sv, wt (red open triangles), clone 1 (green triangles), clone 2 (blue circles). Both clones show a complete restoration of the CS-specific UV-sensitivity, indicating that the GFP-tagged CSB protein is fully functional. (D) Subnuclear localization of GFP-CSB in living stably transfected CS1AN-Sv human fibroblasts. All cells show a strict nuclear distribution and focal and

nucleolar accumulations of GFP-CSB in the nucleoplasm. (E-F) Epifluorescent images of MRC5-Sv human fibroblasts (F) and HeLa cells (G) immuno-stained with affinity-purified anti-CSB antibodies. Scale bars are 10 μm.

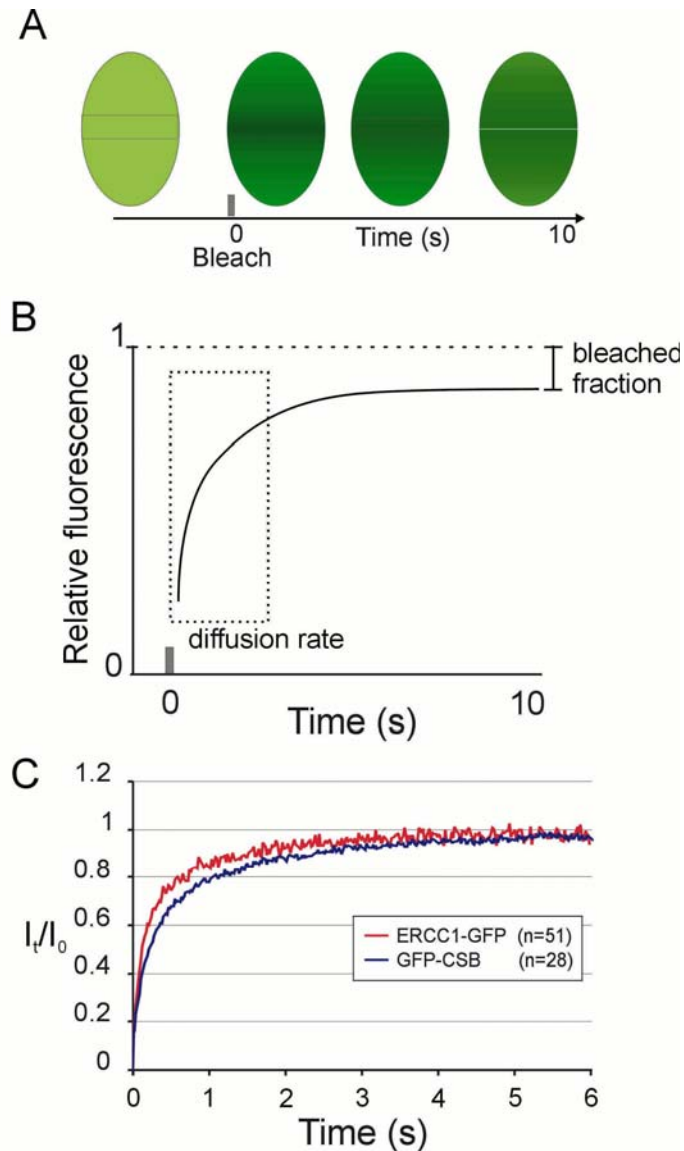### Nuclear mobility of GFP-CSB in living cells

Fig. 2. FRAP analysis of GFP-CSB nuclear mobility. (A) During a FRAP experiment all fluorescent molecules in a small defined strip spanning the nucleus are bleached and subsequent fluorescent recovery is measured. (B) Plotting the recovery relative fluorescent intensity of the strip in time shows a small permanently bleached fraction as caused by the initial bleach pulse. The rate of fluorescent recovery in the strip is a measure for the effective diffusion rate (D_{eff}) of a protein. (C) FRAP analysis of GFP-CSB and ERCC1-GFP expressing cells show a recovery of fluorescence in the strip.

To investigate whether GFP-CSB is bound to subnuclear structures or is moving freely we measured the GFP-CSB nuclear mobility and the dynamic properties of GFP-CSB molecules by applying a FRAP protocol to the cells. Briefly, a 2μm wide strip spanning the nucleus was bleached and fluorescence recovery in the strip was measured at 100 ms intervals (Fig. 2A). The rate of recovery of fluorescence in the bleached strip is a measure for the diffusion rate of the tagged protein (Fig. 2B). Note that the fluorescent intensity in the strip does not recover to prebleach levels (set to one) since a fraction of the molecules is permanently bleached. Analysis of the FRAP data revealed that the majority of GFP-CSB molecules was freely mobile in the nucleoplasm with an effective diffusion coefficient (D_{eff}) of 7 μm^2/s (Fig. 2C). In addition, the 163 kD XPF/ERCC1-GFP complex, which is involved in the core NER reaction (Houtsmuller et al., 1999), had a D_{eff} of 12 μm^2/s, clearly higher than that of GFP-CSB. This suggests that GFP-CSB resides in a high MW complex (>800 kD), confirming our previous gel filtration studies with HA-tagged CSB. (van Gool et al., 1997).

Transient immobilization of GFP-CSB in transcription

Previous *in vitro* experiments suggest that CSB interacts with RNAP II (Tantin et al., 1997; van Gool et al., 1997). Therefore, we studied the dynamic behaviour of GFP-CSB molecules in relation to transcription in living cells, using a combined FLIP/FRAP procedure (Fig. 3A) (Hoogstraten et al., 2002). Briefly, a region at one pole of the nucleus is bleached and the influx of fluorescence in the bleached area is monitored (FRAP) as well as the fluorescence loss in photobleaching (FLIP) at the opposite pole of the nucleus. The difference in relative fluorescent intensity between the FLIP and FRAP region in time is plotted on a logarithmic scale. The time to reach 90% redistribution of GFP-CSB fluorescence was 59 ± 8 seconds. For comparison with other conditions this value was set to 1 in the subsequent experiments. To investigate the relation between GFP-CSB mobility and transcription we incubated cells with various transcription inhibitors. The transcription elongation inhibitor H8 clearly induced a reduction in redistribution time (~20 %) as compared to transcriptionally active cells (Fig. 3B), suggesting a faster overall mobility of GFP-CSB molecules when transcription is inhibited. In sharp contrast, the DNA-intercalating agent Actinomycin D resulted in a severe loss of the ability for GFP-CSB molecules to redistribute, indicative of a long-term immobilization of CSB proteins (Fig. 3C). A similar differential response to transcription inhibitors was reported for RNAP II, where Actinomycin D also resulted in almost complete immobilization,

whereas the H8-like transcription inhibitor DRB led to increased mobility (Kimura et al., 2002). It was argued by the authors that DRB treatment results in release of RNAP II, whereas Actinomycin D irreversibly stalls the polymerase on its template. The similar behaviour in response to transcription inhibitors suggests a close relationship between elongating RNAP II and CSB in living cells. In contrast, XPF/ERCC1-GFP was not immobilized in presence of Actinomycin D, indicating that the immobilization of CSB is not caused by repair activity (data not shown).
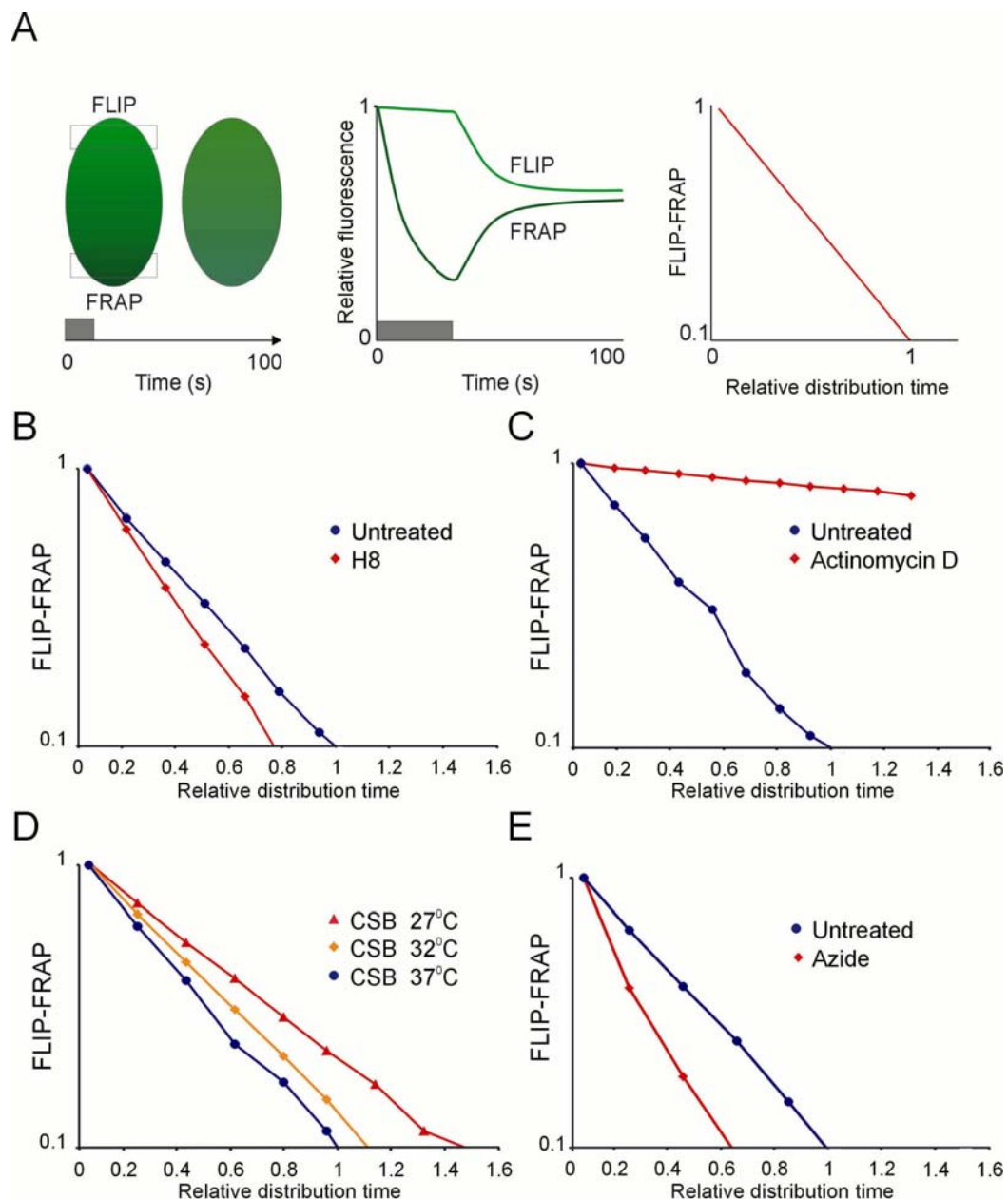

Fig. 3. Dynamic measurements of the GFP-CSB nuclear mobility by combined FLIP/FRAP analysis. (A) Combined FLIP/FRAP analysis was performed by bleaching at one pole of the nucleus and simultaneously monitoring the fluorescent recovery at the bleached (FRAP) and opposite (FLIP)

poles of the cell. After bleaching the FRAP curve shows a drop in fluorescent intensity followed by a recovery of fluorescence and the FLIP curve shows a slow decrease of fluorescent intensity due to redistribution of the bleached molecules. The relative intensities of FLIP and FRAP were subtracted and plotted (Y-axis) against the relative redistribution time of untreated cells (X-axis). (B) Combined FLIP/FRAP experiment of untreated cells (blue circles; n=10) and H8-treated cells (red diamonds; n=10). H8 treated cells display a decreased relative redistribution time as compared to untreated cells. C. Combined FLIP/FRAP experiment of untreated cells (blue circles; n=10) and Actinomycin D-treated cells (red diamonds; n=10). Actinomycin D treatment results in an increased relative redistribution time as compared to untreated cells. (D) Combined FLIP/FRAP experiments at different temperatures (27°C (red triangles), 32°C (orange diamonds) and 37°C (blue circles)). At low temperatures the relative redistribution time is increased. (E) Combined FLIP/FRAP experiment of untreated cells (blue circles, n=10) and azide-treated cells (red diamonds; n=10). Azide treated cells display a decreased relative redistribution time as compared to untreated cells.

Next, we applied the combined FLIP-FRAP procedure to cells cultured at different temperatures. The rationale behind this is that a relatively small difference in (absolute) temperature (Kelvin) has a negligible effect on diffusion rate, but strongly affects the duration of temperature-dependent enzymatic processes such as transcription and active transport (Phair and Misteli, 2000; Hoogstraten et al., 2002). Combined FLIP-FRAP of GFP-CSB expressing cells cultured at respectively 37, 32 and 27 ^{o}C revealed a significant decrease of mobility when temperature was reduced (Fig. 3D). In contrast, diffusion of freely mobile XPF/ERCC1-GFP (Houtsmuller et al., 1999) did not change upon lowering temperature (data not shown). Furthermore, ATP-depletion by azide induced an increased GFP-CSB mobility (Fig. 3E).

In conclusion, these observations strongly suggest that GFP-CSB mobility is decreased in transcriptionally active cells by transient temperature-dependent immobilizations, most likely due to association with elongating transcription complexes. The fluorescence recovery plots fitted best to curves generated by computer simulation of FRAP on molecules (see Materials and Methods) of which a small fraction (~17%) is shortly immobilized (2-5 s).

CSB-associated RNAP II is transcriptionally active in vitro

In order to provide biochemical evidence for the suggested interaction with the transcription machinery we isolated the CSB-RNAP II complex as described before using our previously generated human cell line expressing CSB tagged with a HA epitope (HA-CSB-[His]$_{6}$, referred to as 2tCSB; van Gool et al., 1997) and immunoaffinity purification by binding to an anti-HA antibody resin followed by elution with excess of HA-peptide. Immunopurified CSB was tested in an *in vitro* reconstituted transcription system (RTS) using an adenovirus major late promoter

template (Gerard et al., 1991; Coin et al., 1999). The HA-eluate from dtCSB whole cell extracts (WCE) was able to support the synthesis of the 309 nt transcript when RNAP II was omitted from the RTS (Fig. 4, compare lanes 3 and 14 with lanes 1 and 8, respectively), indicating that the CSB-associated RNAP II is transcriptionally active. In contrast, no signal was detected by addition of HA-eluate from normal HeLa WCE expressing normal CSB without HA-tag (Fig. 4, lane 5) or in the absence of any extract (Fig. 4, lane 7), supporting the specificity of the CSB-RNAP II interaction. To determine the presence of additional basal transcription components in the 2tCSB HA-eluate, transcription was performed in the absence of TBP (lanes 2, 4, 6 and 13), TFIIE, TFIIB, TFIIF, or TFIIH (lanes 9 to 12, respectively). In neither of these cases complementation for the lack of any of these factors was detected (Fig. 4, compare lane 2 with lane 3 and lanes 9 to 12 with lane 14), indicating that none of the transcription initiation factors were present in the 2tCSB (HA-elution) fraction in detectable amounts.
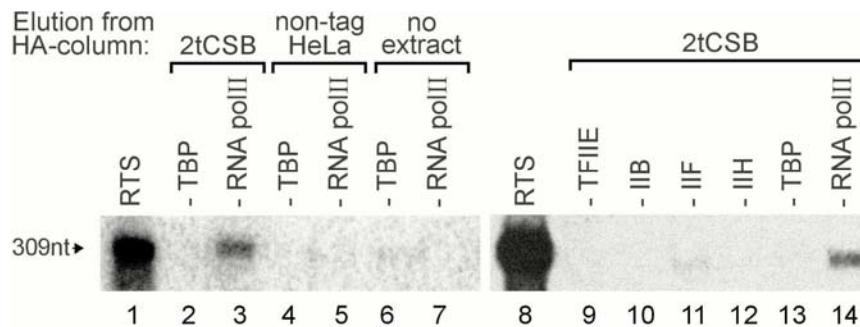

Fig. 4. *In vitro* transcriptional activity of CSB-associated RNA polymerase II. RNAP II transcriptional activity is present in the 2tCSB HA-eluate. *In vitro* transcription was performed in a reconstituted transcription system (RTS) containing human recombinant TBP, TFIIB, TFIIE, and highly purified HeLa TFIIA, TFIIF and RNAP II and the adenovirus major late promoter (AdMLP) as a template (309 nt). Lanes 1 and 8 show complete reactions. To determine the presence of transcription components in the tagged-CSB fraction, individual transcription factors (indicated on top of each lane) were omitted from reactions containing HA-eluate from 2tCSB WCE (lanes 2, 3 and 9 to 14). As a control, HA-eluate from HeLa WCE (lanes 4, 5), or no protein (lanes 6, 7) were added to reactions lacking TBP or RNAP II.

Nuclear mobility of GFP-CSB in UV-irradiated cells

To investigate the behaviour of GFP-CSB in transcription-coupled repair (TCR) we determined the overall nuclear mobility in UV-irradiated cells by FRAP analysis. Fluorescence recovery plots of UV-damaged cells (16 J/m^2, a repair-saturating UV dose; Fig. 5A, red line) revealed a small but reproducible reduction of

fluorescence recovery when compared to non-UV-damaged cells (blue line), indicating that a fraction of GFP-CSB molecules is immobilized for a longer period. In addition, the diffusion rate of the mobile GFP-CSB fraction in untreated and UV-irradiated cells is unaltered, indicating that the size of the CSB complex is not altered upon DNA damage induction (unpublished data).
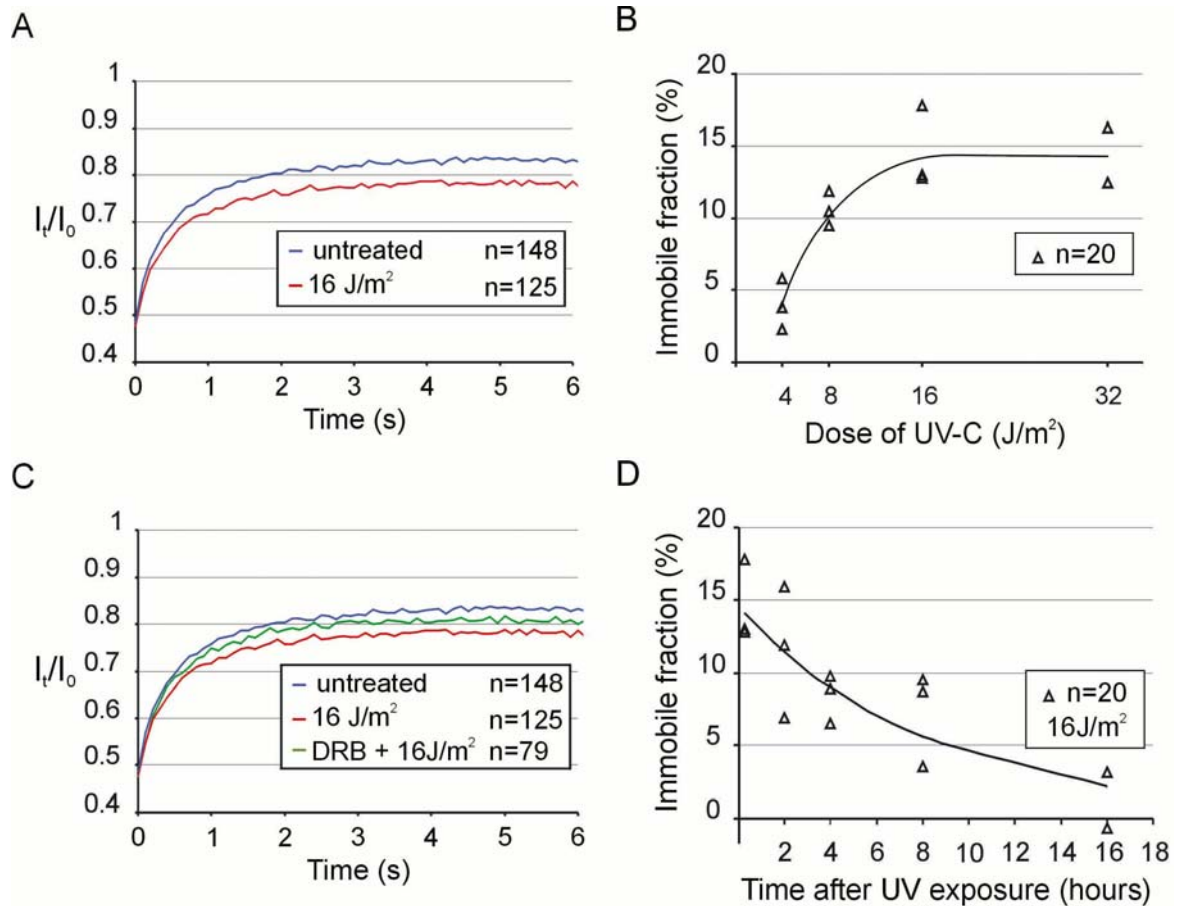

Fig. 5. FRAP analysis of GFP-CSB after UV irradiation. (A) FRAP analysis of untreated cells (blue line; n=148) and UV-irradiated cells (16J/m^2; red line; n=125). GFP-CSB mobility in UV-treated cells is measured between 5 and 25 minutes after irradiation. UV-treated cells show an immobilization of GFP-CSB. (B) Dose-dependency of GFP-CSB immobilization based on three independent experiments. (C) FRAP analysis of untreated cells (blue line; n=148), cells treated with DRB prior to UV irradiation (16J/m^2; green line; n=79) and cells treated with UV solely (16J/m^2; red line; n=125). DRB was added to the medium three hours prior to the experiment. (D) Dynamics of the immobile fraction of GFP-CSB in time after UV (16J/m^2) based on three independent experiments.

The amount of UV-induced immobilized molecules was proportional to UV-dose: from ~ 5% at 4 J/m^2 to a plateau of ~ 15 % at 16 J/m^2 (Fig. 5B). A similar UV-dose dependent immobilization was observed with core NER factors, such as ERCC1-GFP-XPF (Houtsmuller et al., 1999), GFP-XPA (Rademakers et al., 2003),

and TFIIH-GFP (Hoogstraten et al., 2002), although the maximum fraction of GFP-CSB immobilization (~15%) is significantly lower than found with the other NER factors (35-40%). No UV-induced immobilization was found with non-NER factors tagged with GFP (Houtsmuller et al., 1999) stressing the notion that immobilization is related to NER. This suggests that GFP-CSB binds more stably to stalled RNAP II than to elongating RNAP II.

When prolonged immobilization is dependent on stalled polymerases, and implicitly on TCR, we predict that the UV-induced immobilization requires active transcription. To verify this hypothesis we treated the cells with the transcription inhibitor DRB prior to UV irradiation. As shown in the mobility plot of Fig. 5 C (green line) a significant decrease of the immobile fraction upon transcriptional inhibition was apparent when compared to transcriptional active UV-irradiated cells (DRB did not completely prevent UV-induced immobilization, likely caused by incomplete transcription inhibition). This indicates that the observed immobilization of GFP-CSB is most likely due to its engagement in TCR.

When the immobilization of CSB reflects actual participation in TCR we expect that the immobilized fraction would decrease in time depending on progression of repair. Therefore we measured UV-dependent immobilization of GFP-CSB molecules at various time points after irradiation (Fig. 5 D, 16J/m^2). These experiments revealed that the bound fraction gradually decreased to background levels within 16 hours after UV. This indicates that UV-dependent immobilization of GFP-CSB is a reversible process. Interestingly, the kinetics of this process was much slower than anticipated on the basis of the efficient damage repair by TCR measured in selected genes (Mellon et al., 1987).

GFP-CSB mobility in NER-deficient (XP-A) cells

To investigate the effect of defective DNA repair on the mobility of GFP-CSB we examined UV-induced immobilization in repair deficient cells, lacking functional XPA (XP12RO). Comparative analysis of FRAP experiments applied to cells expressing GFP-CSB in either CSB- or XPA-deficient cells showed a slightly larger immobile fraction of CSB molecules in XPA cells upon UV irradiation, using a sub-saturating UV-dose of 8 J/m^2 (Fig. 6, A and B). This contrasts to UV treatment after transcription inhibition, where a smaller immobilized fraction was observed (Fig. 5 C). Importantly, and in contrast to GFP-CSB molecules in repair proficient cells (Fig. 6 C and Fig. 5 B), the fraction of immobilization in XPA-deficient cells did not decrease (nor increase) 4 hours after UV-damage induction (Fig.6D). The notion that the fraction of immobilized molecules is not substantially increased as compared to NER-

proficient cells, suggests that CSB molecules are not permanently trapped in repair complexes, but transiently interact with blocked polymerases. This transient interaction with abortive repair complexes is significantly different from the stable association of CSB with stalled RNAP II by Actinomycin D treatment (Fig. 3C; Kimura et al., 2002).
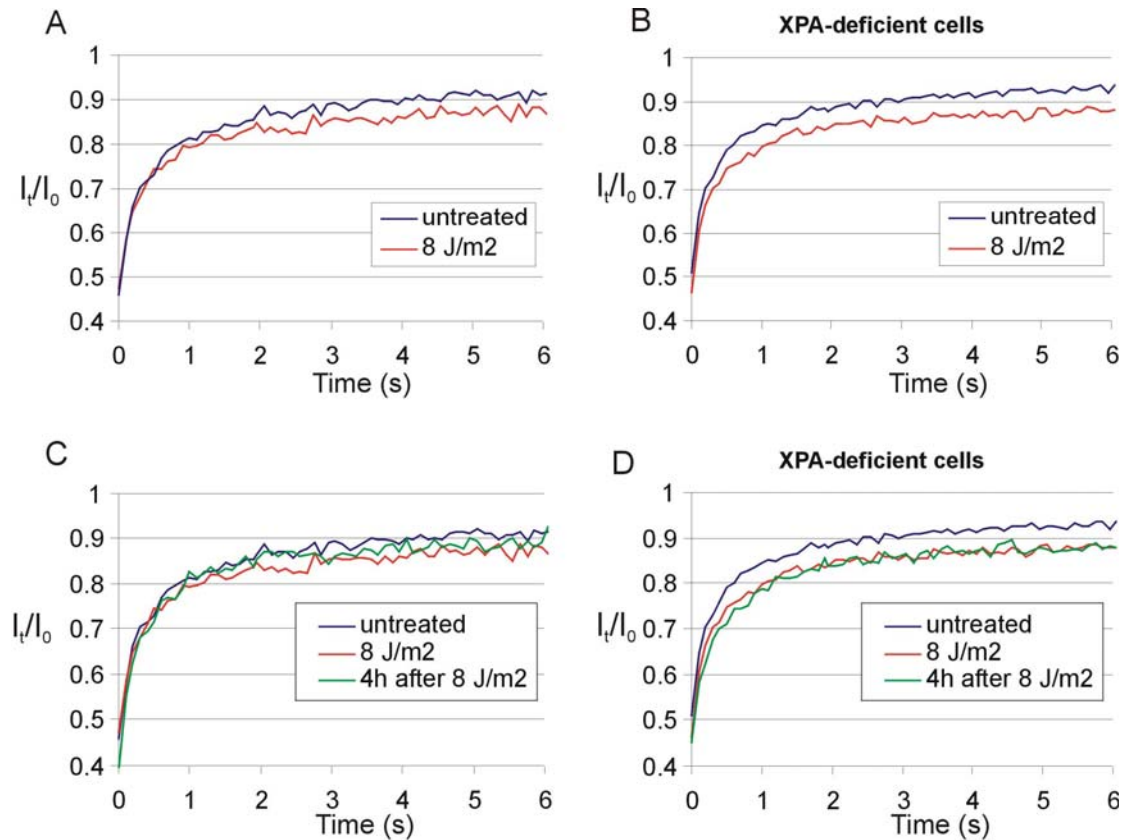

Fig. 6. FRAP analysis of GFP-CSB in NER-deficient (XP group A) cells. (A) FRAP curves of untreated (blue, line; n=20) and 8 J/m^2 UV-irradiated (red line; n= 20) GFP-CSB expressing CS1AN cells, measured between 5 and 15 minutes after UV irradiation. 8 J/m^2 induced a smaller immobile fraction as 16 J/m^2 as shown in Fig.5A. (B) Identical as panel A, however here GFP-CSB is expressed in XP group A cells, lacking functional NER. A slight increase in the immobile fraction is visible as compared to repair-proficient cells in panel A. (C) and (D) Identical to panel A and B respectively, with the exception that here also the FRAP measurements were plotted that were performed 4 hr post UV irradiation, with an intermediate immobilization in NER-proficient cells and no recovery of the immobilized fraction in XP-A cells

GFP-CSB accumulates at sites of local damage

DNA damage-dependent immobilization of GFP-CSB argues for a model in which CSB complexes that transiently interact with the transcription machinery remain longer bound to lesion-blocked polymerases than to elongating complexes.

To obtain further evidence for this hypothesis we locally inflicted UV lesions in cells expressing GFP-CSB using a porous UV-blocking membrane (Volker et al., 2001). Shortly after UV irradiation, we detected accumulations of GFP-CSB similar to those found for other NER proteins such as XPA (Fig. 7 A). XPA is involved in GGR and TCR and is known to accumulate at locally damaged areas in the cell (Rademakers et al., 2003; Volker et al., 2001). This indicates that GFP-CSB also accumulates at sites of DNA damage, most likely active in TCR. Interestingly, the number of accumulated GFP-CSB molecules in the damaged area is relatively stable at least up to 8 hours after UV (Fig. 7 A). These results are in line with our findings that upon overall UV irradiation an immobilization of GFP-CSB is measured until 16 hours after UV. This is in contrast to XPA, which showed an intense concentration of proteins a few minutes after UV that in the first two hours drops to a lower steady-state level (2 h after UV irradiation) and then slowly reduces towards background levels. In addition, immunofluorescence analysis showed that 6-4PPs are removed within 2 hours after UV, whereas the vast majority of CPD lesions are still present up to 8 h after local irradiation (Volker et al., 2001; unpublished data). This suggests that the early intense accumulation of XPA mainly reflects repair of 6-4PPs via the GGR pathway, whereas the subsequent less intense accumulation of XPA represents repair of CPDs.

Do these local accumulations reflect long-term (a few hours) immobilization of CSB molecules or are they the result of a dynamic equilibrium between binding and releasing molecules at the site of damage? To investigate this, we determined the GFP-CSB residence time in the accumulations by FRAP on damaged and non-damaged areas in the nucleus. For this purpose we bleached the fluorescence in the locally damaged region. Interestingly, a quick recovery of fluorescence within the local damaged area was observed (Fig. 7 B), indicating that repair-bound GFP-CSB molecules rapidly exchange with the mobile pool. However, the fluorescence recovery in the damaged area is slower than in an equally sized control region in a non-damaged cell (Fig. 7 B). We calculated an average residence time of GFP-CSB molecules in the local damage of 135 ± 20 seconds. This binding time is short relative to other core NER factors like XPA, TFIIH and ERCC1, which are bound in a locally damaged area for $3 - 5$ min. (Houtsmuller et al., 1999; Hoogstraten et al., 2002; Rademakers et al., 2003).
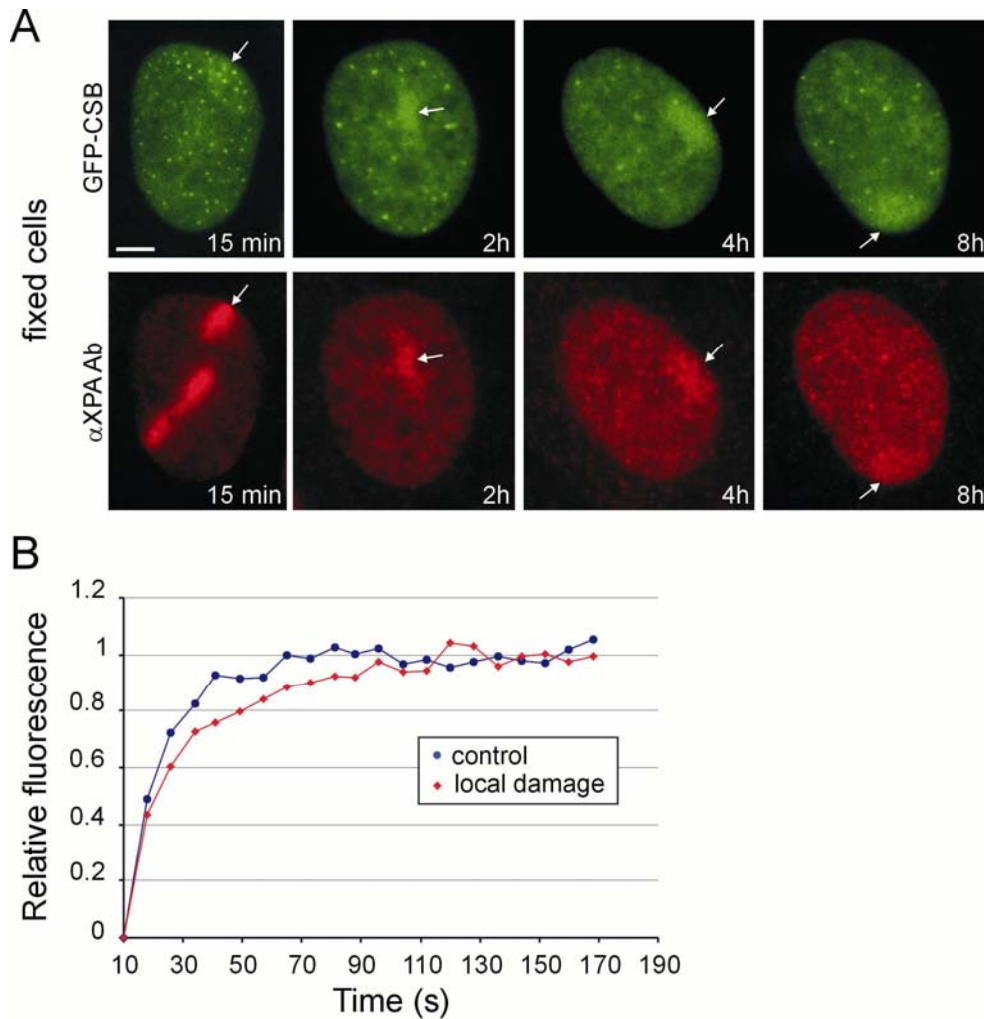
Figure 7. Accumulation of GFP-CSB at local UV-damaged subnuclear areas. (A) Epifluorescent images of fixed GFP-CSB expressing cells at various time points (15 min, 2h, 4h, 8h) after local irradiation. Immuno-fluorescent analysis with anti-XPA antibody shows accumulation of XPA at sites of damage. GFP-CSB shows accumulation in the same areas. Upper panel: GFP signal, lower panel: Cy3 signal. (B) Fluorescence recovery plot of a local damage (red diamonds) and an undamaged control region (blue circles). The calculated average residence time is 135 ± 20 seconds. Scale bar is 5 μm.

Discussion

Here we present a study on the dynamic behaviour of the TCR protein CSB in living cells, using a cell line that stably expresses functional GFP-tagged CSB protein at physiological levels. Confocal microscopy and quantitative digital image analysis of different photobleaching (FRAP) procedures revealed transient interactions of CSB with the transcription machinery, which are prolonged when RNA polymerases are arrested at sites of DNA damage.

Mobility of GFP-CSB

FRAP analysis indicated that the overall CSB mobility is remarkably slow compared to its calculated molecular size and the observed effective diffusion rate (D_{eff}) of other NER-factors (XPA, ERCC1/XPF and TFIIH) tested in a similar fashion that all have a D_{eff} that is in concordance with their molecular sizes, arguing against a stable pre-assembled NER 'holo' complex (Houtsmuller et al., 1999; Hoogstraten et al., 2002; Rademakers et al., 2003). The relatively slow mobility of GFP-CSB *in vivo*, even in transcription inhibited cells, confirms previous biochemical evidence that CSB resides in a complex with an estimated hydrodynamic velocity of particles >700 kD (van Gool et al., 1997).

Dynamic interactions of CSB with the transcription machinery

A significant fraction (~25%) of RNAP II in mammalian cells is bound to DNA and a single polymerase typically is bound for ~ 20 minutes during transcription elongation (Kimura et al., 2002). The suggested role of CSB in transcription elongation predicts that CSB-containing complexes show similar dynamics as RNAP II. However, FRAP studies suggest that only a small fraction of CSB-containing complexes (~17%) are immobilized for approximately 2 to 5 seconds in a transcription-dependent fashion. The drop in mobility at 27 ^{o}C as compared to 37 ^{o}C suggests that CSB is immobilized in a temperature-dependent fashion, most likely due to its involvement in transcription. Interestingly, upon treatment with Actinomycin D an unexpectedly large fraction of CSB is immobilized. A similar strong immobilization, induced by Actinomycin D treatment, was reported for GFP-tagged RNAP II. The authors explain this observation by a permanent block of the elongating complex caused by the DNA intercalating agent (Kimura et al., 2002). Apparently, these 'frozen' complexes permanently trap CSB molecules. In conclusion, our findings suggest a model in which there is a dynamic equilibrium between mobile CSB complexes and CSB transiently bound to elongating RNAP II.

Dynamic interactions of transcription factors with active transcription sites have been noticed before using similar procedures. Hager and colleagues (McNally et al., 2000) described a rapid exchange between chromatin-bound and freely mobile GFP-tagged glucocorticoid receptors. Moreover, our dynamic studies on GFP-tagged TFIIH and androgen receptors (Hoogstraten et al., 2002; Farla et al., 2004), revealed a similar short transcription-dependent interaction. However, both factors stimulate transcription initiation rather than elongation (Chandler et al., 1983; Lu et al., 1992). Obviously, elongating complexes, by virtue of their nature, are longer associated to DNA than we observe here for CSB. The transient interactions of elongation

stimulating factors, such as CSB, may provide a flexible response to different chromatin conformations or changing conditions during elongation allowing different factors to bind on demand. This is the first *in vivo* example of a transcription elongation factor that is not a stably associated component of the RNAP II elongation holo-complex.

Previously, a fraction of CSB molecules was found to interact with RNAP II (Tantin et al., 1997; van Gool et al., 1997). In addition, recombinant CSB was claimed to stimulate RNAP II elongation *in vitro* (Selby and Sancar, 1997) and RNAP II transcription was reported to be slightly impaired in CSB-deficient cells (Balajee et al., 1997; Dianov et al., 1997). Furthermore, a specific role in transcription elongation for the Rad26 protein (the yeast homologue of CSB) was found in yeast (Lee et al., 2001) and deduced from genetic interactions between Rad26 and Spt4 (Jansen et al., 2000), which is implicated in regulation of RNAP II processivity (Hartzog et al., 1998; Wada et al., 1998). Here we demonstrate that in a reconstituted transcription assay CSB-associated RNAP II is transcriptionally competent. No other general transcription initiation factors were detected in the immunoprecipitated fraction. Together these studies support a role for CSB in transcription elongation.

Besides a function in RNAP II-driven transcription a more general role for CSB in RNA polymerase I and III mediated transcription was suggested (Yu et al., 2000; Bradsher et al., 2002). The nucleolar localization of GFP-CSB *in vivo* presented here supports a role of CSB in processivity of other RNA polymerases. Furthermore, the absence of the CSB protein in human fibroblasts derived from CS group B patients caused fragility of metaphase chromosomes at specific loci, these include the U1 and U2 snRNA genes (RNAP II) and the 5S RNA genes (transcribed by RNAP III; Yu et al., 2000). It was suggested that this fragility is provoked by the absence of a (general) stimulating function of CSB in elongation during transcription of these highly structured RNAs.

Participation of CSB in TCR

The fraction of immobilized molecules after UV irradiation decreased to background levels (~16 h) much slower than core NER factors appeared to decrease to background levels in 4 to 6 hrs after UV (Houtsmuller et al., 1999; Hoogstraten et al., 2002; Rademakers et al., 2003). These kinetics of core NER factors were similar to the rate of 6-4PP removal (Van Hoffen et al., 1995) and thus suggest that with the applied methods predominantly repair of 6-4PP was monitored. DNA repair of the most abundant UV lesion, CPD, appeared to occur at much slower rates. Repair of these lesions mainly happens in the transcribed strand of active genes by TCR, in

contrast to 6-4PP removal that are almost as efficiently repaired by GGR as by TCR (Van Hoffen et al., 1995). Assuming that our observed immobilizations of GFP-CSB actually reflect participation in TCR, this further implies that completion of TCR is slower than completion of the bulk of GGR. However, this assumption contrasts to the general accepted model that TCR is more efficient than GGR (Bohr et al., 1985; Mellon et al., 1987). A possible explanation for this apparent contradiction is that the relatively fast removal of CPDs by TCR was measured on frequently transcribed genes (*i.e. DHFR*), whereas our live cell studies are performed on the total pool of transcriptional units, including long and less frequently transcribed genes. Since TCR is likely initiated by the blockage of transcription elongation on lesions, the efficiency of TCR-dependent lesion removal (such as CPDs) is likely determined both by the rate of transcription and the size of the transcriptional unit.

In addition, similar to FRAP analysis, the local accumulation of CSB was observed at least until 8 hours after UV irradiation, further providing evidence for a relatively long lasting active TCR pathway post UV irradiation.

Dynamic interaction of CSB with TCR complexes

The relatively small increase in immobilized GFP-CSB fraction in XPA-deficient cells as compared to NER-proficient cells and the fact that this fraction does not increase in time after UV, suggest that CSB molecules are not permanently bound to lesion-stalled RNAPII complexes that are not further processed because of defective NER. It is remarkable that the absence of repair does not lead to a complete immobilization as observed after treatment with Actinomycin D (Fig. 3 C). The DNA intercalating drug Actinomycin D forms a permanent block for RNAPII thereby capturing the molecule in a template-bound form (Kamitori and Takusagawa, 1992). In contrast, UV-induced stalling of RNAPII in an XPA-deficient background probably induces a different type of conformation that is still permissive to removal from the DNA template by CSB. Evidence for the accessibility of RNAPII stalled on UV lesions was very recently provided by Tremeau-Bravard et al. (2004). This different behaviour of CSB might be explained by differential structural consequences for the stalled RNAPII provoked by Actinomycin D adducts versus bonafide NER lesions such as CPDs. Actinomycin D adducts do have a distinct effect on the DNA structure as compared to NER lesions because this drug does not induce NER (unpublished data).

In addition, lesion-stalled polymerases are targets for ubiquitination (Bregman et al., 1996) and, at least in yeast, proteolysis of polyubiquitinated Rpb1 (largest RNAPII subunit) by Def1 (Woudstra et al., 2002) plays a role in clearing of stalled

RNAPII from the lesion. This process provides an escape route when Rad26 (yeast orthologue of CSB) is exhausted or not present (van den Boom et al., 2002; Woudstra et al., 2002). If a similar system would be present in mammalian cells this would provide an explanation that UV-induced RNAPII are cleared in a Def1-dependent fashion, and do not likely form such permanent roadblocks as Actinomycin D.

Distinct kinetic pools of CSB

Here we have shown that the equilibrium between different kinetic pools of freely diffusing CSB complexes and a "transcription bound" fraction can shift under different transcriptional conditions. The observed temperature-dependence of CSB mobility might be due to its ATPase function during association in transcription. Since CSB is essential for TCR, we investigated the consequences of DNA damage on the distribution of CSB over the distinct kinetic pools. Shortly after UV exposure we observed a change in the duration of the transcription-related immobilization of CSB. The maximal immobilization of ~15% in TCR is significantly smaller than the GGR-induced maximal immobilization of ~40% for other (core) NER factors (Houtsmuller et al., 1999; Hoogstraten et al., 2002; Rademakers et al., 2003). This implies that the molecular equilibrium, which is established between DNA damage-bound and freely diffusing molecules, is different for GGR and TCR. Probably, the immobile fraction of GGR proteins is directly dependent on the DNA damage load, whereas the number of stalled RNAP II elongation complexes in a cell determines the immobile fraction of TCR proteins.

In summary, we find that CSB complexes transiently interact with the transcription machinery during elongation. A possible explanation for this behaviour of CSB is that this protein constantly monitors the elongation status of the transcribing polymerases. When a complex is stalled on a DNA lesion the transient interactions of the CSB protein are stabilized to allow CSB to exert its function in damage removal.

Materials and Methods

Generation and characterization of GFP-CSB fusion protein.

To generate the GFP-CSB fusion gene, the N-terminal HA-tagged CSB cDNA (van Gool et al., 1997) was cloned downstream of the GFP cDNA in the SacI-SalI sites of the pEGFP-C3 expression vector (Clontech). GFP-CSB was stably expressed in CS-B-deficient human fibroblasts (CS1AN-Sv) using SuperFect transfection reagent (Qiagen). After selection with G418 (300 μg/ml), stable transfectants were isolated and selected for UV-resistance by exposing cells three times to a UV dose of 4 J/m^2 UV-C (254 nm) with daily intervals. Stably expressing clones were characterized for protein expression by immunoblot analysis using an affinity-purified rabbit polyclonal anti-CSB and by UV-survival together with VH10-Sv (wt) and untransfected CS1AN-Sv fibroblasts as described (van Gool et al., 1997);

Cell culture and specific treatments

The human fibroblasts; CS1AN-Sv (CS-B), XP12RO-Sv (XP-A) and wild-type VH10-Sv were grown in a 1:1 mixture of Ham's F10 and DMEM (Gibco) supplemented with antibiotics and 10% foetal calf serum at 37° C, 5% CO$_2$. Transcription inhibitors were used according to the following conditions: *N*-(2[methylamino]ethyl)-5-isoquinolinesulfonamide (H8, 100 μM, 2 hours), actinomycin D (10 μg /ml, 2 hours). Treatment with ultraviolet (UV) light was at 254 nm (UV-C) using a germicidal lamp at the indicated doses. DNA damage in localized areas of the nucleus was performed as described (Volker et al., 2001). For azide treatment cells were cultured for 15 minutes in glucose-free medium (Gibco) supplemented with 60mM deoxyglucose and 0.2% Na-azide.

Light microscopy and image analysis

Cells were cultured on sterile glass cover slips. For indirect immunofluorescence (IF), fixation was in 2% parafolmaldehyde in PBS for 10 minutes at room temperature. After fixation, cells were permeabilised with 0.1% TritonX-100 in PBS. Endogenous CSB in wild type VH10-Sv cells was detected with affinity-purified, rabbit polyclonal anti-CSB. Secondary antibody staining was performed with anti-rabbit Alexa 594-conjugated antibodies (Molecular Probes). For fixed cells, fluorescent microscopy images were obtained with a Leitz Aristoplan microscope equipped with epi-fluorescence optics and a PLANAPO 63x/1.40 oil immersion lens. Confocal laser scanning microscopy images of live cells were recorded with a Zeiss LSM 410. GFP images were obtained after excitation with 455-490 and long pass emission filter (>510 nm). Alexa-595 images were obtained after excitation with 515-560 and long pass emission filter (580 nm).

In vitro transcription assay

Transcription was assayed in a reconstituted transcription system containing human recombinant TBP, TFIIB and TFIIE and purified HeLa TFIIA, TFIIF, TFIIH and RNAP II as described earlier (Gerard et al., 1991). Briefly, HA-elution fractions containing CSB were pre-incubated with the indicated transcription factors and with 100 ng of the adenovirus 2 major late promoter (Ad2MLP)-containing template for 15 minutes at 25ºC. After the addition of nucleotides, transcription was allowed to proceed for 45 minutes at 25ºC. The 309 nt [α^{32}P]-CTP run off transcripts were resolved by electrophoresis through a 5% acrylamide/50% urea gel and analysed by autoradiography.

FRAP

A LSM410 (Carl Zeiss MicroImaging, Inc.) was used for the FRAP experiments. Recovery curves for evaluation of protein mobility were obtained as described before (Hoogstraten et al., 2002). For FRAP analysis, a 2μm wide strip, spanning the entire nucleus, was bleached for 200 ms at highest intensity of the 488 nm line of a 15 mW Ar-laser focused by a 40X 1.3 n.a. oil immersion lens. Subsequently the recovery of fluorescence in the strip was monitored at intervals of 100 ms with the same laser at 5% of the intensity applied for bleaching, using a dichroic beamsplitter (488/543nm) and an additional 515-540 nm band pass filter for emission detection. Similarly, combined FLIP and FRAP analysis was performed by giving a 6 second bleach pulse to a strip at the bottom side of the cell. Next, the fluorescent images were made with low laser intensity every 6 seconds for a total of 3 minutes.

Computer simulation

For optimal interpretation of the FRAP data we developed a computer modelling environment to simulate FRAP applied to fluorescent molecules inside a finite volume. The FRAP procedures were simulated using experimentally obtained parameters describing lens (beam shape and 3-D intensity distribution, during monitoring and during bleach pulse), GFP (quantum yield, susceptibility to bleaching) and nuclear properties (size and shape). Three protein mobility parameters, diffusion coefficient, bound fraction and duration of binding of individual molecules were varied and the best fit with experimental data was obtained using least square fitting.

Acknowledgments

References

Balajee, A.S., A. May, G.L. Dianov, E.C. Friedberg, and V.A. Bohr. 1997. Reduced RNA polymerase II transcription in intact and permeabilized Cockayne syndrome group B cells. *Proc. Natl. Acad. Sci. USA*. 94:4306-4311.

Bohr, V.A., C.A. Smith, D.S. Okumoto, and P.C. Hanawalt. 1985. DNA repair in an active gene: removal of pyrimidine dimers from the *DHFR* gene of CHO cells is much more efficient than in the genome overall. *Cell*. 40:359-369.

Bradsher, J., J. Auriol, L. Proietti de Santis, S. Iben, J.L. Vonesch, I. Grummt, and J.M. Egly. 2002. CSB is a component of RNA pol I transcription. *Mol Cell*. 10:819-29.

Bregman, D.B., R. Halaban, A.J. Van Gool, K.A. Henning, E.C. Freidberg, and S.L. Warren. 1996. UV-induced ubiquitination of RNA polymerase II: a novel modification deficient in Cockayne's syndrome cells. *Proc. Natl. Acad. Sci. USA*. 93:11586-11590.

Chandler, V.L., B.A. Maler, and K.R. Yamamoto. 1983. DNA sequences bound specifically by glucocorticoid receptor in vitro render a heterologous promoter hormone responsive in vivo. *Cell*. 33:489-99.

Citterio, E., S. Rademakers, G.T. van der Horst, A.J. van Gool, J.H. Hoeijmakers, and W. Vermeulen. 1998. Biochemical and biological characterization of wild-type and ATPase- deficient Cockayne syndrome B repair protein. *J. Biol. Chem.* 273:11844-11851.

Citterio, E., V. Van Den Boom, G. Schnitzler, R. Kanaar, E. Bonte, R.E. Kingston, J.H. Hoeijmakers, and W. Vermeulen. 2000. ATP-dependent chromatin remodeling by the Cockayne syndrome B DNA repair-transcription-coupling factor. *Mol Cell Biol*. 20:7643-53.

Coin, F., E. Bergmann, A. Tremeau-Bravard, and J.M. Egly. 1999. Mutations in XPB and XPD helicases found in xeroderma pigmentosum patients impair the transcription function of TFIIH. *EMBO J*. 18:1357-1366.

de Boer, J., J.O. Andressoo, J. de Wit, J. Huijmans, R.B. Beems, H. van Steeg, G. Weeda, G.T. van der Horst, W. van Leeuwen, A.P. Themmen, M. Meradji, and J.H. Hoeijmakers. 2002. Premature aging in mice deficient in DNA repair and transcription. *Science*. 296:1276-9.

Dianov, G.L., J.F. Houle, N. Iyer, V.A. Bohr, and E.C. Friedberg. 1997. Reduced RNA polymerase II transcription in extracts of cockayne syndrome and xeroderma pigmentosum/Cockayne syndrome cells. *Nucleic Acids Res*. 25:3636-42.

Donahue, B.A., S. Yin, J.-S. Taylor, D. Reines, and P.C. Hanawalt. 1994. Transcript cleavage by RNA polymerase II arrested by a cyclobutane pyrimidine dimer in the DNA template. *Proc. Natl. Acad. Sci. USA*. 91:8502-8506.

Farla, P., R. Hersmus, B. Geverts, P.O. Mari, A.L. Nigg, H.J. Dubbink, J. Trapman, and A.B. Houtsmuller. 2004. The androgen receptor ligand-binding domain stabilizes DNA binding in living cells. *J Struct Biol*. 147:50-61.

Friedberg, E.C., G.C. Walker, and W. Siede. 1995. DNA repair and mutagenesis. ASM Press, Washington D.C.

Gerard, M., L. Fischer, V. Moncollin, J.-M. Chipoulet, P. Chambon, and J.-M. Egly. 1991. Purification and interaction properties of the human RNA polymerase B(II) general transcription factor BTF2. *J. Biol. Chem.* 266:20940-20945.

Hartzog, G.A., T. Wada, H. Handa, and F. Winston. 1998. Evidence that Spt4, Spt5, and Spt6 control transcription elongation by RNA polymerase II in Saccharomyces cerevisiae. *Genes Dev*. 12:357-69.

Henning, K.A., L. Li, N. Iyer, L. McDaniel, M.S. Reagan, R. Legerski, R.A. Schultz, M. Stefanini, A.R. Lehmann, L.V. Mayne, and E.C. Friedberg. 1995. The Cockayne

syndrome group A gene encodes a WD repeat protein that interacts with CSB protein and a subunit of RNA polymerase II TFIIH. *Cell.* 82:555-564.

Hoeijmakers, J.H. 2001. Genome maintenance mechanisms for preventing cancer. *Nature.* 411:366-74.

Hoogstraten, D., A.L. Nigg, H. Heath, L.H. Mullenders, R. van Driel, J.H. Hoeijmakers, W. Vermeulen, and A.B. Houtsmuller. 2002. Rapid switching of TFIIH between RNA polymerase I and II transcription and DNA repair in vivo. *Mol Cell.* 10:1163-74.

Houtsmuller, A.B., S. Rademakers, A.L. Nigg, D. Hoogstraten, J.H.J. Hoeijmakers, and W. Vermeulen. 1999. Action of DNA repair endonuclease ERCC1/XPF in living cells. *Science.* 284:958-961.

Jansen, L.E.T., H. den Dulk, R.M. Brouns, M. de Ruijter, J.A. Brandsma, and J. Brouwer. 2000. Spt4 modulates Rad26 requirement in transcription-coupled nucleotide excision repair. *EMBO J.* 19:6498-6507.

Kamitori, S., and F. Takusagawa. 1992. Crystal structure of the 2:1 complex between d(GAAGCTTC) and the anticancer drug actinomycin D. *J Mol Biol.* 225:445-56.

Kimura, H., K. Sugaya, and P.R. Cook. 2002. The transcription cycle of RNA polymerase II in living cells. *J Cell Biol.* 159:777-82.

Le Page, F., E.E. Kwoh, A. Avrutskaya, A. Gentil, S.A. Leadon, A. Sarasin, and P.K. Cooper. 2000. Transcription-coupled repair of 8-oxoguanine: requirement for XPG, TFIIH, and CSB and implications for Cockayne syndrome. *Cell.* 101:159-171.

Lee, S.K., S.L. Yu, L. Prakash, and S. Prakash. 2001. Requirement for yeast RAD26, a homolog of the human CSB gene, in elongation by RNA polymerase II. *Mol Cell Biol.* 21:8651-6.

Ljungman, M., and F. Zhang. 1996. Blockage of RNA polymerase as a possible trigger for u.v. light-induced apoptosis. *Oncogene.* 13:823-831.

Lu, H., L. Zawel, L. Fisher, J.-M. Egly, and D. Reinberg. 1992. Human general transcription factor IIH phosphorylates the C-terminal domain of RNA polymerase II. *Nature.* 358:641-645.

McNally, J.G., W.G. Müller, D. Walker, R. Wolford, and G.L. Hager. 2000. The glucocorticoid receptor: rapid exchange with regulatory sites in living cells. *Science.* 287:1262-1265.

Mellon, I., G. Spivak, and P.C. Hanawalt. 1987. Selective removal of transcription-blocking DNA damage from the transcribed strand of the mammalian *DHFR* gene. *Cell.* 51:241-249.

Nance, M.A., and S.A. Berry. 1992. Cockayne syndrome: Review of 140 cases. *Am. J. of Med. Genet.* 42:68-84.

Neer, E.J., C.J. Schmidt, R. Nambudripad, and T.F. Smith. 1994. The ancient regulatory-protein family of WD-repeat proteins. *Nature.* 371:297-300.

Pazin, M.J., and J.T. Kadonaga. 1997. SWI2/SNF2 and related proteins: ATP-driven motors that disrupt protein-DNA interactions? *Cell.* 88:737-740.

Phair, R.D., and T. Misteli. 2000. High mobility of proteins in the mammalian cell nucleus. *Nature.* 404:604-609.

Rademakers, S., M. Volker, D. Hoogstraten, A.L. Nigg, M.J. Mone, A.A. Van Zeeland, J.H. Hoeijmakers, A.B. Houtsmuller, and W. Vermeulen. 2003. Xeroderma Pigmentosum Group A Protein Loads as a Separate Factor onto DNA Lesions. *Mol Cell Biol.* 23:5755-5767.

Selby, C.P., and A. Sancar. 1997. Cockayne syndrome group B protein enhances elongation by RNA polymerase II. *Proc. Natl. Acad. Sci. USA.* 94:11205-11209.

Tantin, D., A. Kansal, and M. Carey. 1997. Recruitment of the putative transcription-repair coupling factor CSB/ERCC6 to RNA polymerase II elongation complexes. *Mol. Cell. Biol.* 17:6803-6814.

Tornaletti, S., and P.C. Hanawalt. 1999 ,. Effect of DNA lesions on transcription elongation. *Biochimie.* 81:139-146.

Tremeau-Bravard, A., T. Riedl, J.M. Egly, and M.E. Dahmus. 2004. Fate of RNA polymerase II stalled at a cisplatin lesion. *J Biol Chem.* 279:7751-9.

Troelstra, C., A. Van Gool, J. De Wit, W. Vermeulen, D. Bootsma, and J.H.J. Hoeijmakers. 1992. ERCC6, a member of a subfamily of putative helicases, is involved in Cockaynes syndrome and preferential repair of active genes. *Cell.* 71:939-953.

van den Boom, V., N.G. Jaspers, and W. Vermeulen. 2002. When machines get stuck-- obstructed RNA polymerase II: displacement, degradation or suicide. *Bioessays.* 24:780-4.

van Gool, A.J., E. Citterio, S. Rademakers, R. van Os, W. Vermeulen, A. Constantinou, J.M. Egly, D. Bootsma, and J.H.J. Hoeijmakers. 1997. The Cockayne syndrome B protein, involved in transcription-coupled DNA repair, resides in a RNA polymerase II containing complex. *EMBO J.* 16:5955-5965.

Van Hoffen, A., A.T. Natarajan, L.V. Mayne, A.A. Van Zeeland, L.H.F. Mullenders, and J. Venema. 1993. Deficient repair of the transcribed strand of active genes in Cockaynes syndrome cells. *Nucl. Acids Res.* 21:5890-5895.

Van Hoffen, A., J. Venema, R. Meschini, A.A. van Zeeland, and L.H.F. Mullenders. 1995. Transcription-coupled repair removes both cyclobutane pyrimidine dimers and 6-4 photoproducts with equal efficiency and in a sequential way from transcribed DNA in xeroderma pigmentosum group C fibroblasts. *EMBO J.* 14:360-367.

Venema, J., L.H.F. Mullenders, A.T. Natarajan, A.A. van Zeeland, and L.V. Mayne. 1990. The genetic defect in Cockayne syndrome is associated with a defect in repair of UV-induced DNA damage in transcripionally active DNA. *Proc. Natl. Acad. Sci. USA.* 87:4707-4711.

Volker, M., M.J. Mone, P. Karmakar, A. van Hoffen, W. Schul, W. Vermeulen, J.H. Hoeijmakers, R. van Driel, A.A. van Zeeland, and L.H. Mullenders. 2001. Sequential assembly of the nucleotide excision repair factors in vivo. *Mol Cell.* 8:213-24.

Wada, T., T. Takagi, Y. Yamaguchi, A. Ferdous, T. Imai, S. Hirose, S. Sugimoto, K. Yano, G.A. Hartzog, F. Winston, S. Buratowski, and H. Handa. 1998. DSIF, a novel transcription elongation factor that regulates RNA polymerase II processivity, is composed of human Spt4 and Spt5 homologs. *Genes Dev.* 12:343-356.

Woudstra, E.C., C. Gilbert, J. Fellows, L. Jansen, J. Brouwer, H. Erdjument-Bromage, P. Tempst, and J.Q. Svejstrup. 2002. A Rad26-Def1 complex coordinates repair and RNA pol II proteolysis in response to DNA damage. *Nature.* 415:929-33.

Yamaizumi, M., and T. Sugano. 1994. U.v.-induced nuclear accumulation of p53 is evoked through DNA damage of actively transcribed genes independent of the cell cycle. *Oncogene.* 9:2775-84.

Yu, A., H.-Y. Fan, D. Liao, A.D. Bailey, and A.M. Weiner. 2000. Activation of p53 or Loss of the Cockayne Syndrome Group B Repair Protein Causes Metaphase Fragility of Human U1, U2, and 5S Genes. *Molecular Cell.* 5:801-810.

Summary

The structure of DNA, the carrier of our genetic information, is continuously challenged as a consequence of replication errors, intrinsic chemical instability or reactive metabolites. Also environmental factors, such as chemical compounds or radiation, can cause serious damage to DNA, which in turn can interfere with an array of DNA-transacting mechanisms. Accumulating lesions cause cellular senescence and cell death, resulting in ageing. In addition, lesions can lead to mutations and as a consequence to cancer, but also inborn diseases. To counteract these deleterious effects, a network of cellular DNA damage response (DDR) mechanisms has evolved. This thesis focuses on the live cell dynamics of DDR systems counteracting UV-induced DNA lesions in mammalian cells.

Chapter 2 is a comprehensive review on the dynamic organization of genome surveillance processes with emphasis on mammalian cells. Diverse DDR systems are introduced, ranging from repair mechanisms and damage avoidance systems to efficient DNA damage signalling. The interconnection of the diverse DNA-transacting mechanisms by dynamic sharing of components, fine-tuned by post-translational modifications of diverse proteins, is outlined. The role of chromatin changes in the spatial organization of DDR mechanisms is discussed, as well as differences in the nuclear organization of diverse genome maintenance mechanisms. Recent studies on live cell dynamics in DDR are summarised, which point towards a general mechanism used in DDR, in which each system reconstitutes larger molecular assemblies by dynamic sharing of small components, rather than utilizing large pre-assembled complexes. This dynamic assembly mechanism enables fast and adequate reaction to a huge variety of genotoxic challenges. Future prospects are mentioned by discussing the applications of new emerging technological possibilities in diverse fields such as biochemistry, cell biology, biophysics, and bioinformatics, and the introduction of the next challenge for a "real-life" understanding of genome surveillance: cells imbedded within the tissue of living organisms.

In **Chapter 3**, we combine two quantitative live cell fluorescence-based techniques, fluorescence recovery after photobleaching (FRAP) and fluorescence correlation spectroscopy (FCS), to unravel the complex nuclear mobilities of biologically functional proteins. As a paradigm, we used the previously well-characterized multi-component nucleotide excision repair (NER) system, which is

specialized on the removal of UV-induced DNA lesions. To analyse the nature of protein mobility in living mammalian cell nuclei, we studied several green fluorescent protein (GFP)-tagged core components of this mechanism in the absence of UV-induced DNA damage, when actual NER activity is minimal. Importantly, we found that most analysed NER factors exhibited mobilities very similar to biologically inert proteins of comparable size; they move corresponding to their molecular size and shape, indicating Brownian motion hindered only by dense nuclear architecture. Exceptions were the multifunctional TFIIH complex and the NER damage sensor XPC. TFIIH showed a small transiently immobilised fraction consistent with its engagement in transcription, whereas the apparent relatively slow mobility of XPC is explained by its intrinsic property to continuously bind to and dissociate from DNA or chromatin.

Chapter 4 presents a study of the dynamic mechanism by which the NER 3'endonuclease XPG is recruited to sites of UV-induced DNA damage. Using confocal photobleaching techniques we analysed the mobility of GFP-tagged XPG stably expressed at physiologically relevant levels in mammalian cells that lack functional endogenous XPG. We found that XPG diffuses freely as a monomer both in Chinese hamster ovary (CHO) cells and in human fibroblasts. It does not show any prominent interactions other than with the nascent NER complex that is formed at DNA damage sites. We could also show that the efficiency of XPG recruitment to DNA lesions was the same in CHO as well as in human cells. Adding DDB2, a protein thought to enhance DNA damage recognition by the NER sensor protein XPC, and which is not expressed in rodent cells, did not have any influence on XPG accumulation at DNA damage sites. XPG recruitment to UV-induced DNA lesions is, however, dependent on the presence of functional TFIIH. Remarkably, the in vivo dynamics of the XPG protein are very similar in human and rodent cells, showing that apparent differences in genetic background hardly affect XPG behaviour.

In **Chapter 5**, an analysis of the dynamic properties of the translesion polymerase eta (Polη) in human cells is presented. This specialized DNA polymerase is known to be able to bypass replication-blocking UV-induced cyclobutane pyrimidine dimers in an error-free manner. Employing photobleaching, we found that Polη, when not recruited into replication foci, moves rapidly throughout the nucleus, suggesting that the majority of the protein is freely mobile and not stably integrated into a large complex. However, a small fraction of Polη molecules appeared to shortly interact in a temperature-sensitive manner with an immobile component in non-S-

phase cells, suggesting another function for this protein besides lesion bypass replication. In S-phase, Polη becomes immobilized very transiently at sites of DNA replication. The extent and duration of Polη immobilization within replication structures after UV-damage induction is increased in a dose-dependent manner, but remains highly dynamic. We could calculate the average binding time to S-phase foci after UV-irradiation to be in the order of only a few seconds. Time-lapse studies of cells with and without locally induced DNA damage showed that the distribution pattern throughout S-phase highly resembles the one of proliferating cell nuclear antigen (PCNA), a well-characterized core factor of replication. This supports previous *in vitro* studies and observations in fixed cells showing that Polη efficiently associates with PCNA in replication foci. Our results underline the highly dynamic, cell cycle-dependent association of Polη with chromatin structures, fine-tuned by the replicative state of the DNA.

Chapter 6 presents a live cell study of the Cockayne syndrome B (CSB) protein, an essential factor in transcription-coupled DNA repair (TCR). TCR is dependent on RNA polymerase II elongation and required to quickly remove cytotoxic transcription-blocking DNA lesions. We expressed functional GFP-tagged CSB at physiologically relevant levels in corresponding human mutant cells. The fusion protein was homogeneously dispersed throughout the nucleus in addition to bright nuclear foci and nucleolar accumulations. Photobleaching studies showed that GFP-CSB moves as part of a high molecular weight complex and transiently interacts with the transcription machinery. Upon DNA damage-induced transcription arrest, CSB binding to the transcription elongation machinery is prolonged, most likely reflecting actual engagement of CSB in TCR. Our findings are consistent with a model in which CSB monitors progression of transcription by regularly probing elongation complexes and becomes more tightly associated to these complexes when TCR is active.

Samenvatting

DNA, de drager van onze genetische informatie, wordt onophoudelijk blootgesteld aan ongewenste veranderingen, ten gevolge van replicatiefouten, intrinsieke chemische instabiliteit of reactieve metabolieten. Ook kunnen omgevingsfactoren, zoals talloze chemische verbindingen of straling (UV licht, röntgenstraling), ernstige schade aan DNA veroorzaken, die vervolgens belangrijke functies van het DNA kunnen aantasten. Een van de nadelige gevolgen is dat beschadigingen kunnen leiden tot blijvende veranderingen in de genetische code (mutaties) die op hun beurt weer kunnen leiden tot kanker of erfelijke afwijkingen. Beschadigingen in het DNA kunnen ook celdood veroorzaken en daarmee een bijdrage leveren aan het proces van veroudering. Om deze schadelijke gevolgen tegen te gaan, is in de evolutie een ingewikkeld netwerk van cellulaire mechanismen ontstaan als antwoord op DNA schade (de 'DNA damage response', DDR). Het hier beschreven promotieonderzoek concentreert zich op de dynamiek van DDR systemen, die zich richten op DNA beschadigingen welke ondermeer door UV-stralen worden veroorzaakt in levende zoogdiercellen.

Hoofdstuk 2 geeft een uitgebreid overzicht van de dynamische aspecten en organisatie van genoomonderhoudsprocessen met nadruk op zoogdiercellen. Diverse DDR systemen worden geïntroduceerd, van reparatiemechanismen en systemen voor schadetolerantie tot het efficiënt signaleren van DNA schade. De samenhang van de diverse DNA-transactiverende mechanismen doordat componenten op een dynamische manier worden gedeeld, en hun regulatie door post-translationale modificaties van diverse eiwitten, is uitgelegd. De rol van chromatineveranderingen in de organisatie van DDR in de celkern wordt besproken, evenals verschillen in de ruimtelijke organisatie van de diverse mechanismen van het genoomonderhoud. Recente studies over DDR dynamiek in levende cellen worden samengevat. Deze wijzen op het bestaan van een algemeen actiemechanisme van DDR systemen, dat is gebaseerd op vele kleine beweeglijke factoren, die op de plaats van de beschadiging een efficiënt werkzaam eiwitcomplex vormen, in plaats van het gebruik van grote voorgevormde eiwitcomplexen, die minder beweeglijk zijn en minder mogelijkheden bieden voor regulatie, multi-functioneel gebruik van onderdelen en reversibiliteit. Toekomstige vooruitzichten worden besproken zoals de aankomende nieuwe mogelijkheden van een multidisciplinaire benadering door de combinatie van steeds meer geavanceerde methoden in biochemie, celbiologie,

biofysica en bio-informatica. Tenslotte wordt de volgende uitdaging voor een „levensechte" inzicht in genoomonderhoud geïntroduceerd, namelijk cellen ingebed in het weefsel van levende organismen.

In **Hoofdstuk 3** worden twee nieuwe kwantitatieve microscopische technieken gecombineerd, redistributie van fluorescentie na foto-bleking (fluorescence redistribution after photobleaching, FRAP) en spectroscopie van de fluorescentiecorrelatie (fluorescence correlation spectroscopy, FCS), om de verschillende celkernmobiliteit van biologisch functionele eiwitten te ontrafelen. Als modelsysteem gebruikten wij het eerder goed karakteriseerde meerstaps DNA reparatiesysteem NER (nucleotide excision repair), dat zich richt op de verwijdering van DNA beschadigingen, die de dubbele helix structuur verstoren zoals DNA lesies veroorzaakt door UV en talloze chemische verbindingen. Om de aard van de mobiliteit van de diverse NER factoren te analyseren, bestudeerden wij verschillende kerncomponenten van dit mechanisme, die met een groen fluorescerend proteïne (GFP) waren gemarkeerd in cellen die niet zijn blootgesteld aan UV bestraling. Onder deze omstandigheden was de daadwerkelijke activiteit van NER minimaal en konden wij de individuele mobiliteit van de verschillende NER eiwitten in de celkern vergelijken. Wij vonden dat de mobiliteit van het merendeel van de geanalyseerde NER factoren vergelijkbaar is met biologisch inerte eiwitten van vergelijkbare grootte, d.w.z. deze NER eiwitten bewegen zich overeenkomstig hun moleculaire grootte en vorm; dit wijst op Brownse diffusie die slechts door de dichte kernarchitectuur wordt belemmerd. Uitzonderingen waren het TFIIH complex, dat naast NER ook betrokken is in het proces van transcriptie en waarvan we vonden dat een kleine fractie voor een korte periode immobiel was, verenigbaar met zijn functie in transcriptie. Een tweede uitzondering was de NER schadesensor XPC. Wij vonden dat een groot deel van de XPC moleculen een interactie met vaste kernstructuren scheen te ondergaan, DNA of chromatine. Deze bindingen waren te kort om ze goed te kunnen onderscheiden van door kernarchitectuur belemmerde diffusie. Dit resultaat suggereert echter dat XPC voortdurend de structuur van DNA aftast op zoek naar helix-vervormende beschadigingen, die een substraat voor NER zouden kunnen zijn.

Hoofdstuk 4 beschrijft een studie van het mechanisme van de dynamische rekrutering van de NER 3' endonuclease XPG aan UV-veroorzaakte DNA schade. In zoogdiercellen die zelf geen functioneel XPG hebben hebben we een GFP-gemarkeerde XPG geïntroduceerd, en cellen met een stabiele fysiologische expressie van het GFP-XPG fusie-eiwit bestudeerd. Met de hulp van

confocale foto-bleking technieken om mobiliteit in de celkern te bepalen, vonden wij dat XPG zowel in Chinese hamster ovarium (CHO) cellen als ook in menselijke fibroblasten vrij als monomeer diffundeert met dezelfde snelheid. Het XPG eiwit toont geen prominente interactie anders dan de associatie met de zich vormende NER complex op een DNA schade. Wij vonden ook dat de effectiviteit van de XPG rekrutering naar plaatsen met DNA schade hetzelfde is in CHO en in menselijke cellen. Toevoeging van DDB2, een eiwit dat de schadeherkenning van DNA door de NER sensor eiwit XPC verbetert, en dat niet in knaagdiercellen wordt geproduceerd, had geen invloed op de accumulatie van XPG aan DNA schadeplaatsen. De rekrutering van XPG aan UV-veroorzaakte DNA lesies is echter afhankelijk van de aanwezigheid van een functioneel TFIIH. Opmerkelijk is dat de dynamiek van XPG zeer vergelijkbaar is in mensen- en knaagdiercellen, hetgeen aantoont dat duidelijke verschillen in genetische achtergronden nauwelijks het gedrag van XPG beïnvloeden.

Hoofdstuk 5 geeft inzicht in de dynamiek van de translesie polymerase eta (Polη) in de kernen van menselijke cellen. Dit gespecialiseerde DNA polymerase is in staat om bij de DNA replicatie over cyclobutane pyrimidine dimeren (CPDs) in het DNA, die door UV worden veroorzaakt, heen te gaan op een relatief foutloze manier. Daarom is het geassocieerd met de replicatiemachinerie in S-fase. Met behulp van confocale foto-bleking methodes vonden wij dat Polη, als het niet wordt gebonden aan DNA replicatie plaatsen, zich snel door kern beweegt. Dit wijst erop, dat het merendeel van het eiwit vrij mobiel is en niet stabiel geïntegreerd in een groot eiwitcomplex. Niettemin, een percentage Polη moleculen wordt korte tijd geïmmobiliseerd op een temperatuur-gevoelige manier in cellen die niet in S-fase zijn en geen (replicatie)structuren bezitten (d.w.z. cellen in G1- of G2-fase van de celcyclus), hetgeen een andere functie voor dit eiwit naast de translesie replicatie suggereert. In S-fase wordt Polη voor een heel korte tijd geïmmobiliseerd aan DNA replicatiestructuren. De omvang en de duur van Polη immobilisatie binnen replicatiestructuren nemen toe door de inductie van UV-schade op een manier, die afhankelijk is van de stralingsdosering. Toch blijft het eiwit ook dan heel dynamisch. Onze berekeningen wijzen uit dat de gemiddelde immobilisatietijd aan individuele replicatiestructuren na UV-bestraling nog steeds in de orde van slechts enkele seconden is. Time-lapse studies van cellen met en zonder plaatselijk veroorzaakte DNA schade toonden aan dat het distributiepatroon door S-fase zeer veel lijkt op die van de basale replicatiefactor en S-fase indicator PCNA (proliferating cell nuclear antigen). Deze resultaten ondersteunen eerdere *in vitro* studies en waarnemingen

aan gefixeerde cellen en tonen aan dat Polη efficiënt met PCNA in replicatiestructuren associeert. Onze resultaten maken de hoogst dynamische, celcyclus-afhankelijke associatie van Polη met chromatinestructuren zichtbaar, die door de replicatieve staat van het DNA verder wordt gereguleerd.

Hoofdstuk 6 beschrijft een levende cel-studie van de Cockayne syndroom B (CSB) eiwit, een essentiële factor in de transcriptie-gekoppelde reparatie (transcription-coupled repair, TCR) van DNA. TCR is afhankelijk van RNA polymerase II elongatie en is nodig voor de efficiënte verwijdering van de cytotoxische transcriptie-blokkerende DNA beschadigingen. Wij exprimeerden functioneel GFP-gemarkeerd CSB op fysiologisch niveau in menselijke cellen die geen functioneel endogeen CSB eiwit aanmaakten. Het GFP-CSB fusieeiwit is homogeen verdeeld over de kern naast enkele heldere punten en nucleolaire accumulaties. Foto-bleking studies toonden aan dat GFP-CSB als deel van een complex met een hoog moleculair gewicht diffundeert en voortdurend kort met de transcriptiemachines in wisselwerking staat. Als het transcriptiecomplex vastloopt op een DNA beschadiging wordt de immobilisatie van CSB aan de transcriptie-machinerie verlengd, wat op een daadwerkelijke functie van CSB in TCR wijst. Onze resultaten zijn verenigbaar met een model waarin CSB de vooruitgang van de transcriptie regelmatig controleert omdat het de verlengingscomplexen sondeert en een sterkere interactie aangaat als TCR actief is.

List of Abbreviations

ATM	ataxia telangiectasia mutated
ATP	adenosine triphosphate
ATR	ATM- and Rad3-related kinase
ATRIP	ATR-interacting protein
BER	base excision repair
BRCA1/2	breast cancer susceptibility 1/2
CAK	cyclin-activating kinase complex
CDK7	cyclin-dependent kinase 7
CEN2	centrin 2 / caltractin 1
Chk1/2	checkpoint protein 1/2
CHO cells	Chinese hamster ovary cells
cs	catalytic subunit
CSA/CSB	Cockayne syndrome A/B protein
CPD	cyclobutane pyrimidin dimer
DDB1/2	damaged DNA-binding protein 1/2
DDR	DNA damage response
D_{eff}	effective diffusion coefficient
ds/ssDNA	double-stranded/single-stranded DNA
DNA	desoxyribonucleic acid
DNA-PK	DNA-dependent protein kinase
Dnmt1	DNA methyltransferase 1
DSB	double-stranded break
EGFP	enhanced green fluorescent protein
ERCC1	human excision repair cross complementing group 1
FCS	fluorescence correlation spectroscopy
FEN1	flap structure-specific endonuclease 1
FLIP	fluorescence loss in photobleaching
FRAP	fluorescence recovery after photobleaching
$G_0/G_1/G_2$	gap 0/1/2 phase of the cell cycle
GFP	green fluorescent protein
GG-NER	global genome NER
h	human

HA	hemagglutinin
hHR23A/B	human homologs of S. cerevisie Rad23A/B
His	histidine
HR	homologous recombination
HU	hydroxyurea
IR	ionizing radiation
kDa	kilodalton
LSM	laser scanning microscope
Mdc1	mediator of DNA damage checkpoint protein 1
MMR	mismatch repair
MMS	methyl methanesulfonate
Mre11	meiotic recombination 11
MRN	Mre11-, Rad50- and Nbs1-containing complex
MW	molecular weight
n.a.	numerical aperture
Nbs1	Nijmegen breakage syndrome 1
NER	nucleotide excision repair
NFP	non-fluorescent protein
NHEJ	non-homologous end-joining
NLS	nuclear localization signal
PCNA	proliferating cell nuclear antigen
Pol	DNA polymerase
PTM	post-translational modification
Rad	radiation sensitive
RFC	replication factor C
RNA	ribonucleid acid
RNAPI/II	RNA polymerase I/II
RPA	replication protein A
S-phase	DNA replication (synthesis) phase of the cell cycle
ssDNA	single-stranded DNA
SV40	simian virus 40
TC-NER	transcription-coupled NER
TCR	transcription-coupled repair
TFIIF/H/S	transcription factor 2 F/H/S
TLS	translesion synthesis
UV	ultraviolet radiation
XPA-F	Xeroderma pigmentosum group A-F
XPV	Xeroderma pigmentosum variant
γ-H2AX	phosphorylated histone H2A
(6-4)PP	6-4 photoproduct (pyrimidine-(6,4)-pyrimidone adduct)

Angelika Zotter

Curriculum vitae

Personal Details

Date of Birth:	18th February 1974
Place of Birth:	Mödling, Austria
Nationality:	Austrian

Education and Qualifications

2005 - 2007: Consiglio Nazionale delle Ricerche, Pisa, Italy, Institute of Neuroscience. **Postdoctoral studies** on Erk activation in neurons. (Prof. L. Maffei, Dr. G.M. Ratto)

2000 - 2005: Erasmus University Medical Center, Rotterdam, The Netherlands, Department of Cell Biology & Genetics. **Ph.D. studies** on nucleotide excision repair in living mammalian cells. (Prof. Jan Hoeijmakers, Dr. Wim Vermeulen)

June 2000: Graduation in Biology / Microbiology with emphasis on Biochemistry and Immunology (**Masters**)

1999 - 2000: Vienna Biocenter, Austria. Department of Microbiology & Genetics. **Diploma thesis** on STAT signalling in mammalian cells. (Prof. Thomas Decker)

1998 - 2000: Vienna Biocenter, University of Vienna, Austria. Specialisation in Microbiology / Biochemistry / Immunology.

1998: **Diplom Vorprüfung (Bachelor)**

1993 - 2000: University of Vienna, Austria. Studies of Biology / Microbiology.

Publications

Recruitment of the nucleotide excision repair endonuclease XPG to sites of UV-induced DNA damage depends on functional TFIIH. **Zotter A**, Luijsterburg MS, Warmerdam DO, Ibrahim S, Nigg A, van Cappellen WA, Hoeijmakers JHJ, van Driel R, Vermeulen W, and Houtsmuller AB.
Molecular Cell Biology 2006 Dec; 26 (23):8868-79. Epub 2006 Sep 25.

DNA damage stabilizes interaction of CSB with the transcription elongation machinery. Van den Boom V, Citterio E, Hoogstraten D, **Zotter A**, van Capellen W, Hoeijmakers J. H. J., Houtsmuller A. B., and Vermeulen W.
Journal of Cell Biology 2004 Jul 5; 166 (1):27-36. Epub 2004 Jun 28.

Specificity of signaling by STAT1 depends on SH2 and C-terminal domains that regulate Ser727 phosphorylation, differently affecting specific target gene expression. Kovarik P, Mangold M, Ramsauer K, Heidari H, Steinborn R, **Zotter A**, Levy D. E., Mueller M, and Decker T. *The EMBO Journal, Vol.20 No. 1 & 2 pp.91-100, 2001.*

Acknowledgements

I would like to thank my promoter Jan Hoeijmakers and my copromoter Wim Vermeulen for the opportunity to join this Ph.D. project including all these possibilities of playing with complicated, interesting, expensive optical devices! :) And, of course, for introducing me into the fascinating world of chromatin-associated processes.

Special thanks to you, Jan, for your contagious energy and enthusiasm and kind motivation ALWAYS! Thank you also for translating my "samenvatting" from my poor online translation-infected attempts into REAL Dutch – at an impossible time in the middle of the night when your email response was actually set to you being out of the office!

Wim, thank you for also noticing when I went through personal trouble and for caring! Thank you for laughing a lot and for your honesty. And I'll never forget your astonishing expertise on Trappist beers! :D

My thanks go also to the members of my small committee, Jan Trapmann, Roel van Driel, and Adriaan Houtsmuller, for reading my thesis in record time and for their kind comments on it.

To Gert van Cappellen: When I went away to Italy for my premature postdoc I already had the strong feeling that I wanted to put you into my pocket and just take you with me. I was right! I really missed your knowledge, support and skilled trouble shooting on the microscopes there!

Many thanks also to our friendly and helpful computer support guys of the Cell Biology & Genetics Department, especially Pim Visser who readily lent his helping hand for nearly EVERY imaginable technical problem.

Thanks to all my colleagues who have positively contributed to my thesis in whatever way and who I cannot mention here by name.

Of course, I cannot leave unmentioned my colleagues who have also become my dear friends:

Shehu, thank you for introducing me into the world of physics (formulas...), as well as to your world of patience, generosity and serenity. You have taught me (with more or less success) never to think negatively of people who act against me, but to

assume first of all that they do not intend to harm. Thank you for your warmth, for your love and for your caring.

Raoul, getting to know you has been a real learning experience, a positive one of course! :D I don't even know where to start – well, thank you for a lot of sober nights under the influence of high quality alcohol and for teaching me about the importance of going your own way! I hope I'll see you back soon from the strange alien worlds your special way has taken you. Thank you for teaching me courage and self respect!

Karl, Astrid, thank you for the good time together during my stay in Rotterdam! Karl, I wish you all the best with your fresh and new family. Man, now it MUST be born finally, what is it, baby-boy or baby-girl?! Astrid: sterkte meisje!!! A pretty, smart, hard-working but still funny and warm-hearted girl like you will soon find her balance back – and above all has friends who stand behind her. :)

Audrey, thanks for cheering up the whole lab – and especially me - in your unmistakeable noisy-humorous way! :D Thank you for being my friend and, above all, my paranimpf! :)

Christina, thank you for being always kind and friendly. Thank you for the shoe-shopping and indulging in chocolate with me in Antwerp! :D And especially for having agreed to still be my paranimpf after all this time! :)

Michael: Where do I start? You are one of the kindest and most generous persons I know. Thank you for helping me driving all my belongings through half Europe from Holland to Italy. Thanks for naturally tucking me in – into your only second room which is your living room! - when I had to come back to Rotterdam in order to finish my thesis. Thank you for all the tips and your support in order to help me in my work. Thank you for being a true friend.

Larissa... you have been my dear friend for so long that I nearly forgot we actually started out as colleagues! :D Thank you, THANK YOU, for ALWAYS being there for me, for even coming to me in person from whatever country you are just in when I need a friend. You are amazing!

Vorrei anche ringraziare i miei gentilissimi colleghi dal C.N.R., sopratutto Riccardo, Roberto, Lisa, Sabrina, Carmela, Andrea, Giuliano e José-Fernando.

Grazie anche a Gimmi ch'era tantissimo paziente con me che non avevo ancora finita la mia tesi!

Raul, Mau, grazie per avermi aiutato in un periodo molto difficile, tutte le due in vostre maniere speciale. :) Non mi dimenticaró mai quell' estate ed autunno con voi e spero di non mai perdervi come amici. "Mangiare questo pedone!!!"

Meine liebe Familie... danke für alles, was Ihr für mich getan habt. Liebe Tante Herta: schlußendlich habe ich's geschafft! :) Danke für Deine Unterstützung in all den Jahren, obwohl Du doch auch noch Heerscharen von Kindern, Enkerln und Urenkerln zu betreuen hast! Danke, dass Du Musik in unser Leben gebracht hast. :)

Schlußendlich möchte ich noch meinen besten und ältesten österreichischen Freunden danken, Walter und Roberto. Walter, danke dass Du Dich aller herumirrenden Gestrauchelten annimmst, inklusive mir! ;) Danke, dass ich weiss, dass ich immer auf Dich zählen kann, danke für Deine Großzügigkeit und Herzlichkeit. Danke fuer gemeinsame Spaziergänge in meinem Heimatwald. Roberto, danke, dass ich weiss dass Du immer da bist, auch wenn wir einmal eine Zeitlang nicht in Kontakt sind, was vor allem an meiner eigenen Trägheit liegt. Wir wissen ja beide, WER von uns nicht sehen kann...

...

Wow, I'm finished!

Well, nearly – I would like to apologize to everyone who has supported me – and hence my thesis work – in these last few years and I didn't mention here. Please be sure to have my gratitude!

I just wish all the best to the world! :)

Angelika

Liebe Oma: Danke für meine Kindheit! Ich vermisse Dich sehr!